HEAT TRANSFER, TRIBOLOGY AND PERFORMANCE OF GRAPHENE NANOLUBRICANTS IN AN IC ENGINE

ABDUL KHALIQ RASHEED

Thesis submitted to the University of Nottingham

for the degree of Doctor of Philosophy

APRIL 2016

Dedicated to

my beloved parents
Nasreen Fathima & Rasheed Kuthos

my loving parents-in-law
Ummul Batiya Banu & Shahul Hameed

my lovely wife
Sharmila Fathima

my adorable children
Abdullah & Hana

Abstract

Improving the thermo-physical and tribological properties of lubricants has been a challenging subject of research. Over the last few years, nanolubricants, which are oils containing nanoparticle have been reported to possess exceptionally higher thermal and tribological properties than the traditional lubricants. However, nanolubricants complying with the American Petroleum Institute (API) and Society of Automotive Engineers (SAE) standards remain largely unexplored. In this dissertation, graphene based automotive lubricants meeting 20W50 API SN/CF and 20W50 API SJ/CF specifications have been investigated using a wide range of analytical methods. Thermal-physical and tribological properties have been thoroughly studied. A four-stroke IC engine test rig has been fabricated to investigate the performance of the formulated nanolubricant. By adding 0.01 wt% of 60 nm graphene and 1% lubricity additive to 20W50 API SN/CF oil, 21% and 23% enhancement in the coefficient of friction (μ) and thermal conductivity (k) at 80°C respectively was observed. Viscosity of SNCF with 0.01 wt% of 60 nm graphene and 1% lubricity increases by ~6% at 25°C, and ~9% at 105°C. Scanning electron microscopy and Energy-dispersive X-ray spectroscopy suggest that many nano-tribo mechanisms occurring simultaneously or subsequently could be the reason for enhanced anti-wear and antifriction behaviour of the nanolubricant. Graphene found in the used engine oil indicates that the multilayer graphene exfoliates, rolls up to become helical coils or tube like structure and subsequently entangles with other flakes. As a result, gradually augmenting the thermal performance of the oil. Thermogravimetric analysis revealed that the onset temperature of oxidation for the SN/CF oil could be delayed by 13-17 °C in the presence of graphene. Moreover, the rate of oxidation when the weight loss of oil in the presence of graphene reaches 40% to 20% could be delayed by more than 30 °C. Resistance to oil degradation depends strongly on the graphene nanoparticle size and concentration. TGA kinetics studies show that the base oils have higher activation energy (E_a) and the addition of graphene significantly reduces E_a. Furthermore, 70% enhancement in heat transfer rate is also achieved in the presence of graphene. SEM images of the piston rings collected after 100 hours of engine operation show that the oil containing graphene (12 nm) decreases the piston wear compared to base oil without graphene. Elemental analysis indicates that the addition of a natural polymeric ester based lubricity additive helps even the graphene of highest thickness to perform better in boundary lubrication conditions.

Essentially, this research has put forth a comprehensive understanding of a novel graphene based nanolubricant. The consolidated approach to understand tribological mechanism proposed in this research is expected to result in de novo strategies for engineering advanced nanolubricants in future.

Keywords: Nanolubricant, tribo-morphological phenomenon, enhanced thermal conductivity, nano-additive

List of publications

Acknowledgements

TABLE OF CONTENTS

List of Tables

List of Figures

Abbreviations

et al.	(*et alia*): and others
Hz	Hertz (Unit of frequency)
Kg	Kilogram (Unit of mass)
m	Meter (Unit of length)
nm	Nanometer (Unit of length)
N	Newton (Unit of force)
s	Second (Unit of time)
API	American petroleum institute
FESEM	Field emission scanning electron microscope
XRD	X-ray diffraction
EDX	Energy-dispersive X-ray
FTIR	Fourier transform infrared spectroscopy
TGA	Thermogravimetric analysis
ICP	Inductively-coupled plasma
CNT	Carbon nanotubes
MWCNT	Multi-walled carbon nanotubes
THW	Transient hot wire
CFD	Computational fluid dynamics
AFM	Atomic force microscopy
G	Graphene

Symbols

Symbol	Definition, Unit(s)
k_{eff}	effective thermal conductivity, $Wm^{-1}K^{-1}$
k_p	thermal conductivity of nanoparticles, $Wm^{-1}K^{-1}$
k_b	thermal conductivity of base fluid, $Wm^{-1}K^{-1}$
n	empirical shape factor ($n = \dfrac{2}{\Psi}$)
k_c	thermal conductivity of the CNTs, $Wm^{-1}K^{-1}$
L	length of CNT, nm
d	diameter of CNT, nm
R_k	thermal resistance of the nanotube-fluid interface
T_0	reference value
g	acceleration of gravity
Δh	upstream hydrostatic head minus downstream hydrostatic head
ν	kinematic viscosity
ΔP	total up-stream pressure minus total downstream pressure
R	capillary radius
L	capillary length
μ	absolute viscosity
ϕ	particle volume fraction
ξ	constant
ψ	sphericity
μ_{eff}	effective viscosity of nanofluids
μ_f	effective viscosity of base fluid
μ_∞	intrinsic viscosity at infinite shear rate
μ_0	reference value
ϕ_m	maximum packing volume fraction
eff	effective
p	nanoparticles
b	basefluid
c	CNT
∞	infinity

CHAPTER 1.   INTRODUCTION

1.1.   Background

Lubricants play a vital role in several areas including manufacturing, transportation and aerospace. Efficiency of lubricants are vital for emissions control and fuel economy. Heavy hydrocarbons acquired during combustion process contribute tremendously to the soluble organic fraction (SOF) and to particle number emissions. Emissions caused due to the lubricants could be controlled by enhancing the engine design and improving the lubricant properties. Performance of lubricants is directly associated with the additives it contain. Over the decades several chemical additives have been developed to overcome or decrease tribological challenges including wear, friction, oxidation, scuffing and corrosion along with extensive studies on lubricant base stocks. In addition, enormous efforts have been made to achieve better thermal performance using multi-grade oils. Organic polysulphides, phosphates, dithiophosphates, dithiocarbamates, molybdenum disulphide, zinc dialkyldithiophosphates (ZDDP), etc., remain popular as anti-wear additives. However, modern technological challenges continue to demand further efficient additives. Since last decade metallic and metal-oxide nanoparticles are being rigorously investigated as potential performance improvers for traditionally used anti-friction and anti-wear additives. The idea of using nanoparticles is derived from the century old idea Maxwell (Maxwell, 1873). He suggested combined effective thermal conductivity of the solid-liquid as,

$$k_{eff} = \frac{k_p + 2k_b + 2(k_p - k_b)\phi}{k_p + 2k_b - (k_p - k_b)\phi} k_b$$

(1.1)

where k_p is the thermal conductivity of nanoparticle, k_f is thermal conductivity of base fluid and ϕ is the volume fraction. Carbon allotropes gained greater attention due to its unique morphology and properties (Zhang et al., 2014). Though graphene is fairly new in the lubrication industry, its outstanding thermo-physical (Novoselov et al., 2004, Berman et al., 2014b, Balandin, 2011) and tribological (Berman et al., 2014a, Berman et al., 2014b, Taha-Tijerina et al., 2013, Eswaraiah et al., 2011) properties have made it a remarkable research subject. Having a theoretical specific surface area up to 2600 m^2/g, graphene is made up of one layer atomic carbon (Chae et al., 2004). It has an excellent in-plane thermal conductivity of approximately 5200 W/mK (Balandin et al., 2008), which makes it one of the potential additives to augment thermal property in a lubricant (Rasheed et al., 2015). Moreover the recent advances in large scale production of graphene (Li and Chopra, 2015a, Li and Chopra, 2015b) at cheaper cost would enable graphene to be used in the engine oils without adding much to the total manufacturing cost. Interestingly graphene concentration as low as 0.01 wt% and below has shown significant improvement in the lubricant performance indicating that this small quantity addition of graphene to oils might not increase the oil cost tremendously. Furthermore, handling of graphene is relatively easy. Although graphene powder can be quite hazardous if inhaled, once dispersed into oil can be considered a regular engine oil waste. Though existing tribological studies unanimously agree to graphene's ability in enhancing lubricant performance (Eswaraiah et al., 2011, Ma et al., 2013), they have not been able to fully

uncover the thermos-physical and tribological characteristics, and their underlying mechanisms. Furthermore, there is no study on the performance of graphene nanolubricant in an actual application i.e., IC engine. Generally, between the surfaces of piston rings and cylinder lines, boundary lubrication conditions exist. This condition is acute particularly when the piston halts briefly at top-dead center (TDC) before reversing towards bottom dead center (BDC). The lubricant film between piston ring and cylinder liner get further deteriorated at this location due to extreme temperatures around the TDC. Low piston speed and high temperatures, along with high gas pressure sabotage the presence of a full film between piston ring and cylinder interface. This leads to wear because of the interlock of surface asperities resulting in break off and melting. Recent reports suggest that the extremely thin laminated structure of graphene allowing it to easily enter the contact areas (Lin et al., 2011) and intrinsic structure and self-lubricating property of graphene augmenting the tribological performance of the lubricants (Ou et al., 2010) could be potential mechanisms. In addition, AFM based studies using graphene on substrates indicate electron-phonon coupling (Filleter et al., 2009), puckering (Lee et al., 2010), interplay of surface attractive forces (Hyunsoo et al., 2009) and other physical phenomenon (Smolyanitsky et al., 2012, Deng et al., 2012, Berman et al., 2014a). However, all these mechanisms explain the tribological enhancement of nanolubricants containing graphene in an isolated approach. Furthermore engine test rigs have not been extensively used to investigate overall heat transfer performance of nanolubricants (Peng et al., 2014). This dissertation therefore, aims to investigate the performance of graphene as a lubricant additive in lubrication regimes (piston ring-cylinder interface) of an

IC engine. Furthermore, thermos-physical and tribological properties are investigated in detail. To achieve this, graphene based 20W50 API SN/CF and 20W50 API SJ/CF nanolubricants are formulated, characterised and studied in a self-fabricated IC engine test rig.

1.2. Problem statement

Graphene based nanolubricants meeting industrial standards require thorough investigation for its properties. Owing to the outstanding properties of graphene, the nanolubricant is expected to outperform the existing lubricants. The factors governing the enhancement of properties such as thermal conductivity, anti-friction and anti-wear behavior and viscosity needs to be investigated. Furthermore, in-situ application of graphene nanolubricant to evaluate its performance is essential. Mechanisms governing the properties and performance of nanolubricant remain unexplored.

1.3. Aims and objectives

This research aims to achieve a comprehensive understanding of graphene nanoflakes based nanolubricants. In order to accomplish this, thermo-physical and tribological investigations are necessary. Furthermore, experiments involving nanolubricant in an IC engine would pave way for uncovering the interaction of graphene with surfaces in a combustion environment. Therefore, the objectives of this study are:

I. To formulate and characterise graphene nanoflakes based nanolubricants

II. To determine thermos-physical and tribological properties of graphene nanolubricants

III. To analyse the thermal and oxidative stability of graphene nanolubricant

IV. To determine the interaction of graphene flakes on the tribological surfaces in an IC engine

1.4. Organization of thesis

A total of six chapters have been written. The **first chapter** gives the background of this study, problem statement and the objectives. **Second chapter** presents an exhaustive review of literature on nanoparticle based suspensions. Experimental investigations and theoretical models pertaining to the subject have been summarized and critically reviewed, leading to the objectives of this research.

Chapter 3 details the materials and methodology adapted in the experimental work of this research. Nanolubricant formulation, graphene's characterization and properties measurements have been elaborated. In addition, all the analytical methods used have been discussed. Engine test rig fabrication and experimental procedure has also been explained. **Chapter 4** reports the characterization of graphene and nanolubricant. Thermal conductivity, rheology and tribological results have been discussed in detail.

Chapter 5 has been dedicated to the observations on the performance of graphene nanolubricant in the IC engine. The heat transfer from the engine in the presence of nanolubricant has been theoretically explained using a modified Maxwell model. **Chapter 6** contains conclusions, limitations and recommendations from this research.

CHAPTER 2.   LITERATURE REVIEW†

2.1.   Introduction

This chapter presents an overview of the remarkable research progress on graphene based nanofluids and nanolubricants witnessed in the recent years. Graphene flakes have been investigated worldwide as an additive for coolants and lubricants due to their excellent thermo-physical and tribological properties. As a result, various synthesis methods, characterization techniques and properties measurement procedures that have been experimented and developed has been highlighted. Moreover, factors affecting the stability, thermal conductivity, viscosity and tribological properties of various nanoparticle based formulations have been delineated in detail. Although very few mechanisms have been proposed to explain the enhancement of thermal conductivity, viscosity and anti-wear behaviour of graphene nanolubricants or nanofluids, some key concerns have been presented. Exhaustive review along with the critical comments and recommendations paved way for forming the objectives of this research.

2.2.   Background

Growing energy demands, precision manufacturing, miniaturization, nuclear regulations and critical economies demand high efficient coolants and lubricants. According to the United Nations industrial commodity statistics

database the annual production, import, export, of lubricants including coolants, insulating oils, white oils, cutting oils, lubricating greases and spindle oils produced by all the countries listed during 2010 amounts to approximately 170,046.9 Metric tons (UNdata, 2013). The performance of such huge quantity lubricants directly affects global energy consumption, wear and tear of machine and vehicle components worldwide. For this reason, enhancing the thermo-physical and tribological properties of coolants and lubricants is imperative. While coolants are primarily used to dissipate heat from a system, lubricants are mainly employed to reduce friction and wear. The addition of chemical compounds (commonly known as additives) has been a well-known practice to enhance the thermal and tribological efficiency of coolants and lubricants. Lubricants are classified for various applications based on certain original Equipment manufacturer (OEM) quality and performance standards. Over the years, the standards have been improving to meet enhanced performance shown in the Figure 2.1.
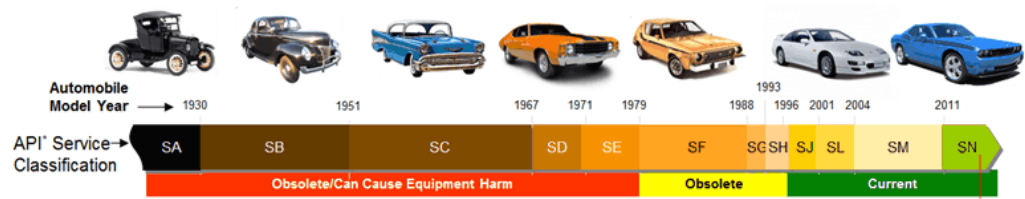
Figure 2.1. API service classification for passenger car engine oil, Petroleum Quality Institute of America, 2013

Lubricants are formulated using base oils which have been categorized by the American Petroleum Institute (API) as shown in Table 2.1. Group I-III are refined from crude petroleum oil. Group IV are full synthetic polyalphaolefin oils. Group V contains base oils not included in the other groups.

Table 2.1. API base oil categories, API 1509 - Appendix E

Base Oil Category	Sulphur (%)	Saturates (%)		Viscosity Index
Group I (solvent refined)	>0.03	and/or	<90	80 to 120
Group II (hydrotreated)	<0.03	and	>90	80 to 120
Group III (hydrocracked)	<0.03	and	>90	> 120
Group IV (Synthetic)	PAO Synthetic Lubricants			
Group V (Synthetic)	All other base oils not included in the above groups			

Various additives perform as thermal conductivity (k) enhancers (Eastman et al., 2001, Yu et al., 2008), friction modifiers (Kosarieh et al., 2013), anti-wear (AW) agents (Haque et al., 2010, Rudenko and Bandyopadhyay, 2013), extreme-pressure (EP) agents (Hernández Battez et al., 2007), anti-oxidants (Nassar et al., 2016, Rasheed et al., 2015), anti-corrosion agents (Wilson and Lyon, 2010), pour point depressants (Hafiz and Khidr, 2007, Taraneh et al., 2008), viscosity index improvers (Mohamad et al., 2012, Vakili-Nezhaad and Dorany, 2012) and so on. Although, some of the additives are multifunctional (Lee et al., 2010), they are commonly known for their primary function. Fine

solid metal particles have also been employed to enhance the efficiency of coolants and lubricants. For instance, micro-scale fine particles of molybdenum disulfide (MoS_2), graphite, etc., have been quite successfully used as anti-friction and anti-wear additives for oils (Martin-Gallego et al., 2011, Cai et al., 2010). However, a number of reports underlined that the micro-particles increase the wear rate and friction coefficient (Liu et al., 2013, Sun et al., 2010). Besides, micro-particles tend to settle down in liquids due to their high density and in case of forced circulation, they clog the channels and wear away the inner-walls of channels. Furthermore strict standards are in place to protect environment from pollution caused by additives such as molybdenum dithiocarbamate (MoDtc), hence mandates alternative additives.

The development of various nanoparticles has opened new opportunities in various fields including lubrication, medicine, composites and space. Metallic and metal oxide nanoparticles (Hernández Battez et al., 2008, Hernández Battez et al., 2010, Yu et al., 2008), carbon family nanostructures (fullerenes, onions, nanotubes and graphene, Figure 2.2) (Nomède-Martyr et al., 2012, Cursaru et al., 2012, Grierson and Carpick, 2007), reverse over based micelles and boron have been used to formulate nanofluids (Das et al., 2007) and nanolubricants (Martin and Ohmae, 2008). In general, nanoparticle based coolants such as water, ethylene glycol, etc., are referred as nanofluids (Das et al., 2007) and oils based nanoparticle suspensions are referred as nanolubricants (Martin and Ohmae, 2008). They carry a number of advantages, including;

1. Better stability is observed while suspended in base oils as compared to macro or micro particles.

2. Nanoparticles enter the contact area easily and also provide a protective coating against wear.

3. Nanoparticles do not require an induction period to obtain the desired tribological properties as they are often efficient at ambient temperature, unlike their micro counterparts.

4. Nanoparticles possess better thermo-physical properties than their bulk counterparts.

In the year 1995, Choi coined the term nanofluids and found that nanoparticles can offer anomalous enhancement of thermal conductivity (k) to the base fluids. Since 1995, research in this area has diversified tremendously into many disciplines as shown in Figure 2.2. A series of breakthroughs were witnessed when Choi (1995), Eastman et al. (2001), and Das et al. (2003) observed 40% enhancement using 0.3% Cu particles of 10 nm size, 150% increase in thermal conductivity of multi-walled carbon nanotubes (MWCNT)-engine oil nanolubricants using 1% volume fraction of nanotubes and strong temperature dependence of nanofluids with Al_2O_3 and CuO particles, respectively.
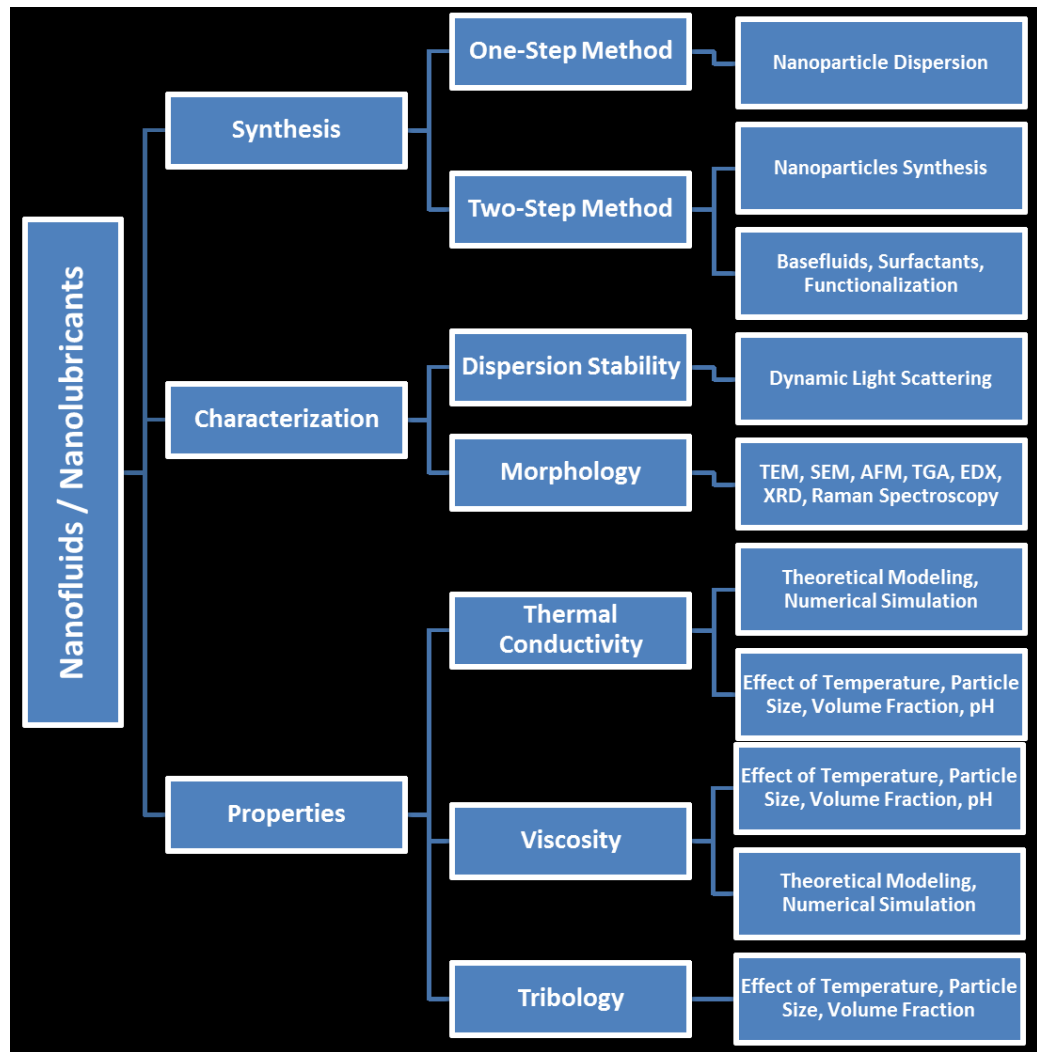
Figure 2.2. Nanofluids and nanolubricants research areas and methodology

Over the years several hundred reports were published on anti-friction (Hernández Battez et al., 2008, Ma et al., 2010, Lahouij et al., 2012), conduction (Fan and Wang, 2011), convection (Daungthongsuk and Wongwises, 2007, Kakaç and Pramuanjaroenkij, 2009, Haddad et al., 2012, Mohammed et al., 2011, Murshed et al., 2011), pool boiling (Taylor and Phelan, 2009), rheology (Kole and Dey, 2013), thermal conductivity mechanisms (Eapen et al., 2007, Chandrasekar et al., 2012, Rashmi et al.,

2014), properties (Murshed et al., 2008b, Özerinç et al., 2010, Thomas and Choondal, 2011, Yu and Xie, 2012, Yu et al., 2008, Nkurikiyimfura et al., 2013, Salman et al., 2013, Rao, 2010), electrical conductivity (Taha-Tijerina et al., 2012, Baby and Ramaprabhu, 2010a, Hadadian et al., 2014, Mehrali et al., 2015), applications (Yu and Xie, 2012, Wen et al., 2009, Yu et al., 2007, Murshed et al., 2008b, Ahmed et al., 2012, Huminic and Huminic, 2012, Mahian et al., 2013), various properties measurement methods (Paul et al., 2010), refrigeration (Saidur et al., 2011, Cheng and Liu, 2013), etc., of various nanolubricants and nanofluids. Interestingly, another wave of serious interest evolved among researchers when single-atom-thick graphene (Figure 2.3) was successfully extracted from bulk graphite in 2004. Several reports have been published on graphene based nanolubricants and nanofluids (Eswaraiah et al., 2011, Rasheed et al., 2015, Senatore et al., 2013). However, a review focusing on graphene nanoparticle based suspensions i.e., graphene nanofluids or nanolubricants is not available yet. It is imperative to understand the anti-friction behaviour, enhanced thermal conductivity phenomenon, rheology and tribology of graphene based nanofluids and nanolubricants owing to its different nature from other nanoparticles.
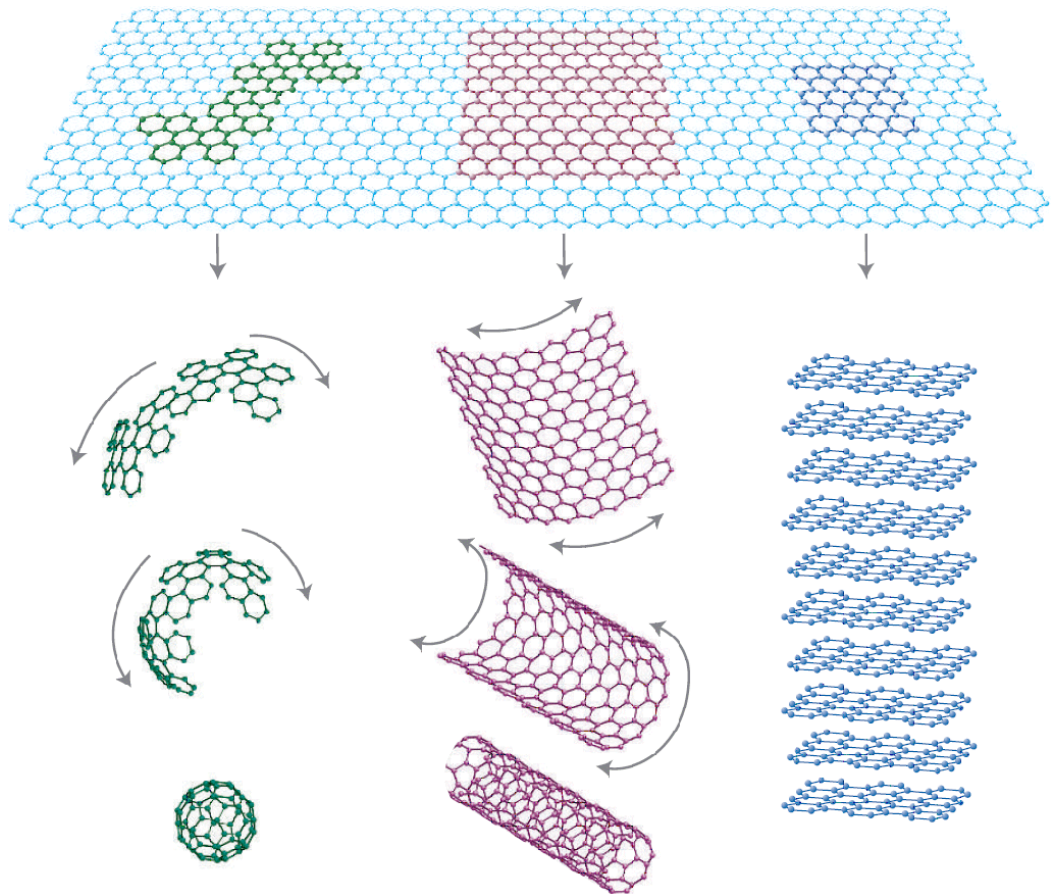
Figure 2.3. Graphene is a 2D building material for carbon materials of all other dimensionalities. It can be wrapped up into 0D buckyballs, rolled into 1D nanotubes or stacked into 3D graphite (Adapted from (Geim and Novoselov, 2007)).

Graphene nano-flakes are made of one layer of atomic carbon with outstanding properties as shown in Table 2.2, including theoretical specific surface area up to 2600 m^2/g (Chae et al., 2004). Exceptionally high thermal conductivity (k) of the range (4.84±0.44) x 10^3 to (5.30±0.48) x 10^3 $W\ mK^{-1}$ was measured for a suspended graphene sheet obtained by mechanical exfoliation (Balandin et al., 2008). These values are greater than that of carbon nanotubes (CNT, ~1500 – 2900 $W\ mK^{-1}$) and diamond (~2200 $W\ mK^{-1}$) obtained experimentally. In addition, few layer graphene is found to have exceptional anti-friction

properties (Berman et al., 2014a, Berman et al., 2014b, Taha-Tijerina et al., 2013, Eswaraiah et al., 2011). These outstanding properties could make graphene one of the ideal additives that may possibly be exploited in the synthesis of coolants and lubricants with enhanced heat transfer and tribological properties.

Table 2.2. Typical properties of graphene

Properties	Graphene
Thermal Conductivity, k	~5000 W m^{-1} K^{-1} (Balandin et al., 2008)
Thermal resistance (interface)	~4 × 10^{-8} K m^2 W^{-1} (r_{Gr-SiO_2}) (Freitag et al., 2009)
Specific surface area	2600 m^2 g^{-1} (Chae et al., 2004)
Young's modulus	~1 TPa (Stankovich et al., 2006a, Lee et al., 2008)
Fracture strength	130 GPa (Lee et al., 2008)
Optical transmittance	~97.7% (Nair et al., 2008)
Sheet resistance	1.3 × 10^4–5.1 × 10^4 Ω sq^{-1} (Nair et al., 2008)
Spin R	1.5–2 μm (Tombros et al., 2007)
Elaxation length	15 000 cm^2 V^{-1} s^{-1} (Novoselov et al., 2004)
Current density	c/300 = 1 000 000 ms^{-1} (Dragoman and Dragoman, 2009)
Fermi velocity	300–500 nm (Dragoman and Dragoman, 2009)
Phase coherence length	3–5 μm (Miao et al., 2007)
Mobility (typical)	200 000 cm^2 V^{-1} s^{-1} (Du et al., 2008)
Mobility (intrinsic)	10^8 A cm^{-2} (Du et al., 2008)

2.3. Synthesis of nanofluids and nanolubricants

Graphene based nanofluids and nanolubricants are synthesized using one-step method or two-step method. The one-step method yields nanofluids directly through chemical methods. In two-step method, graphene is synthesized in powder form by means of physical or chemical methods, e.g. grinding, laser ablation, sol-gel processing, etc., and then dispersed into a base fluid. Dispersion of nanoparticles is aided by stirring, sonication, homogenization or other mixing techniques along with dispersants or surfactants. Both methods have their own advantages and limitations however, the selection of the method depends upon the production scale, quality and functional groups required for stable dispersion into a desired basefluid. Graphene can be obtained either in single layers or multi-layers (Table 2.3). Single-layer graphene is commonly obtained from "highly ordered pyrolytic graphite" (HOPG) by micromechanical cleavage (Novoselov et al., 2004). In this method, a layer is peeled off the HOPG crystal with scotch tape and transferred onto a silicon substrate. Graphene can also be prepared through chemical methods in which single-layer graphene oxide dispersion in dimethlyformamide (DMF) is reduced using hydrazine hydrate (Gilje et al., 2007). Graphite oxide immediately forms a stable colloidal suspension in water after which the suspension is sonicated (300W, 35 kHz) to make graphene oxide (GO). However, this method can lead to graphene with large amount of defects. Chemical vapour deposition (CVD) (Mattevi et al., 2011) of graphene on metals and metal oxide is another way of obtaining graphene but leads to multi-layer graphene production and also they are hard to be taken out from the metal surface. There is no chemical method yet to obtain graphene with definite numbers of layers. Furthermore, the surface area of the

sheets depends on the preparation technique and the number of layers; however, it is usually large (600–1600 m^2 g^{-1}). A number of review articles shed light on the various synthesis methods of graphene and could be useful for deeper insights (Rao et al., 2010, Texter, 2014, Sharma et al., 2016). It has been reported that the defects on graphene could significantly affect the thermal efficiency, as shown in Figure 2.4. Graphene encounters structural defects, atomic vacancies, folding, doping, non-sp^2 carbon defects, Stone-Thrower-Wales (STW)-type defects and so on. It has been reported that by applying photonic engineering, the *k* of graphene could be manipulated.

Table 2.3. Synthesis methods and mechanisms

Synthesis Method	Number and size	Precursors used	Graphene Produced	Mechanism
Epitaxial growth	SLG, FLG; >50 μm	SiC or Ru	Pristine	Thermal decomposition of hydrocarbons on top of SiC or Ru crystals
Mechanical exfoliation (Novoselov et al., 2004)	SLG, FLG; 10 μm	Graphite	Pristine	Peeling off layers using scotch tape
Chemical vapor deposition (Mattevi et al., 2011)	SLG, FLG; >100 μm	Polycrystalline Ni films, copper foils, transition metals	Pristine	Carbon segregation or precipitation over transition metals
Chemical exfoliation (Stankovich et al., 2006b)	SLG, FLG; >100 nm	Graphite oxide (or) GO obtained by processing GICs	Chemically modified graphene	Decomposition of graphite based compounds, reduction and subsequent exfoliation
Liquid phase exfoliation (Hernandez et al., 2008)	SLG, FLG; <20 μm	Graphite (or) graphite oxide	Pristine	Exposing graphite or GO to solvents and applying sonication
Unzipping carbon nanotubes (Kosynkin et al., 2009)	SLG, FLG; <10 nm	MWCNT	Chemically modified graphene	Longitudinal unzipping of CNT
Solvo-thermal synthesis (Choucair et al., 2009)	SLG, FLG; <20 μm	Solvothermal product (*e.g.* Na + C_2H_5OH)	Chemically modified graphene	Pyrolysis and filtering of a solvo-thermal product
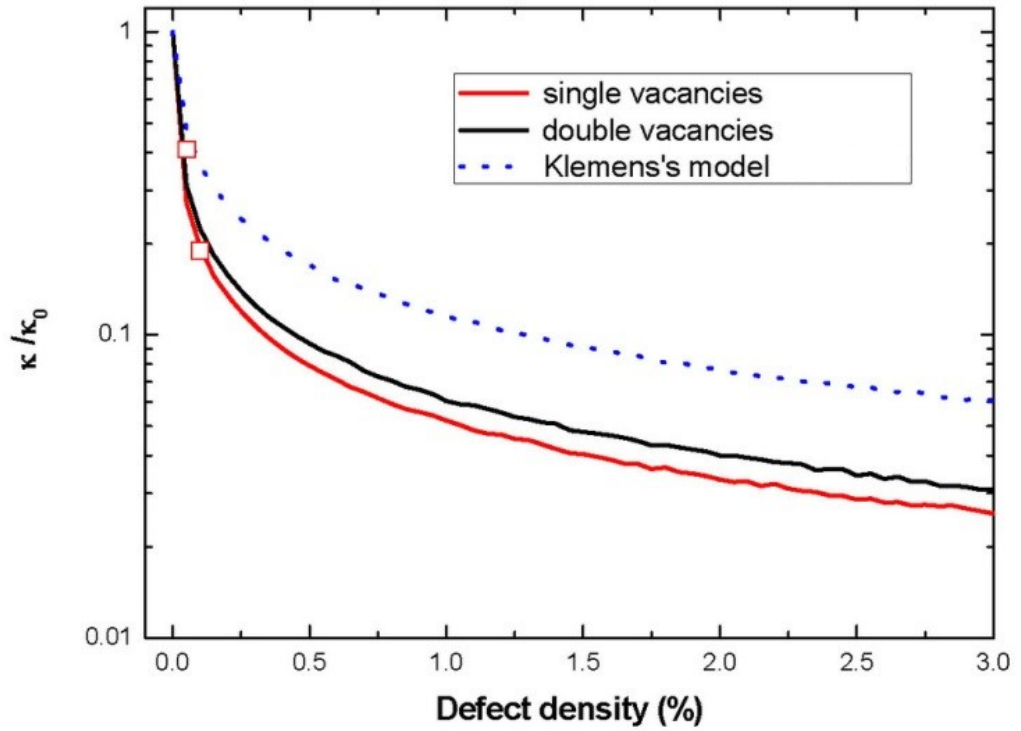
Figure 2.4. The ratio of the *k* of defective graphene to the pristine one at room temperature as a function of defect density (Xie et al., 2014).

The thermal conductivity for different scattering mechanisms are calculated separately and the total is given in the Klemens model as,

$$\frac{1}{k} = \sum_i k_i^{-1}$$

(2.1)

In the Table 2.3 pristine is referred to graphene in its original pure form though it might contain some defects. Chemically modified graphene is referred to the graphene with other atoms attached in place of carbon atoms. Single layer graphene has been reported to have better thermal conductivity than multi-layer graphene. The interlayer linkages could induce substantial decline in the thermal conductivity of bi-layer graphene depending upon the interlayer linkage type, concentration and location. Furthermore, the thermal

conductivity could be severely suppressed if the linkages contain vacancies. While these aspects of graphene synthesis are crucial, they have been largely neglected while explaining the improvement of various properties of nanofluids and nanolubricants. Furthermore, controlled synthesis of graphene and careful characterization could help in understanding the vital parameters that affect various properties of the graphene based suspensions.

2.3.1. Stability of graphene nanofluids

Graphene is hydrophobic in nature and does not disperse in polar solvents. It readily agglomerates and settles when dispersed in water based suspensions. Generally surfactants are added to enhance the stability of the nanoparticle suspensions but the associated disadvantage of poor k of surfactants make it an undesirable option (Mingzheng et al., 2012). Moreover, reports suggest that commonly used surfactants including hexadecyltrimethylammonium bromide (CTAB), gum Arabic and sodium dodecyl sulfate (SDS) have very little impact on the stability of graphene based suspensions (Uddin et al., 2013). The process of dispersing graphene in solvents using stabilizers or surfactants followed by centrifugation to isolate the well dispersed components could be better for lab scale. It might not be suitable for large scale production because such methods lead to wastage of more than 90% graphene (Texter, 2014). Surfactants might not be suitable for lubricants as they would not meet viscosity standards set by original equipment manufacturers and professional bodies. Though mineral oils are generally non-polar, as synthesized graphene is not enough hydrophobic to form homogeneous formulation. Chemical functionalization (Kuila et al., 2012) of graphene helps in modifying the

functional groups which enables the graphene to make bonds with basefluid molecules. Filtration techniques, spin-coating and layer-by-layer assembly in chemical method help to avoid the single layer graphene getting agglomerated during reduction and preserve the intrinsic properties of graphene. Both covalent and non-covalent modification techniques are adopted for functionalizing graphene. In either case, graphene oxide's surface is modified and then reduced. Nucleophilic substitution of an amine-terminated organic modifier under the covalent modification is considered as the easiest method to produce functionalized graphene. However, some reports indicate that the quality of graphene morphologically decreases owing to chemical oxidation and sonication. Furthermore, the thermal and electrical conductivity of functionalized graphene decreases considerably.
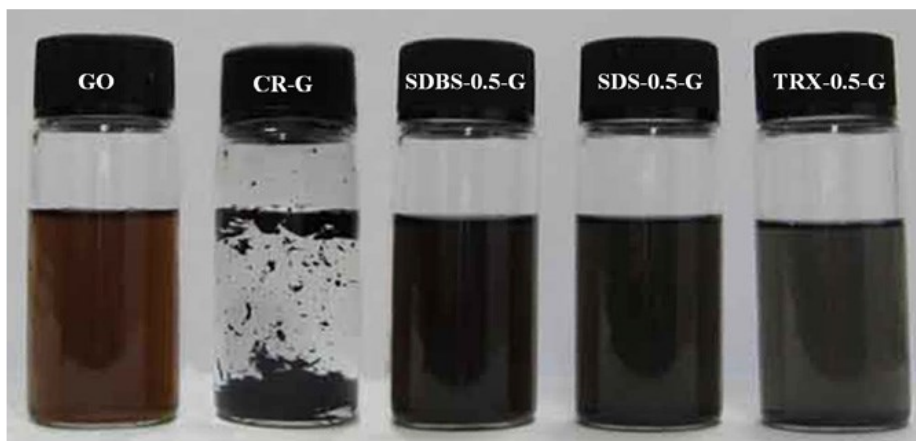
Figure 2.5. Digital photographs of the water dispersion of pure GO, CR-0.5-G, SDBS-0.5-G, SDS-0.5-G and TRX-0.5-G. (Uddin et al., 2013)

In one of the reports (Uddin et al., 2013), 4-(1,1,3,3-tetramethylbutyl) phenyl-polyethylene glycol (Triton X-100), sodium dodecyl benzene-sulphonate (SDBS) and sodium dodecyl-sulphate (SDS) were used as ionic and non-ionic surfactants. The dispersion stability of SDBS functionalized graphene (SDBS-G) was best in water with a concentration of 1.5 mg ml^{-1} (Figure 2.5) but the thermal properties was compromised. Coatings using metals and metal oxides could avoid this problem of thermal property degradation. When SiO_2 was used for coating graphene by chemical liquid deposition using tetraethyl orthosilicate (TEOS) (Li et al., 2014), the stability and thermal conductivity of the suspension increased significantly. Similarly, Ag and CuO coating of graphene has resulted in the excellent stability and thermal conductivity (Baby and Ramaprabhu, 2011a, Baby and Ramaprabhu, 2011b). Obtaining stable suspensions of graphene based mineral oils is difficult unless graphene's surface charges are modified. Eswaraiah et al (Eswaraiah et al., 2011) obtained super hydrophobic, less defective and highly deoxygenated graphene based engine oil formulation by exfoliation of graphite oxide using focused solar electromagnetic radiation. Due to fast heating the elimination of oxygen from groups of GO surpasses the diffusion rate of gasses that emerge back to the graphene. This leads to yielding pressure that exceeds the van der Waals force holding the graphene flakes together in GO. Similarly, Bai et al, (Bai et al., 2014) decorated graphene with well-dispersed cubic fluorite ceria (CeO_2) using a hydrothermal method. They observed that the formulation with high zeta potential (negative or positive) are stable because of the coordination between the residual carboxyl, CeO_2 and phenolic hydroxyl groups present on CeO_2-graphene composites. This makes the electronegativity of O in carboxyl

and phenolic hydroxyl weaker, as a result the surfaces of CeO_2-graphene could lose protons and become more negative than those of graphene. Similarly for various other nanoparticle compositions and hybrid nanolubricants, physical-chemistry approach would help in the formulation of more stable suspensions. Zeta potential, ultra-violet visible (UV-Vis) spectroscopy and digital imaging have been extensively used to study the stability of nanoparticle suspensions. Nevertheless, further emerging technologies based on micro-electrophoresis and electrophoretic light scattering could make zeta potential and electrophoretic mobility measurements more sophisticated, and suitable for nanoparticle suspensions and colloids.

2.3.2. Characterization

Graphene nanoflakes are characterised by a number of analytical methods. Scanning electron microscopy (SEM), transmission electron microscopy (TEM), ultra violet visible absorption spectroscopy and atomic force microscopy (AFM) are useful during the early study period of graphene to identify the number of layers but they are time consuming and require desired sample preparation. In the Figure 2.5, the UV-Vis spectra of monolayer and bilayer graphene measured at 550 nm and high-resolution transmission electron microscopy (HRTEM) picture of the same are shown. It also clearly shows 3–5 layers thick at the edges of PMMA-derived graphene. After the year 2006, Raman spectroscopy is found to be a simple yet powerful tool for quantifying graphene's layers (Ferrari et al., 2006).
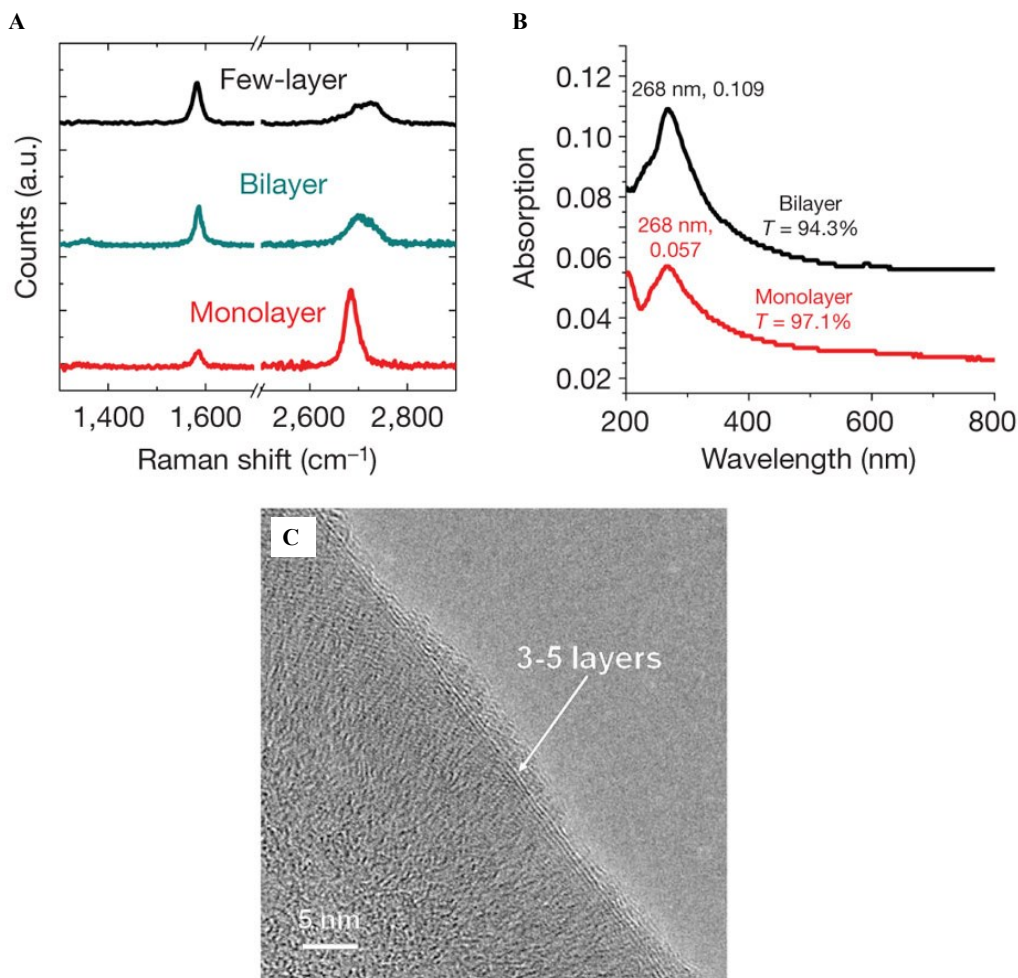
Figure 2.6. PMMA-derived graphene; a, Raman spectra b, The ultraviolet–visible absorption spectra c, HRTEM picture (Sun et al., 2010)

Figure 2.6 shows the disparity in Raman spectra from poly-methyl-methacrylate derived graphene with controllable thicknesses derived from different flow rates of H_2 (Sun et al., 2010). One of the remarkable aspects in the Raman spectra of sp2 hybridized carbon materials is the G-band emerging at *ca.*1580 cm^{-1} and the G-band at *ca.* 2700 cm^{-1} for a laser excitation energy of 2.41 eV. Raman scattering is useful in studying the quality of graphene in which the G-band nearing 1580 cm^{-1} in the Raman spectra is sensitive to doping and other effects. Atomic force microscopy (AFM) also helps in the

24

determination of the number of layers and flakes' features. Scanning tunneling spectroscopy (STS) as well as scanning tunneling microscopy (STM) can be useful in obtaining data pertinent to the defects in graphene flakes nearing Fermi level Lahiri et al. (2010). Nevertheless, explanation of STM and STS data can be complicated, and as a result simulation of such results in the form of images is useful.

Similarly electron diffraction with ideal conditions can be useful to acquire information from structures resembling graphene. The images and the diffraction patterns can also be simulated with the coordinates of the nanostructure and compare the same with the high-resolution images and experimental diffraction patterns. Characterization of graphene after dispersion into liquids is also vital since it could reveal graphene's corrugation and scrolling which is inherent to the two dimensional graphene sheets. It can be seen from the Figure 2.7 that graphene gets folded, coiled and corrugated not only at the edges but also in the middle of its sheets. The defects not only affect the thermal conductivity of graphene but also many other properties. It is not clearly known to what extent the defects can affect the properties. Nevertheless, the characterization techniques seem promising in uncovering further hidden facts about the nanomaterials and graphene in particular
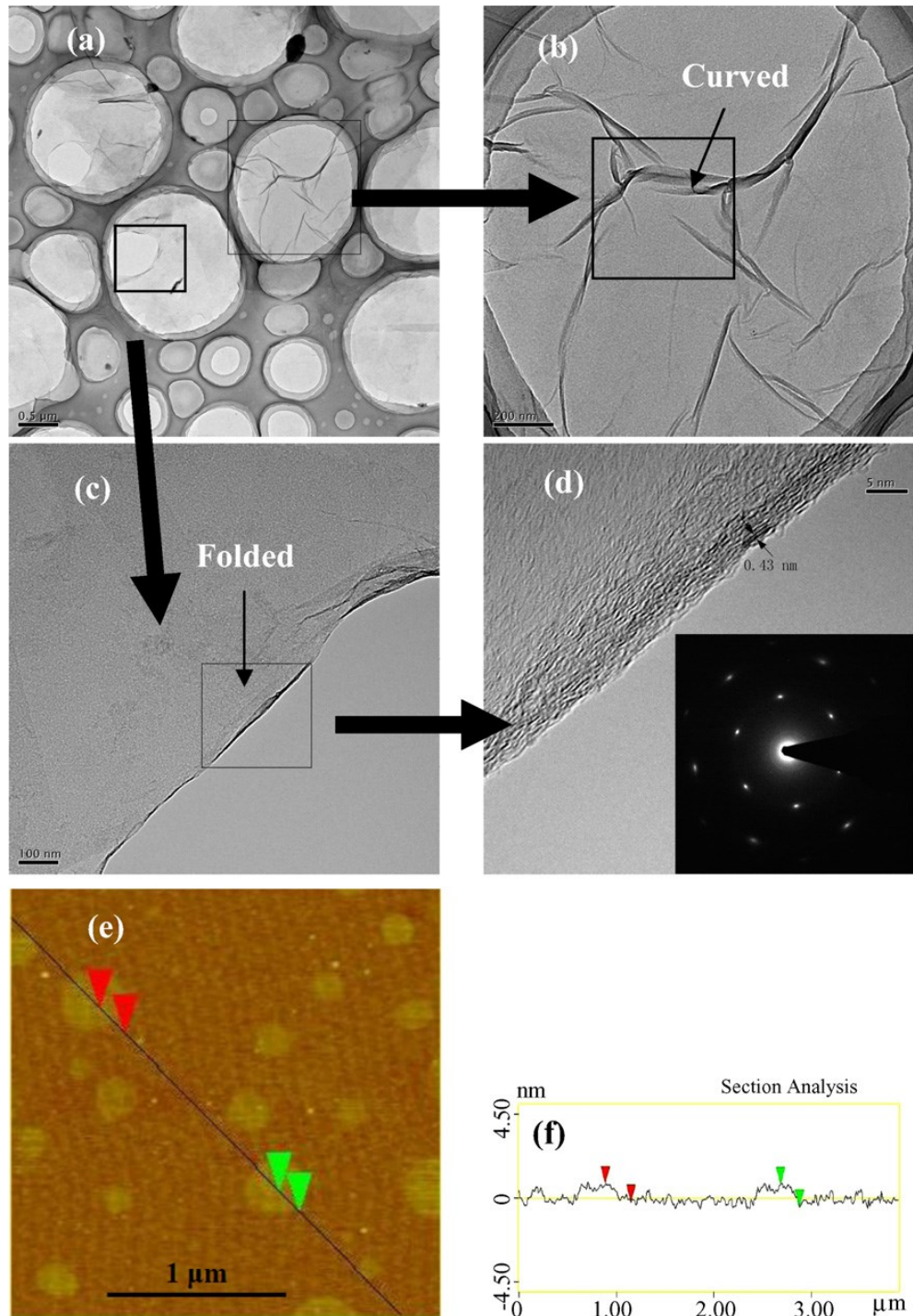
Figure 2.7. TEM and AFM images of as-prepared graphene nanosheets. (a) bar 0.5 μm; (b) bar 200 nm, graphene wave in the middle; (c) bar 100 nm, graphene coiled at the edge; (d) HRTEM image of the graphene; (e) a tapping mode AFM image of graphene nanosheets, and (f) the height profiles in selected location. (Yu et al., 2011)

2.4. Thermal Conductivity (k)

2.4.1. **Experimental**

One of the most common investigations of nanofluids and nanolubricants is on

thermal conductivity (k) owing to its significance in heat transfer applications.

Both coolants and lubricants having various basefluids with poor thermal

conductivity require significant improvement of its thermal properties.

Carbon-based (Ding et al., 2006, Walvekar et al., 2012) particularly carbon

nanotubes (CNT) nanofluids Choi et al. (2001) were known to outperform all

the metallic (Patel et al., 2003, Shahriari et al., 2013, Lotfi and Shafii, 2009,

Eastman et al., 2001) and metal oxide (Li and Peterson, 2007, Eastman et al.,

2001) nanofluids in terms of k. Although graphene has a theoretical k of ~

5000 W m^{-1} K^{-1} (Balandin et al., 2008) which is more than the k of CNT

($\sim 1500 - 2900 \ W \ mK^{-1}$) (Kim et al., 2001), the latest experimental results on

chemical vapour deposition (CVD) grown suspended graphene show lower

values (~2500 W/mK) (Cai et al., 2010). Yet the experimental results (Baby

and Ramaprabhu, 2010a, Yu et al., 2011, Gupta et al., 2011) on graphene

based nanofluids show much higher enhancements than CNT with equal

volume concentrations.   Transient hot wire (THW) method, parallel plate

method and the 3ω method (Table 2.4) are commonly used k measurement

methods.   However, THW technique has been widely used for graphene

nanofluids (Gupta et al., 2011, Sun et al., 2010) because of its reliability in

measuring thermal conductivity and thermal diffusivity. Several investigations

have found that the enhancement of various nanofluids depend on

nanoparticles volume fraction (Walvekar et al., 2012), size (Anoop et al.,

2009, Li and Peterson, 2007, Beck et al., 2009), shape (Jeong et al., 2013), base fluid (Tsai et al., 2008), temperature (Das et al., 2003b), sonication time (Ruan and Jacobi, 2012), pH (Mehrali et al., 2014), etc. Similarly the literature shows that the graphene nanofluids and nanolubricants enhancements depend of several parameters. In the following sections our discussion focusses on the effect of graphene concentration, surface charges, flake size and sample temperature.

Table 2.4. Thermal Conductivity Measurement Techniques

Steady State method (Wang et al., 1999)		**Transient method** (Murshed et al., 2005, Zhang et al., 2007, Zhu et al., 2009, Jiang et al., 2009)					**Thermal Comparator** **(Sherif and Mahmoud, 1966)**
Steady State Parallel Plate	Cylindrical Cell	3ω method	Transient hot wire		Thermal Contacts Analyzer	Temperature Oscillation	
			Liquid –Metal Transient Hot-Wire	*Transient Short Hot-Wire*			

2.4.1.1. **Effect of nanoparticle concentration on thermal conductivity**

As compared to oils and other high-viscous fluids, water and ethylene glycol has been widely used as a base fluid in several reports. Both graphene (Gupta et al., 2011, Baby and Ramaprabhu, 2010a) and graphene oxide (Yu et al., 2010a, Yu et al., 2010b) show increase in thermal conductivity with increasing concentration which is very similar to metallic and metal-oxide nanofluids (Sridhara and Satapathy, 2011, Eastman et al., 2001). While looking at chronological order, in the year 2010, Yu et al showed that the GO can enhance the k of d-H_2O, propyl glycol and liquid paraffin nanofluids by 30.2%, 62.3% and 76.8% respectively using 5.0 vol%, Figure 2.8. In the same year Baby and Ramaprabhu showed that for f-TEG based H_2O nanofluids the enhancement was 64% with volume fraction of 0.056% at 60°C. Their observation was much higher than Yu et al's results. However, in 2011 Yu et al (Yu et al., 2011) found that the graphene treated with sodium dodecyl-benzebe-suefonate (SDBS) perform much better. An enhancement of 86% in thermal conductivity was observed with 5.0 volume% which is 1.42 times than their previous GO nanofluids. Interestingly Gupta et al. (2011) also observed much higher thermal conductivity enhancement of 27% with just 0.2 vol% graphene.
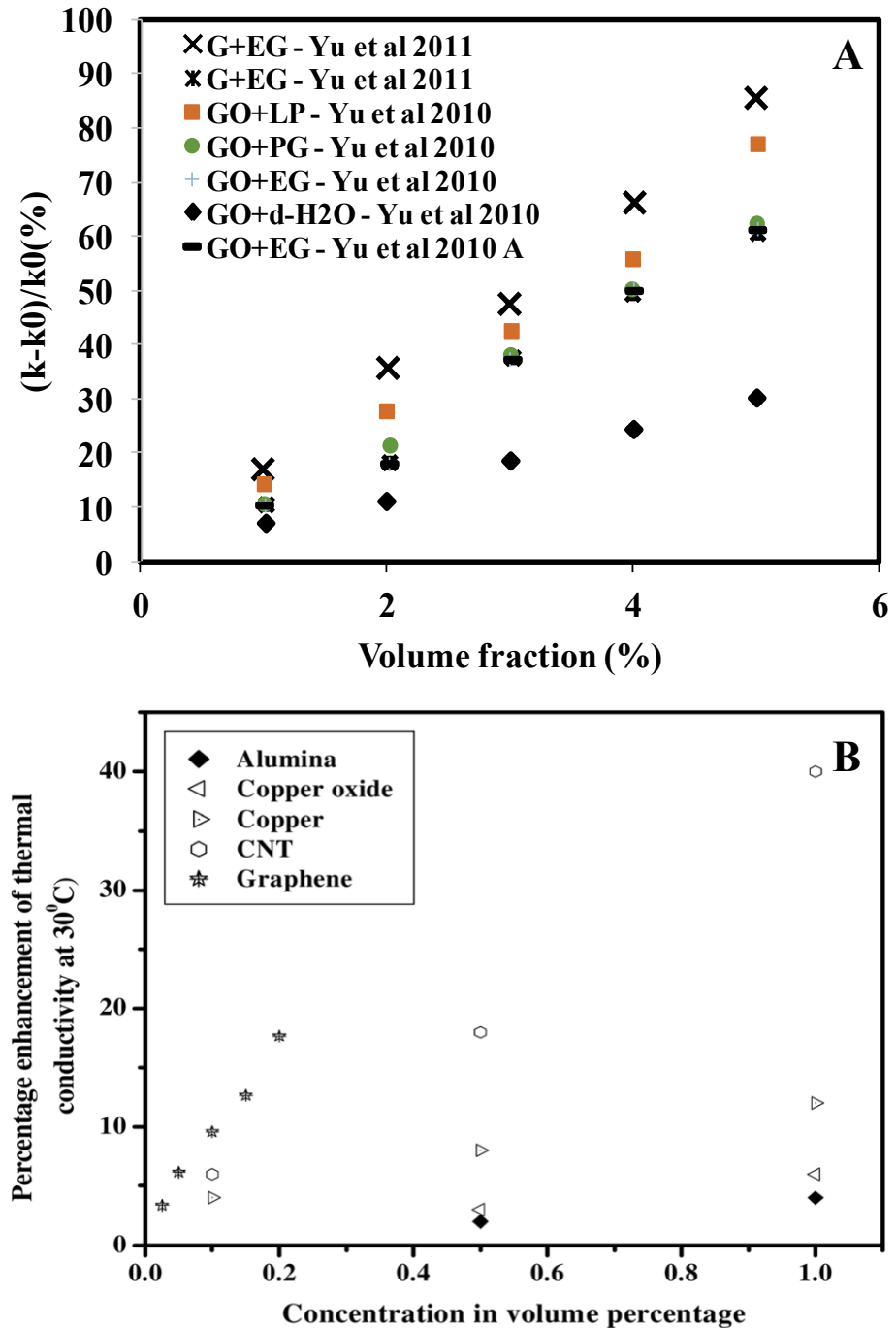
Figure 2.8. A: Thermal conductivity enhancement vs Volume fraction (%) from Yu et al's work (Yu et al., 2011). B: Gupta et al. (Gupta et al., 2011) comparing graphene's enhancement of *k* with other nanoparticles.

Sun et al (Sun et al., 2013) showed a better *k* enhancement of 25% than that of

Gupta et al (Gupta et al., 2011) at a very low concentration of 0.055% volume

fraction (Gupta et al., 2011). However, Kole and Dey (Kole and Dey, 2013) found an enhancement of ~15% with 0.395 vol.% of f-HEG at 30 °C for water-EG based graphene nanofluids. This observation is very close to what Gupta et al (Gupta et al., 2011) found. The thermal conductivity is increasing linearly with graphene concentration. Many reports in the following years, 2013 (Ma et al., 2013, Taha-Tijerina et al., 2013, Ghozatloo et al., 2013)2014 (Fan et al., 2014, Hajjar et al., 2014, Park and Kim, 2014, Mehrali et al., 2014) and 2015 (Mohd Zubir et al., 2015, Rasheed et al., 2015) also reported similar concentration dependent k of graphene nanofluids. Although the increasing concentration will lead to particle aggregation and assist in the formation of percolation (Dhar et al., 2013b) which result in the enhancement of thermal conductivity, graphene tends to settle after the threshold concentration value is reached. Some studies such as by Li et al (Li et al., 2014) on SiO_2-coated graphene-water nanofluids and Moghaddam et al. (Moghaddam et al., 2013) on graphene–glycerol nanofluids did not report the effect of concentration on the thermal conductivity of nanofluids. However, it is expected that the thermal conductivity should be enhanced owing to the identical observations made in all the above reports.

2.4.1.2. **Effect of temperature on thermal conductivity**

According to kinetic theory, the energy of the particles and the base fluid molecules would increase with the increase in temperature. Due to random motion of particles the increase in energy would be readily available for transfer from one place to another. In 2003 Das et al (Das et al., 2003b) found

that the anomalous thermal conductivity enhancement of nanofluids depend on temperature. With the increase in temperature the k is enhanced in most metallic, metal oxide and CNT based nanofluids (Das et al., 2003b, Mintsa et al., 2009). However, reports which contradict this claim have also been surfaced (Buongiorno et al., 2009, Chen et al., 2008, Timofeeva et al., 2007, Yang and Han, 2006). Interestingly, in case of Bi_2Te_3 nanorods based nanofluids, the increase in temperature causes decrease in the thermal conductivity (Yang and Han, 2006). Although this is a unique phenomenon, it shows how diverse observations have been made for various nanoparticles. Similarly, in case of graphene based nanofluids discrepancies exist. Experimental data on graphene and GO by majority of the research groups show that the enhancements are temperature dependent, Figure 8 (Baby and Ramaprabhu, 2010a, Taha-Tijerina et al., 2013, Kole and Dey, 2013, Gupta et al., 2011, Wang et al., 2012). However, Yu et al., (Yu et al., 2010a, Yu et al., 2011) and Sun et al., (Sun et al., 2013) results contradict to show that the thermal conductivity enhancement of GO is independent of temperature as shown in Figure 2.9. This temperature independent behaviour has also been found in the case of CNT (Chen et al., 2008), Al_2O_3 (Timofeeva et al., 2007) and other nanofluids. Timofeeva et al (Timofeeva et al., 2007) contended that the enhancement of thermal conductivity of nanofluids is due to the effect of base fluid rather than the particles themselves. The structure of CNT and graphene offers comparatively large surface area and hence better thermal conductivity than spherical and other shaped particles.
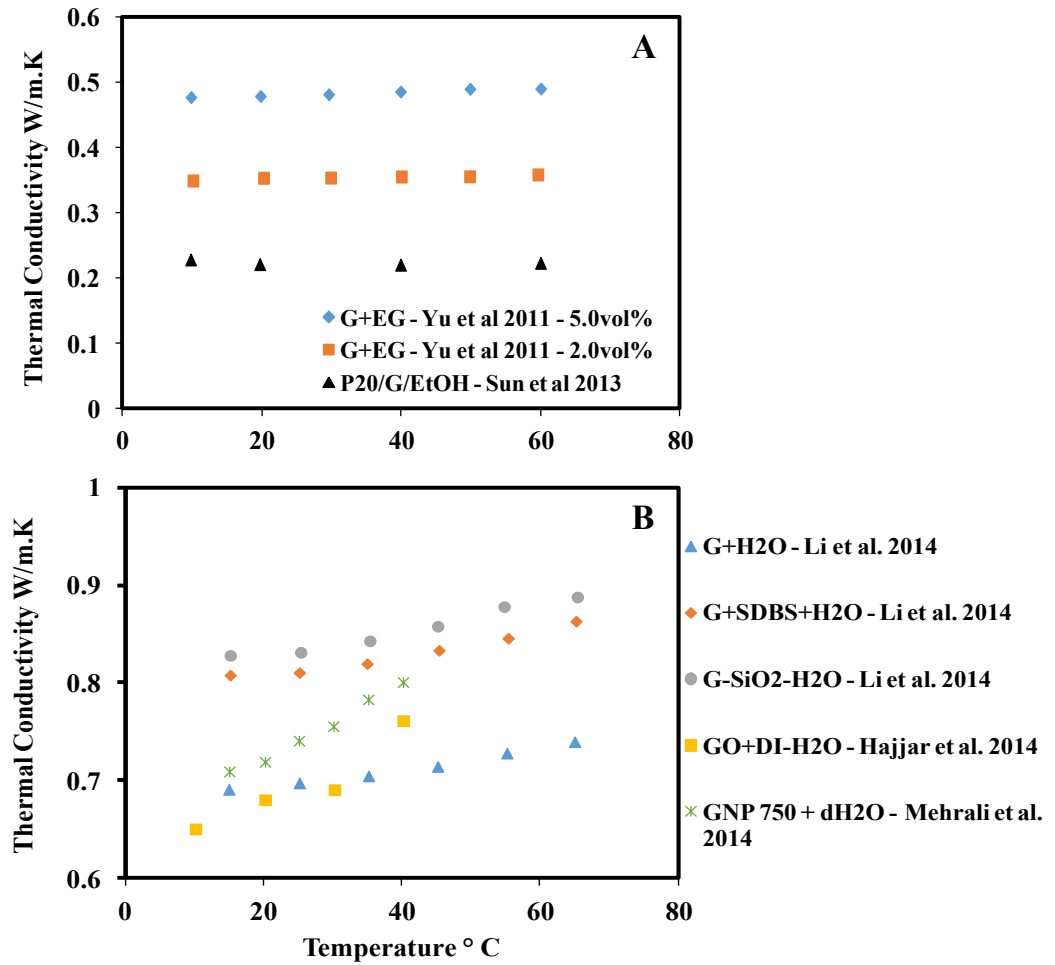
Figure 2.9. A - Temperature independent thermal conductivity of graphene nanofluids. B - Temperature dependent thermal conductivity of graphene and graphene oxide nanofluids

Moreover the aspect ratio of both CNT and graphene make them ideal to form percolation network and thus act as a medium of thermal conduction. It is accepted that due to increase in temperature, the conduction between the graphene flakes would increase leading to *k* enhancement. However, Gupta et al (Gupta et al., 2011) hypothesized that the percolation formation may be less in case of graphene with smaller dimensions and hence chances of ill-connected percolation networks is possible. Since over whelming number of

studies find temperature dependent thermal conductivity enhancement for both graphene and GO nanofluids, future studies will try to validate the minority view and establish the fact. On the other hand future studies should try to investigate the effect of temperature on exfoliation of multilayer graphene suspensions when subjected to shear forces. It is because the exfoliation is a strong function of temperature and shear forces (Kim et al., 2015). As a result the suspension would have more single layer graphene which would lead to better thermal conductivity enhancement.

2.4.1.3. **Surface effects**

In several instances surfactants have been used and functionalization has been done to obtain stable suspensions (Zawrah et al., 2015). Since graphene is hydrophobic in nature, it does not fully disperse in polar solvents. In addition, graphene does not disperse in pure base oils hence require dispersants and surfactants. Nonetheless, GO is more hydrophilic and disperses well in polar solvents. Generally well-dispersed aqueous suspensions are formed when exfoliated graphite oxide is dispersed (Kotov et al., 1996, Cassagneau et al., 2000). Li et al (Chen et al., 2008) suggest that due to the ionization of the phenolic hydroxyl groups and carboxylic acid that exist on the GO sheets, large negative charges seem to appear on GO when suspended in water. As a result they attribute electrostatic repulsion to be the reason for the formation of stable GO suspensions and not the hydrophilicity of GO as understood earlier. It is vital to investigate the effect of surfactants on the k of nanofluids since various studies have shown diverse effects of surfactants (Murshed et al.,

2012, Rashmi et al., 2010, Sadri et al., 2014). Figure 4 shows the stability of water based nanofluids using various surfactants. SDBS functionalized graphene (SDBS-G) was found to enhance the stability significantly however, the k is greatly compromised. A maximum of 3.5 mg ml^{-1} GO could be stable in water based nanofluids due to the presence of oxygen functionality on flake's surface. Although graphene is found to enhance k of various base fluids (Figure 8), it is found (Martin-Gallego et al., 2011) that by adding functionalized graphene to resin, k is not improved. It is noteworthy that the functionalization of graphene may not be an ideal method for obtaining k enhancement in resins. However, the k of graphene-water based suspension has better enhancements. Similarly, Park and Kim (Park and Kim, 2014) observed significant difference in k of graphene and GO after functionalization. The rate at which k of GO nanofluids increases is found to be higher than the graphene based nanofluids. Notably the rate of increase in k for GO nanofluid at 0.01 volume % was 6.24% which is 14% more than that the graphene based nanofluids. In-situ reduction of alkaline graphite oxide method was able to obtain stable suspensions without affecting the thermal properties (Chen et al., 2008, Jyothirmayee Aravind and Ramaprabhu, 2011, Ghozatloo et al., 2013). It is (Ghozatloo et al., 2013) observed that the k is dependent of functional groups which in their case was potassium carboxylate (-COOK) using potassium persulfate (1).

$$\text{(2.2)}$$

Another trend is to synthesis graphene-metal oxide composites which also enhance the thermal conductivity of base fluids significantly (Baby and Ramaprabhu, 2011a, Baby and Ramaprabhu, 2011b, Li et al., 2014, Pasricha et al., 2009). Figure 2.10 shows the decoration of graphene using CuO, silver and SiO_2 nanoparticles. SiO_2 not only increases the hydrophilicity of graphene but also enhances the thermal conductivity (Li et al., 2014). However, the suspension is found to be not very stable after 5 days.
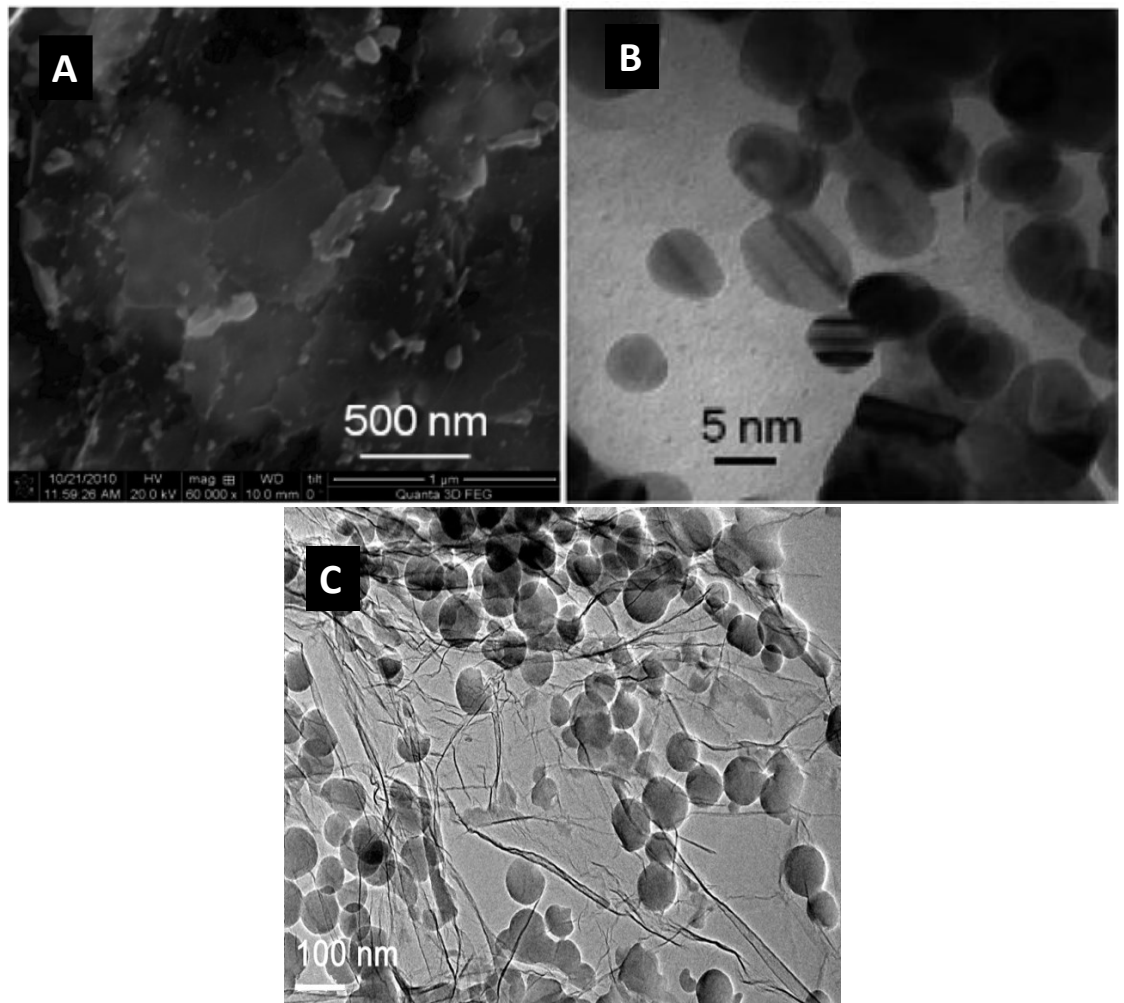
Figure 2.10. (A) FESEM image of CuO decorated graphene (Baby and Ramaprabhu, 2011b) (B) TEM image of Ag decorated graphene (Baby and Ramaprabhu, 2011a) (C) TEM image graphene/SiO_2 (Li et al., 2014)

Similarly, Ag decorated graphene (Ag/HEG) shows considerable enhancement of thermal conductivity which depend on the particle volume fraction and temperature (Baby and Ramaprabhu, 2011a). A simple chemical reduction was done to obtain Ag decoration on graphene;

$$AgNO_3 + NaBH_4 \rightarrow Ag + 1/2\, H_2 + 1/2\, B_2H_6 + NaNO_3 \qquad (2.3)$$

38
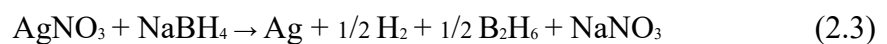
However, before the Ag decoration, functionalization of HEG was done to obtain stable suspension. Likewise, CuO decorated graphene also exhibits enhanced thermal conductivity when suspended in distilled water and ethylene glycol (Baby and Ramaprabhu, 2011b). In all cases, the stability data indicates that the functionalization is necessary before decorating graphene with metal or oxides. Further experimental work using various surfactants, functionalization methods, and hybrid graphene nanofluids could be useful for comprehensive understanding.

2.4.1.4. Effect of graphene size on thermal conductivity

It is well known that the k of nanoparticle suspensions depend on the size (Li and Peterson, 2007) and shape (Nasiri et al., 2012) of the nanoparticles. Although smaller sized particles are expected to be more efficient, clusters formed due to aggregation of particles in a uniform distribution has also been found to enhancement of k of nanofluids (Prasher et al., 2006). Prasher et al (Prasher et al., 2006) pointed out that the radius of gyration and chemical dimension of the aggregates are crucial for the enhancements. Furthermore, some results have shown better enhancements in the presence of larger particles (Wang et al., 1999). In case of CNT nanofluids, the structure of the particle found to influence the thermal conductivity of base fluid (Nasiri et al., 2012), where the single walled nanotube (SWNT) gives the best enhancement as compared to other structures. Similarly Jiang et al (Jiang et al., 2009) observed that when the aspect ratio of CNT is large, the thermal conductivity of the nanofluids is enhanced. One of the first experimental studies on

graphene's *k* revealed that it is size dependent (Balandin et al., 2008). The Klemens theory (Klemens, 2000) predicted that the thermal conductivity in graphene has logarithmic divergence with the layer or grain size and is given by,

$$K = (2\pi\gamma^2)^{-1}\rho_m(v^4/f_mT) \ln(f_m/f_B) \tag{2.4}$$

$$f_B = (Mv^3f_m/4\pi\gamma^2k_BTL)^{1/2} \tag{2.5}$$

where f_m is the upper limit of the phonon frequencies defined by the phonon dispersion, M is the mass of an atom, is the size-dependent low-bound cut-off frequency for acoustic phonons, introduced by limiting the phonon mean-free path with the graphene layer size L. Graphene has large surface area making it one of the best nanomaterials for enhanced heat transfer applications. When graphene nanofluids with three different surface areas were tested for its thermal conductivity, the results show that the thermal conductivity is a strong function of thickness (Mehrali et al., 2014). Similarly, Gupta et al (Gupta et al., 2011) pointed out that there is a high possibility of graphene's size impact on *k* when they used flakes sizes ranging between 5 – 1500 nm as compared to 1 – 3 μm size flakes used by Yu et al (Yu et al., 2010a). Recently Park et al (Park and Kim, 2014) concluded that the graphene oxide with small average particle diameter will offer better properties in contrast to other graphene nanofluids. Synthesis of uniform sized graphene sheets is still challenging area. Any future developments in this aspect could help us understand the effect of size in a much better manner.

Table 2.5. Existing thermal conductivity data of graphene nanofluids (NA - Not available)

Author	Material	Base Fluid	Synthesis method	Nano-particle Size	Concentration	*k* Enhancement
Yu et al (Yu et al., 2010a)	Graphene Oxide	EG	Two step method	NA	0.01–0.05 vol%	61.0% at 5 vol%
Baby and Ramaprabhua (Baby and Ramaprabhu, 2010b)	graphene	H_2O, EG	Two step method	NA	0.005 to 0.056vol%	for 0.056vol% in H_2O, 14% at 25 °C, 64% at 50 °C
Yu et al. (Yu et al., 2010b)	Graphene Oxide	DW,PG,LP	Two step method	NA	0.01–0.05 vol%	30.2%, 62.3%, and 76.8% for DW, PG, and LP at 5vol%
Gupta et al. (Gupta et al., 2011)	Graphene	DI H_2O	NA	NA	0.05–0.2vol%	27% at 0.2vol%
Yu et al. (Yu et al., 2011)	Graphene and Graphene Oxide	EG	Two step method	Range = 0.2–2 μm Thickness = 0.7–1.3 nm	0.01–0.05vol%	At 5 vol%, 86% for Graphene and 61 % for GO

Park and Kim (Park and Kim, 2014)	Graphene M-5, M-15 and Oxidized Graphene (M-5)	DW	Two step method	NA	0.001–0.01 vol%	At 0.01vol%, 5.47% in M-5, 4.45% in M-15 and 6.24% for Oxidized Graphene M-5
Ma et al. (Ma et al., 2013)	FG	Silicone Oil	Two step method	size = 70 μm thickness = 1.1 nm to 2.3 nm	0.01, 0.03, 0.05 and 0.07 wt%	For 0.01wt%, 1.55% at 20 ∘C and 8.48% at 60 ∘C. For 0.07wt%, 18.9% at 60 ∘C.
Kole and Dey (Kole and Dey, 2013)	f-G	DW, EG	Two Step method	NA	0.041-0.395vol%	15% at 0.395 vol.%
Sun et al. (Sun et al., 2013)	Graphene - polymer poly (P20)	Polymer solution	One Step method	lateral sizes of 500–1.5 μm, 0.24 nm thick	0.055 vol.%	~25%
Taha-Tijerina et al. (Taha-Tijerina et al., 2013)		Mineral oil(Nytro10XN), EcoDraw HVE(1:6), Montgomery DB4265C-EX, Metkut H1-EC, Metkool10131TA-S	One Step method	500 x 500nm, 10 atomiclayers	0.01 wt %	23%, 10%, 4%, 15% at 50∘C

Li et al. (Li et al., 2014)	graphene/SiO2	H_2O	One Step method	40 nm	0.1wt%	0.88W/mK at 70 °C
Fan et al. (Fan et al., 2014)	Graphene aerogels GAs	NA	NA	NA	0.67% to 2.5% vol fraction	0.12–0.36 W/(m K).
Hajjar et al. (Hajjar et al., 2014)	GO	H_2O	Two Step method	NA	0.25 wt.%	47.54% enhancement
Kim et al. (Kim et al., 2014a)	GO	NA	NA	NA	0.0005 wt.%	NA
Zhang et al. (Zhang et al., 2014)	Graphene	NA	Two Step method	NA	0.075 mg/ml	NA
Park and Kim (Park and Kim, 2014)	G (M5), G (M5), GO	d-H_2O	One Step method	5x6 μm, 15x6 μm,	0.001–0.01 vol%	5.47%, 4.45%, 6.24%
Mehrali et al. (Mehrali et al., 2014)	Graphene platelets	d-H_2O	One Step method	2 μm dia, 300, 500, and 750 m2/g	0.1 wt.%	27.64%

Ghozatloo et al. (Ghozatloo et al., 2013)	f-Graphene	DI-H_2O	Two Step method	-	0.05 wt.%	14.10%
Moghaddam et al. (Moghaddam et al., 2013)	Graphene	Glycerol	One Step method	15–50 nm thick	2%	NA
Wang et al. (Wang et al., 2012)	Graphene	Ionic Liquid [HMIM]BF4	Two Step method	NA	0.06% wt	15.5% and 18.6% at 25 °C and 65 °C respectively
Ijam et al. (Ijam et al., 2014)	GO	glycerol–water	Two Step method	NA	0.1 wt%	11.7 % at 45 °C
Aravind and Ramaprabhu (Jyothirmayee Aravind and Ramaprabhu, 2011)	Graphene wrapped MWCNT	DI-H_2O EG	One Step Method	NA	0.009-0.14 vol% 0.008-0.14 vol%	94.3 % at 50 °C 36.1 % at 50 °C
Baby and Ramaprabhua (Baby and Ramaprabhu, 2011a)	HEG coated with Ag	DI-H_2O EG	One Step Method	NA	0.005–0.05 vol% 0.01–0.07 vol%	86% at 70°C 14% at 70°C
Zubir et al. (Mohd Zubir et al., 2015)	RGO-CNT	DI-H_2O	One Step Method	NA	3:1; 0.05wt%	25% at 40°C

44

2.4.2. **Theoretical thermal conductivity**

Several mechanisms such as micro convection (Patel et al., 2005), liquid layering theory (Xue et al., 2004), Brownian motion (Jang and Choi, 2004), percolation theory (Dhar et al., 2013b), and ballistic heat transport (Keblinski et al., 2002) have been proposed to explain the enhanced k effect of various nanofluids. A summary of several thermal conductivity models for nanoparticle suspensions are listed in Table 2.6. Particle volume fraction (Walvekar et al., 2012), size (Anoop et al., 2009, Li and Peterson, 2007, Beck et al., 2009), shape (Jeong et al., 2013) and temperature (Das et al., 2003b) are well-known to affect the enhancements of k in most nanolubricants and nanofluids. The enhancement in k due to increase in temperature and concentration has been explained using Brownian motion (Jang and Choi, 2004) and micro convection model (Patel et al., 2005). However, some reports have dismissed the micro-mixing effects due to Brownian motion which leads to micro convection (Wang et al., 1999, Keblinski et al., 2002). Later, Jang and Choi (Jang and Choi, 2004) came up with a four-modes of energy transfer model by considering kinetics, Kapitza resistance, and convection. Although the model considers the effects of particle size, temperature and concentration, the Brownian effect was ignored. Models based on Brownian motion and micro-convection explained the enhancement with respect to concentration and temperature but could not account for other parameters such as size, shape, etc. When the distance between nanoparticles is very small, ballistic heat transport takes place due phonons initiated in one particle persisting through base fluid and getting transported to other particles (Xue, 2003). Likewise liquid layering theory explain that the nanoparticles act as insulators

when their characteristic length is much bigger than the particle size due to interfacial resistance which decreases the effective *k* rather than increasing it (Xue et al., 2004). Models based on both ballistic heat transport and liquid layering theory well predicted the increase in metallic nanoparticles at lower concentrations but unsuccessful to explain the behaviour of CNT. It is mainly because CNT showed no enhancement with increasing temperature. Later the development of percolation model (Sastry et al., 2008) explains the CNT nanofluids enhancement by taking into consideration the temperature independence and chain formation of CNT nanotubes. Nevertheless, a large group of researchers worldwide (Buongiorno et al., 2009) concludes after a benchmarking study that their experimental data are in good agreement with the effective medium theory developed for dispersed particles by Maxwell (Equation 2.6) and generalized by Nan et al (Nan et al., 1997). Thermal conductivity using Maxwell's equation (1.1) relies on the volume fraction, spherical shape of the particle and base fluid thermal conductivity. According to Nan's model (Nan et al., 1997), nanofluids *k* can be calculated as:

$$k_{nf} = k_{bf} \frac{3 + \phi[2\beta_{11}(1-L_{11}) + \beta_{33}(1-L_{33})]}{3 - \phi(2\beta_{11}L_{11} + \beta_{33}L_{33})} k_f \tag{2.6}$$

where L_{11} and ϕ are the geometrical factor and the volume fraction of particles, respectively. B_{11} is defined as,

$$\beta_{11} = \frac{k_p - k_{bf}}{k_{bf} + L_{11}(k_p - k_{bf})} k_f \tag{2.7}$$

where k_p is the *k* of the particles. Since graphene has very high aspect ratio, $L_{11} = 0$ and $L_{33} = 1$. The benchmark study was argued to be limited to the

samples considered and the observations may not be universal. Hence a model by taking into account an elemental analytical domain or cell within the graphene flake was proposed by Dhar et al (2011), Figure 2.11. Although this model is quite similar to the other existing hybrid models, it considers graphene sheet percolation and temperature dependent sheet dynamics to be governing the heat conduction within the domain. Graphene sheet size distribution influences the thermal transport in graphene nanofluids because the synthesized graphene flakes do not have uniform size leading to a poly-dispersed nanofluid.
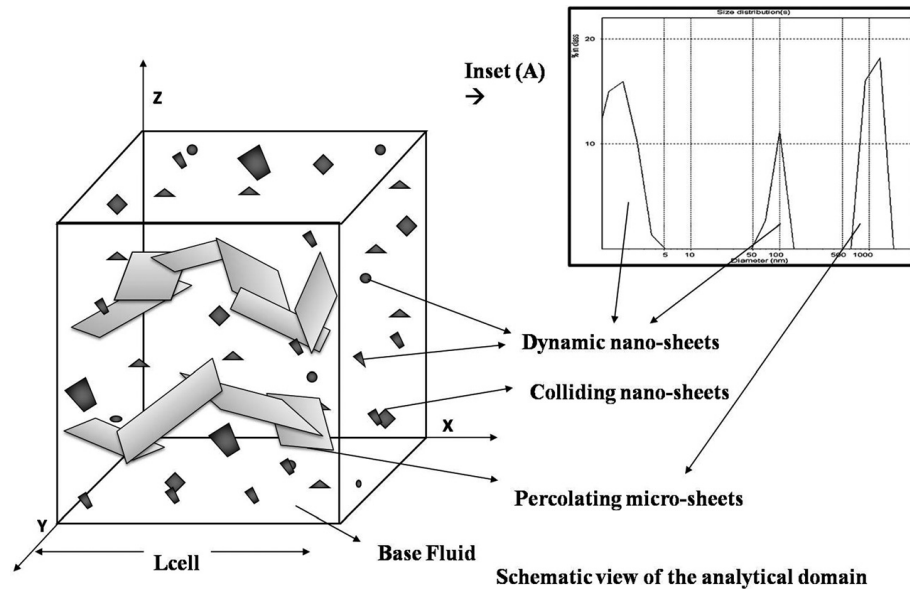
Figure 2.11. The analytical domain of Dhar et al., 2013. Insert A - DLS data (Gupta et al., 2011)

The effective thermal conductivity according to Dhar's model is calculated as,

$$k_{gnf} = k_{sd}^{\alpha} k_{effective}^{(1-\alpha)} \qquad (2.8)$$

where k_{sd} is the sum of thermal conductivities of the medium, k of the fluid solely due to the presence of the nanosheets and dynamic conductivity which is the function of all the factors that accurately describe the dynamic heat transport behaviour of a nano-particle within a fluid domain. The results show that the model accurately predicted the k however, at low concentrations enhancement is very low as the percolating length of graphene flakes is small. However, the assumptions made in this model may not fully reflect the energy transport in real conditions. Furthermore, the effect on k due to defects and morphological changes in the graphene still remains unanswered. Graphene is prone to getting coiled, folded and corrugated at the edges and surface. This might influence the pattern of energy transfer (Wei et al., 2011a) and hence limiting enhance k models to a particular shape may not reflect the real mechanism. Details insights on various existing models could be found in other review works (Kleinstreuer and Feng, 2011, Özerinç et al., 2010).

Table 2.6. Thermal conductivity models for nanoparticle suspensions

Models	Expression	Remarks
(Bruggeman, 1935)	$\frac{1}{4}[(3\phi-1)]\frac{k_p}{k_f}+(2-3\phi)+\frac{1}{4}\sqrt{\Delta}$	$\Delta=[(3\phi-1)^2\left(\frac{k_p}{k_f}\right)^2+(2-3\phi)^2+2(2+9\phi+9\phi^2)k_p/k_f]$
(Sastry et al., 2008)	$k_{eff}=\frac{x}{A}\left(\sum_{i=1}^{N}\dfrac{1}{\dfrac{k_{Fluid}A}{dx_i}+\dfrac{M}{\dfrac{L_i}{\pi k_{CNT}d^2+\dfrac{2}{Gd^2}}}}\right)^{-1}$	Predicts the k_{eff} of CNT suspensions considering the contact resistance in a thermal resistance network. A dimensionless parameter $GL_{CNT}\alpha/k_{Fluid}$ is introduced to represent the role of percolation as a mechanism of thermal transport in CNT-based nanofluids.
(Xue and Xu, 2005)	$\dfrac{1-\phi+2\phi\dfrac{k_p}{k_p-k_b}\ln\dfrac{k_p+k_b}{2k_b}}{1-\phi+2\phi\dfrac{k_b}{k_p-k_b}\ln\dfrac{k_p+k_b}{2k_b}}$	Model for CNTs-based nanofluids. Includes the axial ratio and the space distribution.

49

(Jang and Choi, 2004)	$k_b(1-\phi) + k_p\phi + 3C\dfrac{d_b}{d_p}k_b\,\mathrm{Re}^2_{d_p}\,\mathrm{Pr}\,\phi$	Four modes: • Collisions between fluid molecules • Thermal diffusion of nanoparticles • Collisions between nanoparticles due to Brownian motion • Thermal interaction of dynamic nanoparticles with base fluid molecules
(Xuan et al., 2003)	$k_{eff} = k_f\left\{\dfrac{k_p + 2k_f - 2(k_f - k_p)\phi}{k_p + 2k_f + (k_f - k_p)\phi}\right\} + \dfrac{\rho_p\phi C_p}{2}\sqrt{\dfrac{k_B T}{3\pi r_{cl}\mu}}$	The model takes into account of Brownian motion and clusters of nanoparticles.
(Jeffrey, 1973)	$k_{eff} = k_f\left\{\begin{array}{l} 1 + \dfrac{3\phi(k_p/k_f - 1)}{k_p/k_f + 2} + 3\phi^2\left(\dfrac{k_p/k_f - 1}{k_p/k_f + 2}\right)^2 \\ \left[1 + \dfrac{1}{4}\left(\dfrac{k_p/k_f - 1}{k_p/k_f + 2}\right) + \dfrac{3}{16}\left(\dfrac{k_p/k_f - 1}{k_p/k_f + 2}\right)\left(\dfrac{k_p/k_f + 2}{2k_p/k_f + 3}\right) + ..\right] \end{array}\right\}$	Higher order terms represent pair interactions of randomly dispersed particles; vanishing interfacial thermal resistance
(Davis, 1986)	$k_{eff} = k_f\left\{1 + \dfrac{3\phi(k_p/k_f - 1)\left[\phi + f\phi^2 + O\phi^3\right]}{(k_p/k_f + 2) - (k_p/k_f - 1)\phi}\right\}$	Higher order terms due to pair interactions of randomly dispersed spheres, f= 2.5 & 0.5 for kp/k_f= 10

		and ∞ respectively; vanishing interfacial thermal resistance
(Wasp et al., 1998)	$$k_{eff} = \frac{k_p + 2k_f - 2(k_f - k_p)\phi}{k_p + 2k_f + 2(k_f - k_p)\phi} k_f$$	Special case of Hamilton and Crosser model with $\Psi = 1$
(Yu and Choi, 2003)	$$k_{eff} = \frac{k_{pe} + 2k_f + 2(k_{pe} - k_f)(1-\beta)^3 \phi}{k_{pe} + 2k_f - (k_{pe} - k_f)(1+\beta)^3 \phi}$$	Modified Maxwell model k_{pe} is equivalent thermal conductivity of particles
(Wang et al., 2003)	$$k_{eff} = \frac{(1-\phi) + 3\phi \int_0^\infty k_{cl}(r) n(r)/[k_{cl}(r) + 2k_f] dr}{(1-\phi) + 3\phi \int_0^\infty k_f(r) n(r)/[k_{cl}(r) + 2k_f] dr}$$	A fractal model based on the multi-component Maxwell model by substituting the effective thermal conductivity of nanoparticle clusters, $k_{cl}(r)$, and the radius distribution function, n(r)
(Xue, 2003)	$$0 = 9\left(1 - \frac{\phi}{\lambda}\right)\frac{k_{eff} - k_f}{2k_{eff} + k_f} + \frac{\phi}{\lambda}\left[\frac{\frac{k_{eff} - k_{c,x}}{k_{eff} + B_{2,x}(k_{c,x} - k_{eff})}}{+ 4\frac{k_{eff} - k_{c,y}}{2k_{eff} + (1 - B_{2,x})(k_{c,y} - k_{eff})}}\right]$$ *with* $$\lambda = abc/(a+t)(b+t)(c+t)$$	Model for elliptical nanoparticles with radii in three directions of x, y and z respectively as a, b and c; model based on the average polarization theory taking into account of the effect of an interfacial shell of a thickness t between nanoparticles and base liquid; $k_{c,x}$ – effective dielectric constant and $B2,x$ - depolarization factor along x-symmetrical axis.

(Nan et al., 2003)	$$\frac{k_{cl}}{k_f} = \frac{3 + \phi\left[2\beta_x\left(1 - L_x\right) + \beta_z\left(1 - L_z\right)\right]}{3 - \phi\left[2\beta_x L_x + \beta_z L_z\right]}$$	Proposed model for CNT nanofluids. Account for cluster thermal conductivity. Does not consider the effect of temperature.
(Yu and Choi, 2004)	$$k_{eff} = \left(1 + \frac{n\phi_{eff} A}{1 - \phi_{eff} A}\right) k_f$$	Modified Hamilton-Crosser model
(Kumar et al., 2004)	$$k_{eff} = k_f + c\frac{2k_B T}{\pi\mu d_p^2}\frac{\phi r_f}{\left(1 - \phi\right) r_a}$$	Model taking into account Brownian motion
(Bhatta charya et al., 2004)	$$\frac{k_p}{k_f}\phi + (1 - \phi)$$ $$k_p = \frac{1}{k_B T^2 V}\sum_{j=0}^{n}\langle Q(0)Q(j\Delta t)\rangle\Delta t$$	The model takes into account of Brownian motion
(Koo and Kleinstr euer, 2004)	$$\frac{k_{eff,Maxwell}}{k_f} + 5\times10^4 \beta\phi\rho_p C_p\sqrt{\frac{k_B T}{\rho_p D}}\frac{f(T,\phi)}{k_f}$$	The Model takes into account micro-convection due to the Brownian motion; β – volume fraction of fluid moving with a particle; $f(T,\phi)$ – factorial function depending on fluid properties and inter particle interactions

(Xue and Xu, 2005)	$$0 = \left(1 - \frac{\varphi}{\phi}\right)\frac{k_{eff} - k_f}{2k_{eff} + k_f} + \frac{\varphi}{\phi}.$$ $$\left[\frac{(k_{eff} - k_i)(2k_i + k_f) - \phi(k_f - k_i)(2k_i + k_{eff})}{(2k_{eff} + k_i)(2k_i + k_p) + 2\phi(k_p - k_i)(k_i - k_{eff})}\right]$$	Effect of interfacial shell. No effect of temperature studied
(Xie et al., 2005)	$$k_{eff} = 1 + 3\Theta\phi_T + \frac{2\Theta^2\phi_T^2}{1 - \Theta\phi_T}$$	Considers effect of nanolayer
(Chon et al., 2005)	$$k_{eff} = k_f\left\{1 + 64.7.\phi^{0.7460}\left(\frac{d_f}{d_p}\right)^{0.3690}\left(\frac{k_p}{k_f}\right)^{0.7476} \Pr^{0.9955} \mathrm{Re}^{1.2321}\right\}$$	For Al_2O_3-water nanofluids
(Shukla and Dhir, 2005)	$$k_{eff} = k_f\left\{\frac{k_p + 2k_f + 2\phi(k_p - k_f)}{k_p + 2k_f - \phi(k_p - k_f)}\right\} + C\frac{\phi(T - T_o)}{\mu r_p^4}$$	Modified Hamilton-crosser model using diffusion coefficient.
(Prasher et al., 2005)	$$\left(1 + A\mathrm{Re}^m \Pr^{0.333}\phi\right)\left\{\frac{k_p + 2k_f + 2(k_p - k_f)\phi}{k_p + 2k_f - (k_p - k_f)\phi}\right\}$$	Model takes into account micro-convection induced by Brownian motion; A and m are constant.

(Patel et al., 2005)	$$k_{eff} = \frac{k_p}{k_f}\left(1 + C\frac{V_{Br}d_p}{\alpha_f}\right)\frac{d_f}{d_p}\frac{\phi}{1-\phi}$$	Micro-convection model taking into account surface area of particles and Brownian motion.
(Xu et al., 2006)	$$k_{dynamic} = k_f c\frac{Nu.d_f(2-D_f)D_f\left[\left(\frac{d_{p,max}}{d_{p,min}}\right)^{1-D_f}-1\right]}{(1-D_f)^2\left(\frac{d_{p,max}}{d_{p,min}}\right)^{2-D_f}-1}\frac{1}{d_p}$$ $$D_f = 2 - \frac{\ln\phi}{\ln\left(\frac{d_{p,min}}{d_{p,max}}\right)}$$	Static part is determined from Hamilton-Crosser model (1962). Here, c is an empirical constant.
(Leong et al., 2006)	$$k_{eff} = \frac{(k_p - k_i)\phi_l k_i[2\beta_l^3 - \beta^3 + 1] + (k_p + 2k_i)\beta_l^3[\phi_l\beta^3(k_i - k_f) + k_f]}{\beta_l^3(k_p + 2k_i) - (k_p - k_i)\phi_l[\beta_l^3 + \beta^3 - 1]}$$	The Model takes into account the effect of interfacial layer thickness $$\gamma = \frac{h}{a}$$
(Jwo et al., 2007)	$$k_{eff} = k_f\left\{\frac{k_p + 2k_f + 2(k_p - k_f)\psi\phi}{k_p + 2k_f - (k_p - k_f)\psi\phi}\right\}$$	Explores the effect of rotation of acicular particles on the changes in volume concentration

(Koo et al., 2008)	$$k_{eff} = \frac{X}{A}\left(\sum \frac{1}{\dfrac{k_f A}{dx} + \dfrac{M}{\dfrac{L}{\pi k_p d_p^2} + \dfrac{2}{Gd^2}}}\right)^{-1}$$ $$M = \frac{4\phi X^3}{\pi d_p^2 L N_c}$$	Modified model of Sastry et al. [71]. Included the effect of excluded volume concept given by $V_{ex} \approx \dfrac{\pi}{2} L^2 d_p$ And number of contacts per cylinder $$N_c = \frac{\pi}{2} L^2 d_p \frac{\phi}{\dfrac{\pi}{4} d_p^2 L} = 2\phi\left(\frac{L}{d_p}\right)$$
(Yu-Hua et al., 2008)	$$k_{eff} = k_f \left\{ \frac{k_p + 2k_f - 2\phi(k_f - k_p)}{k_p + 2k_f + \phi(k_f - k_p)} + \frac{\rho_p \phi C_{p,p}}{2k_f}\sqrt{\frac{k_B T}{3\pi r_{cl} \mu}} \right\}$$	Considered the effect of Brownian motion, liquid layering around nanoparticles, and clustering. The effect of temperature on average cluster size and Brownian motion.
(Chen et al., 2009)	$$k_{eff} = k_f \left\{ \frac{k_{cl} + (n-1)k_f - (n-1)\phi_{cl}(k_f - k_{cl})}{k_{cl} + (n-1)k_f + \phi_{cl}(k_f - k_{cl})} \right\}$$	Model is a function of cluster radii, it's a modified Hamilton-Crosser model.

(Mogha dassi et al., 2009)	$$k_{eff} = k_f \left\{ 1 + \gamma \left(\frac{k_i}{k_p} \right)^a \left(\frac{t}{d_p} \right)^b \phi^c \right\}$$	γ, a,b,c are constants and depends upon type of nanofluid.
(Hosseini et al., 2011)	$$k_{eff} = k_f \left\{ 1 + m \left(\frac{1}{d_p} \right)^a (aR)^b (\phi)^c \right\}$$	m, a,b andc are constants for CNT nanorefrigerant systems.

2.5. Critical heat flux (CHF)

Nucleate boiling is considered to be one of the efficient methods of heat transfer because of its ability of transferring large heat flux with not as much of wall superheat compared to a single-phase heat transfer or other boiling regime heat-transfer processes. Consequently, electronic chips and power plants utilize nucleate boiling for effective cooling. However, problems associated with CHF limits the efficiency of nucleate cooling. Several reports have confirmed that a very small amount of nanoparticles can considerably enhance the CHF both in pool boiling and flow boiling conditions (Murshed et al., 2011). In the presence of various kinds of nanoparticles, the surface morphology, surface wettability, and capillarity of the heater surface are affected, a major reason for enhancements (Fan et al., 2015). Graphene is two-dimensional and has a very high stiffness and aspect ratio which makes it an outstanding additive for enhancing thermal properties of nanofluids. The reported enhanced k of graphene based suspensions in the literature is owing to largest surface area of graphene compared with the other types of nanoparticles. Therefore, graphene will have significantly larger contact area with the base fluid, so the contact resistance at the graphene–fluid interface will be reduced significantly [6]. Some of the recent observations and results pertaining to CHF of graphene has been summarized in the Table 2.7.

Table 2.7. CHF data of nanofluids

Author	Material + Basefluid	Nano-particle Size	Concentration	CHF	Remarks
Park et al. (Park et al., 2010)	graphene/ GO + H_2O	powder size = 45μm	0.001 vol %	CHF enhancement 179%	Graphene's own self-assembly characteristic can lead to a geometrically altered critical instability wavelength.
Park et al. (Park et al., 2012)	GO + flooding H_2O	-	0.0001 vol%.	CHF enhanced 40% at 90∘, 200% 0∘	GO nanofluids can be very stable under external reactor vessel cooling (ERVC) coolant chemical environments.
Kim et al. (Kim et al., 2014b)	GO + H_2O	-		-	Thickness of GO deposition on the wire surface is proportional to the increase in the CHF observed.
Park and Bang (Park and Bang, 2014)	GO + d-H_2O and R-123	<45 μm	0.01% vol	CHF enhancement ~150%	The change to the Rayleigh–Taylor wavelength influences the bubble diameter, the portion of the heating element area covered by evaporating vapour and the velocity of the escaped vapour.

Kim et al. (Kim et al., 2014a)	GO	-	0.0005 wt.%	-	The rate of change of the wall temperature in the quasi-transition boiling regime was proportional to the heat flux, even if the higher heat flux was applied following the onset of the increase in the wall temperature.
Ahn et al. (Ahn et al., 2014b)	reduced-GO + H_2O	-	0.001 wt.%, 0.0001 wt.%	4.70% 200%	-
Ahn et al. (Ahn et al., 2014a)	reduced-GO + H_2O	-	0.0001 wt.%	200%	The CHF enhancement was due to the development of RGO coating layers such as the base graphene layer (BGL), self-assembled foam-like graphene structure (SFG), and thickly aggregated graphene layer (TGL).
Park et al., (Park et al., 2015) 2015	GO +	15 μm lateral; 6-8 nm thick	-	54.54%, 67.27% for 9.9°, 0°	Decrease of heat transfer coefficient is attributed to a fouling effect.

Park et al., recently spray-deposited oxidized graphene onto heat-transfer samples to augment safety and reduce cost of the heat-transfer apparatus. They observed at 21.7° and at 12.5° maximum and decreased pool-boiling heat-transfer coefficients, respectively (Park et al., 2015). Though Rohsenow's model is widely used for calculating and comparison of CHF, Park et al derived a formulation by introducing a correction factor to Kandlikar's prediction formula (equation 2.9),

$$q_{CHF}^{"} = C_{cf} h_{fg} \rho_g^{1/4} \left(\frac{1+\cos\beta}{16} \right) \left[\frac{2}{\pi} + \frac{\pi}{4}(1+\cos\beta)\cos\phi \right] \left[\sigma g(\rho_l - \rho_g) \right]^{1/4} \quad (2.9)$$

$$C_{cf} = 1.154 \exp(-0.1\sin\beta) \quad (2.10)$$

where C_{cf}, h_{fg}, ρ_g, ρ_l, are the correction factor, evaporative latent heat (*kJ/kg*), vapor density (kg/m^3), liquid density (kg/m^3) respectively. β, ϕ, σ and g denote contact angle of heat-transfer specimen surface (°), basic contact angle of heat-transfer specimen surface, surface tension (N/m), and acceleration of gravity (m/s^2), respectively. They compared their model with Zuber's correlation which showed consistency with 5% error. Fan et al., attributed the enhancement in boiling heat transfer to morphology, wettability, and roughness, on the quenched surfaces. Though the fundamental reason for improved CHF remains increased surface roughness serving as paths to facilitate solid−liquid contacts (Fan et al., 2015). Surface charges and surfactants have an impact on the contact angle and wettability (Lim et al., 2015). It would be interesting to comprehend the effect of various surface effects on the CHF of graphene based suspensions. Murshed et al (Murshed et al., 2011) in their review on convective and boiling heat transfer also stressed

that the data on flow boiling heat transfer is very limited. They asserted that further studies are required by focusing on physical-chemistry to avoid presumptions such as nanoparticle deposition on heat transfer surfaces and surface wettability.

2.6. Rheological studies

Rheological behaviour of nanolubricants has great significance owing to the relationship between viscosity, shear rates, pumping power and pressure drop. Newtonian or non-Newtonian behaviours are associated with many factors such as nanoparticle size (Kole and Dey, 2013, Masuda et al., 1993, Moghaddam et al., 2013), shape (Ettefaghi et al., 2013), concentration (Murshed et al., 2008a), surfactants, shear rate range and so on. Several papers have described the rheological behaviour of various nanofluids and nanolubricants (Sharma et al., 2016) including graphene (Ahammed et al., 2015, Sadeghinezhad et al., 2015, Sadri et al., 2014, Dhar et al., 2013a) and carbon nanotubes based suspensions (Chen et al., 2008). One of the common observations is the change in viscosity with the increasing nanoparticle concentration and temperature respectively (Masuda et al., 1993, Chen et al., 2008). However, discrepancies exist over the relationship between viscosity and various parameters (Mahbubul et al., 2012). Furthermore, reports have also shown the relationship between k and viscosity of nanofluids (Tsai et al., 2008). Although similar observations like the metallic and metal-oxide nanofluids are expected from the graphene based nanofluids, the sheet shape of graphene could be a distinct factor. In a recent observation, it is found that

15.65% rate of viscosity increase of graphene (15 μm average length) nanofluid at 0.01 vol% at room temperature (Park and Kim, 2014). It was higher than the nanofluids containing lower average flake size indicating that the increase in flake size can increase the rate of viscosity increase.
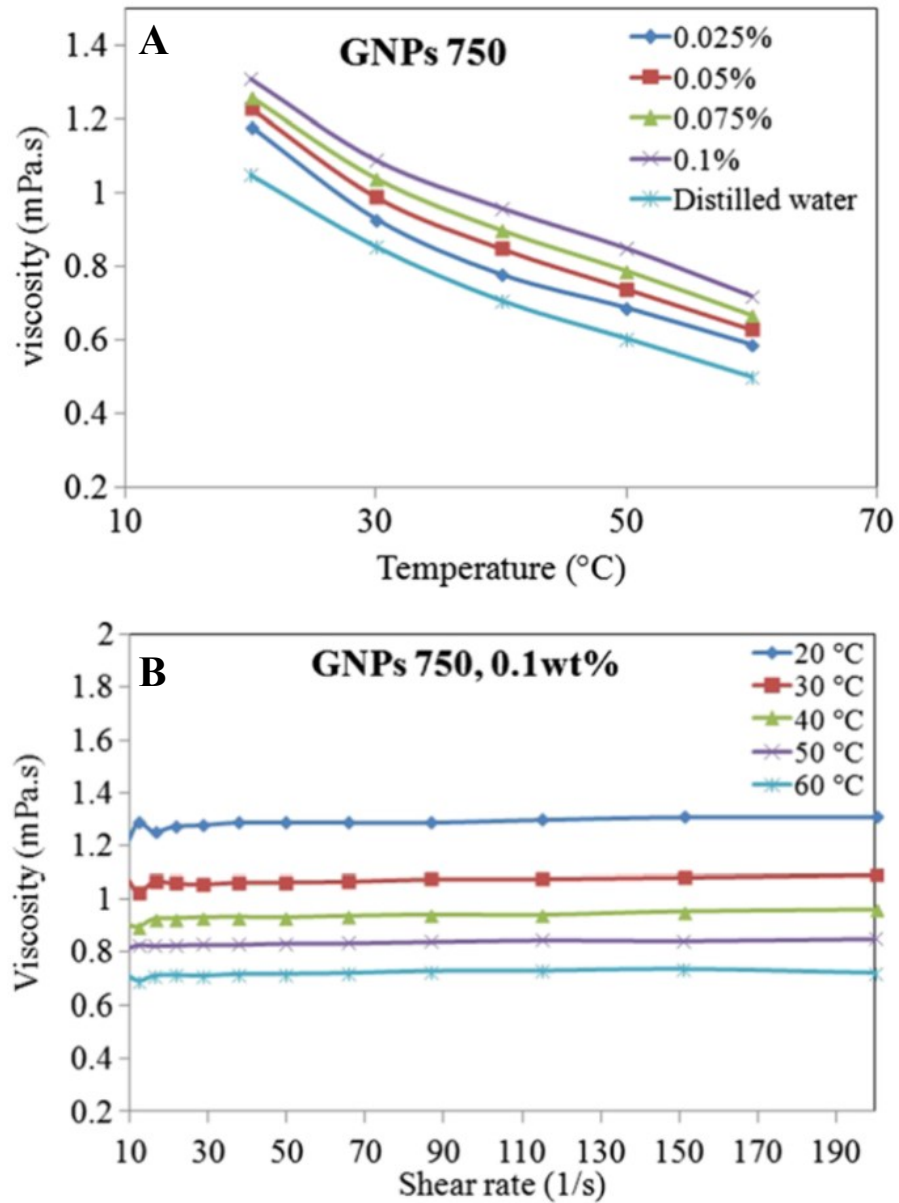
Figure 2.12. A - Viscosity versus temperatures; B - Viscosity versus shear rate; Mehrali et al (Mehrali et al., 2014)

Mehrali et al (Mehrali et al., 2014) found 44% enhancement of viscosity with 0.1 wt.% graphene addition in water based nanofluids as shown in Figure 2.12. Similar to Moghaddam et al, the viscosity was found to decrease with the increase in temperature and shear rate. In contrary to glycerol, water based graphene nanofluids show non-Newtonian pseudo-plastic behaviour. Kole and Dey (Kole and Dey, 2013) observed approximately 100% viscosity enhancement over the base fluid (30% EG+30% H_2O) using graphene flakes. They observed non-Newtonian behaviour of with the increase of both graphene concentration and temperature. Similar to (Mehrali et al., 2014) shear thinning behaviour was found in this case. Furthermore, it was found that the classical models (Table2.9) including Krieger and Dougherty (Krieger and Dougherty, 1959), Brinkman (Brinkman, 1952), Einstein(Einstein, 1956), Kitano et al (Kitano et al., 1981), Batchelor (Batchelor, 1977) and Neilsen (Nielsen, 1970) could not predict the enhancement in the viscosity.

Table 2.8. Viscosity models for nanofluids

Model	Expression	Remark
(Einstein, 1906)	$\mu = \mu_f(1 + 2.5\phi)$	Interaction between liquid and particle with volume concentration less than 1% is used.
(Mooney, 1951)	$\mu = \mu_f e^{2.5\phi(1-\phi/\phi_c)}$	Infinitely dilute suspension of spheres
(Krieger and Dougherty, 1959)	$\mu = \mu_f(1 - \phi/\phi_c)^{-2.5\phi_c}$	Semi-empirical equation
(Nielsen, 1970)	$\mu = \mu_f(1 + 1.5\phi)e^{\phi/(1-\phi_c)}$	Used for low volume concentration
(Batchelor, 1977)	$\mu = \mu_f(1 + 2.5\phi + 6.5\phi^2)$	Used for low volume concentration up to 10%
Brinkman-Roscoe, 1952	$\mu = \mu_f(1 - \phi)^{-2.5}$	Extended Einstein model with a volume concentration up to 4%
(Frankel and Acrivos, 1967)	$\mu = \mu_f \dfrac{9}{8}[(\phi/\phi_m)^{1/3}/[(\phi_m - \phi)^{1/3}/\phi_m^{1/3}]]$	Semi-empirical equation
(Lundgren, 1972)	$\mu = \mu_f[1 + 2.5\phi + 6.25\phi^2 + f(\phi^3)]$	Semi-empirical equation

Graham, 1981

$$\mu = \mu_f \left(1 + 2.5\phi + 4.5 \left[\frac{1}{\left[\left(\frac{h}{d_p} \left(2 + \frac{h}{d_p} \right) \right) \left(1 + \frac{h}{d_p} \right)^2 \right]} \right] \right)$$

Introduces particle radius and inter particle spacing

Kitano et al., 1981

$$\mu = \frac{\mu_f}{\left[1 - \left(\frac{\phi}{\phi_m} \right) \right]^2}$$

Predicts viscosity of two phase suspension

White, 1991

$$\ln \frac{\mu_f}{\mu_0} \approx a + b \left(\frac{T_0}{T} \right) + c \left(\frac{T_0}{T} \right)^2$$

a=-2.10, b=-4.45, c=6.55

Model for pure fluids between viscosity and temperature

Bicerano et al., 1999

$$\mu = (1 + \mu\phi + k_H \phi^2]$$

Viscosity of particles and base fluid is considered

Wang et al., 1999

$$\mu_{nf} = \mu_{bf}(1 + 7.3\phi + 123\phi^2)$$

Volume concentration up to 8% at room temperature

Tseng and Chen, 2003

$$\mu = \mu_f \times 0.4513 e^{0.6965\phi}$$

Volume concentration 5-12%

Avsec and Oblac, 2007

$$\mu_{nf} = \mu_{bf} \left[1 + 2.5 \left(\phi_{eff} + 2.5\phi_{eff} + (2.5\phi_{eff})^2 + ... \right) \right]$$

Considers Ward model and Einstein model

Chen et al., 2007	$\mu_{nf} = \mu_{bf}\left(1 - \dfrac{\phi_a}{\phi_m}\right)^{-2.5\phi_m}$		$\phi_a = \phi\left(\dfrac{a_a}{a}\right)^{3-D}$
Masoumi et al., 2009	$\mu_{nf} = \mu_{bf}\left(1 + \dfrac{\rho_N V_b d_N^2}{72 C \delta \mu_f}\right)$		Considered Brownian motion of Al_2O_3 particles in water
Pak and Cho, 1998	$\mu_{nf} = \mu_{bf}\left(1 + 39.11\phi + 533.9\phi^2\right)$		Volume concentration 0.99 – 10% at 25 °C
Kulkani et al., 2006	$\ln(\mu_{nf}) = -\left(2.8751 + 53.548\phi - 107.12\phi^2\right)$ $+ \dfrac{\left(1078.3 + 15857\phi + 20587\phi^2\right)}{T}$		Temperature (5-50°C) dependent
Nguyen et al. 2007	$\mu_{nf} = \left(2.1275 - 0.0215T + 0.00027T^2\right)$		Temperature dependent model for concentration 1-4%
Namburu et al. 2009	$Log(\mu_{nf}) = Ae^{-BT}$		Temperature (-35to50°C) dependent model for 1-10% of Al_2O_3 particles
Chandrasekhar et al. 2010	$\mu_{nf} = \mu_{bf}\left[1 + b\left(\dfrac{\phi}{1-\phi_m}\right)^n\right]$		Effect of electromagnetic and mechanical-geometrical factors considered

Abu-Nada 2009

$$\mu_{nf} = -0.155 - \frac{19.582}{T} + 0.794\phi + \frac{2094.47}{T^2}$$

$$-0.192\phi^2 - 8.11\frac{\phi}{T} - \frac{27463.863}{T^3} + 0.127\phi^3$$

$$+1.6044\frac{\phi^2}{T} + 2.1754\frac{\phi}{T^2}$$

μ_{nf} is a function of temperature and particle volume fraction. Used Nguyen et al. experimental data to develop the model.

Masud Hosseeini, et a., 2010

$$\mu_{nf} = \mu_f \left[\exp\left(m + \alpha\left(\frac{T}{T_0}\right) + \beta(\phi_h) + \gamma\left(\frac{d}{1-r}\right) \right) \right]$$

Dimensionless group model taking into account volume concentration, particle size, temperature and capping layer effect

Dhar et al., 2013

$$\mu_{nf} = \mu_{percolation} + \mu_{sheetdynamics}$$

$$\mu_{percolation} = \mu_f(1 + L^* d\phi\alpha)$$

$$\mu_{sheetdynamics} = (\rho_G \lambda U_B \theta)\phi(1-\alpha)$$

Izadi et al. 2015 (Izadi et al., 2015)

$$\mu_{eff} = (\beta_0 + \beta_1 Wt\% + \beta_2 T + \beta_{12} Wt\% \times T) \times 10^{-3}$$

Empirical model considering temperature and wt%

However, existing temperature dependent viscosity models were able to predict the measured viscosity with an r^2 value of 0.97728 and 0.98763. On the other hand, the highest enhancement (401.49% with 2% graphene at 20 °C.) in viscosity of glycerol due to graphene addition was reported by Moghaddam et al. (2013). Although glycerol behaves as Newtonian fluids, the addition of graphene makes it to behave like non-Newtonian. Moreover, their results were able to fit with the Vogel–Tammann–Fulcher equation [58],

$$\eta(T) = A \exp\left(\frac{B}{T + T_0}\right) \tag{2.11}$$

where η is the shear viscosity, T is the temperature, and A, B, and To are constants. A is the value of g at the infinite temperature. B corresponds to the energy barrier associated with the so-called 'cage' confinement due to the close packing of liquid molecules, implying any structural rearrangement of liquid molecules would need to overcome the energy barrier. Savithiri et al. used scaling analysis to probe the effect of slip mechanisms in nanofluids. It was observed that all of the slip mechanisms are dominant in cylindrical shaped particles than the spherical or sheet shaped particles. The investigation also found that the Brownian force is more active for smaller sized and cylindrical shaped particles at low concentration and low viscosities. Similarly, Mehrali et al (Mehrali et al., 2014) explained that the cause of non-Newtonian shear thinning behaviour in case of graphene-water based nanofluid could be due to the gradual alignment of fluid molecules along the direction of increasing shear resulting in less resistance and decrease in viscosity. Although these two works briefly relate some mechanisms to viscosity, no other work exists to completely explain the viscosity

enhancement of base fluids due to the addition of graphene. On the other hand, graphene based hybrid nanofluids and nanolubricants remain unexplored. Zubir et al (Mohd Zubir et al., 2015) observed a 4% improvement of viscosity for reduced graphene oxide and CNT based deionized water hybrid nanofluids. The cause for such low improvement in viscosity is unclear. It will be also interesting to probe the effect of graphene on the viscosity of oils. Though low concentration of nanoparticles does not after the Newtonian behaviour of oils, the higher concentration could alter the behaviour. Furthermore, the effects of graphene's aspect ratio, concentration, pH, stability and temperature on the viscosity enhancements remain unexplained and hence require further studies.

2.7.   Tribology of graphene nanolubricants

Engines experience three types of lubrications during operation as shown in the Figure 2.13. The Stribeck curve in this figure provides the overall view of friction variation in the entire range of lubrication, including the hydrodynamic, mixed, and boundary lubrication. Friction and wear are two types of responses from any tribo-system, which are desired to be minimal. Conventional lubricants are required to be superior for modern engineering challenges. Traditional additives have reached threshold point of enhancing base oils. Remarkable tribological properties of nanomaterials have made them attractive in the field of lubricants (Zhmud and Pasalskiy, 2013).
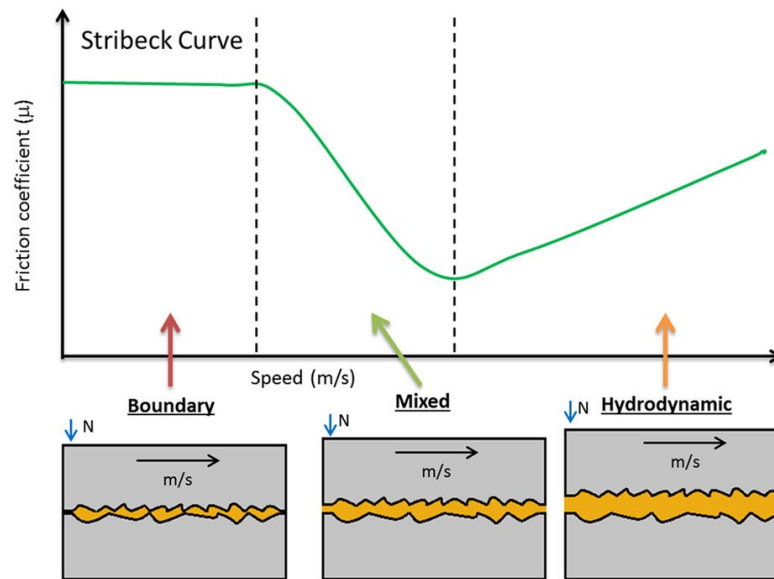
Figure 2.13. A Stribeck curve and illustrations of the 3 lubricant regimes occurring simultaneously in an engine

Graphene has been investigated by many research groups as an additive for lubricants. Significant improvement in anti-wear (Ahammed et al., 2015, Eswaraiah et al., 2011, Senatore et al., 2013, Wei et al., 2011a) and anti-oxidation (Rasheed et al., 2015) of lubricants has been found reported. Several factors such as the concentration of nanoparticles in oil, temperature, sliding speed, applied load, contact form of friction pairs and lubricating oils that influence the tribology of nanolubricants have been studied. Moreover, many techniques and methods have been developed to determine the friction co-efficient, mechanisms and various other aspects of lubrication (Zhang et al., 2012, Martin and Ohmae, 2008). One of the most common observations is the entry of nanoparticles into contact area due to its small size, providing lubrication effect. It has been found that the Cu nanoparticles fill the scars and grooves on the friction surface as per AFM and EDS analysis, when the deposition of nanoparticles occurs between the friction surfaces (Nika et al.,

2012). Another study denotes that the nanoparticles agglomerates on the surface therefore reduces abrasive action and provides protective film (Jang et al., 2010). It has also been stated that the nanoparticles get dragged into contact area and interact with the surface, causing an improvement in the tribological behaviour of the lubricating oil (Chou et al., 2010). Significant attention has been paid to study the effect of various other metallic, metal-oxides and inorganic nanoparticles as lubricating oil additives (Hernández Battez et al., 2008, Ma et al., 2010, Lahouij et al., 2012). Carbon family has also received tremendous attention due its unique structures and properties. Although graphite is well known solid lubricant, graphene is relatively new in the lubrication industry. Similar to other nanoparticles (Nika et al., 2012, Hu et al., 2002), it is believed that graphene due to its thin atomic sized thickness fills the contact area or forms a film on the surface of the sliding metal. It has been observed that the friction coefficient is lower for the graphitized nanodiscs due to its highly organized structure compared to the other nanocarbons such as graphitized carbon blacks and carbon nanofibres (Nomède-Martyr et al., 2012). Zhang et al., (Zhang et al., 2014) studied the tribological properties of graphene and MWCNTs as additives in diamond-like carbon/ionic liquids hybrid films in different lubricating states at high vacuum. The results indicated that MWCNTs and graphene present the different nano-scale tribological mechanisms and produce different lubricating effect on the hybrid films at different lubricating states, Figure 2.14.
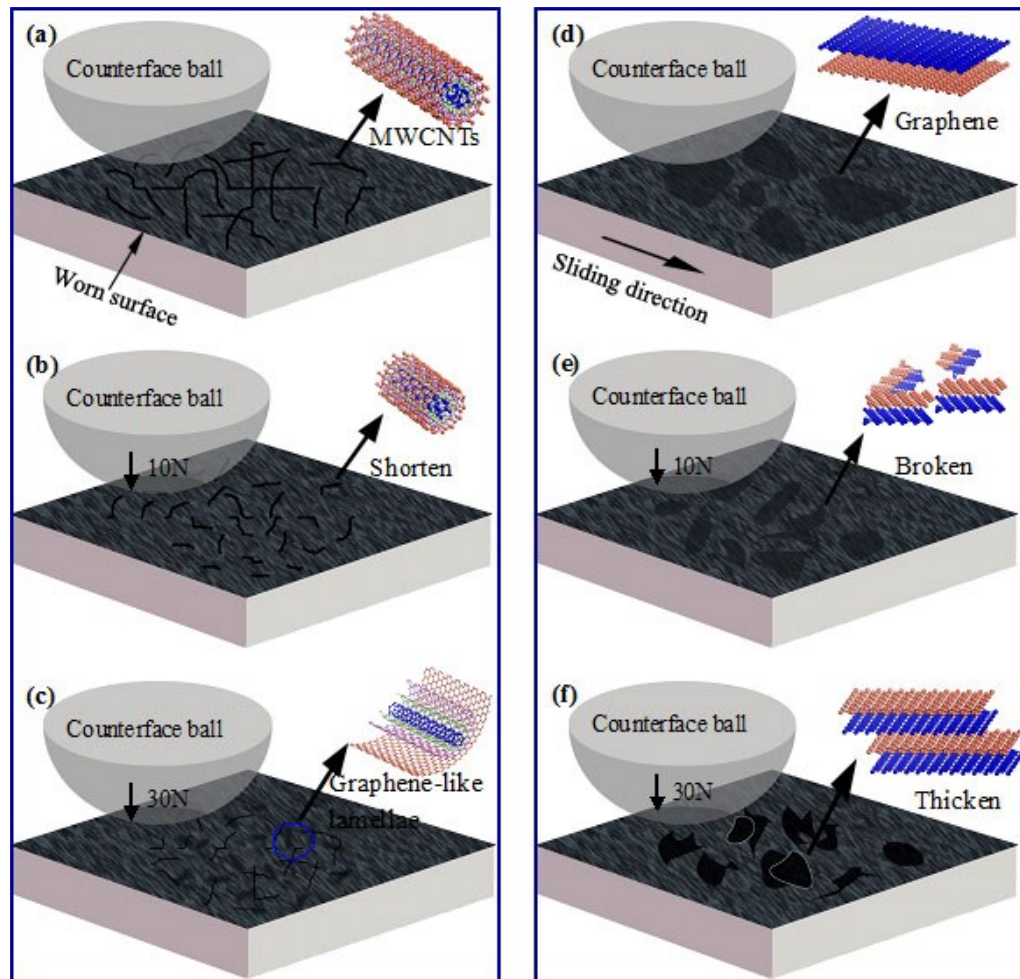
Figure 2.14. Schematic presentation of friction mechanism at different loads. (a), (d) the contact schematic sketch of the ball-on-disk pair; (b), (c), (e), (f) the different changing process of nano-additives after friction testing. Zhang (Zhang et al., 2014)

Wei et al., (Wei et al., 2011b) used liquid phase exfoliated graphene modified by oleic acid as additives (0.02–0.06 wt%) in lubricant oil which showed enhanced performance, with friction coefficient and wear scar diameter reduced by 17% and 14%, respectively. Similarly, Lin et al (Lin et al., 2011) found that the surface modified graphene enhances the wear resistance and load-carrying capacity of the machine. SEM and EDX results show that the enhancement might be due to extremely thin laminated structure, allowing the

graphene to easily enter the contact area. Kinoshita et al (Kinoshita et al., 2014) found that by adding graphene oxide nanoparticles in water based coolant for friction testing, no surface wear was found for over 60000 cycles and the coefficient of friction was reduced to 0.05. Eswaraiah et al (Eswaraiah et al., 2011) found 80, 33, and 40% enhancement of frictional characteristics, anti-wear, and extreme pressure properties respectively for engine oil with 0.025 mg/mL of graphene added to it. They attributed nano-bearing mechanism of graphene as the reason behind the enhancements. Ou et al (Jang et al., 2010) using their micro-tribological studies showed that the reduced graphene oxide possesses good friction reduction and antiwear ability. They attributed the enhancement to graphene's intrinsic structure, and self-lubricating property. Lee et al (Lee et al., 2010) demonstrated that when the thickness of graphene is decreased, the friction monotonically increases. It was similar to other nanomaterials such as niobium diselenide, hexagonal boron nitride and molybdenum sulfide. The results further suggest that the trend arises from the thinner sheets' increased susceptibility to out-of-plane elastic deformation which could be a universal characteristic of nanoscale friction for atomically thin materials weakly bound to substrates. On the other hand, grease containing alternately stacked single graphene sheets and a C60 monolayer showed that the intercalated C60 molecules can rotate in between single graphene sheets by using 13C NMR measurements (Miura and Ishikawa, 2010). Miura et al (Miura and Ishikawa, 2010), claimed that the grease with this novel additive was providing better lubricating performance than all the other existing additives. Although there seems to be unanimous agreement on graphene's role in enhancing the anti-friction and anti-wear

properties of lubricants, the approach to underlying mechanisms are diverse. Graphene flakes size is not uniform and its planar shape does not remain intact after dispersion into lubricants. These particular aspects have been mostly neglected while explaining the mechanisms. Furthermore, when graphene is subjected to shear forces, it undergoes buckling, puckering, rippling, exfoliation and in some cases rupture (Shenoy et al., 2008, Dikin et al., 2007). Hence consolidation of multiple mechanisms can only explain the enhanced tribological phenomenon instead of isolated mechanisms. On the other hand, base oils from paraffinic, naphthenic, aromatic and synthetic blends contain different chemistries, sulphur content and viscosities. Integrating graphene flakes into such base oils and API group I-IV might need different methodologies and therefore requires further detail investigations.

2.8. Studies of nanolubricants in engines

Scientists and engineers had no option in the last few decades but to develop better fuel efficient and compact engines for the automotive industry (Roberts et al., 2014). This eventually lead tribologist to encounter higher speeds, specific loads and temperatures on the major engine components including the valve train, piston-cylinder and bearings. Moreover, the lubricant used should have lower viscosity which certainly decreases oil film thickness between contacting surfaces (Mufti and Priest, 2009). Limited *in situ* studies have been performed by using nanolubricants in engines. Often studies are limited to lab bench tribology equipment which limits the scope of the investigations (Liu et al., 2014, Laad and Jatti, 2016, Wan et al., 2015). Although bench tests are

useful in determining the suitable formulation, they often lack realistic conditions where engine components undergo all modes of lubrication regimes from boundary to hydrodynamic. Graphene nanolubricants have not been investigated in an IC engine. Any data obtained on this subject would be a significant addition to knowledge base.

2.9. Conclusion from literature

Several existing reports indicate that graphene and its allotropes are potential enhancers of thermal conductivity, viscosity, electrical conductivity and tribological properties of polar solvents, oils and grease. The following conclusion could be drawn from the present exhaustive review of the literature;

- Nanoparticles can significantly enhance the thermo-physical and tribological properties of base oils and coolants.

- The stability of nanolubricants is crucial for long lasting enhancement of most properties. As compared to using surfactants, functionalization of graphene seems to be an effective existing method to achieve stable suspensions. pH and zeta-potential can also be very helpful in obtaining stable suspensions. Hence more attention should be paid on optimization of various factors on individual basefluid basis.

- From the existing reviews on models, it can be confirmed that the existing theoretical models and empirical models are tailor made for one type of nanoparticle or nanotube based suspensions. They are

unable to explain all aspects about the enhancements of thermal conductivity and rheology of graphene nanofluids and nanolubricants. Therefore, a model could be proposed in future to explain thermal conductivity and rheology in general.

- Very limited application oriented studies focusing on single phase flow, convective heat transfer, etc., have been done using high viscous nanolubricants. It could be interesting to study these aspects besides tribological studies.

- Graphene allotropes, graphene based hybrid materials and surface modified graphene also show remarkable enhancements. If a simple procedure to identify the suitability of functionalization methods and materials for coating is developed, it could help researchers significantly.

- Further detailed tribological studies using DLS, TEM and AFM are required to comprehend the interaction between graphene flakes and contact surfaces. Although, a common notion in several reports is the sedimentation of nanoparticles in the gaps and grooves of the metal surfaces, the claims should be substantiated using appropriate experimental results and theoretical models. Moreover, vital aspects such as number of layers of graphene, puckering, bending, twisting, exfoliation and so on should be considered simultaneously due to the polydispersed nature of graphene based suspensions.

- Limited applications based studies have been carried out. Application oriented studies to evaluate the performance of nanolubricants could help in the better understanding of the graphene based nanolubricants.

2.10. Summary

In this chapter, an overview of the enhanced thermal conductivity and tribology of graphene based suspensions has been presented. Progress and key challenges associated with synthesis, characterization and properties have also been addressed. Furthermore, existing results on k measurements and tribology investigations have been critically reviewed. The key parameters that affect the *k*, viscosity and tribology have been explained. Gaps in research findings and suggestion for further research have also been delineated.

CHAPTER 3.   METHODOLOGY

3.1.   Introduction

This chapter details the materials and methods adapted in this study. Methodologies pertaining to material characterization, measurement of oil properties and its tests in IC engine is discussed.

3.2.   Materials

Graphene flakes powder (Table 3.1) was purchased from Graphene Labs Inc, USA. Based on availability and cost, 8, 12 and 60 nm graphene was purchased for this study. Paraffinic oil with 150, 500, 2100 SUS viscosity, API 20W50 SN/CF and API 20W50 SJ/CF mineral oils (Table 3.2) were obtained from Lube World, Malaysia. American Petroleum Institute (API) service category SN grade is the current oil standard for gasoline engines approved by the International Lubricants Standardization and Approval Committee (ILSAC). It is expected to offer improved high temperature deposit protection for pistons, rigorous sludge control, and seal compatibility. API SJ grade oils are suitable for 2001 and older automotive engines. Test criteria for oil meeting API SN or API SN/Resource Conserving determined by the American Petroleum Institute (API) in 2010 is in Appendix 3. Natural polymeric ester based lubricity additive was acquired from Apar Industries Limited, India.

Table 3.1. Graphene dimensions as per supplier:

Sample ID	Material	Specific surface area	Lateral dimensions
G60	Graphene (60 nm)	$<15 \ m^2/g$	3000 - 7000 nm
G12	Graphene (12 nm)	$80 \ m^2/g$	1500 - 10000 nm
G8	Graphene (8 nm)	$\sim100 \ m^2/g$	150 - 3000 nm

Table 3.2. List of base fluids used

Sample ID	Oil	Kinematic Viscosity at 40°C, cSt
SN/CF	API SN/CF 20W50	159.700
SJ/CF	API SJ/CF 20W50	176.000
150 SUS	Base mineral oil 150 SUS (Paraffinic oil)	029.247
500 SUS	Base mineral oil 500 SUS (Paraffinic oil)	099.847
2100 SUS	Base mineral oil 2100 SUS (Paraffinic)	457.431
H_2O	H_2O	121.000

3.3. Nanolubricant formulation

The graphene powder was suspended in various base oil at 0.01 – 0.1 wt% concentration. Figure 3.1 shows some of the stock solutions and their diluted forms. In the Figure 3.1 E-G, plain base stock with graphene dispersed with poor stability is shown. To ensure proper blending of the nanoparticles in oil, stirring and sonication was performed for 4 hours using bath-sonicator (JAC Sonicator 1505, 4 kHz). Garg et al., (Garg et al., 2009) suggested that an optimum sonication time does not alter the performance of nanoparticles. They found optimal sonication time for aqueous-CNT nanofluids to be 40 min using a 130 W, 20 kHz sonicator. Ruan and Jacobi (Ruan and Jacobi, 2012) found that the CNT length was not affect significantly by sonication as compared to breaking agglomerates. It was assumed that due to a lower frequency sonication at 4 KHz for 4 hours, the graphene flakes should have lesser agglomerates and also few ruptures only.
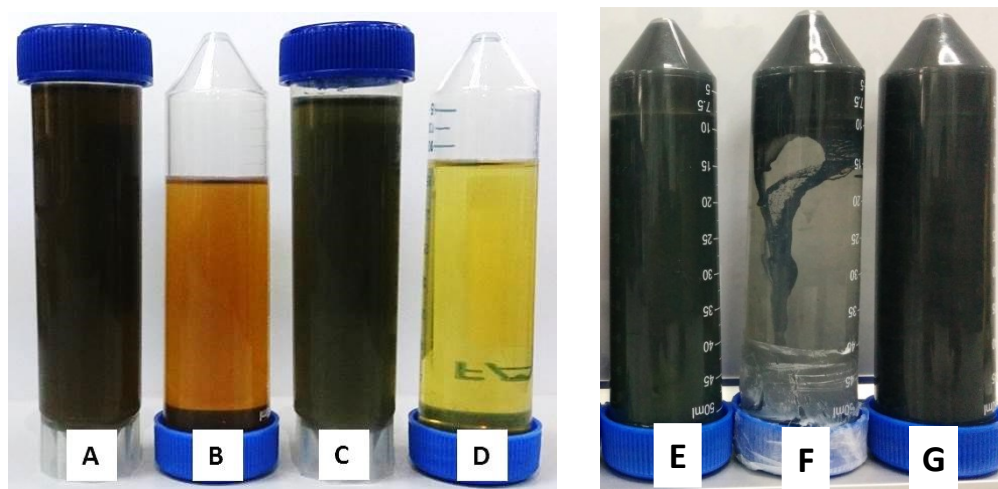
Figure 3.1. 0.01 wt% graphene added to various base oils. A-1:20 dilution of B; B – 20W50 SN/CF+G60 nm; C-1:20 dilution of D; D – 20W50 SJ/CF+G60 nm; E – SUS 150+G60; F – SUS 500+G60; G – SUS 2100+G60;

3.4. Material characterisation

The samples were physically monitored to examine settling of nanoflakes. Field Emission Scanning Electron Microscopy (FESEM) of the graphene nanoflakes were performed by mounting the samples on stubs with conductive carbon tape using FEI Quanta 400F, USA. The machine was operated under high vacuum at 20 kV. Different magnifications were selected to obtain morphological details of the samples. Graphene and other samples were also analysed for their elemental compositions with energy-dispersive X-ray spectroscopy (EDX). XRD data was carried out through PANytical X-ray Diffractometer. Graphene 60 nm sample were scanned from 20 to 80 degrees with a step size of 1 degree/min. Divergence slit size is 0.9570 degrees. X-rays were produced through Copper material, with wavelength (K aphla) of 1.54 angstroms. Filtering of X-ray was done through Ni using an operational

voltage of 45 kV and current 27 mA. The stability of suspensions was measured by finding the zeta potential using Zetasizer Nano (Malvern). It is electric potential existing between the particle surface and the dispersing liquid at the slipping plane. The equipment uses combination of electrophoresis and laser Doppler velocimetry, where the velocity of a particle in a liquid is measured when an electrical field is applied. Since the viscosity and the dielectric constant of the oil is known, Henry equation is applied and followed by obtaining the Zeta potential by solving Smoluchowski equation. Functional groups of graphene powder was identified by mixing it with KBr powder in 1:10 ratio to form a pellet and placing the same for characterization using FTIR, Perkin Elmer. Similarly oil drops were placed between the two KBr pressed pellet in the 1:100 ratio and were characterised by FTIR spectrometer, BRUKER Germany.

3.5. Measurement of nanolubricant properties

3.5.1. Thermal conductivity measurements

Thermal conductivity measurements of the graphene nanolubricants were performed using a portable thermal conductivity measurement device KD2 Pro (Decagon Devices, Inc. USA).
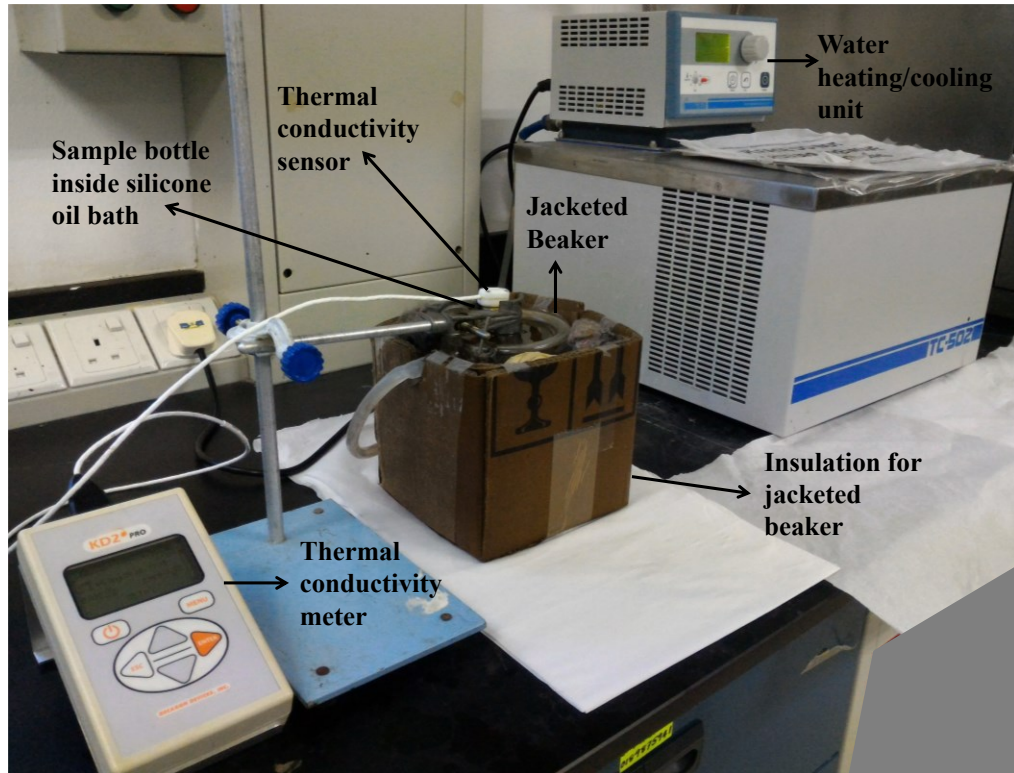
Figure 3.2. Thermal conductivity measurement setup

As shown in the Figure 3.2, the sample in 30 ml glass tube was placed inside silicone oil contained in a jacketed beaker. Water circulates through the jacket to maintain sample temperature. All the measurements were performed inside a fume hood to avoid any inconsistencies due to environmental changes. The transient line source (TLS) in the thermal conductivity meter uses a sensor (single needle with 1.3 mm diameter and 60 mm in length) to measure the thermal conductivity. A measurement similar to thermocouple with relationship between thermal conductivity and temperature change given as,

$$T(t) - T_{ref} = \frac{q}{4\pi k}\left[\ln(t) - \gamma - \ln\left(\frac{a^2}{4\alpha}\right)\right] \qquad (3.1)$$

Where $T(t)$ is the temperature at time t, T_{ref} a reference temperature, q electrical power applied to the transient line, k is the thermal conductivity, γ is

the Euler's constant, a wire radius and α is the thermal diffusivity of the fluid. T- T_{ref} and $\ln(t)$ are linearly related with a slope equal to $q/4\pi k$. Linear regression of ΔT on $\ln(t)$ yields thermal conductivity given by,

$$k = \frac{q}{4\pi k} \qquad (3.2)$$

A measurement cycle consists of 30 s of each equilibration, heating and cooling time. Standard glycerin was used for calibrating the device. The temperature measurements were made at the intervals of 1 s during both heating and cooling. Measurements are then fit with exponential integral functions using a non-linear least squares procedure. A linear drift term corrects for temperature changes of the sample during the measurement, to optimize the accuracy of the readings. Nearly five readings were taken at each temperature to ensure uncertainty in measurement with in ±5%.

3.5.2. Rheology measurements

MCR302 modular compact rheometer, Anton Paar GmbH Austria as shown in Figure 3.3 was used for dynamic viscosity measurements. The machine uses C-PTD200 measuring cell with Peltier system to maintain sample temperature. 1-100 1/s shear rate was used to measure viscosity and shear stress between 25-105 °C. Spindle CC45 DIN was used in the rheometer. The Graphene nanofluid was poured in the sample chamber of the rheometer. Subsequently, the viscous drag of the fluid against the spindle is measured by the deflection of the calibrated spring. The shear rate, shear strain and viscosity data at room temperature was recorded by a data logger. The rheometer is guaranteed to be

accurate to within ±1% of the full scale range of the spindle speed combination in use reproducibility is within ±.2%.
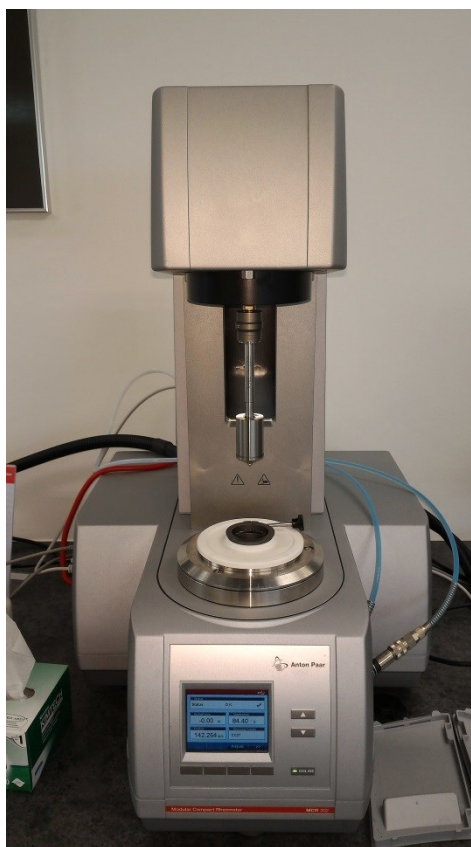
Figure 3.3. MCR302 modular compact rheometer, Anton Paar

3.6. Thermogravimetric analysis

Thermal degradation studies[‡] were performed using Simultaneous Thermal Analyzer (STA) 6000, Perkin Elmer. Oil samples <15 mg were used in the analysis under both oxygen and nitrogen gas with a purge rate of 20 mL/minute. The samples were maintained at 30°C isothermal state and then gradually raised up to 800°C with a heating rate of 5°C/min, 10°C/min, 15°C/min and 20 °C/min according to the desired experiment. Onset

---

[‡] TGA studies have been published in the Journal of Materials Research

temperature or the initial decomposition temperature, which is the measure of thermal stability of that material, was recorded from the TGA graphs obtained. Activation energy (Ea.) which is the minimum amount of energy needed to initiate the oxidation process was obtained after calculations using TGA decomposition kinetics software.

3.7. Tribology experiments

ASTM D 2266 / IP 239 and ASTM D 2783 standard methods are followed for the tribological investigations using 4-ball tribometer (TR 30 L, Ducom), Figure 3.4. The test conditions include temperature 75°C ± 1.7°C, speed 1200 ± 50 rpm, load 40 ± 0.2 kg and test duration of 60 ± 1 min. The steel balls surface was analysed using FESEM (Figure 3.4) and non-contact profiler, Taylor Hobson Inc. USA.
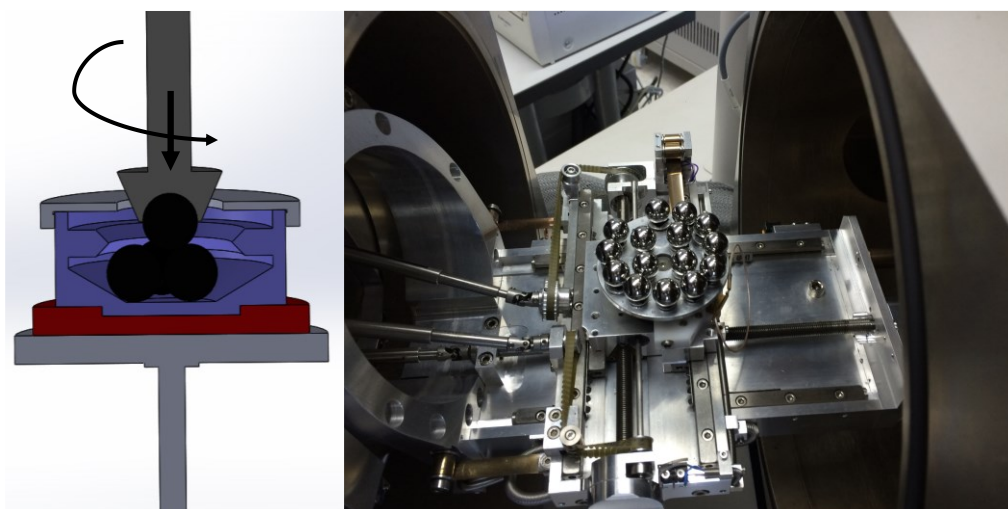
Figure 3.4. Graphical representation of four-ball tribometer test section. Steel ball samples inside FESEM test stage.

3.8. Engine test rig fabrication and operation

An engine test bed has been fabricated with temperature monitoring and data logger system (TMDLS) as shown in Figure 3.5. 4-stroke petrol engine (Hero Motocorp Ltd., India), 97.2 cc, single-cylinder air-cooled having overhead valve (OHV) is integrated with TMDLS. It has a bore of 50 mm and 49.5 mm stroke. The engine consumes approximately 25 litres of petrol during 100 hours of idle operating condition at 1000 rpm. Having four temperature sensors (at test rig, cylinder head adjacent to spark plug, cylinder lining and engine case/crank case) and an engine-on sensor, TMDLS is a protocol system developed (See Appendix 1) to measure the temperature at the surrounding surfaces of the engine. Data collected from the input sensors are processed with Arduino processor board. Logarithmic trend lines are obtained for the temperature profiles by using slope and y-intercept method.
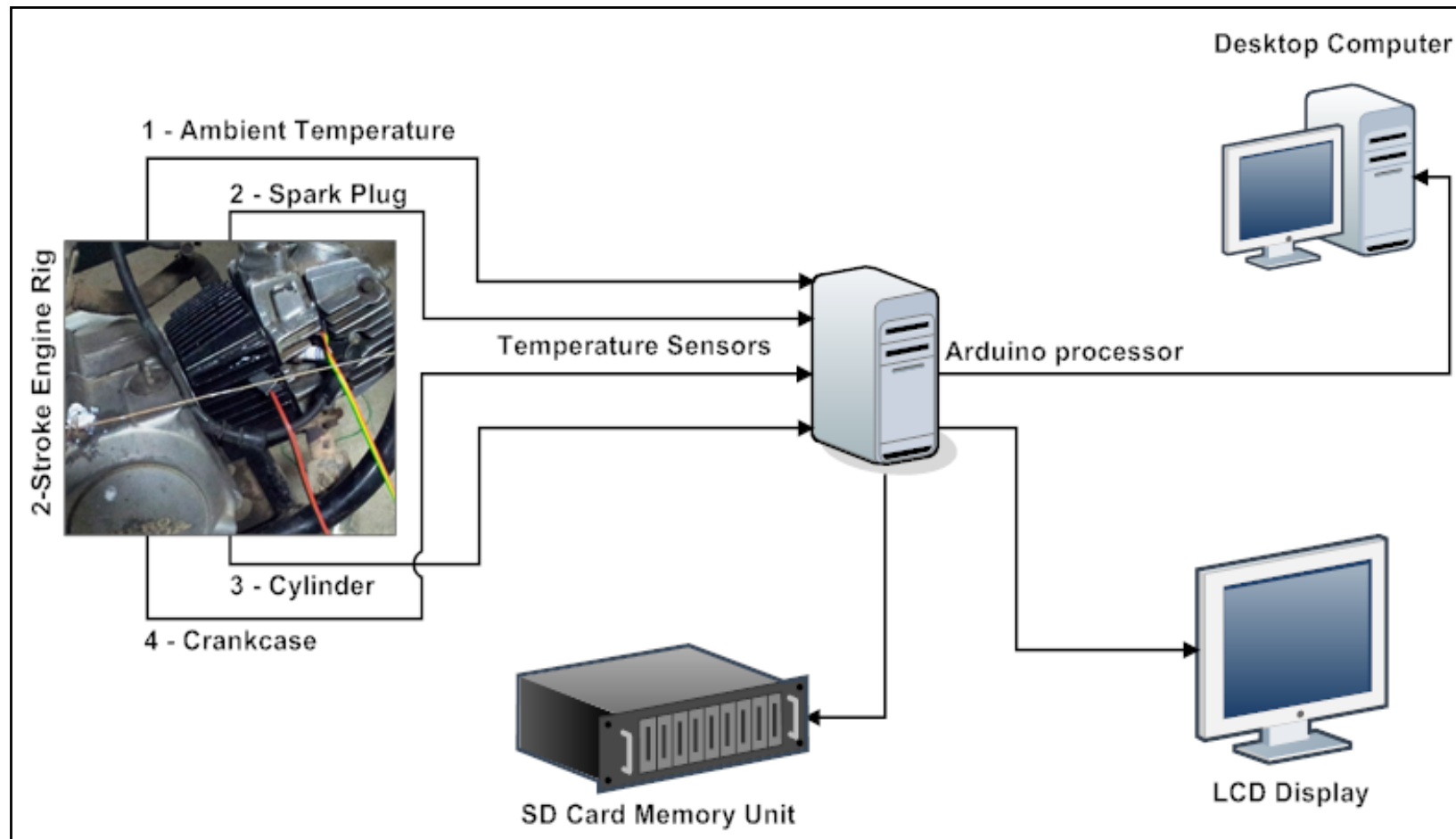
Figure 3.5. 4-stroke petrol engine test rig with TMDLS system;
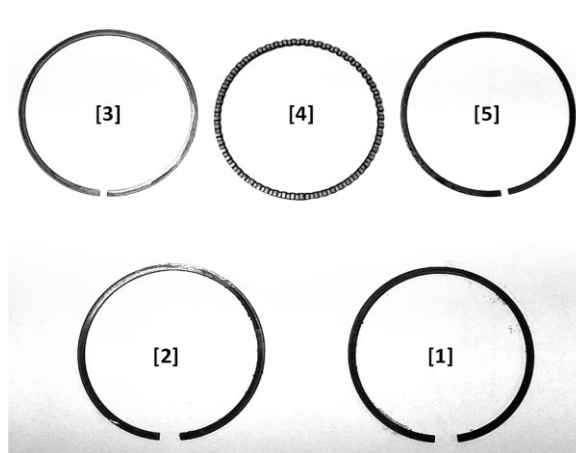
Figure 3.6. Piston rings recovered from engine after after 100 hours operation

The used piston rings (Figure 3.6) comprising, 1 – top compression ring; 2 – lower compression ring; 3 – upper oil ring rail; 4 – oil ring expander; 5 – lower oil ring rail are cut into pieces, and its surfaces are analysed using FESEM and EDX.

3.8.1. Used oil analysis

Elemental analysis of the used oil is performed using various ASTM methods as listed in Table 5.2. FTIR was performed using Bruker instrument by placing the oil drops between two KBr pressed pellet in the 1:100 ratio. Inductively-coupled plasma (ICP) mass spectrometry was performed according to ASTM D5185. As per the standard procedure, thoroughly homogenized used engine oil was diluted ten-fold by weight with mixed xylene solvent. The samples were introduced to the ICP instrument by free aspiration. By comparing elemental intensities measured with the standards, the concentration of elements were determined. Nanoparticle Tracking Analysis (NTA) has been

done using NanoSight NS300, Malvern Inc. USA to analyse the particle size distribution in the engine oil before and after 100 hours of operation. It employs the properties of both light scattering and Brownian motion in order to obtain the size distribution within 2 micron range and concentration measurement of particles in oil formulation.

CHAPTER 4. RESULTS: THERMO-PHYSICAL AND TRIBOLOGICAL PROPERTIES

4.1. Introduction

This chapter explains the characteristic properties of graphene nanoflakes and nanolubricant concisely. Thermal conductivity, rheology and tribological properties of the graphene nanolubricant have been discussed in detail. These results would provide the basis for further analysis of nanolubricant using the IC engine.

4.2. Material characterization[§]

Figure 4.1 shows the SEM images of non-uniform sized graphene flakes in powder form. Thicknesses of flakes are found to be approximately 60, 12 and 8 nm when the edges of the flakes were measured. The appearance of graphene shows that most flakes are planar and few flakes seem bent. Moreover, few flakes are stacked up and appear agglomerated.

[§] The material characterization results have been published in the Journal of Materials Research and also submitted to Tribology International for peer review.
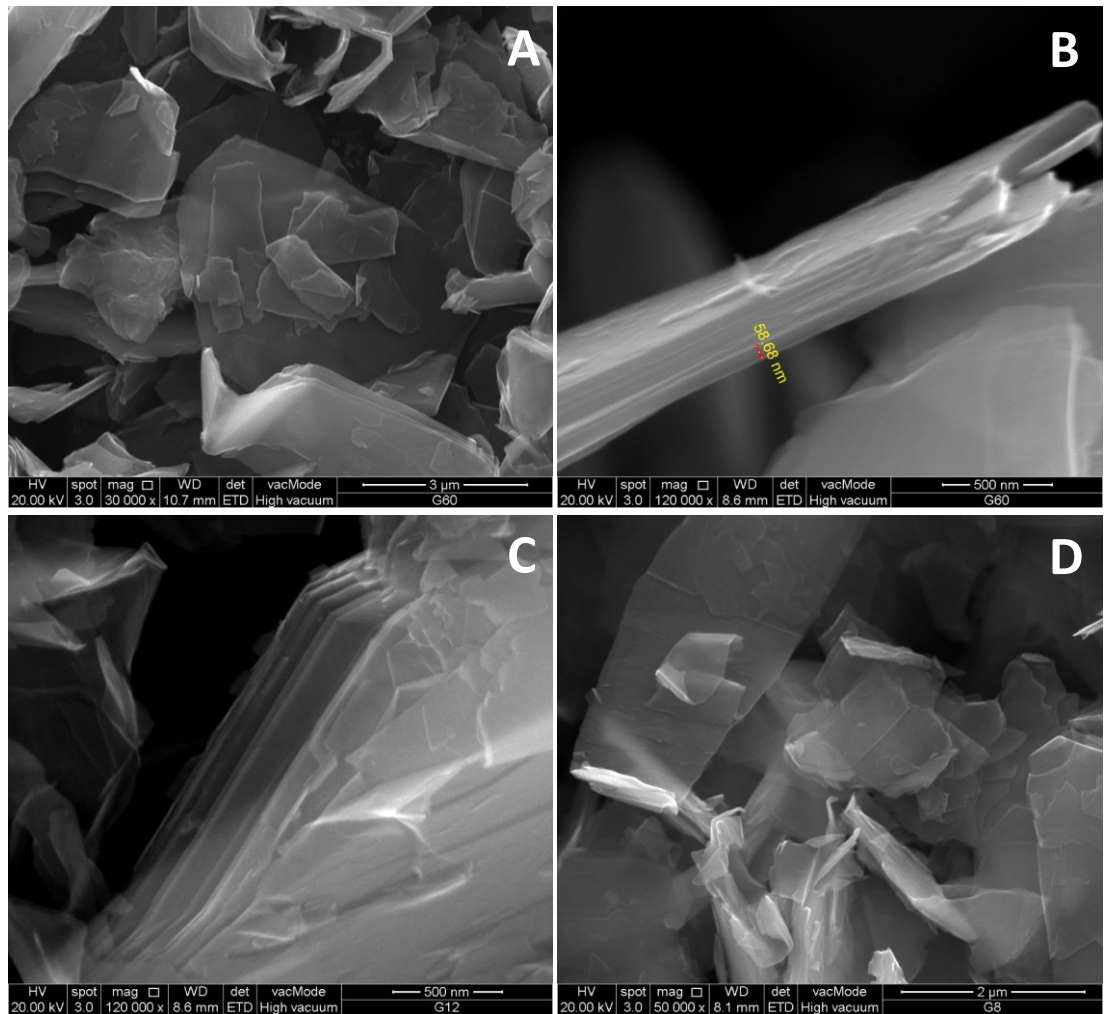
Figure 4.1. Scanning electron microscope graphs of graphene: G-graphene; A-60 nm, B- Three stacked graphene flakes showing multilayers of G60, C - G12, D - G8.

EDX analysis as shown in the Figure 4.2A show that the atomic composition of graphene comprises of more than 95 % carbon. The presence of sodium and sulphur and chlorine would be potentially due to contamination during sample preparation. Single peak in XRD spectrum matches with ICSD (inorganic crystal structure database) pattern # 98-005-2916 as shown in Figure 4.2 B.
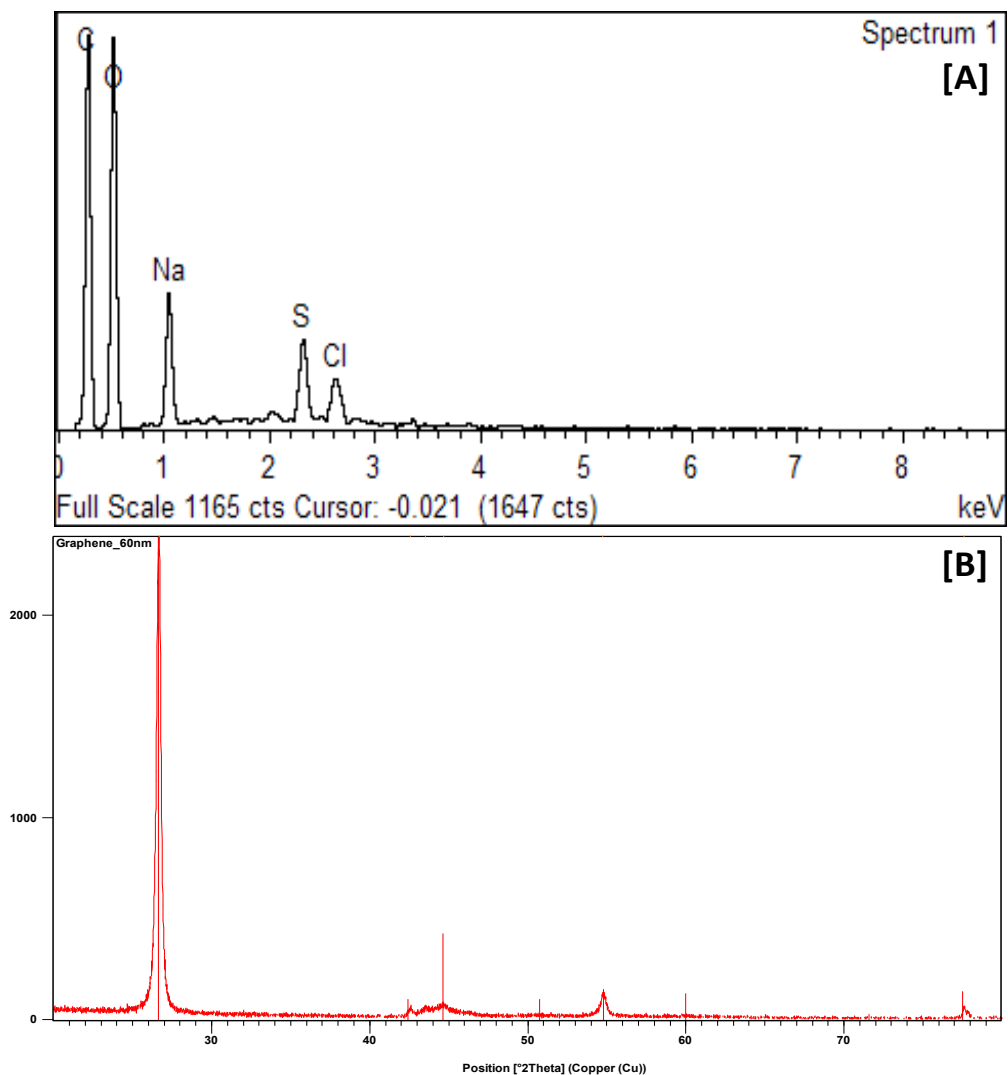
Figure 4.2. A - Energy-dispersive X-ray spectroscopy graph of Graphene flakes; B - X-ray diffraction pattern of graphene flakes;

Figure 4.3 is the Fourier transform infrared spectroscopy (FTIR) graph of graphene (G60) and the functionalized graphene (f-G60). Acid

functionalization of graphene was performed according to Hummers method (Kuila et al., 2012). This method assists in obtaining highly oxygenated graphene containing carboxyl, hydroxyl, ketone, epoxide and diol functional groups that can alter the van der Waals interactions significantly. Prominent peaks from the FTIR are enumerated in Table 4.1. The peaks were determined or verified using the FTIR application library and the literature. The carbonyl, hydroxyl and other functional groups aid the graphene flakes to be hydrophilic. The peaks at 1750 and 1350 cm^{-1} could be due to C=O and C-O stretching vibrations of COOH, carboxylic acid. Peaks corresponding to carbonyl and hydroxyl groups are not prominent in the as-synthesised graphene. However, the small traces of such groups keep G60 from becoming super-hydrophobic. This has the potential to affect the stability of graphene in oil.
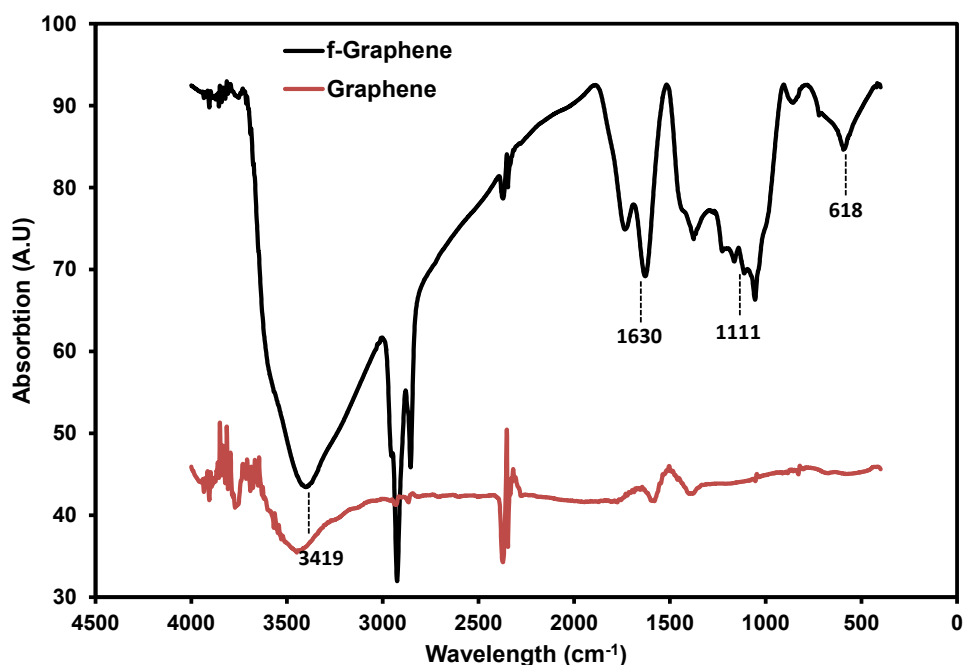
Figure 4.3. Fourier transform infrared spectroscopy graph of graphene and functionalized-graphene flakes.

Table 4.1: Attached Functional Groups of graphene 60 nm

Peaks	Attached Functional Groups - graphene 60 nm		
618.37	C-H bend acetylenic (alkynes)	C-Cl (acid chloride)	C-Cl stretch (alkyl halides)
1111.65	C-O Stretch (alcohol)	C-O-C (dialkyl-ethers)	C-C stretch (ketone)
1630.93	C-C (alkene)	C=O stretch (amides)	-
3419.81	O-H stretch (alcohols)	O-H stretch (carboxylic acids)	-

Zeta potential results show that the as-synthesized graphene in the oil formulation is stable, Table 4.2. It was visually observed that the stability decreases with the increase in graphene concentration from $0.01 - 0.1$ wt% in oil. Therefore, the lowest concentration 0.01 wt% was chosen for various investigations in this research. Furthermore, studies in the past (Rasheed et al., 2016, Sadeghinezhad et al., 2016) have found 0.01 wt% to be stable. API grade samples had inbuilt dispersants and therefore sonication was performed to obtain uniform distribution of graphene in the oil. Similarly for water and pure base oils sonication was helpful in obtaining uniform distribution of graphene. Particle agglomeration, hydrophobicity, fluid polarity, surface charges of the particle and other factors determine the stability of the suspensions. According to DLVO theory, the sum of van der Waals attractive and electrical double layer (EDL) repulsive forces that exist between particles as they approach each other due to the Brownian motion determines the stability. Furthermore, Gupta et al., (Sen Gupta et al., 2011) suggested that the stability can be explained by sedimentation ratio, from Stokes-Einstein theory (1897) [Eq. (4.1)], which is given by,

$$v = \frac{2r_p^2 \left| \rho_p - \rho_m \right| g}{9\varepsilon_m} \tag{4.1}$$

where ρ_m = density of the medium, ε_m = viscosity of the fluid, ρ_p = density of the particle, and r_p = radius of the nanoparticle. Lower the value of sedimentation ratio, higher the stability of the suspension. In case of water based stable suspension, the density of graphene is comparable to the density of water and the sedimentation ratio is close to zero (Sen Gupta et al., 2011)

resulting in the higher stability of the suspension. However, the density of graphene is higher as compared to oil (0.865 g/cm^3). As denoted in Table 4.2, pure base mineral oil has comparatively poor stability also owing to its strong nonpolar nature and also particle agglomeration.

Table 4.2. Zeta potential of oil samples

Basefluid	Graphene concentration, wt%	Stability Improvement Method/Factor	Zeta Potential, mV	Stability Remarks
API 20W50 SN/CF	0.01 - 0.1	In-built Dispersants+ Sonication	1160	Stable below 1 month
API 20W50 SJ/CF	0.01 - 0.1	In-built Dispersants+ Sonication	714	Stable below 1 month
Deionised H_2O	0.01 - 0.1	Acid Functionalization of Graphene + Sonication	-70	Stable for over 2 years
Base Oil 150 SUS	0.01 - 0.1	Sonication	18.4	Stable for 2 hrs
Base Oil 500 SUS	0.01 - 0.1	Sonication	22.1	Stable for 4 hrs

4.3. Thermal conductivity

Figure 4.4 shows that the concentration of graphene as low as 0.01 wt% could enhance the thermal conductivity of engine oil (API 20W50 SN/CF) upto 22.3% at 80 °C. The API 20W50 SJ/CF showed an enhancement of 19.9% which is 5.4% lower enhancement than SN/CF oil formulation. The thermal conductivity was found to be the function of nanoparticle concentration as shown in Figure 4.5. Mineral oils having different viscosities show that the thermal conductivity is a function of concentration. However, the chances of thermal conductivity dropping after a particular concentration (>0.1 wt%) is highly possible owing to particle agglomeration due to increased van der Waals forces of attraction, restricting its Brownian motion (both rotational and translational motions) (Timofeeva et al., 2009).
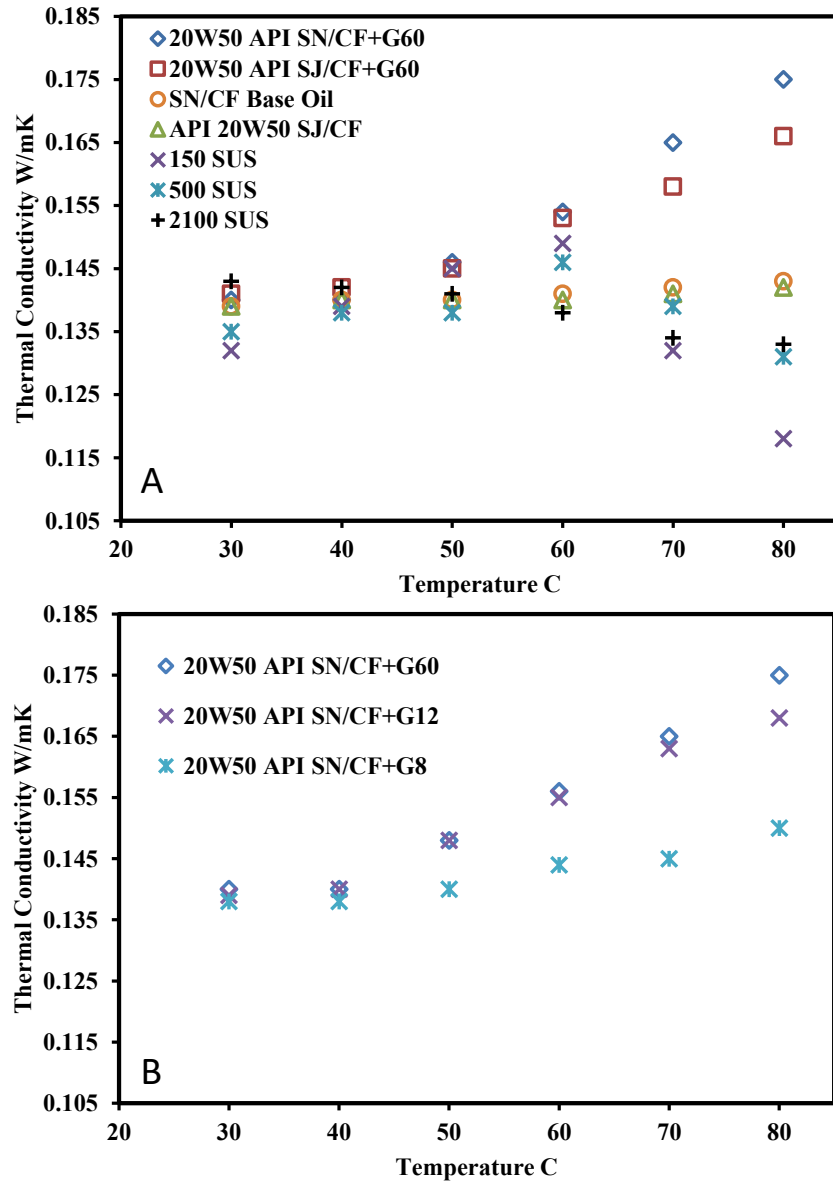
Figure 4.4. A: Thermal conductivity with respect to temperature of base oils with and without 0.01wt% graphene (60 nm); B: Size dependent thermal conductivity of API SN/CF oil.
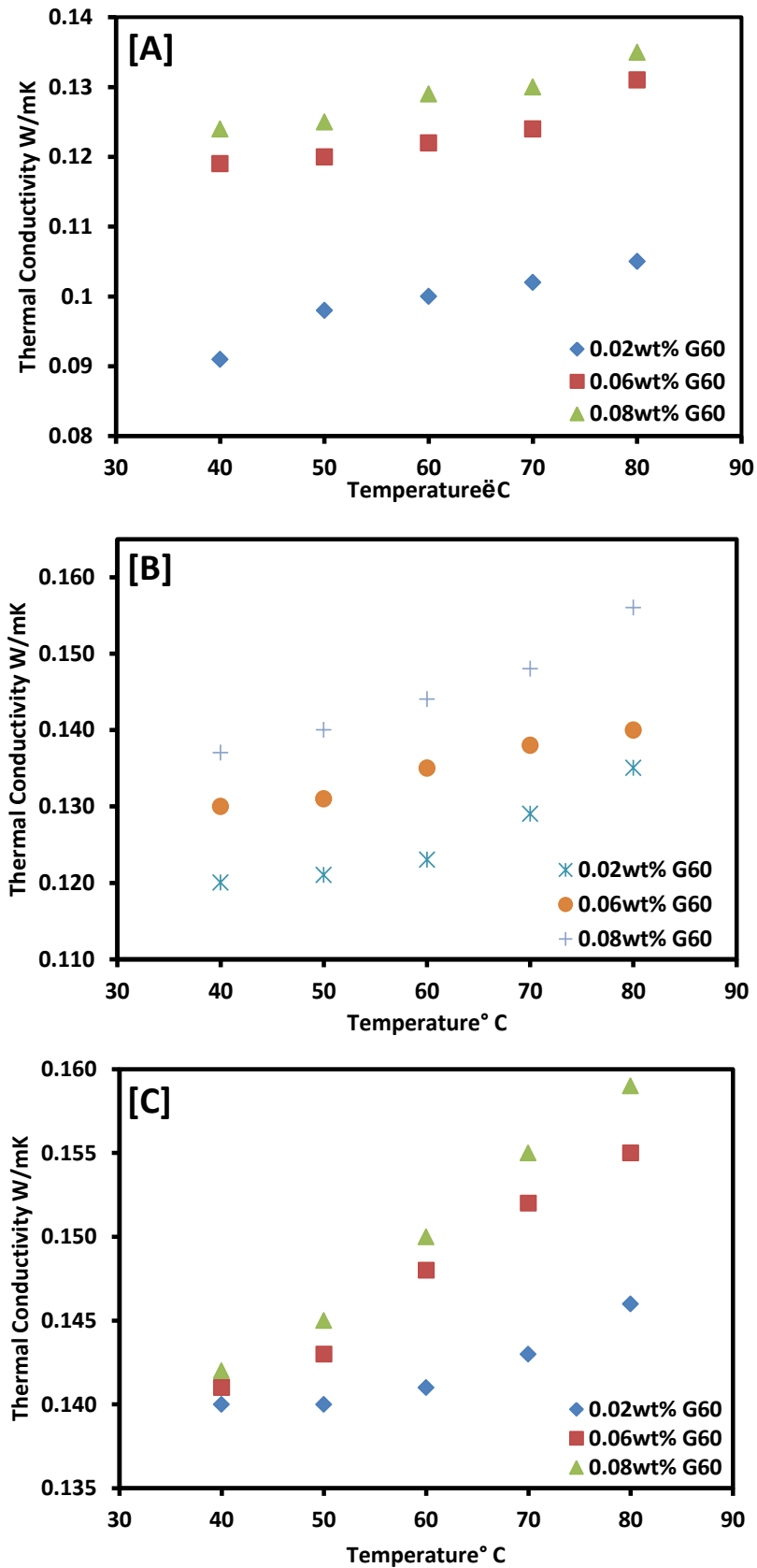
Figure 4.5. Effect of G60 concentration on thermal conductivity of mineral oil. A-150 SUS+G60; B – 500 SUS+G60; C – 2100 SUS+G60;

Furthermore, it was observed that the oil formulation help graphene to remain stable due to the presence of inbuilt additives whereas, the stability of pure base oil decreases due to poor dispersion. Hence the thermal conductivity of oil formulation is better than that of pure base oil containing graphene with identical concentration. As the temperature is increased the thermal conductivity of the base oil also increases, Figure 4.5. Three base oils having different viscosities were tested with G60. All three samples showed temperature dependent thermal conductivity enhancement. It has been suggested that the higher temperature enhances the Brownian motion which is a significant contributor to thermal conductivity improvement. Brownian motion has more impact on the smaller particles than large flakes, whereas the large flakes seem to form percolation network (Dhar et al., 2013b). Similarly the thermal conductivity enhancement is found to be strongly depend on graphene flakes thickness and specific surface area, Figure 4.4B. Previous studies suggest that the thermal conductivity of graphene based suspensions is enhanced as the heat is conducted faster along the surface. As the surface area is reduced the thermal conductivity decreased. Moreover with the increase in flake thickness i.e increase in the number of layers the thermal conductivity increases (Ahn et al., 2014, Zhou et al., 2016, Mehrali et al., 2014).

The experimental thermal conductivity results of graphene-oil formulation were compared with Maxwell, Hamilton-Crosser and Nan's models as shown in the Figure 4.6. Thermal conductivity using Maxwell's equation (1.1) relies on the volume fraction, spherical shape of particle and base fluid thermal conductivity. Hamilton-Crosser model (equation 4.1) is a

modification of Maxwell's model which is applicable to non-spherical particles,

$$k_{eff} = \frac{k_p + (n-1)k_f - (n-1)\phi(k_f - k_p)}{k_p + (n-1)k_f + \phi(k_f - k_p)} k_f \qquad (4.1)$$

where k_p is thermal conductivity of nanoparticle, k_f is thermal conductivity of base fluid, $k_p/k_f > 100$, n is an empirical shape factor $n = \dfrac{2}{\Psi}$ and Ψ is the sphericity. Interestingly, here it was observed that at low temperature range (25 - 45 °C) thermal conductivity values from Maxwell model is close to the experimental results, and the results from H-C model are slightly higher. However, similar to presents results shown in the Figure 4.6, in some studies, it was found that even at low concentration the measured thermal conductivity of nanofluids is greater than that predicted by classical models (Maxwell, 1892, Hamilton and Crosser, 1962, Bruggeman, 1935). This is due to the fact that these models were developed for milli or micro sized particles as discontinuous phase. In addition they do not account for particle geometry, temperature effect, Brownian motion of nanoparticles, the effect of interfacial layer at particle/liquid interface, and the effect of nanoparticles clustering, which are considered as important mechanisms for enhancing the thermal conductivity of nanofluids (Lee et al., 1999, Keblinski et al., 2002, Eastman et al., 2001, Xue et al., 2004, Das et al., 2003a). However, some reports found Nan's model (Nan et al., 1997) to be closely predicting k_{eff} and it expresses the resulting effective thermal conductivity of the composite for completely disoriented ellipsoidal particles as,

$$k = k_0 \frac{3 + \varphi[2\beta_{11}(1 - L_{11}) + \beta_{33}(1 - L_{33})]}{3 - \varphi(2\beta_{11}L_{11} + \beta_{33}L_{33})} \qquad (4.2)$$

$$\text{where } \beta_{ii} = \frac{k_p - k_0}{k_0 + L_{11}(k_p - k_0)} \qquad (4.3)$$

where L_{11} and φ are the geometrical factors and the volume fraction of particles, respectively. k_p is the thermal conductivity of the ellipsoidal particles. For graphene and graphene oxide, the aspect ratio is very high, so it is assumed that L11=0 and L33=1.
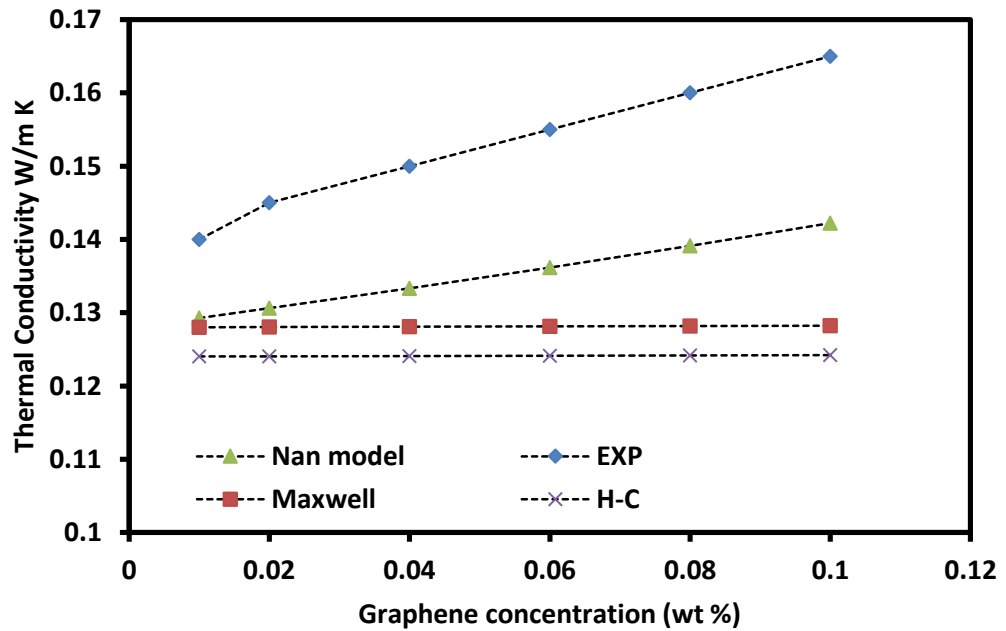
Figure 4.6. Comparison between experimental and theoretical thermal conductivity data

4.4.   Rheological analysis

4.4.1. Kinematic viscosity of graphene nanolubricants

Viscosity results obtained by following ASTM D-445 procedure are presented in the Figure 4.7. The kinematic viscosity of the base oils and the

nanolubricant has negligible difference with the addition of 0.01 wt% graphene. Furthermore, when the viscosity was measured at a temperature of 105 °C, the difference in viscosity further reduces. Compared to base fluids such as water and emulsions, the increase in viscosity of mineral oils samples after the addition of graphene flakes is insignificant. The reason for this behaviour remains unclear as most of the existing explanations seem to be speculative (Ettefaghi et al., 2013, Kole and Dey, 2013). However, Heine et al (Heine et al., 2010) showed through the molecular dynamics simulations of equilibrium structure and the response to imposed shear on suspensions of spheres, rods, plates, and jacks, that the rod and plate systems show noticeable particle alignment, which helps to minimize the frequency of particle collisions. Similarly it is expected that the graphene having sheet structure could align itself along the shear direction. Nevertheless, this claim requires experimental validation.
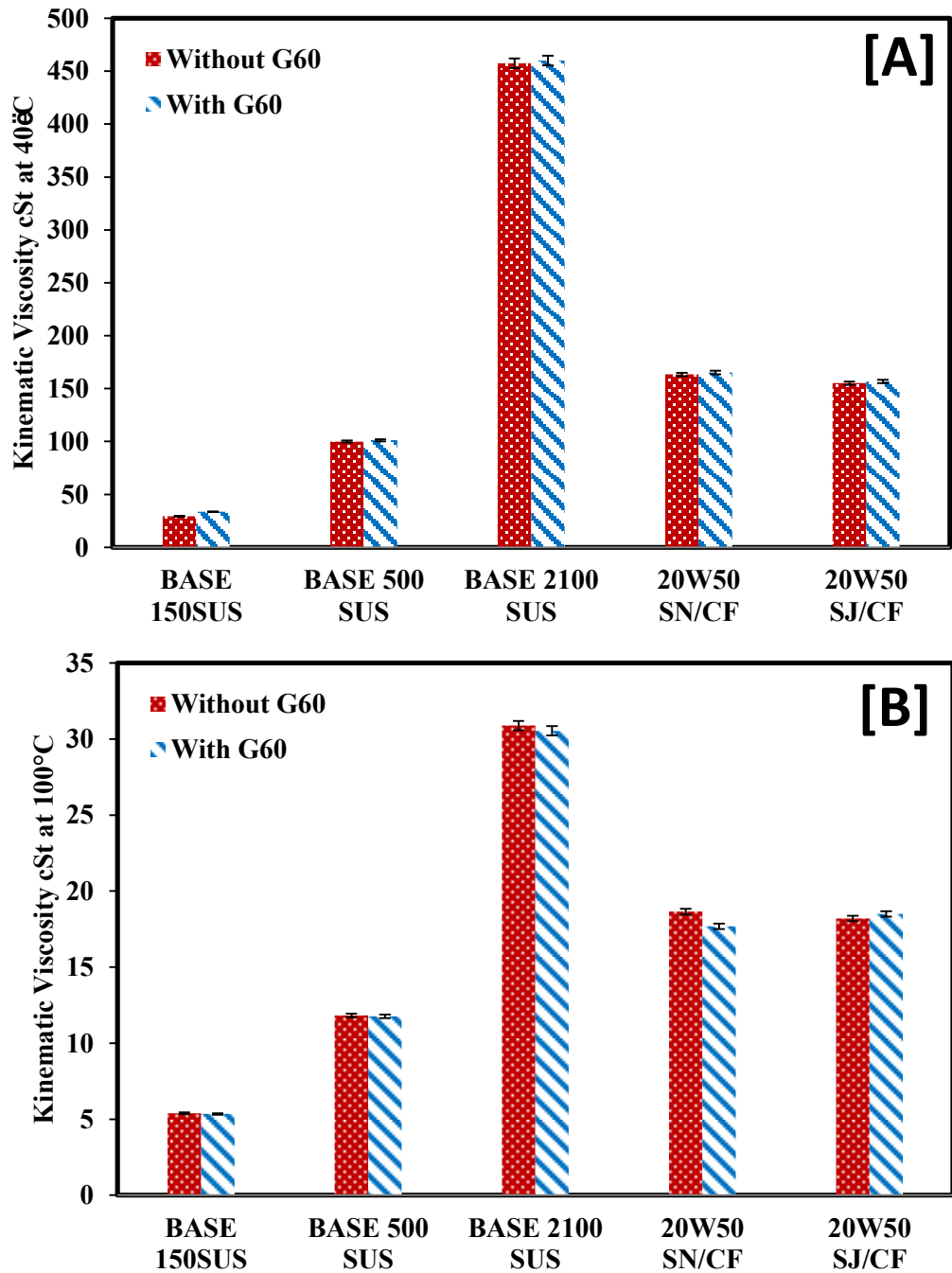
Figure 4.7. Kinematic viscosity of various base oils with and without graphene (60 nm) at A-40°C and B-100°C

4.4.1.1. **Effect of graphene size on viscosity**

The viscosity was found to be a function of graphene flake thickness. While enhancement of viscosity due to G8 is comparatively low, G12 and G60 nm have nearly same enhancement as shown in the Figure 4.8. At low temperatures, the viscosity of all the different sized graphene nanolubricant seems to be of negligible difference. Furthermore as shown in the Figure 4.9 the nanolubricant exhibits Newtonian behaviour since the base fluid is mineral oil (Dyson, 1965). Interestingly the 60 nm thick flake based lubricant has slightly lower viscosity at low shear rate. It might be due to the fact that the initial spinning stage the graphene flakes are disoriented and as the spindle speed increased, the flakes align themselves along with the direction of shear force (Tian and Ahmadi, 2013, Tian et al., 2012).
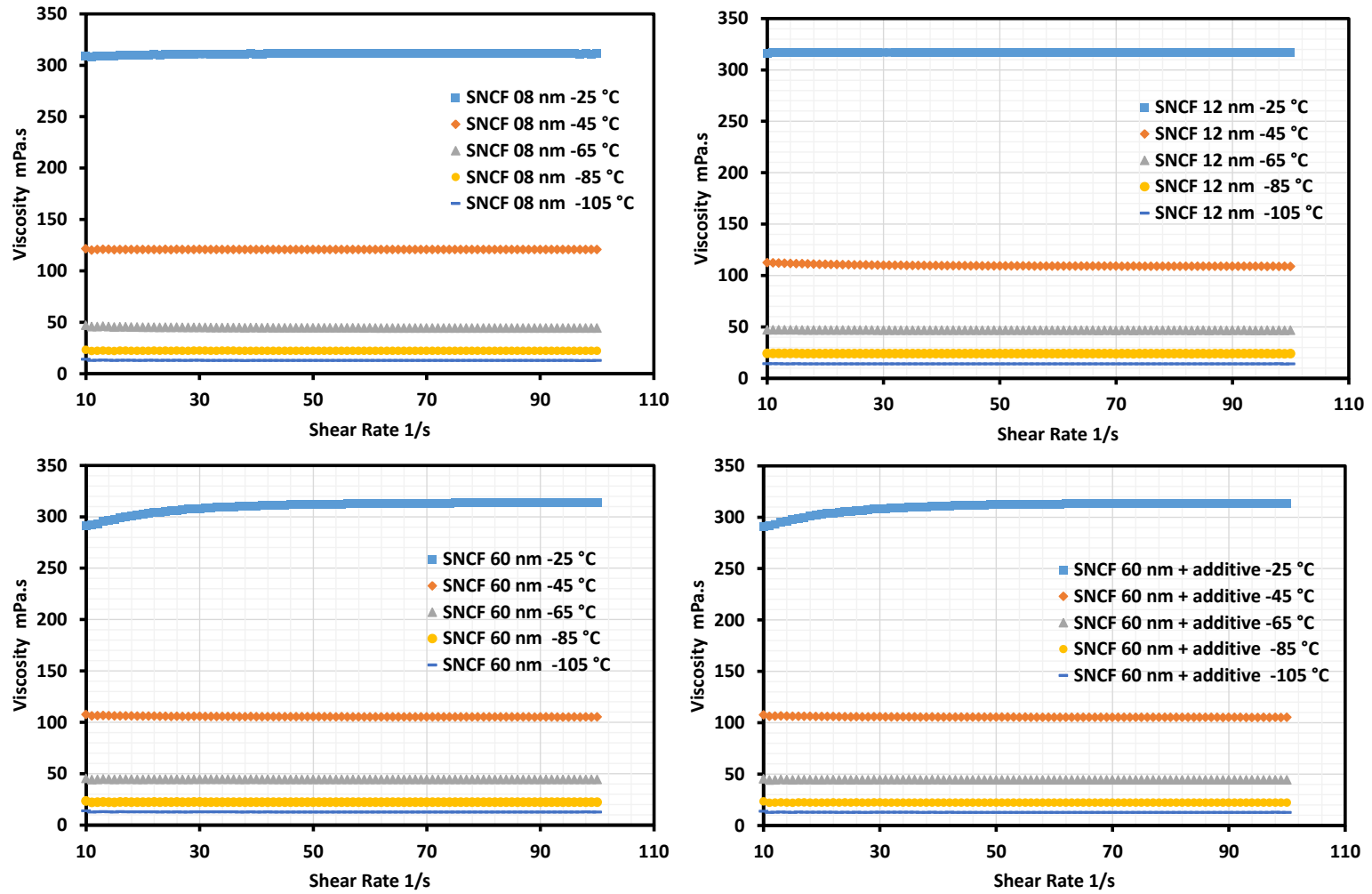
Figure 4.8. Dynamic viscosity of nanolubricant containing different sized graphene
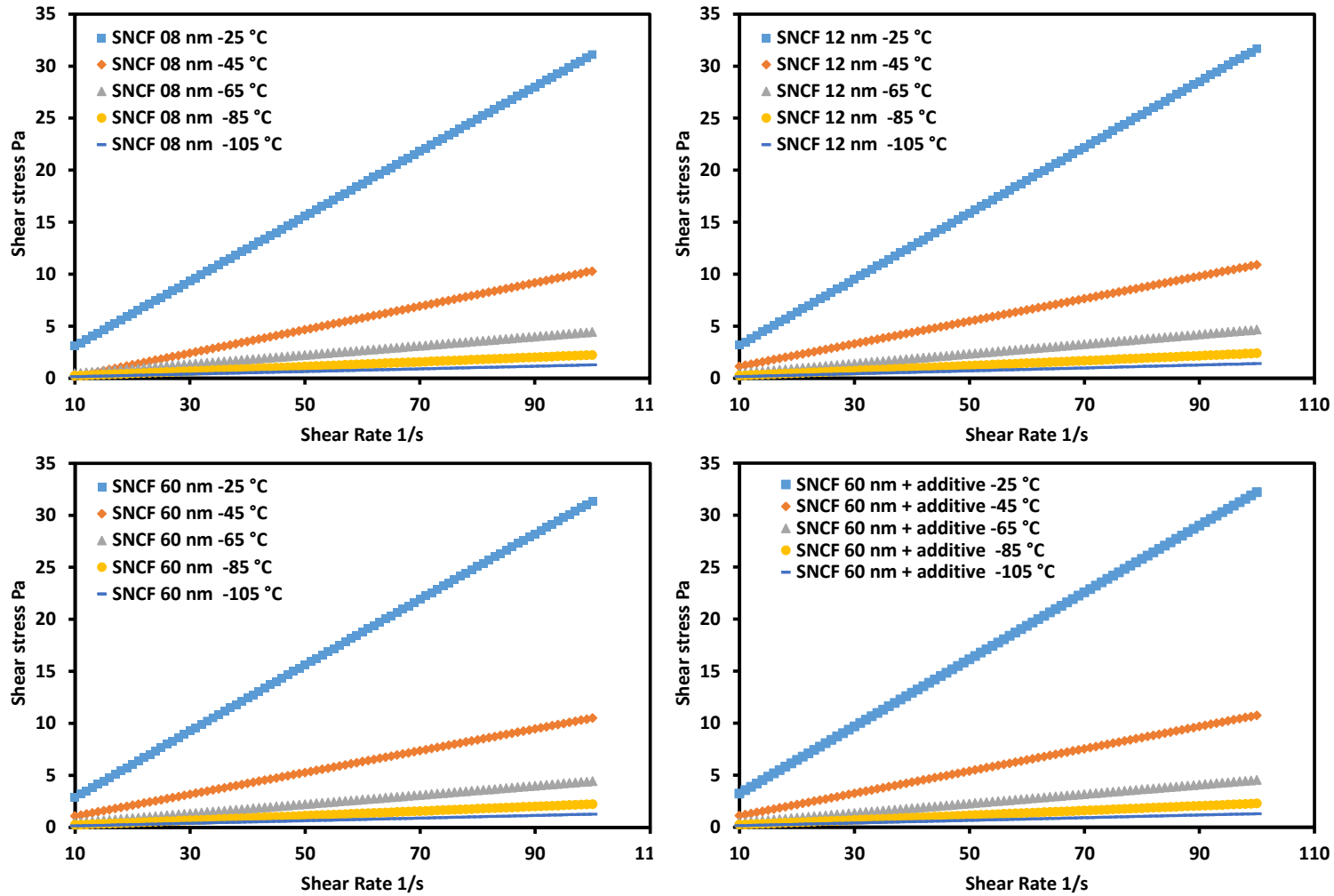
Figure 4.9 Newtonian behaviour derived using shear-strain curves of nanolubricant containing different sized graphene

4.4.1.2. **Effect of temperature on viscosity**

Figure 4.8 shows that the viscosity of graphene nanolubricnats significantly reduces with temperature. The viscosity drops intensely from 60 to 40°C. It might be due to the inter-molecular and inter-particle adhesion forces become weak with the increase in temperature, causing decrease in viscosity. Moreover, increased Brownian diffusion at elevated temperatures can reduce viscosity. Whereas below 40°C, the Brownian diffusion might be weak owing to higher base-fluid viscosity. At very high-shear rates, the Brownian diffusion plays a negligible role in comparison with the convective contribution and hence independent of the high-shear viscosity on the temperature. Similar behaviour has been witnessed in many previous studies consisting different nanoparticles and base fluids (Mahbubul et al., 2012, Sharma et al., 2016). For instance, Nguyen et al. (2008) found that the dynamic viscosity of nanofluids increases considerably with particle volume fraction but clearly decreases with a temperature increase. However, for higher volume fraction samples, it was observed that a critical temperature (T_{cr}) exists beyond which the particle suspension properties seem to be drastically altered, triggering a hysteresis phenomenon (Nguyen et al., 2008). For a particular concentration, the critical temperature corresponds to last data point which has the highest temperature on corresponding curve. Hysteresis phenomenon occurs in nanofluids when the viscosity does not change with respect to the factor that causes its change. The critical temperature is found to be strongly dependent of particle size. In case of graphene nanolubricants, the viscosity is clearly the function of temperature but no critical temperature exists which could cause hysteresis phenomenon. It also noteworthy that Nguyen et al experimented water based

Al$_2$O$_3$ nanofluids which is very different from the mineral oil based formulation. The addition of the lubricity additive has neutral effect on the behaviour of the nanolubricant. It is because the additive enhances the base fluid viscosity and has no effect on the graphene directly.
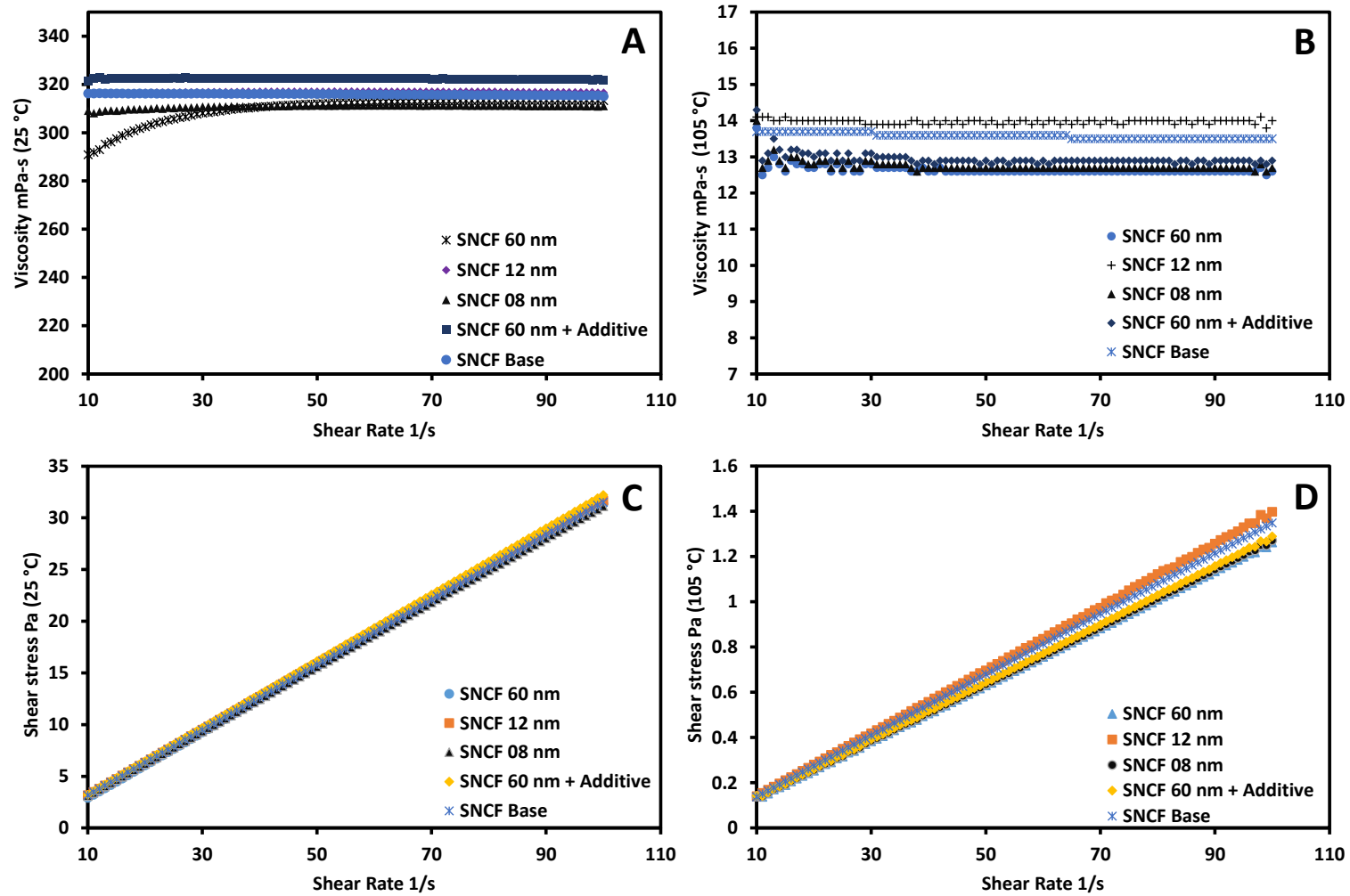
Figure 4.10. Viscosity vs shear rate at A-25°C and B-105°C; Shear stress vs shear rate at C-25°C and D-105°C; of graphene nanolubricant.

4.4.1.3. **Theoretical viscosity**

Several reports have compared the experimental values against the Einstein's model which predicts the effective viscosity of a fluid according to the following equation,

$$\mu_{eff} = \mu_b (1 + 2.5\phi) \tag{4.4}$$

where μ_b is the viscosity of base fluid and ϕ is the volume fraction. The temperature dependent viscosity can be calculated from equation (4.4) provided that the viscosity of the base fluid at the corresponding temperature is known. Few classical models (Brinkman, 1952, Bruggeman, 1935, Mooney, 1951) used the differential effective medium approach for spherical particle suspensions to extend the Einstein's formula for a moderate particle volume fraction. Although the graphene is hydrophobic, it requires further acid treatments to become super hydrophobic. This is one of the reasons why the stability of graphene reduces over time and temperature. However, exact prediction of viscosity for graphene nanofluids using these classical models is not possible. Based on Mooney (1951) model, another expression was developed for non-spherical particles (Choi et al., 2000, Kwon et al., 1998) as,

$$\ln\left(\frac{\mu}{\mu_f}\right) = \frac{\mu_\infty \phi}{1 - \phi/\phi_m} \tag{4.5}$$

where ϕ the volume fraction and ϕ_m is the maximum packing volume fraction. This model (4.5) can be use to predict the viscosity of graphene flakes based nanofluids which are similar to plate-like Ba-Ferrite. Using $\phi_m = 0.65$, the expression (4.5) fitted very well with their measured viscosities for plate-like

Ba–Ferrite particle for volume fraction up to 0.04. From this expression the intrinsic viscosity at infinite shear rate was also evaluated where μ_∞ = 12 cP for plate-like Ba–Ferrite particle. In the present study, the experiments were limited to a single concentration of graphene with different base fluids. The experimental results were compared with both Newtonian and non-Newtonian fluid viscosity models such as Newton, Casson, Bingham and Herschel Buckley models as shown in the Figure 4.11. No significant variation in viscosity was observed with any of the models used.
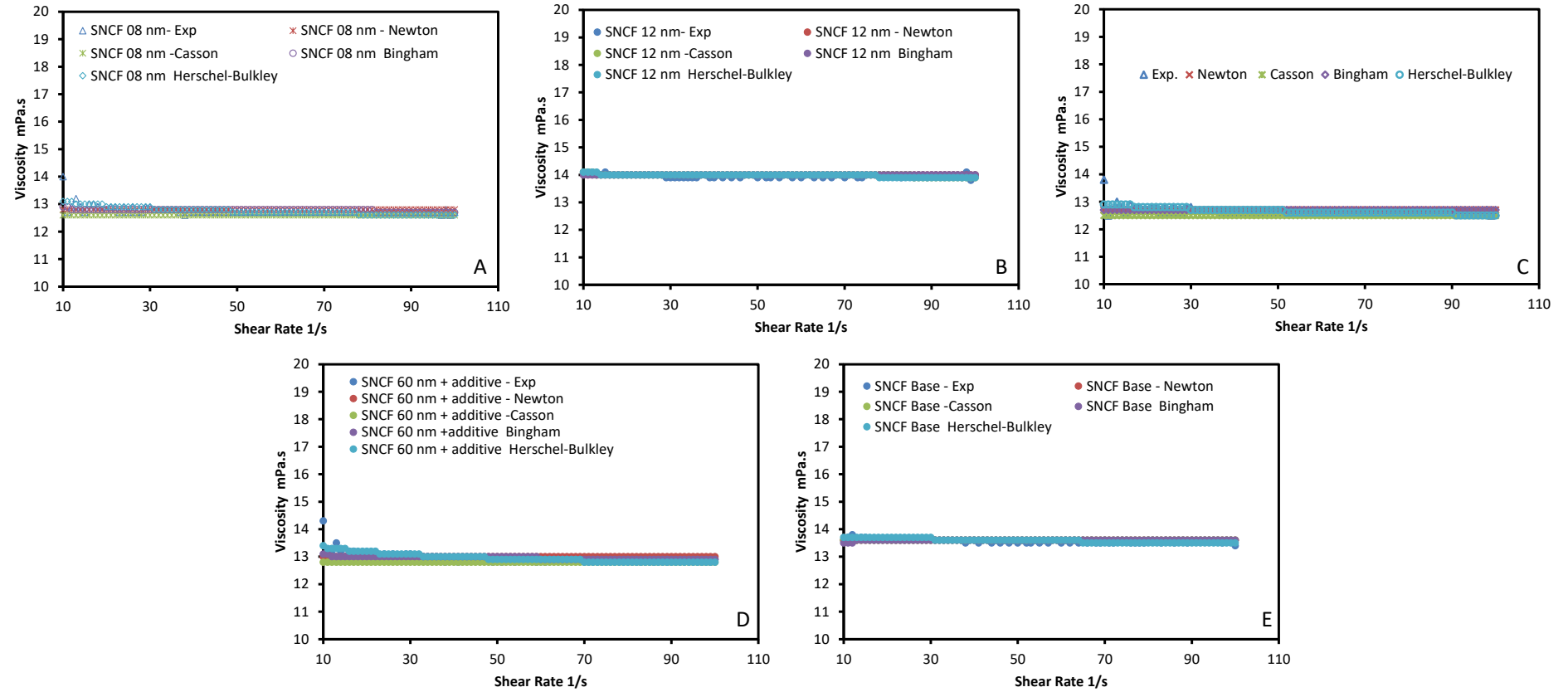
Figure 4.11. Experimental and theoretical viscosity of graphene nanolubricant. A-SN/CF+G8; B-SN/CF+G12; C-SN/CF+G60; D-SN/CF+G60+Additive; E-SN/CF Base;

4.5. Thermogravimetric analysis[**]

Thermo (oxidative) degradation of lubricants in thermogravimetric analyzer (TGA) is a fundamental technique to evaluate the stability of engine oils under isothermal and dynamic heating conditions. Figure 4.12 shows the thermogravimetry curves of oil samples (SN/CF). The sample loses its moisture content and is quite stable until approximately 250 ºC. Oxidation and the elimination of low molecular weight products including from aliphatic and aromatic hydrocarbons occurs at 297.79 ºC, followed by the degradation of remaining hydrocarbon. The graph shows that after at 450 ºC decomposition of remaining hydrocarbons of higher molecular weight take place. The maximum weight loss is noticed at 353ºC in case of G60 nm however, the maximum weight loss temperature decreases with the graphene size. Furthermore, the onset temperature at which the oxidation starts for SNCF formulation is delayed in the presence of graphene flakes and depends on the size of the graphene as well.

[**] TGA studies have been published in the Journal of Materials Research
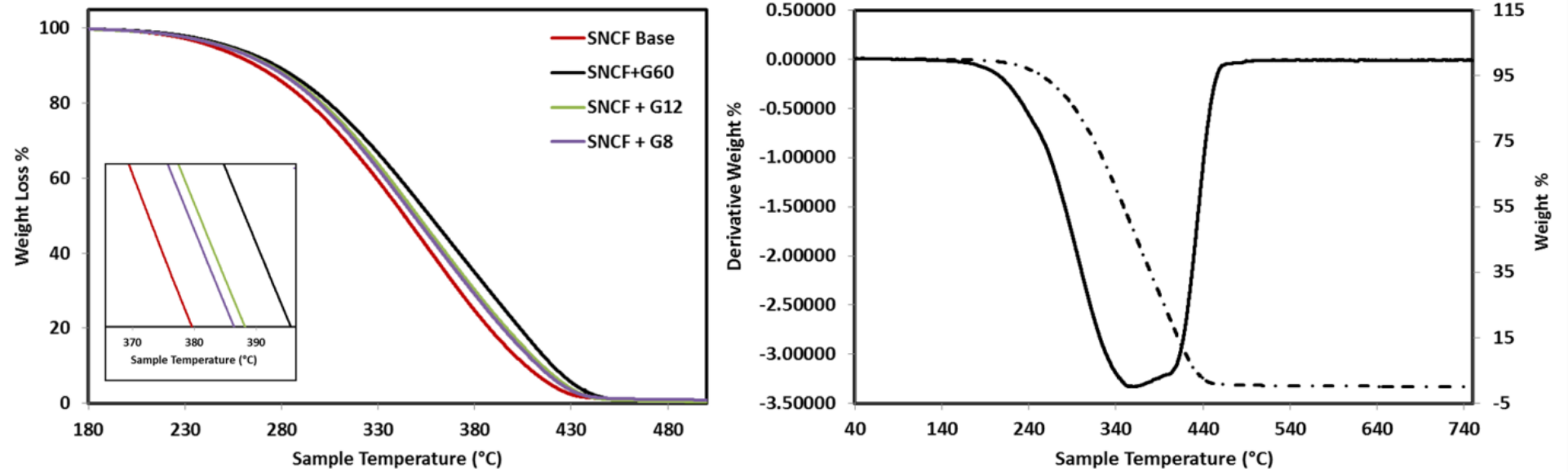
Figure 4.12. Left: TG curves of 20W50 API SN/CF with graphene (60, 12, 8 nm). Right: Derivative weight % of API 20W50 SN/CF with graphene (12 nm) at a heating rate of 5 ºC/min under a nitrogen purge of 20 ml/min.

It is well known that various properties especially thermal conductivity of nanoparticle based suspensions depend on the size (thickness, length and diameter) of nanoparticles. Many molecular dynamics studies have found that the thermal conductivity of graphene also depends on lateral dimensions and the thickness owing to two-dimensional nature of phonons in graphene (Xu et al., 2014, Balandin et al., 2008). When Xu et al (Xu et al., 2014) measured the thermal conductivity of single-layer graphene at 27 ºC with respect to graphene's length and temperature, thermal conductivity was increasing and remained logarithmically divergent with sample length. Nika et al (Nika et al., 2012) found that the long mean free path of the long-wavelength acoustic phonons in graphene can lead to an unusual nonmonotonic dependence of the thermal conductivity on the length L of a ribbon. The results also confirmed that the effect is pronounced for the ribbons with the smooth edges (specularity parameter p > 0.5) and scaling of the phonon thermal conductivity with the lateral sizes in graphene. Similarly, thermal conductivity of graphene was found to increase with the number of layers, approaching the in-plane thermal conductivity of bulk graphite for the thickest samples, while showing suppression below 160 W/m-K at room temperature for single-layer graphene (Jang et al., 2010). The observation in our experiments could also be essentially due to the phonon effect in graphene which depend on the length and thickness of the graphene. Mehrali (Mehrali et al., 2014) used three different surface area (300, 500, and 750 m^2/g) graphene and found that the graphene with specific surface area 750 m^2/g dispersersed in water could enhance thermal conductivity upto 27.64% at 0.1 wt.%. However, contrarily it

was observed that the initial oxidation is delayed more in the presence of 60

nm think flake which las low specific surface area.
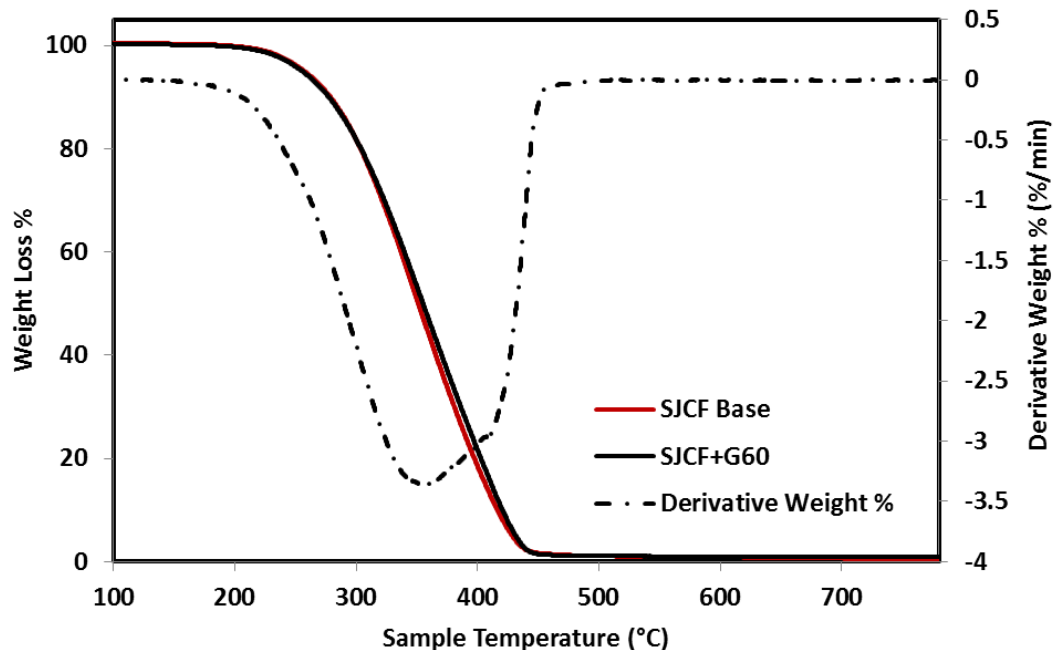
Figure 4.13. TG and DTG curves of API 20W50 SJ/CF with and without graphene 60 nm at a heating rate of 5 ºC/min under a nitrogen purge of 20 ml/min.

Furthermore, it is understood from the broader peak of derivative weight %

that the oil sample contains many other compounds (additives) similar to base

oil. SN/CF oil in the presence of graphene seems to perform better than SJ/CF

as seen in the Figure 4.13. Both the onset temperature and maximum oxidation

temperature are almost same however, the oxidation speed of graphene based

nanolubricant is slightly delayed than the base oil. However, in the case of API

SN/CF oil the improvement is prominent both interms of oxidation onset

temperature and the rate of oxidation. This observation is similar to Zhang et

al (Zhang et al., 2012) who studied the thermal properties of Ag–MoS$_2$

nanoparticle based multi-component lubricating system. Their TGA results showed that the starting temperature of oxidation for both cases, with and without nanoparticle is approximately 360 ºC. It is interesting to note that the hydroperoxide concentration level in Cu-kerosene nanofluids was found to be low after a thermal oxidation reaction (Li et al., 2011). Indicating that the Cu nanoparticles reacted with the oxygen before the kerosene was oxidized. This shows that a suitable amount of nanoparticles added into a base oils and fuels can enhance its thermal oxidation stability. Similarly, graphene suspended in the oil could have the potential to get oxidized in an oxygen rich environment. In a thermal treatment, the polyhydrocarbon template has helped to produce high-quality reduced graphene oxide compared to good-quality reduced graphene oxide through a chemical reduction method (Some et al., 2013). Heteroatom-free rGOs is referred to as high-quality reduced graphene oxide.
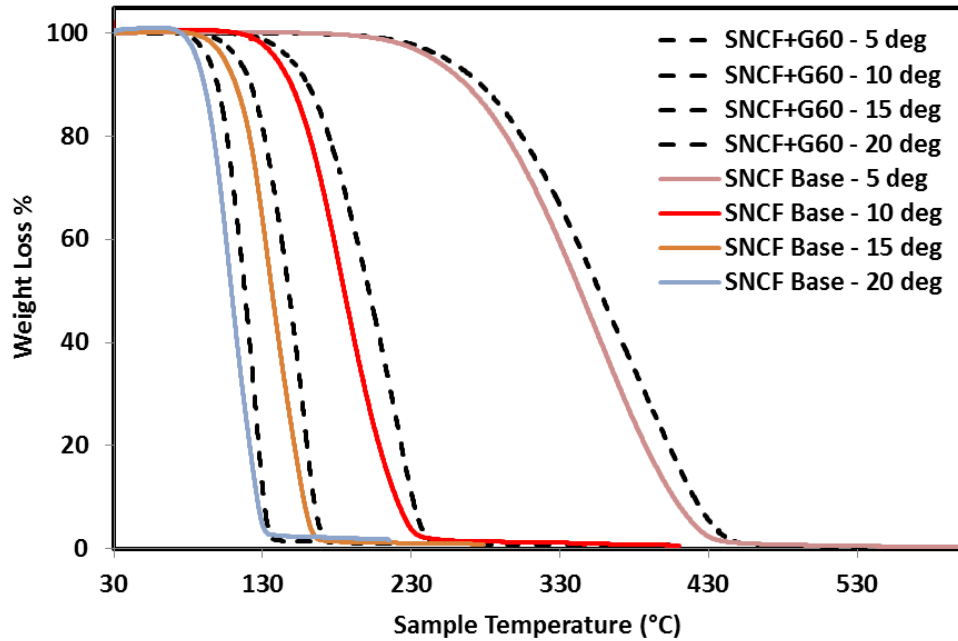
Figure 4.14. Effect of heating rate on API 20W50 SN/CF + Graphene. Nitrogen purge rate of 20 ml/min

In order to ensure the repeatability of the TGA curves, the heating rate was varied from 5 to 10, 15 and 20 ºC/min, Figure 4.14. It was observed that the initial decomposition temperature increase with the heating rate in all the four cases. Moreover, the presence of graphene helps in the oxidation delay of approximately 13-17 ºC.

4.5.1.1. Kinetic studies

TGA kinetics approach of this study uses the well-known variable heating method developed by Flynn and Wall (1966). It relates the pre-exponential factor A, the activation energy E, and the reaction model f(α) as seen in the following expression:

$$\frac{da}{dt} = A \exp\left(\frac{-E}{RT}\right)(1-a)^n \qquad (4.6)$$

where da/dt is the rate of mass loss, a is the conversion or the fraction of material reacted, n is the reaction order, E is the Arrhenius activation energy (J/mole), T is the temperature (K), R is a constant (8.314 J/mole K) and A is the pre-exponential factor (sec^{-1}). The conversion 'a' is given by $(w_0 - w_t)/(w_0 - w_f)$, where w_0 denotes initial sample weight, w_t denotes sample weight at time t, and w_f is the weight of remaining char. Under the application of a constant heating rate, ϕ, and assuming a first order reaction (n =1), the rate expression becomes:

$$\frac{da}{(1-a)} = \left\{\frac{A}{\phi}\right\} \exp\left(\frac{-E}{RT}\right) dT \qquad (4.7)$$

Since a value of n=1 is used (first order kinetics) this method is essentially the same as that used by ASTM Standard Test Method E 1641. Salehi et al. (2012) discussed the suitability of using model free isoconversional methods to analyse thermal decomposition of metal injection moulding (MIM) feedstocks (Salehi et al., 2012). Since the knowledge of the reaction mechanism is not required, model free methods are regarded as most reliable way to determine kinetic parameters of thermally activated complex reactions. These methods are based on studying the degree of conversion with respect to temperature at different heating rates (Figure 4.14). In the model free methods, activation energy is calculated directly from the TGA curves. Activation energy takes into consideration several processes occurring simultaneously. The rate of degradation, da/dt, is assumed to depend on the temperature and weight of the sample. Therefore, the main advantage of eliminating the necessity of a kinetic

model is clouded by the influence of the sample mass and size in the apparent kinetics parameters calculated. To reduce possible errors regarding size and mass, samples of similar dimensions and masses were employed. It is assumed for the thin disks employed that the binder removal rate is predominantly determined by decomposition rates of organics and not by transport processes. For pyrolysis of engine oils, the function f(a) that signifies the variation of conversion with time is characterized by a decelerating kinetics. This implies that in the initial phase the reaction rate is maximum and decreases continuously as conversion is increased. Therefore, f(α) is given by nth order kinetics, $(1 - a)^n$. Usually, engine oil decomposition is characterized by first order kinetics, i.e., n = 1. Kinetics Committee of International Confederation for Thermal Analysis and Calorimetry (ICTAC) recommends the evaluation of apparent activation energy at different mass conversions using isoconversional models that utilize TGA data at a minimum of three heating rates for kinetic predictions, and to understand the regimes and mechanism of mass loss. Table 4.3 contains the kinetic parameters that were obtained by processing the TGA data using Perkin Elmer kinetic software.

The change in activation energy with the addition of graphene reflects differences in the decomposition kinetics due to several factors including oxidation. It is apparent that the pure oil formulation has higher activation energy, whereas the addition of graphene significantly reduces its activation energy. Furthermore, the reduction in graphene tickness which is essentially decrease in the number of layers further decreases the activation energy. Figure 4.15 shows the temperature required to achieve a 3% conversion at different holding times. The considerable increase in onset temperature for the

oxidation of the oil with the increase in holding time is clearly evident from the results. Furthermore, in the presence of graphene 60 nm the complete conversion happens after 400 ºC which is 100 ºC more than the oil without graphene. Similarly, with the addition of graphene 12 nm, the complete conversion happens around 600 ºC (out of scale in the Figure 4.13B). This shift in the required temperature for the complete conversion in the presense of different sized graphene shows that the graphene size plays a crucial role.

Table 4.3. Kinetic parameters obtained from the reactions

% Conversion	Activation Energy Ea (KJ/mole)	+/-	pre-exponential factor lnZ (1/s)	+/-
API 20W50 SN/CF Base				
3.0	134.47	78.17	23.46	18.71
5.0	158.46	0.87	28.80	0.20
8.0	170.80	122.32	31.14	27.81
API 20W50 SN/CF + G60				
3.0	76.62	27.41	8.79	6.44
5.0	75.98	37.72	8.62	8.64
8.0	77.66	40.92	8.94	9.10
API 20W50 SN/CF + G12				
3.0	44.35	32.48	1.48	8.20
5.0	45.21	27.01	1.92	6.61
8.0	46.75	19.77	2.47	4.70
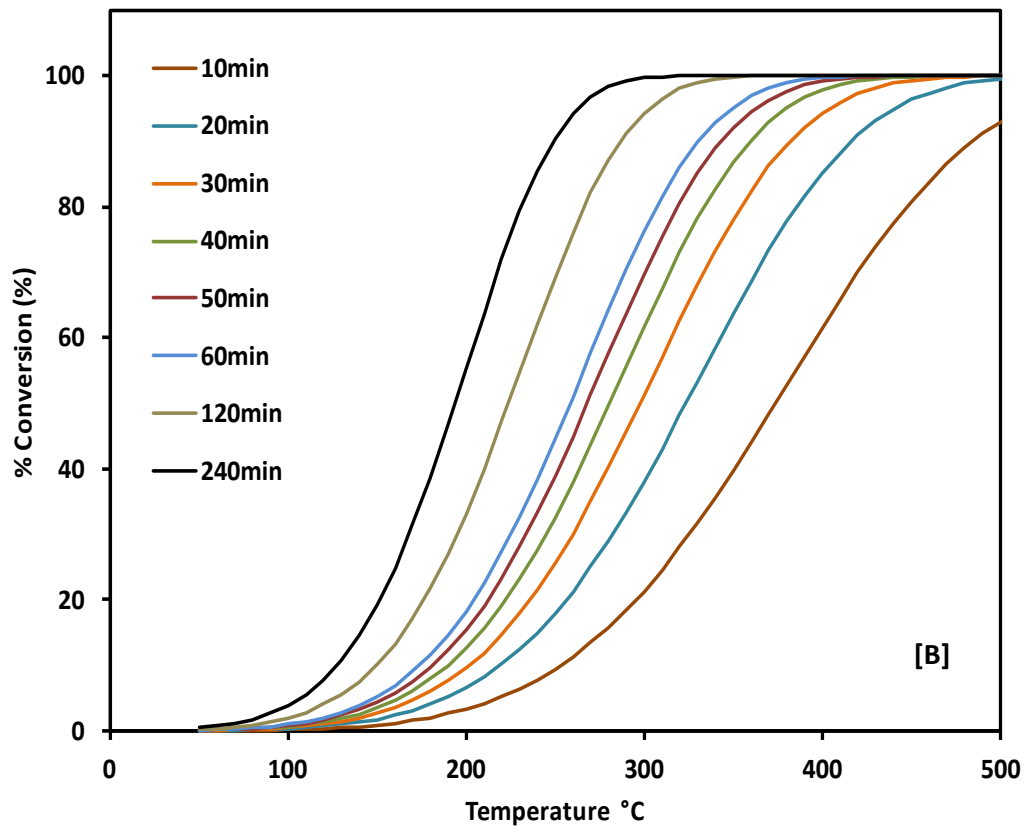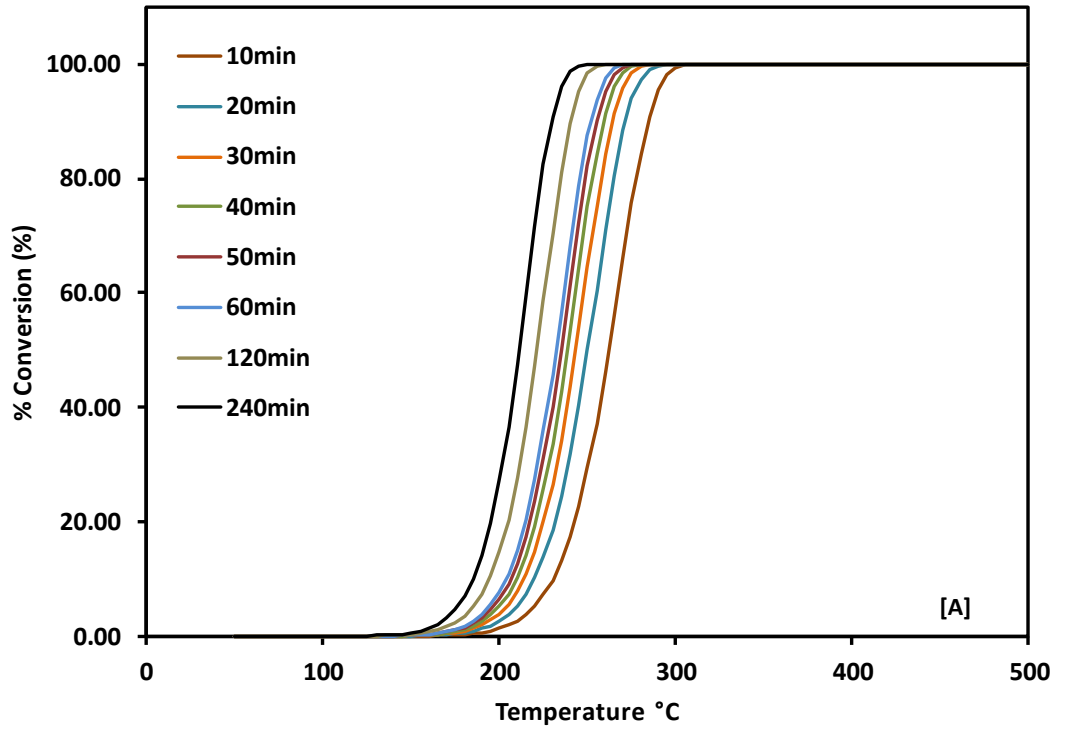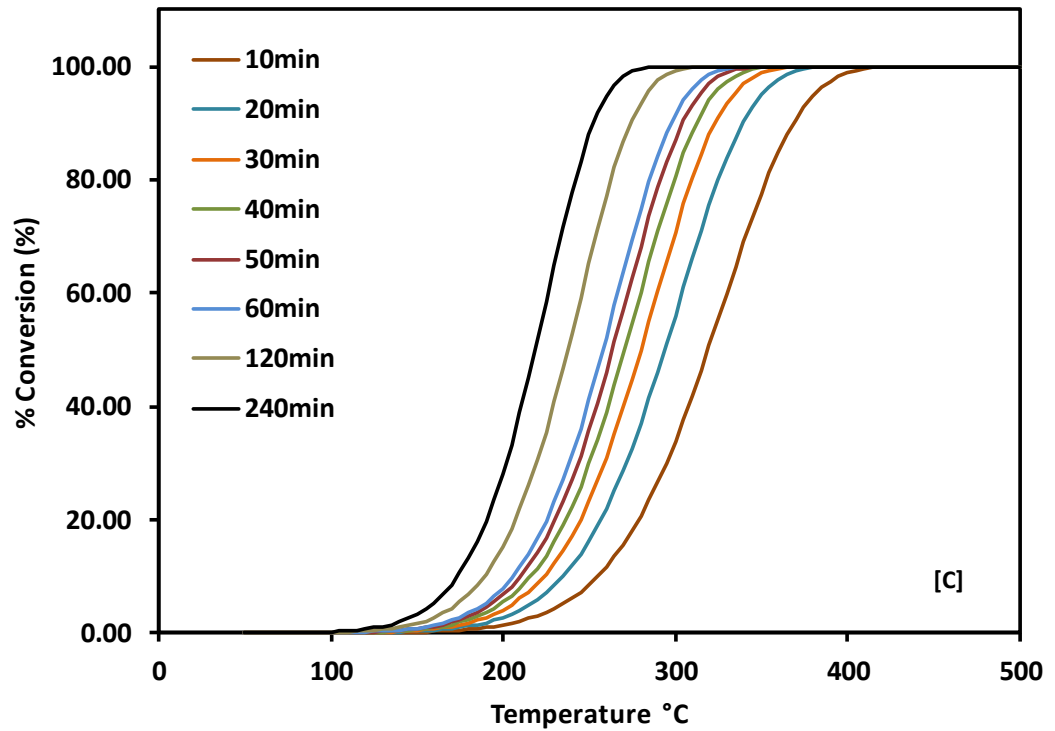
Figure 4.15. Isochronal decomposition predictive curves; [A] – SN/CF Oil; [B] - SN/CF Oil+G12; [C] - SN/CF Oil+G60;

Under isothermal conditions the activations energy remains same as in the isochronal conditions. Isochronal implies a condition where the reaction occurs at equal intervals of time. However, there is significant delay in oil oxidation time in the presence of graphene flakes as shown in the Figure 4.15. It also further confirms that the oxidation depends strongly on the size of the graphene.
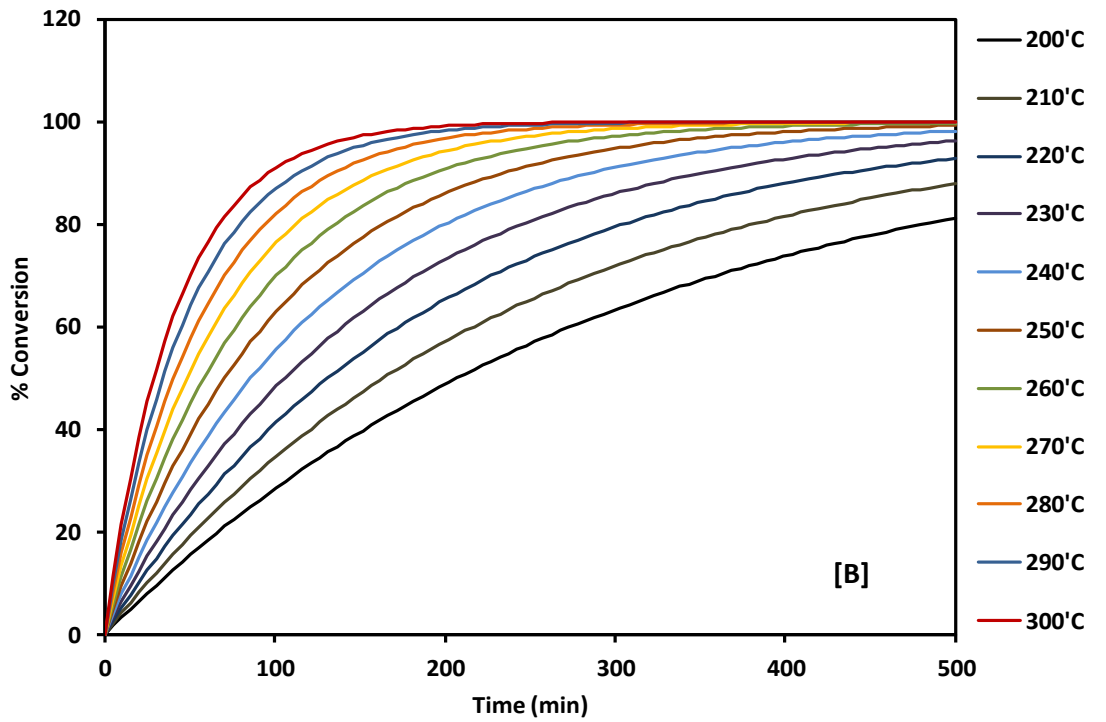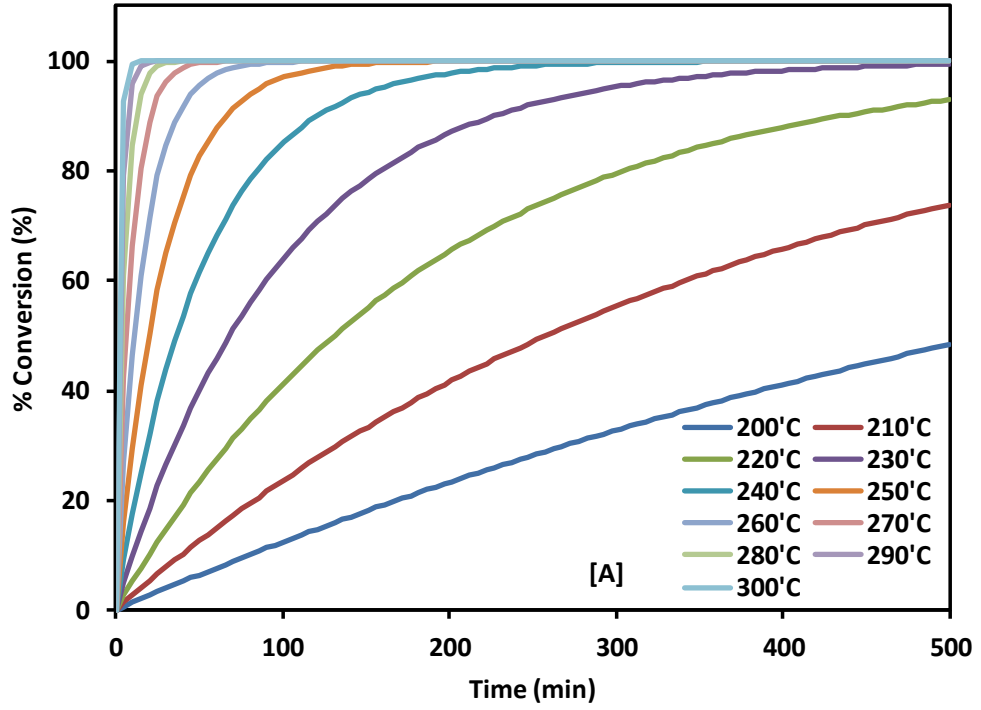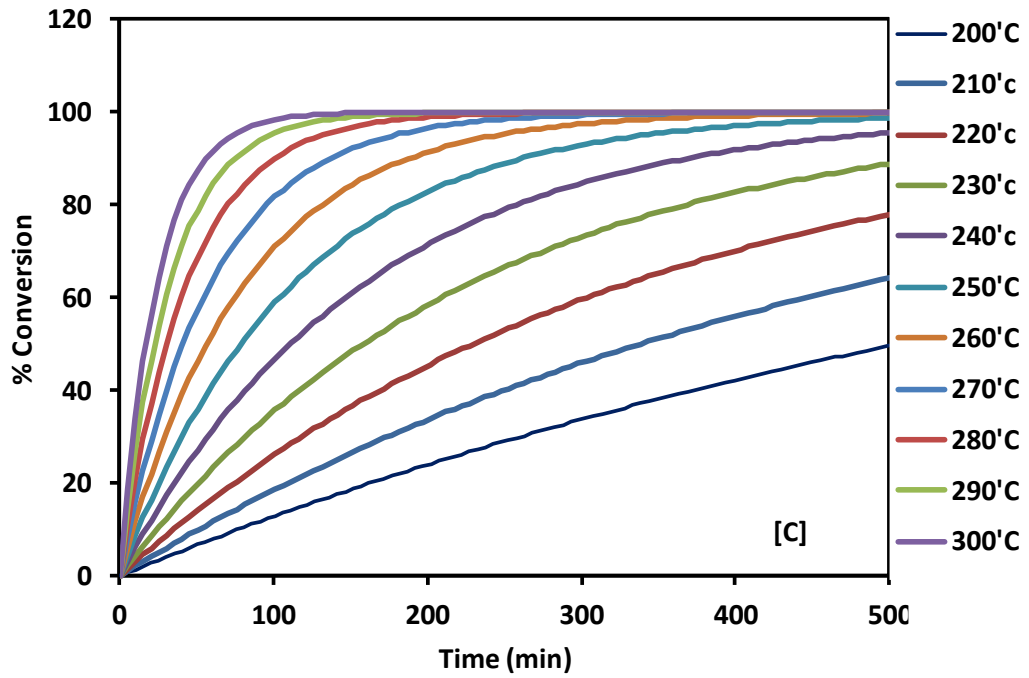
Figure 4.16. Percentage Conversion vs Time (min) under isothermal conditions. [A] – SN/CF Oil; [B] - SN/CF Oil+G12; [C] - SN/CF Oil+G60;

It is observed from the Figure 4.16, that while the base oil formulation at higher temperatures ranging from 300 ºC - 260 ºC oxidises within 50 minutes of the reaction, the nanolubricant resists oxidation beyond 100 mins at the same temperature range. Graphene 60 nm helps the base oils remain stable with a conversion value of just 45% for 500 mins. However, at higher temperatures the onset temperature for oxidation is slightly higher than that of oil containing graphene 12 nm. This indicates that the heat dissapation in oil varies with the size of the graphene flake. The major reason behind the enhancement of thermal properties of the oil could be attributed to the superior thermal conductivity of graphene flakes.

4.6.   Tribology results

The results show that the average coefficient of friction (μ) of API SJ/CF in the presence of 0.01wt% G60 is decreased considerably as shown in Table 4.4. The addition of a lubricity additive, natural polymeric ester, lead to enhanced anti-friction effect in both SN/CF and SJ/CF formulations. It is because more graphene flakes are brought in between contact areas as the graphene in oil is more stable. This is evident from the EDX analysis (Figure 4.20) which confirms graphene's presence on the surfaces comparatively higher than other the oil samples that doesn't contain lubricity additive. It is noteworthy that the addition of 1 wt% lubricity additive has negligible effect on overall behaviour of the base stock oil. API SN/CF with 0.01wt% of all the three different sizes of graphene shows decrease in both the wear scar diameter and the average μ. The improvement is insignificant or absent with G60 and G8 might be because of the additional lubricity additives in the oil formulation competing with the available tribological surfaces. In the SJ/CF formulation, the top treat of lubricity additive is absent and therefore nanoparticles play a significant role in acting upon the tribological contacts.

Table 4.4. Tribology results of oil samples

API SNCF 20W50			API SJCF 20W50		
Sample	% decrease - μ	% decrease of wear scar	Sample	% decrease - μ	% decrease of wear scar
API SN/CF 20W50 + Additive + G60	21.42	3.33	API SJ/CF 20W50 + Additive + G60	19.04	18.03
API SN/CF 20W50 + G60	-	2.22	API SJ/CF 20W50 + G60	14.28	13.11
API SN/CF 20W50 + G12	7.14	12.50	API SJ/CF 20W50 + G12	19.04	18.03
API SN/CF 20W50 + G8	-	4.44	API SJ/CF 20W50 + G8	16.66	14.75

Furthermore, the anti-wear enhancement depends on the number of graphene layers as shown in Figure 4.17. 12 nm thick graphene offers better antifriction effect than 8 nm and 60 nm thick graphene as indicated in the Table 4.4 and Figure 4.18. It is well known that the few layer graphene offers better anti-friction effect than a single layer graphene (Smolyanitsky et al., 2012, Lee et al., 2010). In single layer graphene puckering effect happens due to adhesion of flakes to the peaks and valleys of microscopic surfaces. This creates out-of-plane deformation of a graphene sheet, leading to increased contact area and friction (Lee et al., 2010). Shear force acting on a few layer graphene helps its exfoliation (Paton et al., 2014, Chen et al., 2012) thereby contributing to the lubrication effect of the oil. Moreover, it was reported that the folded graphene has higher compressive strength and strain compared to planar graphene (Yongping et al., 2011). Therefore due to relatively low bending stiffness, the sheets could also possess buckling effect and sometimes might behave as rollers. In case of very few layers graphene, the repeated exfoliation due to shear forces could form several single layer graphene sheets which could undergo puckering effect. This is evident when traces of small pieces of graphene on the surface of the ball were noticed.
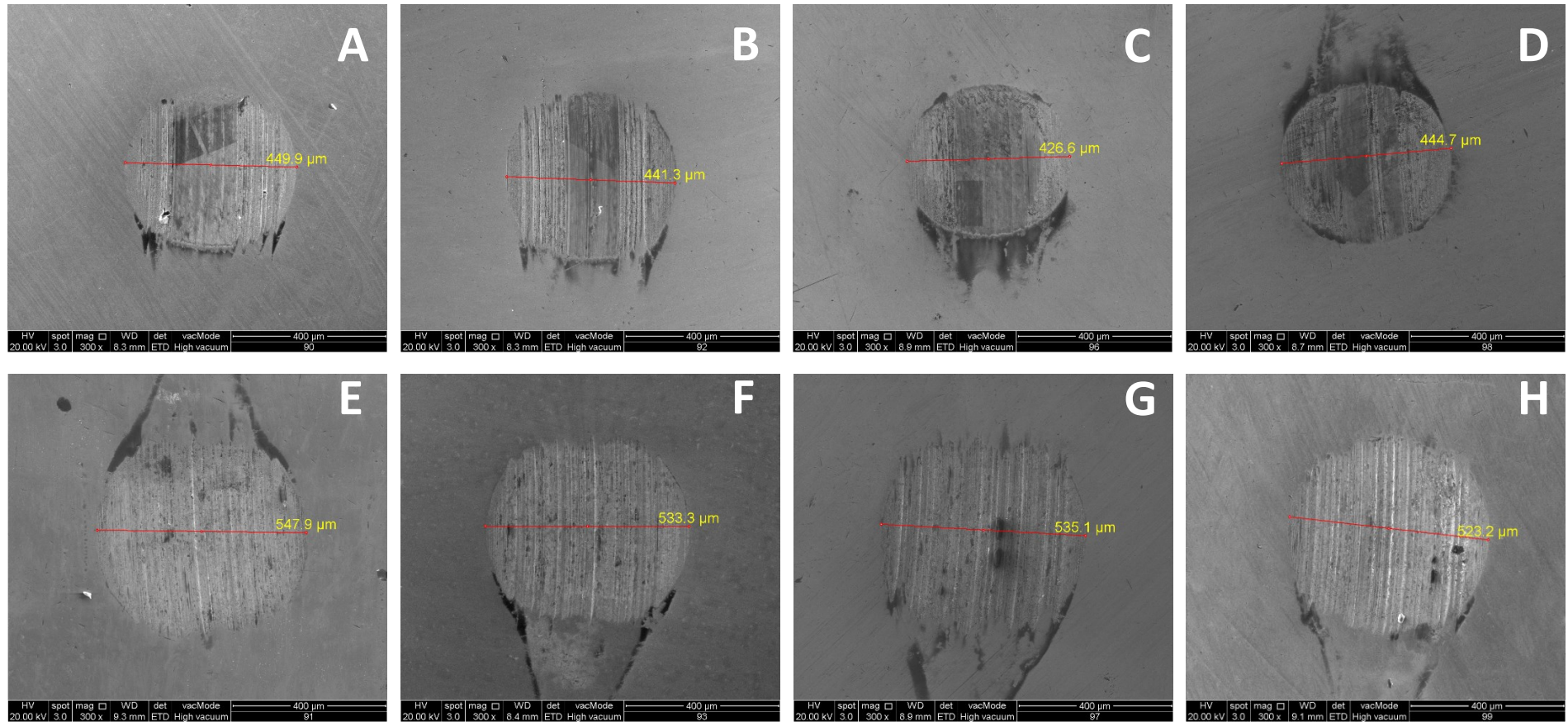
Figure 4.17. Wear Scar diameter on steel balls after tribology experiments. A-D: API SN/CF 20W50, with G60, G12, G8 respectively; E-H: API SJ/CF 20W50, with G60, G12, G8 respectively.

However, multilayer graphene (G60) did not have significant enhancement effect and also in some cases found to counter the enhancement effect, Figure 4.18. It could be due to the bending rigidity of multilayer graphene which results its interlayer shear deformation (Chen et al., 2015). Bending rigidity of multilayer graphene is influenced by the interlayer shear interaction and the number of graphene layers (N). Based on classical continuum mechanics theories, it was expounded that the physical properties including bending rigidity of graphene will be influenced significantly by its interlayer shear rigidity (Chen et al., 2015). Hence the multilayer graphene has more potential to impart higher momentum on the microscopic contacts thereby causing friction.

	Ball 90, 91	Ball 92, 93	Ball 96, 97	Ball 98, 99
SNCF	0.0872	0.0932	0.489	0.157
SJCF	0.154	0.248	0.412	0.4018
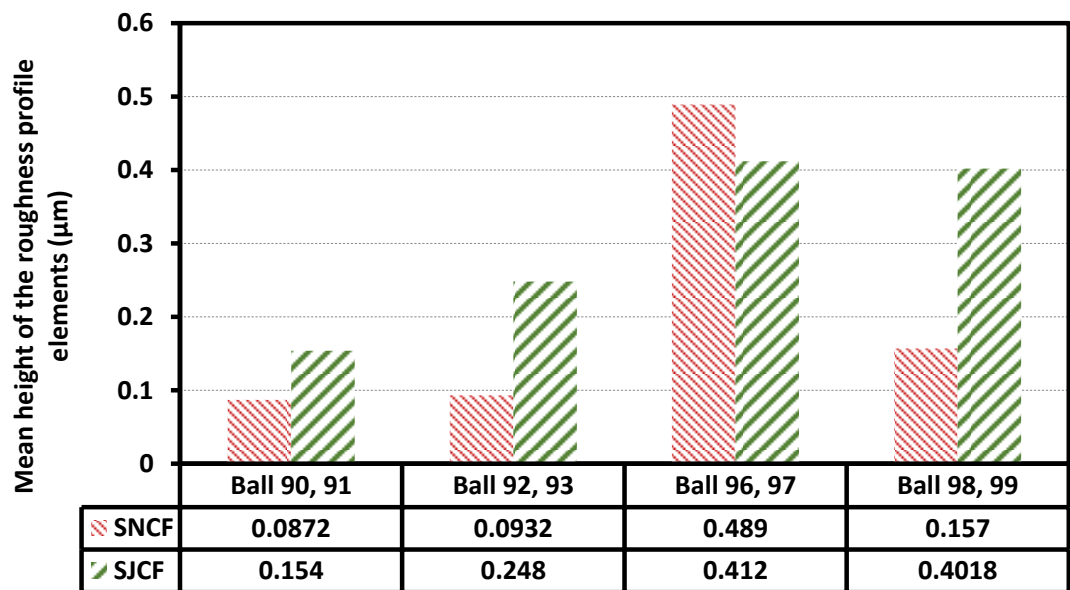
Figure 4.18. Mean height of the roughness profile elements (μm) of the steel balls.
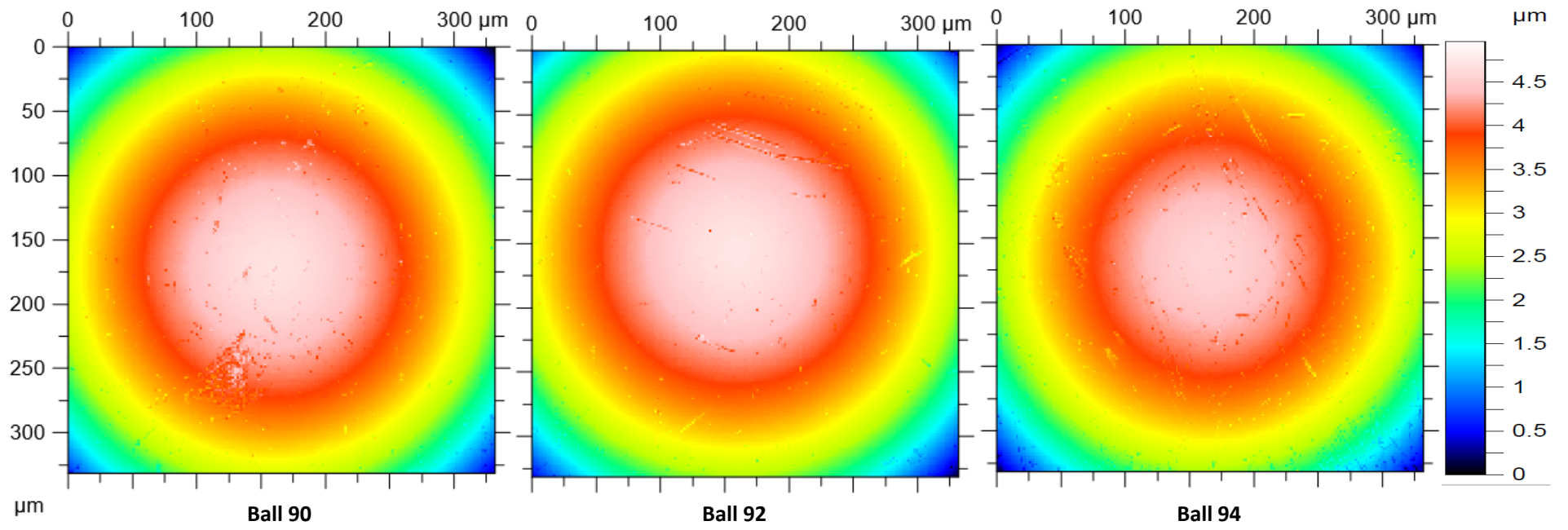
Figure 4.19. Surface profiles of the steel balls.

The surface profiles of the steel balls as shown in the Figure 4.19 were also obtained. The profile data obtained correlates with the SEM observations. Mean height of the roughness profile elements (Appendix 4) of the base oil is significantly lower than the oils containing graphene. Mean height of the roughness profile elements (Rc) is calculate as,

$$R_c = \frac{1}{m}\sum_{i=1}^{m} Z_{ti} \tag{4.8}$$

where Z_t is mean of height of the profile curve elements in a sampling length (ℓ). The graph indicates that the peaks and grooves of the balls tested with base oil were greatly subjected to friction and wear.

4.6.1.1. Tribology mechanism

A number of mechanisms have been proposed for various tribological enhancements using graphene as an additive. Wei et al., (Wei et al., 2011b) used liquid phase exfoliated graphene modified by oleic acid as additives (0.02–0.06 wt%) in lubricant oil which showed enhanced performance, with friction coefficient and wear scar diameter reduced by 17% and 14%, respectively. Similarly, Lin et al (Lin et al., 2011) found that the surface modified graphene enhances the wear resistance and load-carrying capacity of the machine. Their SEM and EDX results show that the enhancement might be due to extremely thin laminated structure, allowing the graphene to easily enter the contact area. Micro-tribological studies by Ou et al (Ou et al., 2010) showed that the reduced graphene oxide possesses good friction reduction and antiwear ability. They attributed the enhancement to graphene's intrinsic

structure and self-lubricating property. Lee et al (Lee et al., 2010) demonstrated that when the thickness of graphene is decreased, the friction monotonically increases. It was similar to other nanomaterials such as niobium diselenide, hexagonal boron nitride and molybdenum sulfide. The results further suggest that the trend arises from the thinner sheets' increased susceptibility to out-of-plane elastic deformation which could be a universal characteristic of nanoscale friction for atomically thin materials weakly bound to substrates. On the other hand, grease containing alternately stacked single graphene sheets and a C60 monolayer showed that the intercalated C60 molecules can rotate in between single graphene sheets (Miura and Ishikawa, 2010). Miura et al (Miura and Ishikawa, 2010), claimed that the grease with this graphene was providing better lubricating performance than all the other existing additives. Moreover atomic force microscopy (AFM) based friction studies of graphene substrates have been instrumental in explaining various possible mechanisms (Smolyanitsky et al., 2012, Deng et al., 2012, Lee et al., 2010, Berman et al., 2014a). Electron-phonon coupling (Filleter et al., 2009), puckering effect (Lee et al., 2010) and interplay of surface attractive forces (Hyunsoo et al., 2009) in graphene have major role in reducing friction. Although there seems to be unanimous agreement on graphene's role in enhancing the anti-friction and anti-wear properties of lubricants, the approach to underlying mechanisms are diverse. Whether only one tribo-morphological phenomenon responsible for the tribological enhancements as indicated by the existing reports is questioned? Or a culmination of various mechanisms when the nature of graphene is polydispersed?

Based on the experimental observations and review of the existing literature, it was understood that the occurrence of several morphological transformations of graphene simultaneously or subsequently could be the key. Large variation in flake size exists when graphene is synthesized and dispersed in fluids using sonication techniques (Chew et al., 2010, Zhang et al., 2015). Therefore graphene based suspension should be a poly dispersed graphene-oil mixture (Dhar et al., 2013c). Small flakes could easily deposit in the valleys and prevent the deepening of the same. Large flakes could provide coating effect by sliding, buckling, bending or by turning into semi tubes as the shear forces act on them. Furthermore, since the shape and size of the peaks and ridges of the tribological surfaces differ considerably, the amount of resulting shear forces would be different. As a result different tribological phenomenon could transpire simultaneously. Graphene slides between the contacts (Eswaraiah et al., 2011) especially during mixed and hydrodynamic lubrication thereby furthering the formation of a protective film (Lin et al., 2011) could be mainly possible due to its planar structure. SEM images show that the graphene is deposited in valleys and ridges, Figure 4.20. EDX analysis further confirmed high carbon deposition in wear tracks.
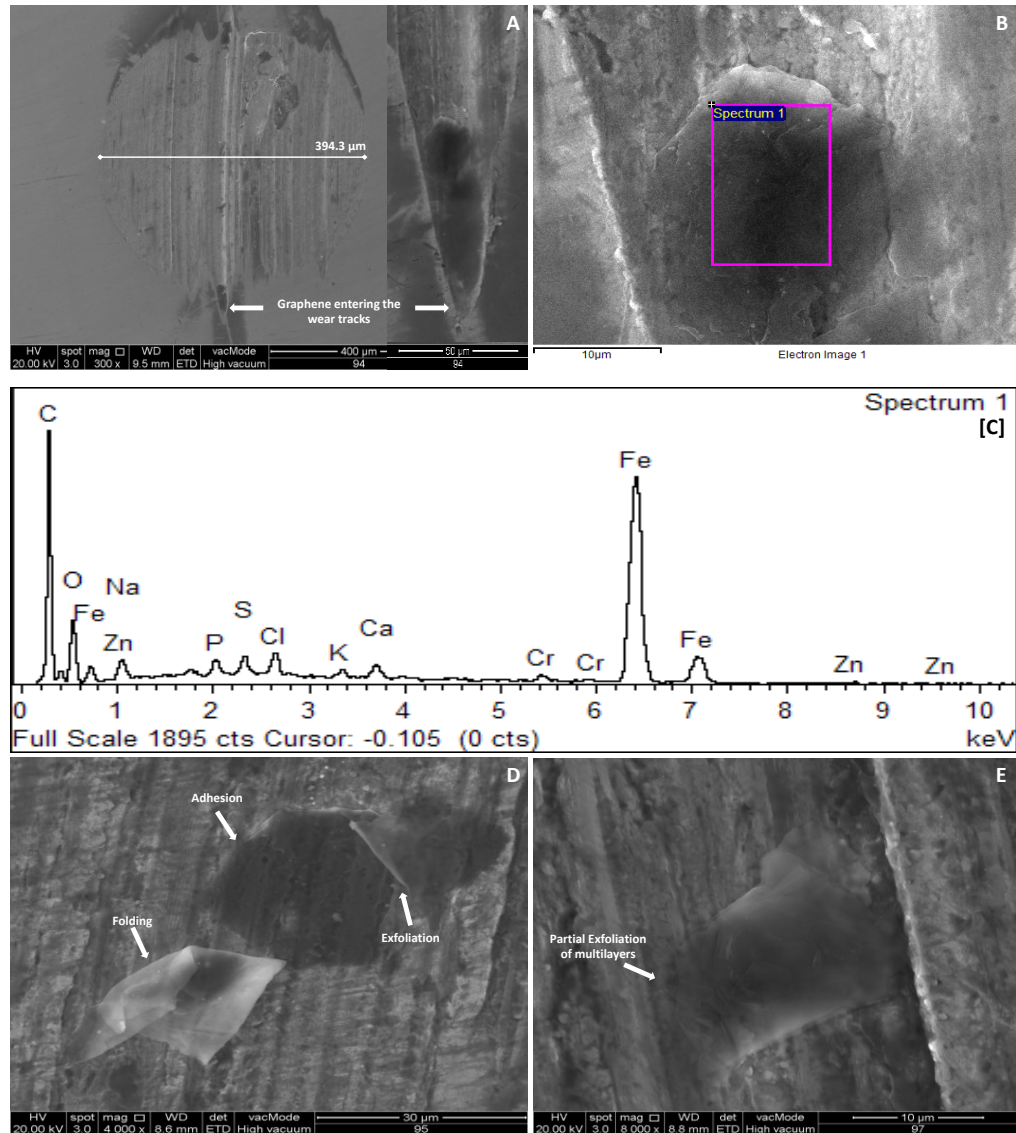
Figure 4.20. A - Graphene flakes sliding through the scars tracks; B - Graphene deposited in valleys of steel ball; C - EDX graph corresponding to B; D - Folded, twisted, adhered and exfoliated graphene sheet on wear track; E - partially exfoliated graphene sheets deposited in the wear tracks;

Also found sliding of flakes through the propagating wear tracks to be the primary reason for graphene's deposition in the wear tracks, Figure 4.19A. While the graphene slides through the contacts, the interplay of surface attractive forces could be more pronounced (Hyunsoo et al., 2009). In several scar areas adhesion of single layer graphene sheets in addition to ruptured

flakes could be found, Figure 4.20B. It is also interesting to find some multi layered graphene flakes in the contact areas having bent layers and buckled morphology, Figure 4.20D. It is because at the inner surface between flakes, the stress is compressive in nature, which leads to local shear and buckling of the layers (Dikin et al., 2007). Shenoy et al., (Shenoy et al., 2008) showed that the edge stresses can contribute to warping and rippling of graphene sheets, which could deform the bulk sheet due to the reduction of the edge energy. They also observed that the morphology of the warped sheets depends strongly on graphene sizes and shapes besides the magnitude of the edge stresses. Although the thermal performance of bent sheets are not compromised (Yang et al., 2013), the tribological performance is a concern. When the sheets are bent or twisted it will observe more stress compared to a planar flake. There are contradicting views on the effects of ruptured graphene tribology. High contact pressures (≈0.5 GPa) do not deter graphene from protecting the specimen from wear (Berman et al., 2014a). It was predicted that the extraordinary wear performance originates from hydrogen passivation of the dangling bonds in a ruptured graphene, leading to significant stability and longer lifetime of the graphene protection layer (Berman et al., 2014a). Furthermore, Figure 4.20D shows the evidence of folding, adhesion, twisting and exfoliation of graphene taking place simultaneously. Such observations were also made in many other locations of the wear tracks. Suggesting the fact that many tribo-morphological phenomenon simultaneously augment the anti-wear and anit-friction behaviour of the lubricants. However, further research is needed to determine the sequence of such phenomenon and their intensities by considering all possible factors.

4.6.1.2. **Morphological transformation of graphene in used oil**

Engine operation is a complex process involving high shear forces, temperatures, pressure and various lubrication regimes. Engine oil is expected to withstand such extreme conditions for a prolonged period and offer good performance. Graphene, a stack of carbon layers are together due to Van der Waals forces. Graphene in the oil has a strong potential to get exfoliated and even rupture due to engine operation. Figure 5.8 is the optical microscope images showing graphene particles present in the oil before and after 100 hours of engine operation respectively. The graphene's structure has transformed significantly after the engine operation as shown in the Figure 5.8 C-D. The formation of graphene tube and ruptured flakes are clearly evident. Partial stacking of graphene is witnessed in the used oil (Figure 5.8 C). Though graphene's exfoliation is generally due to various forces including shear and forces acting normal to the flakes, the microscopic observation suggest that the exfoliation in oil could be predominantly due to the shear forces. Liquid phase exfoliation (LPE) is known to happen due to sonication, heating and centrifugation. Similarly the graphene nanolubricant experiences high temperatures and pressures in the engine which could cause exfoliation. Smaller net energies cause such exfoliation, and the energy balance for the graphene and oil can be expressed as the enthalpy of mixing per unit volume,

$$\frac{\Delta H_{mix}}{V_{mix}} \approx \frac{2}{T_{flake}}\left(\delta_G - \delta_{sol}\right)^2 \phi \qquad (4.9)$$

Where T_{flake} is the thickness of a graphene flake, ϕ is the graphene volume fraction, δ is the square root is the square root of the surface energy of phase

graphene or solvent which is defined as the energy per unit area required to overcome the van der Waals forces when peeling two sheets apart. Moreover the large presence of ruptured flakes could be due to the fragmentation as a result of flakes collision during turbulence and flow thru channels. Edge collisions are expected to happen when the flakes flow near the boundaries and hit the engine components. Random collisions between the flakes can also result in fragmentation of large flakes. Similarly the wear particles from the engine components can assist in mechanical exfoliation. Sharp wedges can pears thru the layers interface or the compressive stress exerted normal to the flake can cause exfoliation and fragmentation. According to the theory of stress waves, once the compressive wave spreads to the free interface of multilayer graphene, a tensile stress wave will be reflected back to the body. In addition to exfoliation, rolling and entangling of graphene seems to be prominent as shown in the figures 5.8 C- 5.8 D respectively. It is propounded that the twisted graphene flakes might be devoid of sliding through the contact areas or piston rings due to its non-planar structure. Hence it could be found suspended in the oil sump contributing to the heat transfer rate. Moreover, when the shear forces overcome the bending stiffness of graphene, the flakes get further twisted and eventually become tubes as shown in Figure 5.8 C. Formation of too many tube like graphene could result in their entanglement as shown in the Figure 5.8 D. The entanglement of large flakes would keep them from taking part in tribological activity. Rather such flakes would be improving the thermal conductivity of the oil in the engine sump. It is noteworthy that the entangled graphene flakes could act similar to percolation network which is one of the major contributors in the enhanced thermal

conductivity effect of nanolubricants. This phenomenon could be further validated from our previous report whereby entangled flakes were not seen on the contact surfaces including the piston rings. The fragmented graphene flakes assisted by Brownian motion enhances the thermal conductivity further.

Due to extreme dynamic mechanical and tribological loads, piston rings tend to wear out even in the presence of good lubricants. Such loads necessitates the use of materials with high strength particularly at temperatures of 200-300°C capable of withstanding the elastic range, thermal expansion and bending. Piston rings are made of cast iron alloys. Flakes with high bending stiffness can be detrimental, to engine components especially piston rings, when used as additives in lubricants. Multilayer graphene used in the present experiments contain approximately 30 layers making the flakes rigid with high bending stiffness. It causes higher wear compared to base oil without graphene. The piston rings might be largely affected as the ICP analysis (Table 5.3) has detected the worn out materials particularly from the piston ring. The addition of few layer graphene G12 significantly lowers the engine wear. The detected materials including iron and chromium are significantly low in the oil containing G12. Hence G12 is found to be a potential additive in terms of enhancing both the thermal properties and anti-wear properties of the base oil. Although adding G60 could be detrimental to the engine components, it can significantly enhance the thermal properties of the oil.
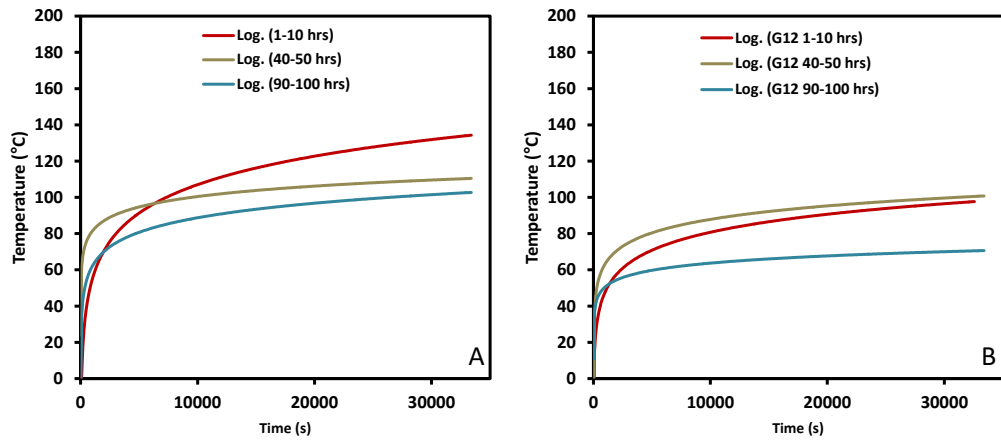
Figure 4.21. Temperature recorded at the crank case of IC engine in the presence of [A] API SN/CF+G60+Additive; [B] API SN/CF+G12+Additive.

.

Figure 4.21 A and B is the logarithmic trend of the temperature recorded with respect to time during 100 hours operation of IC engine in the presence of API SN/CF+G60+Additive and API SN/CF+G60+Additive respectively. The data clearly shows that the rate of hear transfer significantly increases from the initial 10 hours to the final 10 hours. This enhancement in the heat transfer rate could be because of the accumulation of entangled graphene flakes besides the relatively small flakes in the oil. It could also be propounded that the exfoliation of G60 in the engine oil is directly proportional to entanglement of graphene. Thus contributing to the overall heat transfer rate. Future research is essential to delineate the quantum of exfoliation due to various engine lubrication regimes, oil flows and conditions. It is also vital to further understand the different stages of lubricant depletion with respect to graphene's morphological transformation.

4.7. Summary

This chapter discusses the characterization of nanolubricants formulated using graphene nanoflakes and engine oil meeting API 20W50 SN/CF and API 20W50 SJ/CF specifications. Both the nanoflakes and the oil formulation are characterised using several analytical methods such as FTIR, XRD, FESEM, EDX, TGA, zeta potential and nanoparticle tracking analysis. By adding 0.01 wt% of 60 nm graphene and 1% lubricity additive to API 20W50 SN/CF oil, 21% and 23% enhancement in the coefficient of friction (μ) and thermal conductivity (k) at 80$°C$ respectively was observed. 12 nm graphene enhanced μ of the oil without lubricity additive by approximately 7%, whereas 8 nm and 60 nm had little or no enhancement. Scanning electron microscopy and Energy-dispersive X-ray spectroscopy analysis suggest that the single or very few layer graphene and multilayer graphene has the disadvantage of puckering, rupture and bending stiffness. Based on our experimental findings and review of existing literature, it is understood that the existing nano-scale tribology mechanisms cannot be isolated while explaining the underlying physics; rather multiple tribological phenomenon should be considered simultaneously or subsequently.

CHAPTER 5.   RESULTS: PERFORMANCE OF GRAPHENE NANOLUBRICANT IN AN IC ENGINE

5.1.   Introduction

It is well known that several factors determine the complex heat transfer performance of a lubricant in an IC engine. Thermal conductivity and film thickness of the lubricant between piston-cylinder are crucial for both conduction and convection (Harigaya et al., 2004). In the presence of 0.01 wt% G60, the thermal conductivity of API SN/CF 20W50 was found to enhance by 23% at $80°C$. This enhancement is a function of graphene flake thickness, concentration and temperature. Polydispersity of graphene allows graphene to augment thermal conductivity of oil by Brownian motion, flake clustering, liquid layering and particle interaction (Li et al., 2013, Dhar et al., 2013b). Dhar et al (2013) suggests that the small graphene flakes assist heat conduction through Brownian motion induced sheet dynamics and the large sheets form percolation network or matrix of graphene to fast conduct heat (Dhar et al., 2013b). However, when the lubricant reaches the gap between piston-cylinder the percolation and Brownian motion related effects might weaken. Though boundary lubrication conditions exist during piston-cylinder action, trailing edge of the ring leaves a lubricant film which acts as a potential convective medium. A highly conducting oil layer around graphene might further augment the enhancement effect so long as the film's thickness is significant. Hence the major reason for heat transfer between piston-cylinder could be mainly due to combined thermal conductivity effect of graphene-oil and direct conduction between asperities of piston-cylinder and graphene. The

thermal conductivity effect of graphene nanolubricant can be simply calculated using a modified Maxwell (Maxwell, 1873) expression,

$$k_{eff}^{\cdot} = \frac{k_G + (\psi - 1)k_b + (\psi - 1)\phi_{eff}(k_G - k_b)}{k_G + (\psi - 1)k_b - \phi_{eff}(k_G - k_b)} k_b \qquad (5.1)$$

where k_G is the thermal conductivity of graphene flake, k_b is the thermal conductivity of base oil, ϕ_{eff} is the volume fraction, expressed as,

$$\phi_{eff} = (1 + \frac{t}{r_G})^3 \phi \qquad (5.2)$$

r_G is the average radius graphene flake, t is thickness of the liquid layer based on Langmuir theory,

$$t = \frac{1}{\sqrt{3}} \left(\frac{4M}{\rho_b N_A} \right)^{1/3} \qquad (5.3)$$

where M is the molecular weight of the liquid on the solid interface, ρ_b is the density of base liquid, N_A is Avogadro's constant and ψ is the shape factor for graphene when it is considered as a disk,

$$\psi = \frac{2\pi d^2 + 2\pi r_G t}{4\pi \left(\left(\frac{3}{4} \right)^{\frac{2}{3}} r_G^{4/3} t^{2/3} \right)} \qquad (5.4)$$

where r_G is the average radius of the graphene and t is the thickness of the flake. Figure 5.1B shows that the graphene flakes have adhered to the piston

ring surface which could pave way for heat conduction through direct contact between piston ring surface-graphene-cylinder. Assuming a steady quasi-one-dimensional heat flow condition where the temperature depends only on a single coordinate (r), the rate of heat transfer for piston-cylinder geometry (Figure 5.1A) can be determined using equation (1),

$$\dot{Q} = \left[\frac{T_{\infty 1} - T_{\infty 2}}{\dfrac{1}{h_{GN1} 2\pi r_1 L} + \dfrac{1}{h_{GN1} 2\pi r_2 L} + \dfrac{\ln(r_3 / r_2)}{k_3 2\pi r_3 L} + \dfrac{1}{h_2 2\pi r_3 L}} \right] \tag{5.5}$$

where $\dot{Q}$ is rate of hear transfer and h_{GN1} is the heat transfer coefficient of graphene nanolubricant.
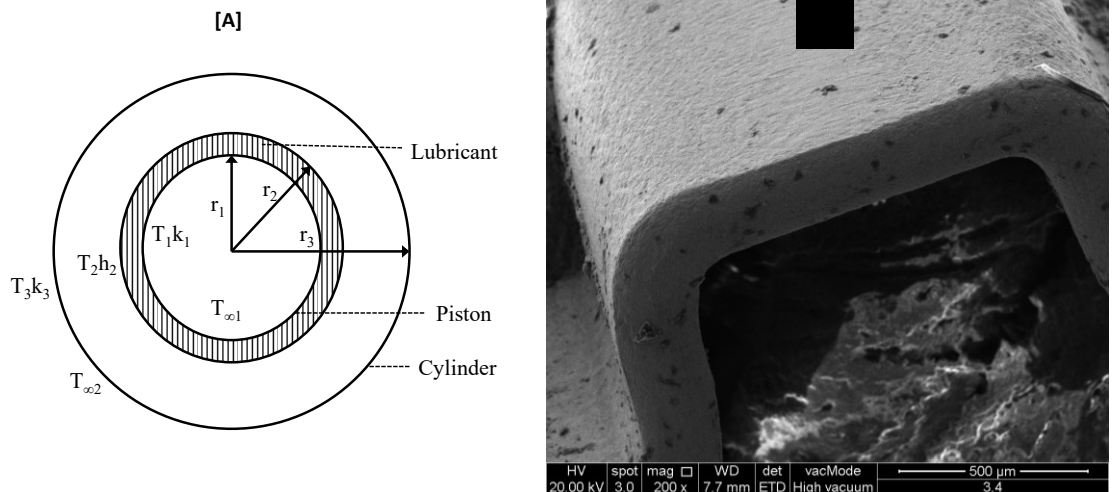
Figure 5.1. A - Piston-lubricant-cylinder geometry; B – Graphene flakes deposited over oil ring surface;

The temperatures recorded at the spark plug, cylinder and the crankcase clearly show that the heat transfer rate in the presence of graphene based oil is significantly high as shown in Figure 5.2. An enhancement in heat transfer rate of 70.6%, 71.4% and 80.0% was observed at the spark plug, cylinder and crankcase respectively for G60 with SN/CF.
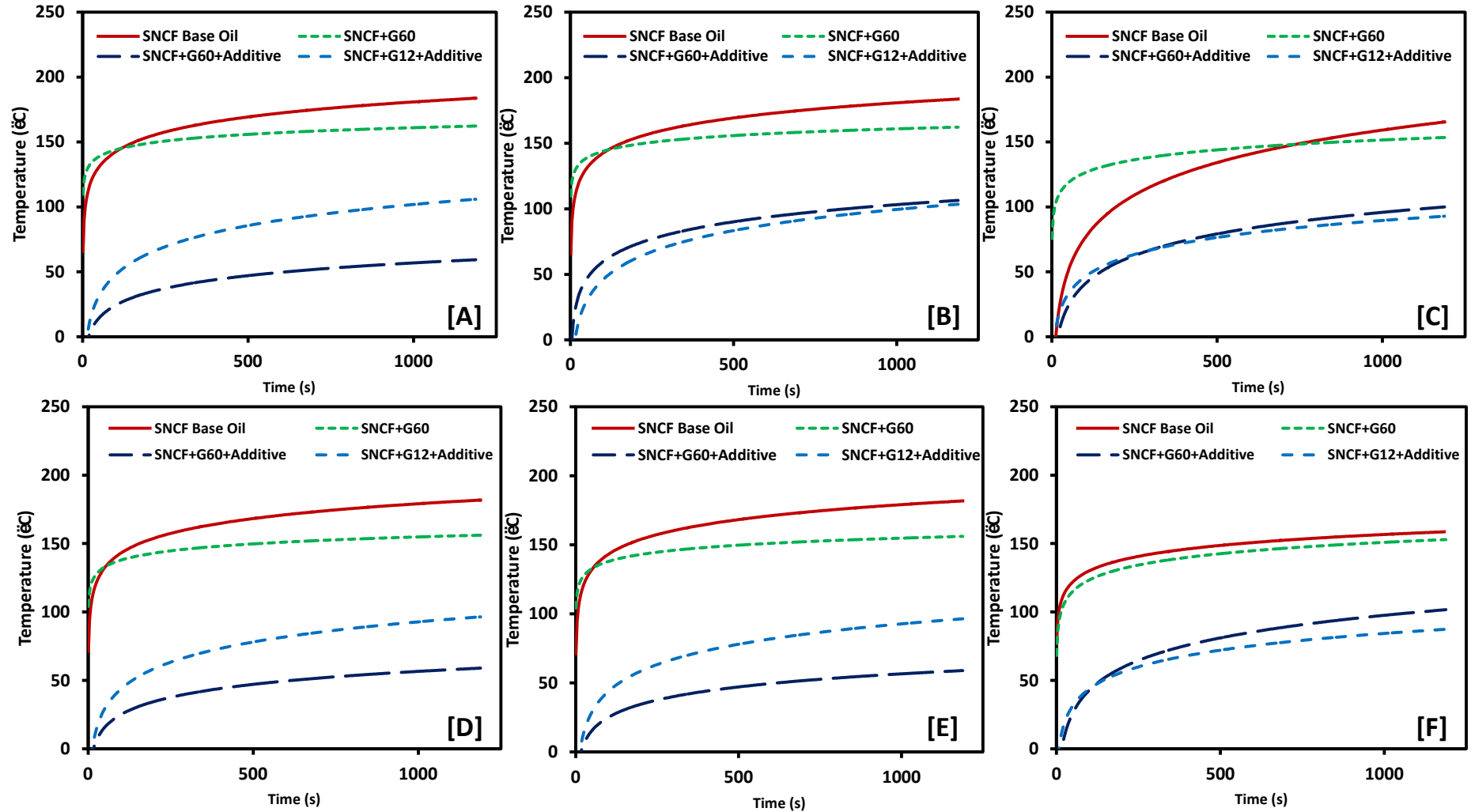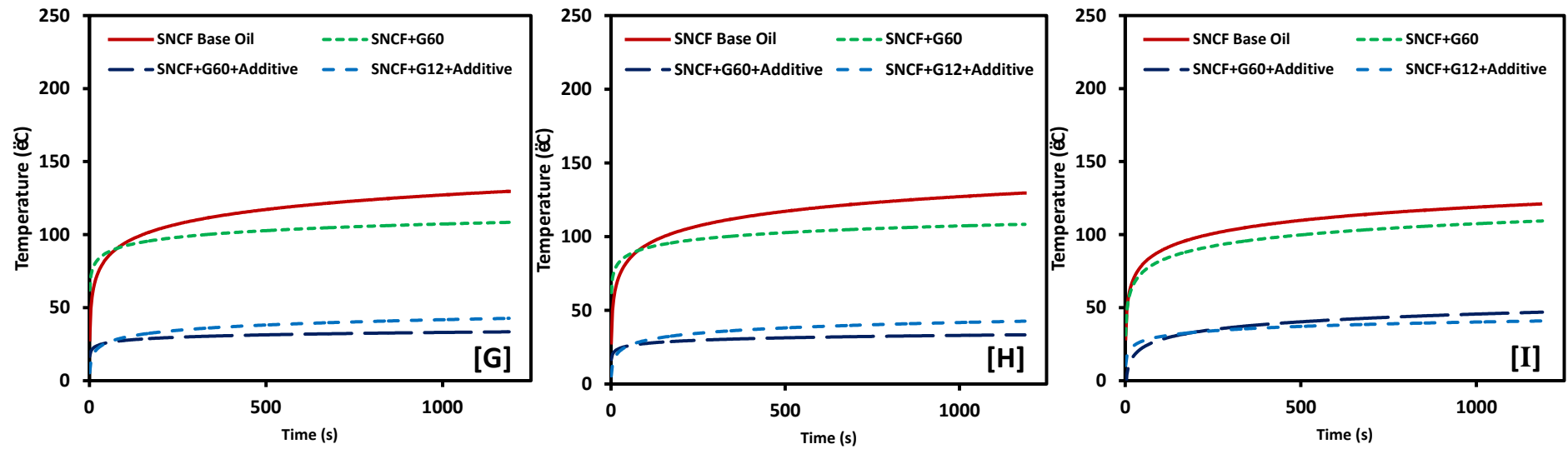
Figure 5.2. Temperature recorded at sparkplug [A-C], cylinder [D-F] and crankcase [G-I] after 30, 60 and 90 hours operation.

Although G60 based oil seems better in the early hours of operation, there is a clear indication that both G60 and G12 based oils perform the same as the oil ages. The accumulation of combustion products and wear debris in the oil degrades the additives present in it. Hence the oxidation onset temperature is nearly the same for the oil samples with and without graphene as shown in Figure 5.6. The difference between G60 with and without additive also shows the significance of suspension's stability in the enhancement of both thermal and tribological performance.

5.2. Piston-ring tribology

The 4-ball tribometer test results indicate that the addition of graphene has significant enhancement in the anti-friction property of the lubricant as shown in section 4.6, Table 4.4. An enhancement of 7.14% and 19.04% was observed in the coefficient of friction (μ) of 20W50 SN/CF and 20W50 SJ/CF, respectively. The addition of natural polymeric ester, a lubricity additive in 20W50 SN/CF oil with the same graphene concentration increased the enhancement to ~21%. It is due to the fact that the lubricity additive helps graphene remain in between contact areas due to increased stability, Figure 5.3A, B. This is evident from the EDX analysis which confirms graphene's presence on the surfaces comparatively higher than the oil samples that doesn't contain lubricity additive, Figure 5.3C.
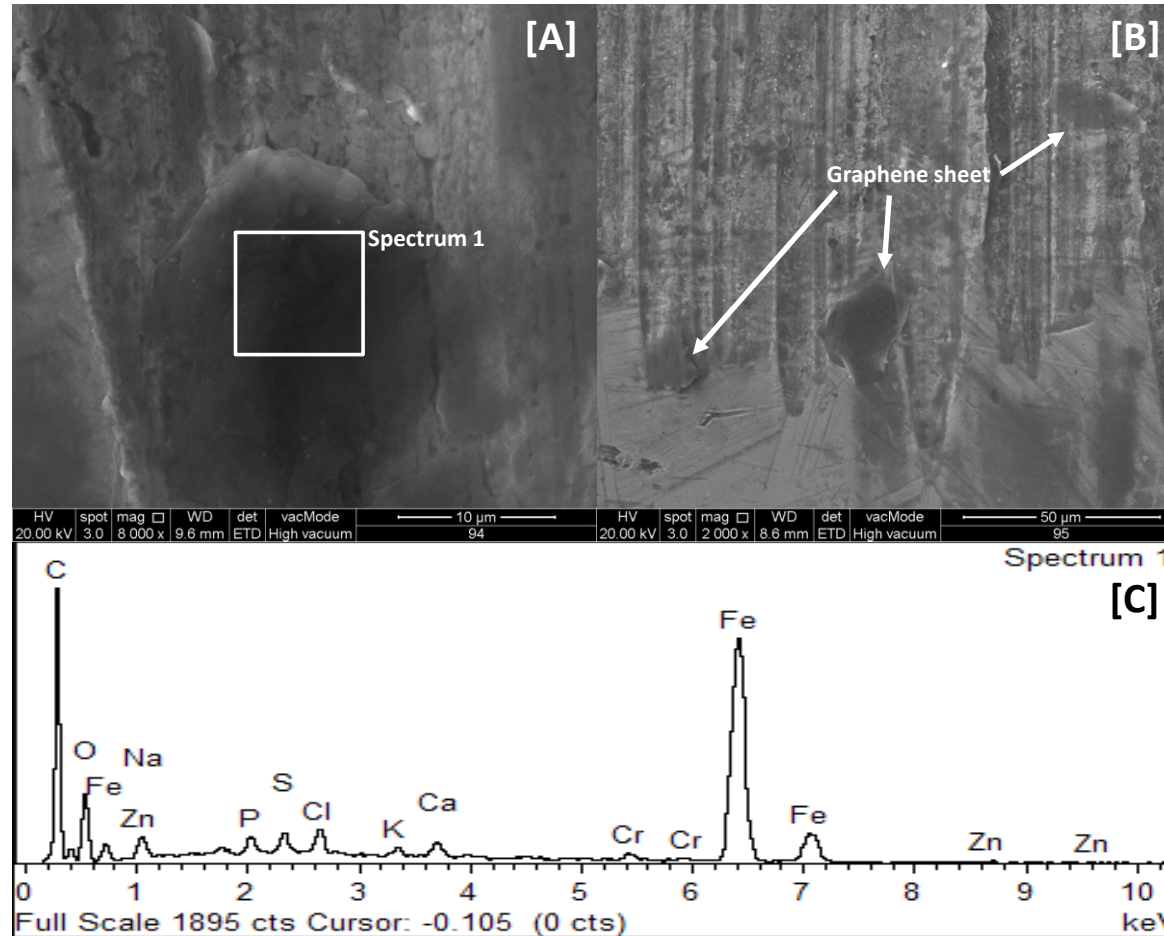
Figure 5.3. 4-ball wear scar having graphene flakes adhered on its surface due to natural polymeric ester based lubricity additive. A – API SN/CF 20W50 + G60 + additive; B – API SJ/CF 20W50 + G60 + additive; C – Corresponding EDX graphene of [A];

Similarly, the piston rings obtained after 100 hours of engine operation show anti-wear behaviour of graphene nanolubricant. The top compression ring is primarily expected to seal the combustion gasses and act as a heat transfer bridge between piston and cylinder wall. Boundary lubrication condition exists at this interface where the graphene present in oil could contact the asperities. It is hard to ascertain the level of wear in the top rings of SNCF base oil and SNCF+G60 by using the SEM images, Figure 5.4A-C. However, it is clear that there is significant improvement in anti-wear property of oil by using graphene 60 nm with the lubricity additive. In 4-ball test it has been found that G60 might counter the enhancement effect. It could be due to the bending rigidity of multilayer graphene which results its interlayer shear deformation (Chen et al., 2015). Bending rigidity of multilayer graphene is influenced by the interlayer shear interaction and the number of graphene layers (N). Based on classical continuum mechanics theories, it is found that the physical properties including bending rigidity of graphene will be influenced significantly by its interlayer shear rigidity (Chen et al., 2015). Hence the multilayer graphene has more potential to impart higher momentum on the microscopic contacts thereby causing friction. Second or lower compression ring aids the top ring but it does not encounter harshest conditions with respect to thermal and mechanical loading as the top ring. Figure 5.4D shows that the SLG has adhered to the surface of the lower compression piston-ring when SNCF+G60 was used. The presence of graphene was confirmed with EDX analysis. The surface of rings from nanolubricant samples appear with relatively less wear and few deep ridges. Multilayer graphene has exfoliated and adhered to ring surface due to very high shear stress acting on the

lubricant subjected to boundary lubrication (Paton et al., 2014, Chen et al., 2012). The addition of lubricity additive retains the film thickness and thereby graphene keeps its multilayers. Furthermore, folded and morphed graphene flakes are found on the wear tracks of additive based G60 sample. Folded graphene has higher compressive strength and strain compared to planar graphene (Yongping et al., 2011). Owing to relatively low bending stiffness, the sheets could also possess buckling effect and sometimes might behave as rollers.
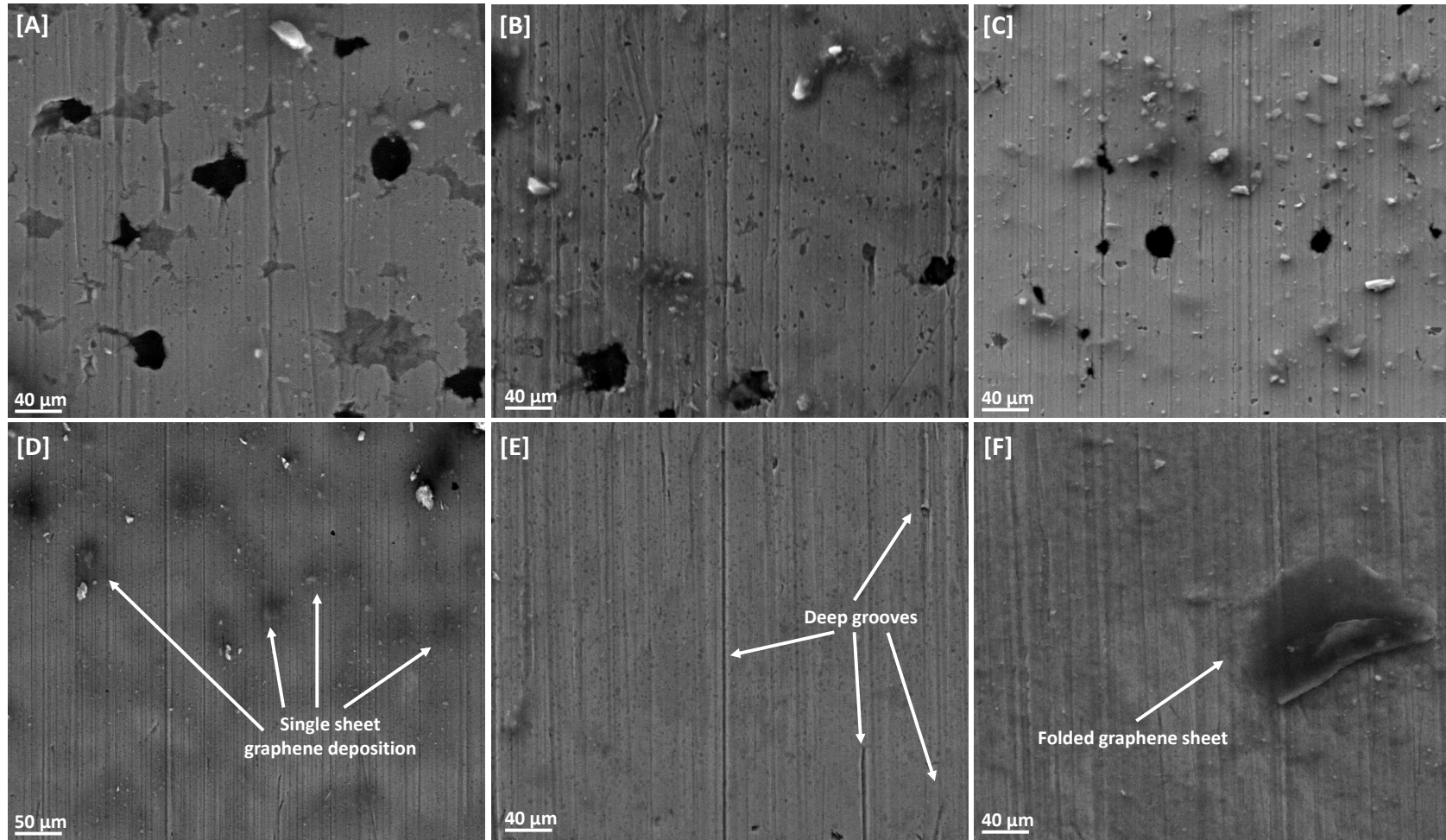
Figure 5.4. Top (A,B,C) and second (D,E,F) compression rings after 100 hours of engine operation. [A,D] - SNCF+G60; [B,E] - SNCF Base oil; [C,F] - SNCF+G60+Additive;

5.3. Used oil analysis

5.3.1.1. FTIR of used oil

The bands observed in the FTIR spectrum (Figure 5.5) of the used engine oil and their corresponding combustion products, presence and depletion of additives is listed Table 5.1. The additives components were identified using the FTIR system database and literature. The degree of oxidation and the depletion of various additives is significantly low in case of nanolubricants. Furthermore, the anti-oxidation and anti-depletion effect of graphene is clearly graphene flake size dependent. However, the depletion of phenol inhibitors is considerably high in the presence of graphene. During phenol inhibition, free-radicals that cause oxidation are neutralized. In addition, the oil containing natural polymeric ester based lubricity additive and graphene is susceptible to early depletion of its most additives compared to oil containing graphene only. Nevertheless, the lubricity additive in the engine oil can still be favourable compared to the original formulation.

Table 5.1. FTIR observations

Wavenumber cm^{-1}	Observed element/reaction
3648 cm^{-1}	Phenolic antioxidant
2924 cm^{-1}	C-H stretching
2350 cm^{-1}	C-O stretching
1773 cm^{-1}, 1704 cm^{-1}, 1366 cm^{-1}	Succinimide dispersant
1714 cm^{-1}	Carbonyl
1494 cm^{-1}	Detergent's carbonate
1460 cm^{-1}	CH$_2$ scissoring
1376 cm^{-1}	Symmetric bending of CH$_3$
1169 cm^{-1}, 1158 cm^{-1}	Sulfonate detergent
1230 cm^{-1}	Succinimide Detergent
978 cm^{-1}, 654 cm^{-1}	Zinc dialyldithiophosphate - ZDDP
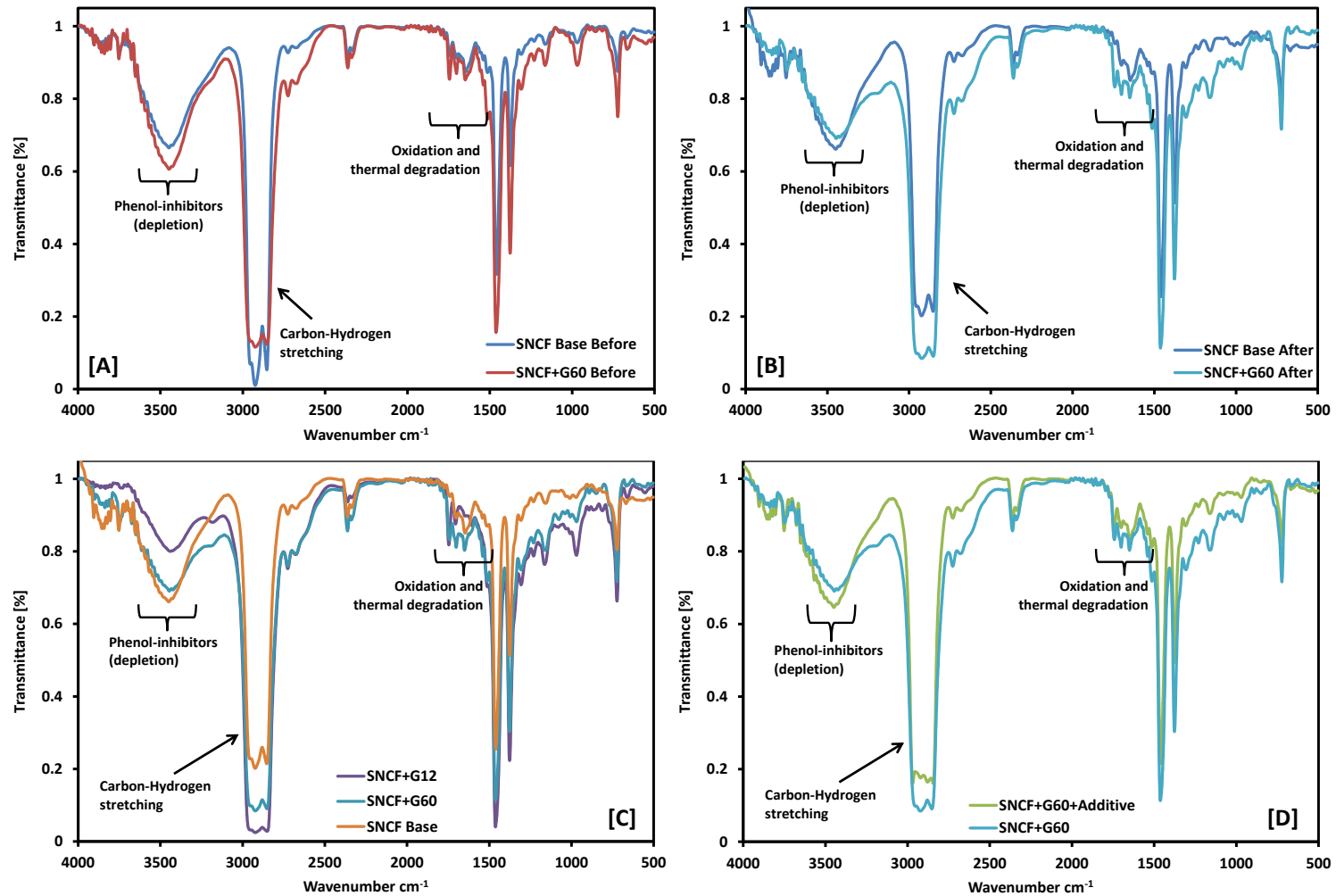
Figure 5.5. FTIR graphs; A – Fresh API SN/CF oil with and without graphene. B – Used API SN/CF oil with and without graphene. C - Used API SN/CF oil with 12 and 60 nm graphene. D - Used API SN/CF oil + graphene with and without lubricity additive.

Various ASTM based characterization show that the addition of graphene has both advantages and disadvantages, Table 5.2. However, G12 with the lubricity additive shows overall better performance. Total base number (TBN) being the acid-neutralizing capacity of the lubricant, was found to be highest in G12 based engine oil. Suggesting that the amounts of active additives in oil are more. Kinematic viscosity of the used oil typically increases due to the presence of contaminants or oxidation. It might also decrease due to the presence of fuel and SN/CF+G12 has both low flash point and low kinematic viscosity.

5.3.1.2. **TGA of used oil**

TGA and DTGA thermograms of used oil obtained after the operation of 100 hours is shown in Figure 5.6. Two distinct weight loss regimes from 150 to 380 °C and 380 to 470 °C are apparent from the TGA profiles of the used engine oils. Lehrle et al. (Lehrle et al., 2002) confirmed using mass spectrometric measurements that evaporation and degradation of hydrocarbons present in the low end of the molecular weight distribution happen in for the temperature range of 150 to 350 °C. Decomposition of long chain hydrocarbons take place in the second weight loss regime.
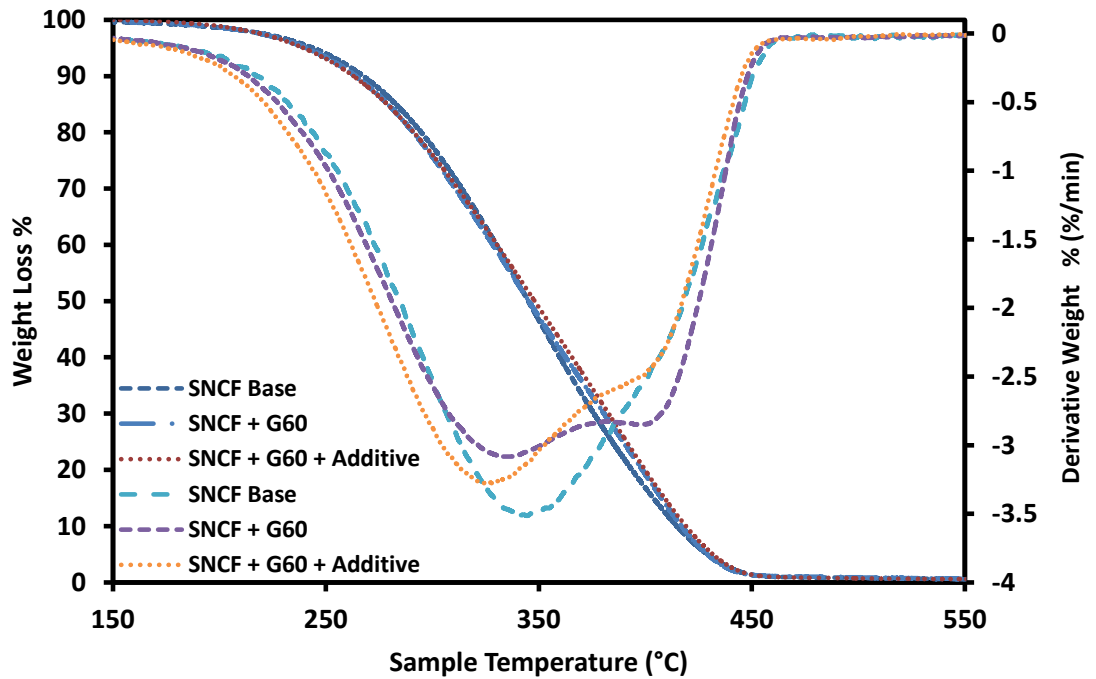
Figure 5.6. TGA and DTGA curves of used engine oil.

Comparatively higher derivative weight loss can be noticed for used engine oil without graphene. Nonetheless, the oxidative onset temperature of the used oil with and without graphene has negligible difference. It would have been interesting to see the difference between oils after periodic intervals but due to limitations of the experimental setup and limited oil sample, it was not achieved.

5.3.1.3. **Elemental analysis of used oil**

Similarly elemental analysis of used oil reveals that nickel (Ni), titanium (Ti), tin (Sn), vanadium (V) and silver (Ag) are of similar levels in both used oils with and without graphene, Table 5.3. Commonly scuffing on piston skirts as

it strokes repeatedly along the length of a cylinder leads to wear of aluminium (Al). Bearings and engine block also wears during engine operation which could contribute to the Al levels in used oil. Although aluminium level is comparatively higher in nanolubricants, magnesium (Mg), molybdenum (Mo), zinc (Zn) and iron (Fe) levels are significantly high in base oil without graphene. A number of engine components including cylinder head covers, rocker arm covers, valve covers, intake manifolds, air intake adaptors, induction systems, and accessory drive brackets are made using magnesium alloys. It appears that enormous wear has taken place due to friction in components other than piston ring and cylinder liner when base oil is used. It could be interesting to draw a contrast between oils before and after testing to estimate the presence of carbon levels. However, ICP based elemental analysis was limited to used oils only.

Table 5.2 Characteristic properties of the used oil samples

Test Characteristics	Test Method	SN/CF Base Oil	SNCF + G60	SN/CF+G60+ Additive	SN/CF+G12+ Additive
Appearance	Visual	Dark Brown Liquid	Dark Brown Liquid	Dark Brown Liquid	Dark Brown Liquid
Colour visual	ASTM D 1500	D.8.0	D.8.0	D.8.0	D.8.0
Flash point, COC, ºC	ASTM D 92	234	240	240	222
Density at 29.5ºC, gm/cc	ASTM D 1298	0.867	0.868	0.869	0.867
kinematic viscosity at 40ºC, cSt (mm^2/s)	ASTM D 445	157.20	157.40	168.20	142.10
kinematic viscosity at 100ºC, cSt (mm^2/s)	ASTM D445	17.71	18.56	18.97	17.21
Viscosity index	ASTM D 2270	124	133	128	132
Total Acid Number (TAN), mgKOH/gm	ASTM D 974	2.06	1.60	1.74	1.80
Total Base Number (TBN), mgKOH/gm	ASTM D 2896	7.04	7.75	7.58	8.41

Table 5.3 Elemental analysis of used engine oil by using inductively-coupled plasma (ICP) mass spectrometry ASTM D5185

Element detected	SN/CF Base Oil	SNCF + G60	SN/CF+ G60+Ad	SN/CF + G12
Aluminum (Al), ppm	13	31	28	21
Boron (B), ppm	75	3	< 1	1
Barium (Ba), ppm	1	1	1	< 1
Cacium (Ca), ppm	83	2383	2204	2089
Chromium (Cr), ppm	1	2	1	1
Copper (Cu), ppm	2	5	2	2
Iron (Fe), ppm	40	106	43	26
Magnesium(Mg), ppm	1283	21	22	30
Potassium (K), ppm	4	4	4	2
Molybdenum (Mo), ppm	99	42	41	40
Sodium (Na), ppm	6	14	5	3
Phosphorous (P), ppm	709	683	687	710
Lead (Pb), ppm	< 1	1	< 1	< 1
Silicon (Si), ppm	179	24	163	234
Zinc (Zn), ppm	841	821	794	826

5.4.   Viscosity of used oil

Figure 5.7 shows the viscosity and shear stress with respect to shear rate (1/s). The used engine oil after 100 hours operation continues to have Newtonian behaviour. The increase in viscosity of the used oil samples is <3%. It is known that the combustion products coupled with wear debris can increase the viscosity of used oil. Therefore, the anti-wear performance of oil is directly associated with the viscosity of engine oil. However, an increase of ~6% in viscosity of SNCF+G60 with lubricity additive is noticeable at 25°C, and ~9% at 105°C. It could be because of the show degradation of lubricity additive based oil sample compared to other oil samples.

Furthermore, morphological changes are noticed in graphene from used oil. The flakes have largely entangled and seem to have rolled into tubes as shown in Figure 5.8C-D. Graphene has the tendency to form tube like structure when subjected to twisting Kit et al. (2012). The pristine tube structure is formed after the flat sheets undergo buckling. Formulation of nanolubricant involves blending of graphene by means of stirring and sonication. Although sonicating could break large flakes, stirring could lead to buckling of graphene as shown in Figure 5.8A.
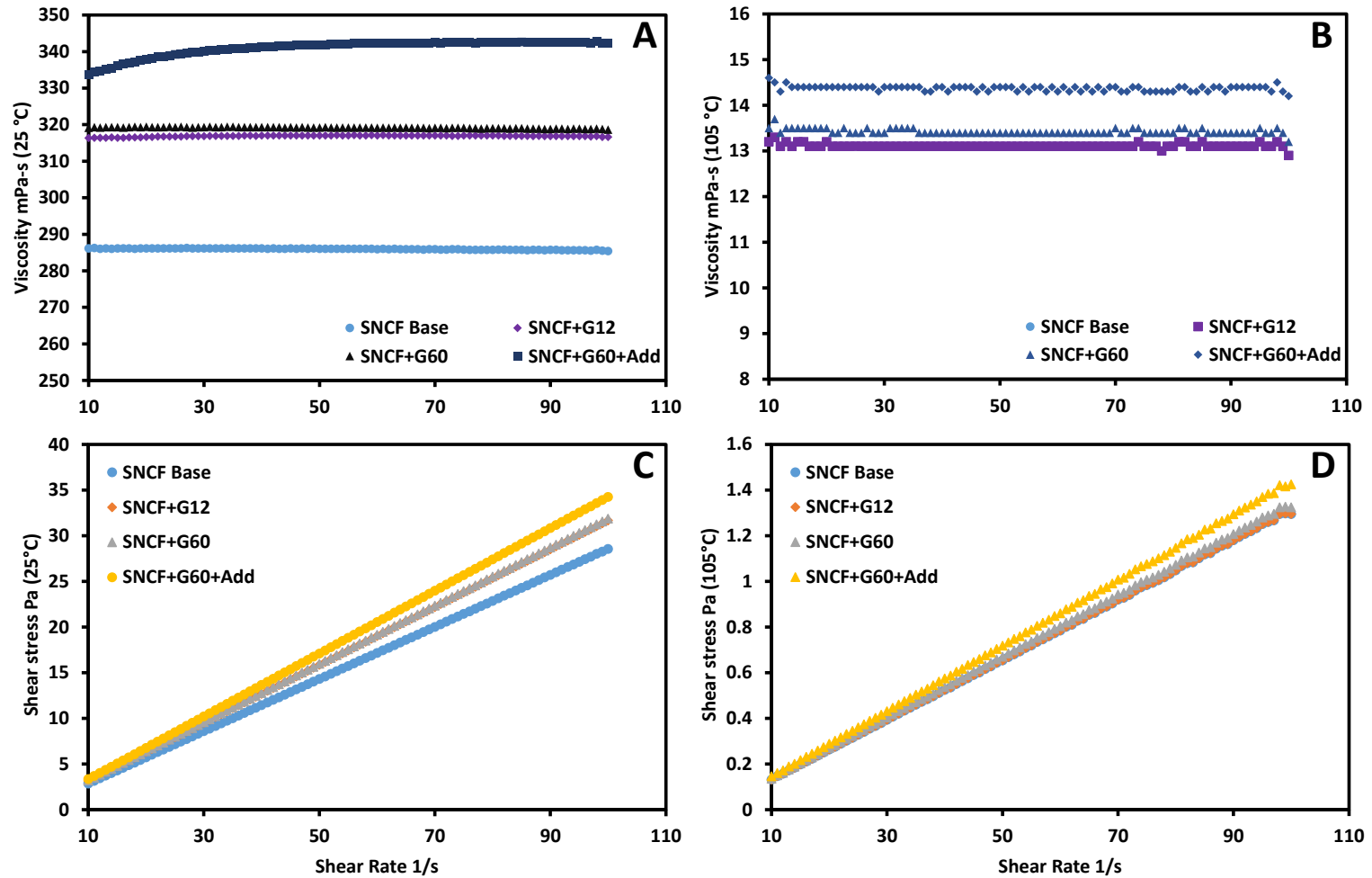
Figure 5.7. Viscosity vs shear rate at A-25°C and B-105°C; Shear stress vs shear rate at C-25°C and D-105°C;
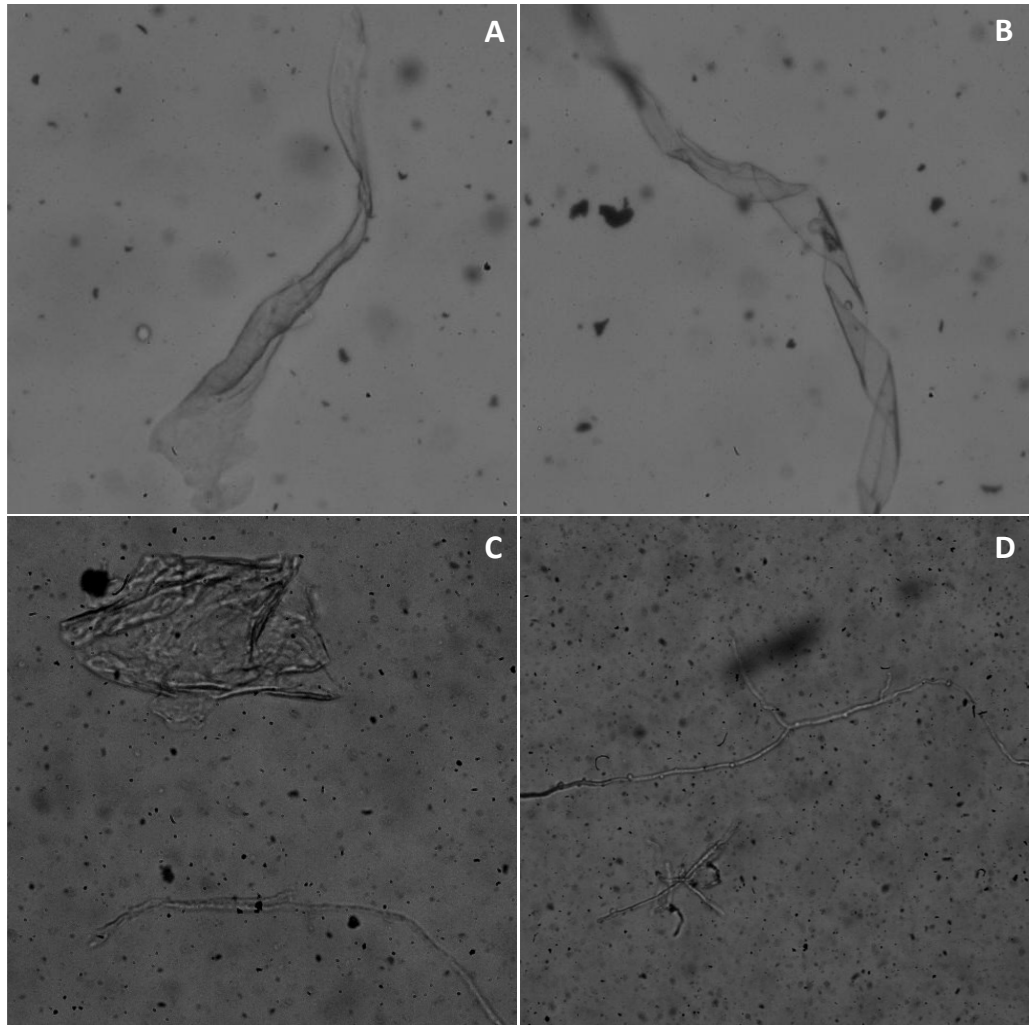
Figure 5.8. Graphene in oil before engine test, A - partially rolled, B – Twisted; Graphene in oil after engine test, C - Fulled rolled and partially exfoliated, D – Entangled;

It was noticed that a distinct transition from a twisted configuration to a helical (coil-like) configuration was a function of rotation and graphene layers (Steven and Markus, 2011). Hence the cause of many coil-like flakes in the used oil could be because of rotations. Furthermore, the flakes seem to have partially exfoliated (Figure 5.8C). Existing reports suggest that when graphene is subjected to shearing vortex fluidic films, it can exfoliate (Chen et al., 2012).

Similarly turbulent assisted shear forces can exfoliate graphene flakes (Paton et al., 2014).

5.5. Mechanism and discussion

SEM and EDX analyses of the piston rings suggest that many tribo-morphological phenomena such as rippling (Gallagher et al., 2016), puckering (Lee et al., 2010), bending (Chen et al., 2015), warping (Shenoy et al., 2008), buckling (Chen and Chrzan, 2011), chemisorption and physisorption (Kozlov et al., 2012), etc., could occur simultaneously or in combinations under specific operating conditions. Because of the non-uniform size distribution of graphene, it could involve in diverse physical interactions while encountering shear forces and varying temperatures. NTA reveals that the formulated oil has a wide range of graphene flakes with sizes <100 nm, >100 nm and >1000 nm. Sonication assisted lubricant blending operation ruptures large flakes (Chew et al., 2010, Zhang et al., 2015). Flakes having defects could further contribute to the increase of the ruptured flakes (Rajasekaran et al., 2016). The prominent flake size in the used oil after 100 hours engine operation is found to be 60 nm unlike the wide range of flake sizes in freshly prepared oil samples. This observation leads to the fact that the flakes <60 nm gets deposited or adsorbed into the valleys and ridges of the piston-cylinder assembly. It is reported that graphene has great tendencies for chemisorption and physisorption on metal surfaces (Kozlov et al., 2012). Further the studies on bi-layer and tri-layer graphene has weak physisorption on Al, Ag, Cu, Au, and Pt substrates (Zheng et al., 2013) and a strong chemisorption on Ti, Ni, and Co substrates. A stacking-insensitive

band gap is opened for the two uncontacted layers of TLG which could assist in exfoliation when shear forces act on top layers. Moreover the interplay of surface attractive forces are more pronounced (Hyunsoo et al., 2009) when flakes are between two surfaces. Deposition and adhesion of flakes on the surface of rings as shown in the Figure 5.9A and 5.5D is found on almost all piston rings. EDX analysis (Figure 5.9B) on the dark sites of the ring confirms the presence of transparent graphene sheets. Large flakes slide on the surface of the piston rings when shear forces act on them. The evidence of which is found in many piston ring surfaces (Figure 5.9-5.10). Nanoscale thickness helps it slide (Eswaraiah et al., 2011) between contacts and prevents deepening of grooves and wear tracks as it forms a protective film (Lin et al., 2011). In Figure 5.9A, graphene deposited in the groove track is bent inwards which indicates that the flake was pressed by the opposite surface in contact, preventing direct contact between asperities of piston and cylinder. Contact pressures as high as ~0.5 GPa does not prevent graphene from protecting the piston surface from wear (Berman et al., 2014a). Literature also suggests that the exceptional wear performance of graphene is suggested to have originated from hydrogen passivation of the dangling bonds in a ruptured graphene, leading to significant stability and longer lifetime of the graphene protection layer (Berman et al., 2014a).
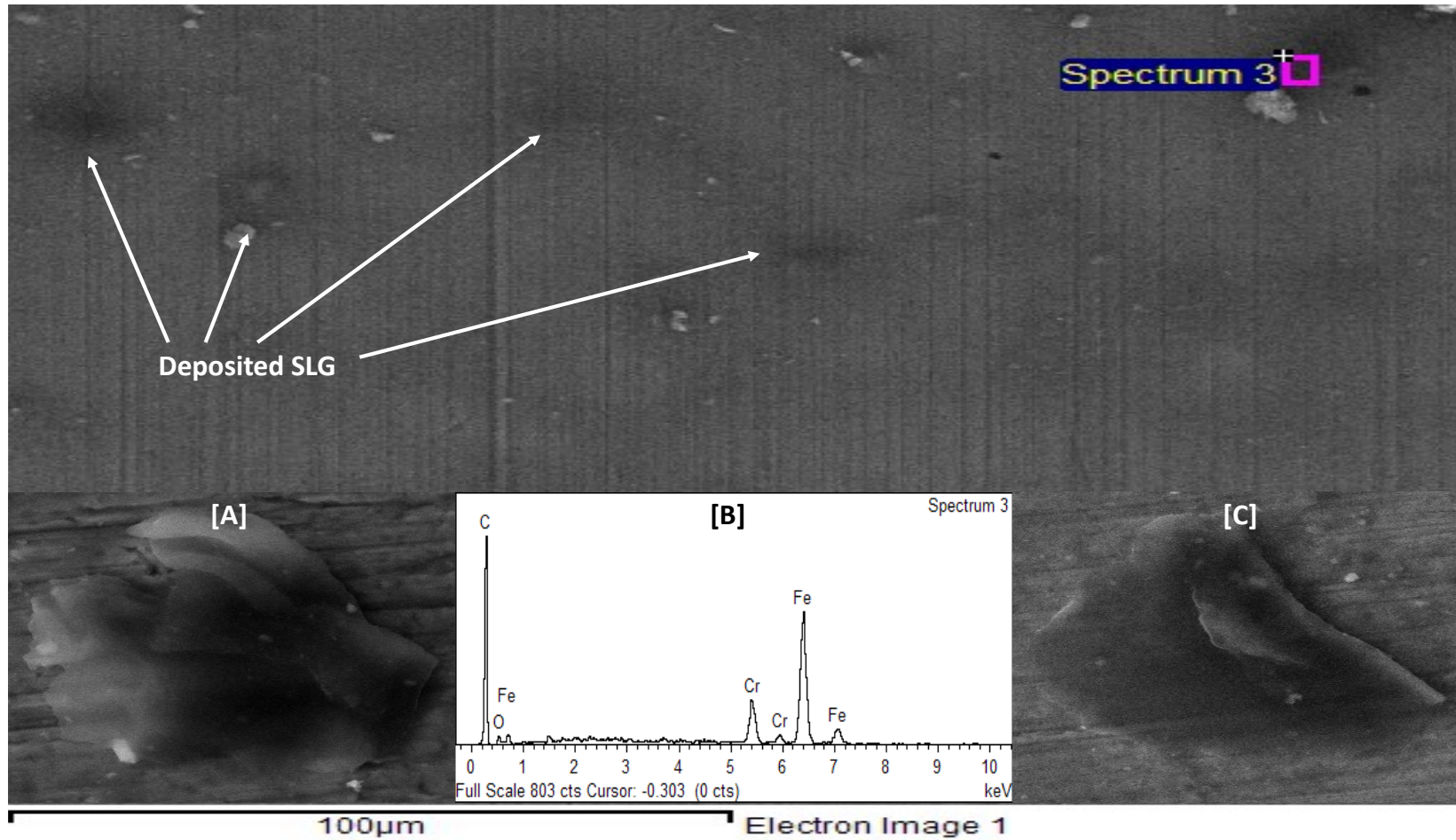
Figure 5.9. Transparent sheets of exfoliated graphene deposited on the surface of piston rings and cylinder. A – Entangled flakes near the deposited graphene site; B – EDX of dark areas on the piston surface indicating graphene; C – Folded graphene flake near the dark sites;

Results indicate that the anti-wear performance of the nanolubricant is graphene thickness i.e., number of layers dependent. While few layer graphene (G12) shows significant enhancement, multilayer graphene (60 nm) has negligible improvement or in some cases detrimental effects. The out-of-plane deformations in multilayer graphene when the tip from the asperities comes in contact increases friction (Reguzzoni et al., 2012). Though puckering (Lee et al., 2010) of graphene is primarily responsible for the increased friction, higher momentum imparted through the stiff flakes when the shear forces act on it could be another major factor (Wei et al., 2016). When few layer graphene (G12) is strongly bound to the ring surface or it is struck between asperities, the puckering effect will be suppressed (Li et al., 2010). Besides being able to slide between contacts easily, few layer graphene also has the advantage of shear driven exfoliation and warping as shown in Figure 5.10D. Many morphological changes of graphene due to shear forces (Paton et al., 2014) have the potential of offering better anti-friction effect. Multilayer graphene flakes in the contact areas have folded and buckled, as shown in Figure 5.9B. It is because at the inner surface between flakes, the stress is compressive in nature, which leads to local shear and buckling of the layers (Dikin et al., 2007). Some multilayer flakes as shown in Figure 5.10C retain its planar structure which might be due to the cross-linkages that reduces the buckling strain and the buckling force per unit length. Shenoy et al., (Shenoy et al., 2008) shows that the edge stresses can contribute to warping and rippling of graphene sheets, which could deform the bulk sheet due to the reduction of the edge energy. They also observe that the morphology of the warped sheets depends strongly on graphene sizes and shapes besides the magnitude of the

edge stresses. Although the thermal performance of bent sheets does not deteriorate (Yang et al., 2013), the tribological performance is has not been thoroughly investigated. When the sheets are bent, twisted or warped it could withstand higher impacts compared to a planar flake because the bending stiffness. However, over time the interfacial bonds weaken and the top layers will rupture. As the multilayer graphene continues to exfoliate it would gradually lose its anti-friction property. On the other hand, when puckering happens on a graphene flake, it increases the friction (Lee et al., 2010).
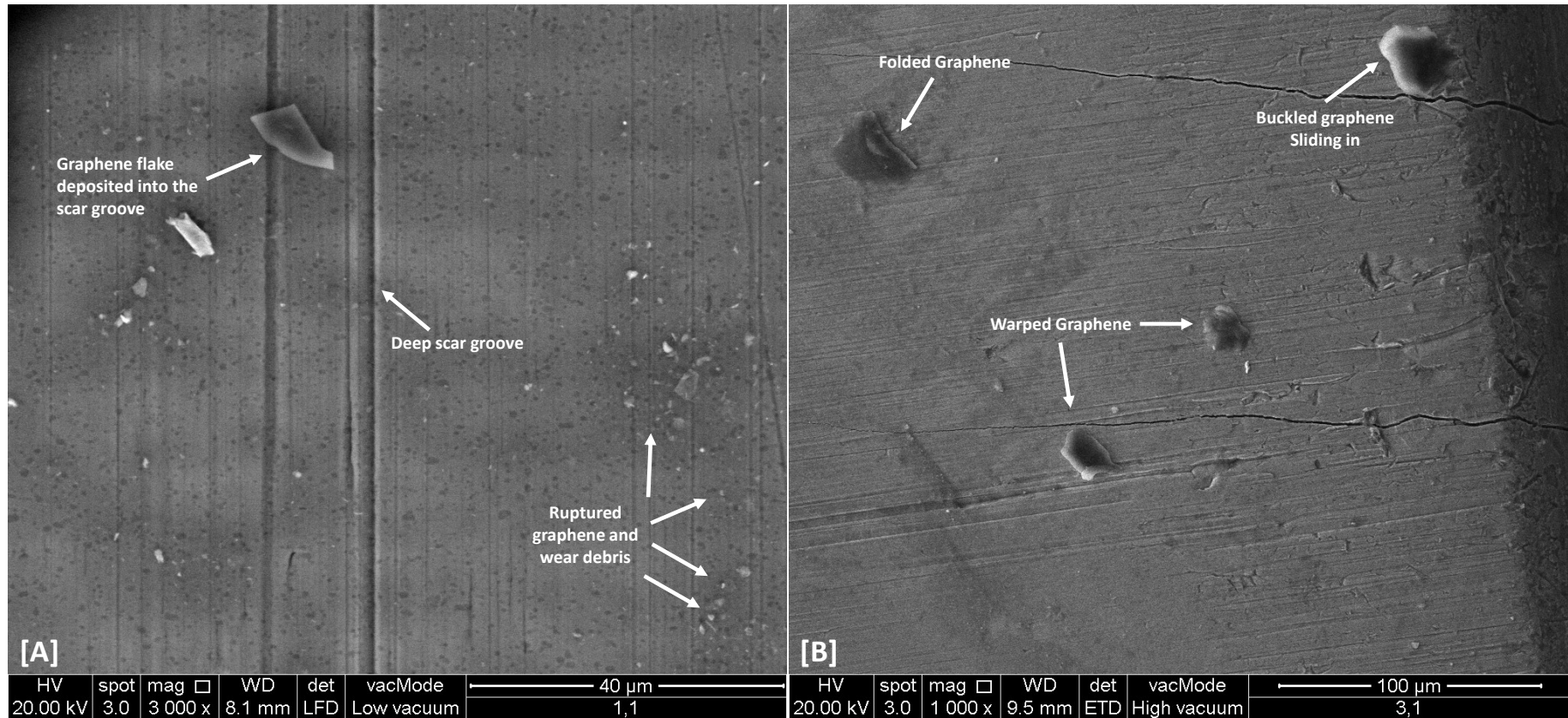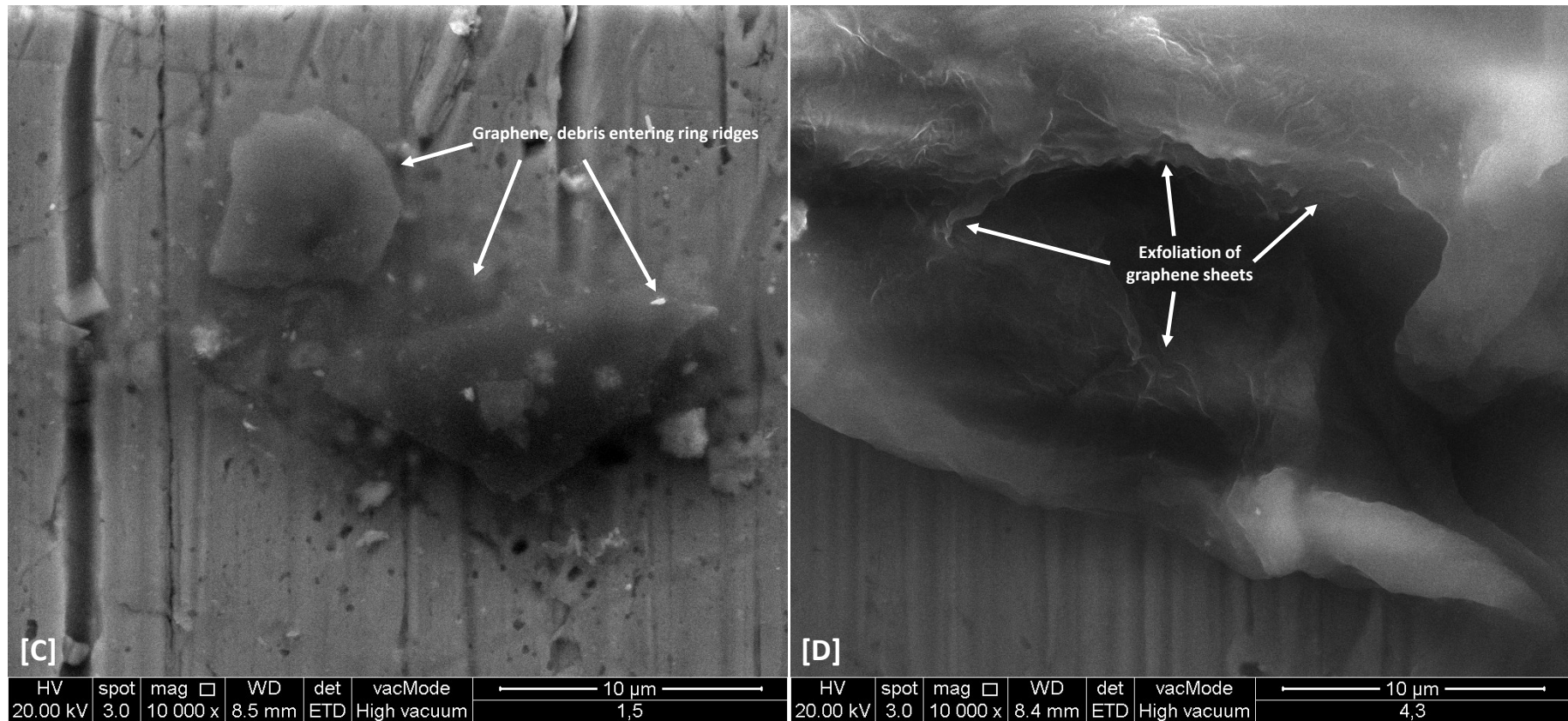
Figure 5.10. A – Graphene flake sliding from the edge of a piston ring; B – Folded, buckled and warped graphene found on a single location of a piston ring; C – Debris adhered to graphene flake; D – Exfoliated G12 due to shear forces;

The quality of graphene which includes the number of layers graphene retained and morphology are crucial for the continuous performance. Due to the reservoir limitation in engine test rig and limited engine oil samples, results could not determine the rate of graphene flake rupture or degradation. So the effects of ruptured graphene on the tribological performance are difficult to ascertain. However, as the large flakes continue to rupture, it would enhance the thermal conductivity of the lubricant. Furthermore turbulence assisted shear exfoliation (Varrla et al., 2014) of very few layer graphene can add to the number of single layer flakes in the engine oil. Continuous exfoliation due to engine operation is an irreversible damage caused to graphene flakes which could make it to lose its anti-friction property gradually. Of the many factors, increase of combustion products which are acidic in nature can also rupture graphene (Yu et al., 2016). Furthermore, oil oxidation would induce oxygen intercalation (Ma et al., 2015) associated decoupling of graphene adhered on piston surface. This could damage the protective film formed initially by exfoliated single flakes.

5.6. Summary

In this chapter an investigation onto the performance of graphene based nanolubricant using a 4-stroke IC engine test rig has been described. The addition of 0.01 wt% graphene to API 20W50 SN/CF results in 70% enhancement in heat transfer rate from the engine. SEM images of the piston rings collected after 100 hours of engine operation show that the oil containing graphene (12 nm) decreases the piston wear compared to base oil without

graphene. Elemental analysis indicates that the addition of a natural polymeric ester based lubricity additive helps even the graphene of highest thickness to perform better in boundary lubrication conditions. Furthermore, occurrence of several tribo-morphological phenomenon including sliding, puckering, rolling, buckling, twisting, shearing and exfoliation of graphene on the surface of piston ring has been identified. As a result multiple tribological phenomenon occurring simultaneously or subsequently is suggested to be the mechanism behind the tribology improvement.

CHAPTER 6.   CONCLUSION

6.1.   Introduction

This thesis has demonstrated that graphene can be an outstanding additive for engine oils. Graphene which has superior thermal conductivity not only enhances the thermal properties of the lubricant but also significantly improves its tribological properties. A novel consolidated approach to understand the tribological phenomenon has been presented with significant experimental evidence. For the first time, graphene's anti-oxidation ability has been presented with TGA-kinetics studies. Furthermore, an IC engine test rig was successfully fabricated with TMDLS to study the used oil and heat transfer from the engine. Elemental analysis of the used oil shows that graphene can significantly prevent wear at various interfaces. A remarkable heat transfer rate improvement is possible with the graphene as an additive in engine oil.

6.2.   Principal findings

1. Results show that concentration of graphene as low as 0.01 wt% could enhance the thermal conductivity of engine oil (API 20W50 SN/CF) up to ~23% at 80 °C. The API 20W50 SJ/CF has 5.4% low enhancement than SN/CF oil formulation. The thermal conductivity was found to be the function of nanoparticle concentration however, after a particular concentration (>0.1 wt%) the conductivity doesn't enhance further. It

might be due to the agglomeration of nanoparticles at higher concentrations due to van der Waals forces of attraction, restricting its Brownian motion (both rotational and translational motions).

2. By adding 0.01 wt% of 60 nm graphene and 1% lubricity additive to API 20W50 SN/CF oil, 21% enhancement in the coefficient of friction (μ) was observed. 12 nm graphene enhanced μ of the oil without lubricity additive by approximately 7%, whereas 8 nm and 60 nm had little or no enhancement. Scanning electron microscopy and Energy-dispersive X-ray spectroscopy analysis suggest that the single or very few layer graphene and multilayer graphene has the disadvantage of puckering, rupture and bending stiffness. Based on our experimental findings and review of existing literature, we understand that the existing nano-scale tribology mechanisms cannot be isolated while explaining the underlying physics; rather multiple tribological phenomenon should be considered simultaneously or subsequently.

3. The results showed that the increase in viscosity of engine oil after the addition of graphene is insignificant. The nanolubricant showed Newtonian behavior both with the increase in shear rate and temperature.

4. The TGA findings indicate that graphene could be an excellent additive to improve anti-oxidation property of base oils used for engine applications. TGA curves show that in the presence of graphene flakes the onset temperature for oxidation could be delayed by 13-17 °C. The thermal effect of graphene depends on the flake size and the length. The TGA results were also verified using four different heating rates

which show similar effects of graphene. The activation energies of the oil formulation is strongly affected in the presence of graphene flakes. The onset temperature of oxidation gets significantly higher in the presence of graphene.

5. A remarkable 70% enhancement in heat transfer rate is achieved in the presence of graphene. SEM images of the piston rings collected after 100 hours of engine operation show that the oil containing graphene (12 nm) decreases the piston wear compared to base oil without graphene. Elemental analysis indicates that the addition of a natural polymeric ester based lubricity additive helps even the graphene of highest thickness to perform better in boundary lubrication conditions. Furthermore, occurrence of several tribo-morphological phenomenon including sliding, puckering, rolling, buckling, twisting, shearing and exfoliation of graphene on the surface of piston ring has been identified. As a result multiple tribological phenomenon occurring simultaneously or subsequently is suggested to be the mechanism behind the tribology improvement.

6.3. Limitations

Given the interdisciplinary nature of this study, there are some limitations as the following.

1. Graphene nanoflakes of sizes 8, 12 and 60 nm were chosen based on the availability in the market and cost. Although the graphene powder is poly-sized, it is assumed to be of the sizes mentioned above. Defects

and morphological deformations are assumed to negligible owing to the complex polydispersity of graphene in oil formulation.

2. All the experimental investigations except thermal conductivity measurements were limited to 0.01 wt% graphene concentration.

3. Similarly API 20W50 SN/CF and API 20W50 SJ/CF base fluids were used in most experiments. Owing to the superiority of API 20W50 SN/CF over the other base fluids in terms of overall performance, it was alone used for engine tests.

4. Brownian motion and percolation effects as suggested by Dhar et al. (2011) for thermal conductivity calculations of nanolubricant are neglected while calculating the heat transfer rate from the engine. It is because of the assumption that the lubricant film between piston ring and cylinder would be very thin to allow such microscale phenomenon.

6.4. Recommendation for future studies

1. Based on the findings in this thesis, stability of nanolubricant is vital for its optimal performance. Studies to improve the hydrophobicity of graphene without damaging its morphology would be significantly helpful. Acid functionalization methods to make graphene highly hydrophobic could be explored.

2. This research has been able to explore few of the essential properties including, thermal conductivity, viscosity and anti-oxidation property of graphene nanolubricants only. Further research on other aspects of the lubricant including sludge and soot control would be interesting.

3. Scanning electron microscopy has led to a phenomenal understanding of the tribological behavior of graphene on piston ring surfaces. Further studies should investigate the factors responsible for the morphological changes on flakes on the surfaces. AFM and XPS based studies should be carried out to further the understanding of graphene-metal surface bonding.

4. Sampling methods from engine tests should be improved to assess oil condition at regular intervals. It would help in determining the critical point of additives degradation.

5. CFD studies on lubrication behaviour, lubricant film, etc., could also help in reducing extensive experimental work.

6. Graphene together with other nanomaterials forming hybrid nanolubricants would be another interesting research. The culmination of various properties in a hybrid nanolubricant system could outperform a nanolubricant with a single nanomaterial.

7. Research should also be done on used nanolubricant disposal or recycling and used oil filters as it may have serious implications.

REFERENCES

AHAMMED, N., ASIRVATHAM, L. G. & WONGWISES, S. 2015. Effect of volume concentration and temperature on viscosity and surface tension of graphene–water nanofluid for heat transfer applications. *Journal of Thermal Analysis and Calorimetry,* 123**,** 1399-1409.

AHMED, H. E., MOHAMMED, H. A. & YUSOFF, M. Z. 2012. An overview on heat transfer augmentation using vortex generators and nanofluids: Approaches and applications. *Renewable and Sustainable Energy Reviews,* 16**,** 5951-5993.

AHN, H. S., KIM, J. M., KAVIANY, M. & KIM, M. H. 2014a. Pool boiling experiments in reduced graphene oxide colloids part II – Behavior after the CHF, and boiling hysteresis. *International Journal of Heat and Mass Transfer,* 78**,** 224-231.

AHN, H. S., KIM, J. M., KAVIANY, M. & KIM, M. H. 2014b. Pool boiling experiments in reduced graphene oxide colloids. Part I – Boiling characteristics. *International Journal of Heat and Mass Transfer,* 74**,** 501-512.

AHN, H. S., KIM, J. M., KIM, T., PARK, S. C., KIM, J. M., PARK, Y., YU, D. I., HWANG, K. W., JO, H., PARK, H. S., KIM, H. & KIM, M. H. 2014. Enhanced heat transfer is dependent on thickness of graphene films: the heat dissipation during boiling. *Scientific Reports,* 4**,** 6276.

ANOOP, K. B., SUNDARARAJAN, T. & DAS, S. K. 2009. Effect of particle size on the convective heat transfer in nanofluid in the developing region. *International Journal of Heat and Mass Transfer,* 52**,** 2189-2195.

BABY, T. T. & RAMAPRABHU, S. 2010a. Investigation of thermal and electrical conductivity of graphene based nanofluids. *Journal of Applied Physics,* 108**,** 124308-6.

BABY, T. T. & RAMAPRABHU, S. 2010b. Investigation of thermal and electrical conductivity of graphene based nanofluids. *Journal of Applied Physics,* 108**,** -.

BABY, T. T. & RAMAPRABHU, S. 2011a. Synthesis and nanofluid application of silver nanoparticles decorated graphene. *Journal of Materials Chemistry,* 21**,** 9702-9709.

BABY, T. T. & RAMAPRABHU, S. 2011b. Synthesis and Transport Properties of Metal Oxide Decorated Graphene Dispersed Nanofluids. *The Journal of Physical Chemistry C,* 115**,** 8527-8533.

BAI, G., WANG, J., YANG, Z., WANG, H., WANG, Z. & YANG, S. 2014. Preparation of a highly effective lubricating oil additive - ceria/graphene composite. *RSC Advances,* 4**,** 47096-47105.

BALANDIN, A. A. 2011. Thermal properties of graphene and nanostructured carbon materials. *Nat Mater,* 10**,** 569-581.

BALANDIN, A. A., GHOSH, S., BAO, W., CALIZO, I., TEWELDEBRHAN, D., MIAO, F. & LAU, C. N. 2008. Superior Thermal Conductivity of Single-Layer Graphene. *Nano Letters,* 8**,** 902-907.

BATCHELOR, G. K. 1977. The effect of Brownian motion on the bulk stress in a suspension of spherical particles. *Journal of Fluid Mechanics,* 83**,** 97-117.

BECK, M., YUAN, Y., WARRIER, P. & TEJA, A. 2009. The effect of particle size on the thermal conductivity of alumina nanofluids. *Journal of Nanoparticle Research,* 11**,** 1129-1136.

BERMAN, D., DESHMUKH, S. A., SANKARANARAYANAN, S. K. R. S., ERDEMIR, A. & SUMANT, A. V. 2014a. Extraordinary Macroscale Wear Resistance of One Atom Thick Graphene Layer. *Advanced Functional Materials,* 24**,** 6640-6646.

BERMAN, D., ERDEMIR, A. & SUMANT, A. V. 2014b. Graphene: a new emerging lubricant. *Materials Today,* 17**,** 31-42.

BHATTACHARYA, P., SAHA, S. K., YADAV, A., PHELAN, P. E. & PRASHER, R. S. 2004. Brownian dynamics simulation to determine the effective thermal conductivity of nanofluids. *Journal of Applied Physics,* 95**,** 6492-6494.

BRINKMAN, H. C. 1952. The Viscosity of Concentrated Suspensions and Solutions. *The Journal of Chemical Physics,* 20**,** 571-571.

BRUGGEMAN, D. A. G. 1935. The calculation of various physical constants of heterogeneous substances. I. dielectric constants and conductivities of the mixtures composed of isotropic substances. *Annals of Physics,* 24**,** 636-664.

BUONGIORNO, J., VENERUS, D. C., PRABHAT, N. & AL., E. 2009. A benchmark study on the thermal conductivity of nanofluids. *Journal of Applied Physics,* 106**,** 094312-14.

CAI, W., MOORE, A. L., ZHU, Y., LI, X., CHEN, S., SHI, L. & RUOFF, R. S. 2010. Thermal Transport in Suspended and Supported Monolayer Graphene Grown by Chemical Vapor Deposition. *Nano Letters,* 10**,** 1645-1651.

CASSAGNEAU, T., GUÉRIN, F. & FENDLER, J. H. 2000. Preparation and Characterization of Ultrathin Films Layer-by-Layer Self-Assembled from Graphite Oxide Nanoplatelets and Polymers. *Langmuir,* 16**,** 7318-7324.

CHAE, H. K., SIBERIO-PEREZ, D. Y., KIM, J., GO, Y., EDDAOUDI, M., MATZGER, A. J., O'KEEFFE, M. & YAGHI, O. M. 2004. A route to high surface area, porosity and inclusion of large molecules in crystals. *Nature,* 427**,** 523-527.

CHANDRASEKAR, M., SURESH, S. & SENTHILKUMAR, T. 2012. Mechanisms proposed through experimental investigations on thermophysical properties and forced convective heat transfer characteristics of various nanofluids – A review. *Renewable and Sustainable Energy Reviews,* 16**,** 3917-3938.

CHEN, H., WITHARANA, S., JIN, Y., KIM, C. & DING, Y. 2009. Predicting thermal conductivity of liquid suspensions of nanoparticles (nanofluids) based on rheology. *Particuology,* 7**,** 151-157.

CHEN, L., XIE, H., LI, Y. & YU, W. 2008. Nanofluids containing carbon nanotubes treated by mechanochemical reaction. *Thermochimica Acta,* 477**,** 21-24.

CHEN, S. & CHRZAN, D. C. 2011. Continuum theory of dislocations and buckling in graphene. *Physical Review B,* 84**,** 214103.

CHEN, X., DOBSON, J. F. & RASTON, C. L. 2012. Vortex fluidic exfoliation of graphite and boron nitride. *Chemical Communications,* 48**,** 3703-3705.

CHEN, X., YI, C. & KE, C. 2015. Bending stiffness and interlayer shear modulus of few-layer graphene. *Applied Physics Letters,* 106**,** 101907.

CHENG, L. & LIU, L. 2013. Boiling and two-phase flow phenomena of refrigerant-based nanofluids: Fundamentals, applications and challenges. *International Journal of Refrigeration,* 36**,** 421-446.

CHEW, H. B., MOON, M.-W., LEE, K. R. & KIM, K.-S. 2010. Compressive dynamic scission of carbon nanotubes under sonication: fracture by atomic ejection. *Proceedings of the Royal Society of London A: Mathematical, Physical and Engineering Sciences*.

CHOI, H. J., KWON, T. M. & JHON, M. S. 2000. Effects of shear rate and particle concentration on rheological properties of magnetic particle suspensions. *Journal of Materials Science,* 35**,** 889-894.

CHOI, S. U. S., ZHANG, Z. G., YU, W., LOCKWOOD, F. E. & GRULKE, E. A. 2001. Anomalous thermal conductivity enhancement in nanotube suspensions. *Applied Physics Letters,* 79**,** 2252-2254.

CHON, C. H., KIHM, K. D., LEE, S. P. & CHOI, S. U. S. 2005. Empirical correlation finding the role of temperature and particle size for nanofluid (Al2O3) thermal conductivity enhancement. *Applied Physics Letters,* 87**,** -.

CHOU, R., BATTEZ, A. H., CABELLO, J. J., VIESCA, J. L., OSORIO, A. & SAGASTUME, A. 2010. Tribological behavior of polyalphaolefin with

the addition of nickel nanoparticles. *Tribology International,* 43**,** 2327-2332.

CHOUCAIR, M., THORDARSON, P. & STRIDE, J. A. 2009. Gram-scale production of graphene based on solvothermal synthesis and sonication. *Nat Nano,* 4**,** 30-33.

CURSARU, D.-L., ANDRONESCU, C., PIRVU, C. & RIPEANU, R. 2012. The efficiency of Co-based single-wall carbon nanotubes (SWNTs) as an AW/EP additive for mineral base oils. *Wear,* 290–291**,** 133-139.

DAS, S. K., CHOI, S. U., YU, W. & PRADEEP, T. 2007. *Nanofluids: Science and Technology*, Wiley-Interscience.

DAS, S. K., P., P. N. T. & ROETZEL, W. 2003a. Temperature dependence of thermal conductivity enhancement for nanofluids. *J. Heat Transfer,* 125**,** 567.

DAS, S. K., PUTRA, N., THIESEN, P. & ROETZEL, W. 2003b. Temperature Dependence of Thermal Conductivity Enhancement for Nanofluids. *Journal of Heat Transfer,* 125**,** 567-574.

DAUNGTHONGSUK, W. & WONGWISES, S. 2007. A critical review of convective heat transfer of nanofluids. *Renewable and Sustainable Energy Reviews,* 11**,** 797-817.

DAVIS, R. H. 1986. The effective thermal conductivity of a composite material with spherical inclusions. *International Journal of Thermophysics,* 7**,** 609-620.

DENG, Z., SMOLYANITSKY, A., LI, Q., FENG, X.-Q. & CANNARA, R. J. 2012. Adhesion-dependent negative friction coefficient on chemically modified graphite at the nanoscale. *Nat Mater,* 11**,** 1032-1037.

DHAR, P., ANSARI, M. H. D., GUPTA, S. S., SIVA, V. M., PRADEEP, T., PATTAMATTA, A. & DAS, S. K. 2013a. Percolation network dynamicity and sheet dynamics governed viscous behavior of polydispersed graphene nanosheet suspensions. *Journal of Nanoparticle Research,* 15**,** 1-12.

DHAR, P., GUPTA, S. S., CHAKRABORTY, S., PATTAMATTA, A. & K. DAS, S. 2013b. The role of percolation and sheet dynamics during heat conduction in poly-dispersed graphene nanofluids. *Applied Physics Letters,* 102**,** 163114-5.

DHAR, P., SEN GUPTA, S., CHAKRABORTY, S., PATTAMATTA, A. & DAS, S. K. 2013c. The role of percolation and sheet dynamics during heat conduction in poly-dispersed graphene nanofluids. *Applied Physics Letters,* 102**,** 163114.

DIKIN, D. A., STANKOVICH, S., ZIMNEY, E. J., PINER, R. D., DOMMETT, G. H. B., EVMENENKO, G., NGUYEN, S. T. & RUOFF,

R. S. 2007. Preparation and characterization of graphene oxide paper. *Nature,* 448**,** 457-460.

DING, Y., ALIAS, H., WEN, D. & WILLIAMS, R. A. 2006. Heat transfer of aqueous suspensions of carbon nanotubes (CNT nanofluids). *International Journal of Heat and Mass Transfer,* 49**,** 240-250.

DRAGOMAN, M. & DRAGOMAN, D. 2009. Graphene-based quantum electronics. *Progress in Quantum Electronics,* 33**,** 165-214.

DU, X., SKACHKO, I., BARKER, A. & ANDREI, E. Y. 2008. Approaching ballistic transport in suspended graphene. *Nat Nano,* 3**,** 491-495.

DYSON, A. 1965. Flow Properties of Mineral Oils in Elastohydrodynamic Lubrication. *Philosophical Transactions of the Royal Society of London A: Mathematical, Physical and Engineering Sciences,* 258**,** 529-564.

EAPEN, J., LI, J. & YIP, S. 2007. Beyond the Maxwell limit: Thermal conduction in nanofluids with percolating fluid structures. *Physical Review E,* 76**,** 062501.

EASTMAN, J. A., CHOI, S. U. S., LI, S., YU, W. & THOMPSON, L. J. 2001. Anomalously increased effective thermal conductivities of ethylene glycol-based nanofluids containing copper nanoparticles. *Applied Physics Letters,* 78**,** 718-720.

EINSTEIN, A. 1906. A New Determination of Molecular Dimensions. *Annals of Physics,* 324**,** 289-306.

EINSTEIN, A. 1956. *Investigations on the Theory of the Brownian Movement*, Dover, New York.

ESWARAIAH, V., SANKARANARAYANAN, V. & RAMAPRABHU, S. 2011. Graphene-Based Engine Oil Nanofluids for Tribological Applications. *ACS Applied Materials & Interfaces,* 3**,** 4221-4227.

ETTEFAGHI, E.-O.-L., RASHIDI, A., AHMADI, H., MOHTASEBI, S. S. & POURKHALIL, M. 2013. Thermal and rheological properties of oil-based nanofluids from different carbon nanostructures. *International Communications in Heat and Mass Transfer,* 48**,** 178-182.

FAN, J. & WANG, L. 2011. Review of Heat Conduction in Nanofluids. *Journal of Heat Transfer,* 133**,** 040801-14.

FAN, L.-W., LI, J.-Q., LI, D.-Y., ZHANG, L., YU, Z.-T. & CEN, K.-F. 2015. The effect of concentration on transient pool boiling heat transfer of graphene-based aqueous nanofluids. *International Journal of Thermal Sciences,* 91**,** 83-95.

FAN, Z., MARCONNET, A., NGUYEN, S. T., LIM, C. Y. H. & DUONG, H. M. 2014. Effects of heat treatment on the thermal properties of highly

nanoporous graphene aerogels using the infrared microscopy technique. *International Journal of Heat and Mass Transfer,* 76**,** 122-127.

FERRARI, A. C., MEYER, J. C., SCARDACI, V., CASIRAGHI, C., LAZZERI, M., MAURI, F., PISCANEC, S., JIANG, D., NOVOSELOV, K. S., ROTH, S. & GEIM, A. K. 2006. Raman Spectrum of Graphene and Graphene Layers. *Physical Review Letters,* 97**,** 187401.

FILLETER, T., MCCHESNEY, J. L., BOSTWICK, A., ROTENBERG, E., EMTSEV, K. V., SEYLLER, T., HORN, K. & BENNEWITZ, R. 2009. Friction and Dissipation in Epitaxial Graphene Films. *Physical Review Letters,* 102**,** 086102.

FRANKEL, N. A. & ACRIVOS, A. 1967. On the viscosity of a concentrated suspension of solid spheres. *Chemical Engineering Science,* 22**,** 847-853.

FREITAG, M., STEINER, M., MARTIN, Y., PEREBEINOS, V., CHEN, Z., TSANG, J. C. & AVOURIS, P. 2009. Energy Dissipation in Graphene Field-Effect Transistors. *Nano Letters,* 9**,** 1883-1888.

GALLAGHER, P., LEE, M., AMET, F., MAKSYMOVYCH, P., WANG, J., WANG, S., LU, X., ZHANG, G., WATANABE, K., TANIGUCHI, T. & GOLDHABER-GORDON, D. 2016. Switchable friction enabled by nanoscale self-assembly on graphene. *Nat Commun,* 7.

GARG, P., ALVARADO, J. L., MARSH, C., CARLSON, T. A., KESSLER, D. A. & ANNAMALAI, K. 2009. An experimental study on the effect of ultrasonication on viscosity and heat transfer performance of multi-wall carbon nanotube-based aqueous nanofluids. *International Journal of Heat and Mass Transfer,* 52**,** 5090-5101.

GEIM, A. K. & NOVOSELOV, K. S. 2007. The rise of graphene. *Nat Mater,* 6**,** 183-191.

GHOZATLOO, A., SHARIATY-NIASAR, M. & RASHIDI, A. M. 2013. Preparation of nanofluids from functionalized Graphene by new alkaline method and study on the thermal conductivity and stability. *International Communications in Heat and Mass Transfer,* 42**,** 89-94.

GILJE, S., HAN, S., WANG, M., WANG, K. L. & KANER, R. B. 2007. A Chemical Route to Graphene for Device Applications. *Nano Letters,* 7**,** 3394-3398.

GRIERSON, D. S. & CARPICK, R. W. 2007. Nanotribology of carbon-based materials. *Nano Today,* 2**,** 12-21.

GUPTA, S. S., SIVA, V. M., KRISHNAN, S., SREEPRASAD, T. S., SINGH, P. K., PRADEEP, T. & K. DAS, S. 2011. Thermal conductivity enhancement of nanofluids containing graphene nanosheets. *Journal of Applied Physics,* 110**,** 084302-6.

HADADIAN, M., GOHARSHADI, E. K. & YOUSSEFI, A. 2014. Electrical conductivity, thermal conductivity, and rheological properties of graphene oxide-based nanofluids. *Journal of Nanoparticle Research,* 16**,** 1-17.

HADDAD, Z., OZTOP, H. F., ABU-NADA, E. & MATAOUI, A. 2012. A review on natural convective heat transfer of nanofluids. *Renewable and Sustainable Energy Reviews,* 16**,** 5363-5378.

HAFIZ, A. A. & KHIDR, T. T. 2007. Hexa-triethanolamine oleate esters as pour point depressant for waxy crude oils. *Journal of Petroleum Science and Engineering,* 56**,** 296-302.

HAJJAR, Z., RASHIDI, A. M. & GHOZATLOO, A. 2014. Enhanced thermal conductivities of graphene oxide nanofluids. *International Communications in Heat and Mass Transfer,* 57**,** 128-131.

HAMILTON, R. L. & CROSSER, O. K. 1962. Thermal Conductivity of Heterogeneous Two-Component Systems. *Industrial & Engineering Chemistry Fundamentals,* 1**,** 187-191.

HAQUE, T., MORINA, A. & NEVILLE, A. 2010. Influence of friction modifier and antiwear additives on the tribological performance of a non-hydrogenated DLC coating. *Surface and Coatings Technology,* 204**,** 4001-4011.

HARIGAYA, Y., SUZUKI, M., TODA, F. & TAKIGUCHI, M. 2004. Analysis of Oil Film Thickness and Heat Transfer on a Piston Ring of a Diesel Engine: Effect of Lubricant Viscosity. *Journal of Engineering for Gas Turbines and Power,* 128**,** 685-693.

HEINE, D. R., PETERSEN, M. K. & GREST, G. S. 2010. Effect of particle shape and charge on bulk rheology of nanoparticle suspensions. *The Journal of Chemical Physics,* 132**,** 184509.

HERNÁNDEZ BATTEZ, A., GONZÁLEZ, R., FELGUEROSO, D., FERNÁNDEZ, J. E., DEL ROCÍO FERNÁNDEZ, M., GARCÍA, M. A. & PEÑUELAS, I. 2007. Wear prevention behaviour of nanoparticle suspension under extreme pressure conditions. *Wear,* 263**,** 1568-1574.

HERNÁNDEZ BATTEZ, A., GONZÁLEZ, R., VIESCA, J. L., FERNÁNDEZ, J. E., DÍAZ FERNÁNDEZ, J. M., MACHADO, A., CHOU, R. & RIBA, J. 2008. CuO, ZrO2 and ZnO nanoparticles as antiwear additive in oil lubricants. *Wear,* 265**,** 422-428.

HERNÁNDEZ BATTEZ, A., VIESCA, J. L., GONZÁLEZ, R., BLANCO, D., ASEDEGBEGA, E. & OSORIO, A. 2010. Friction reduction properties of a CuO nanolubricant used as lubricant for a NiCrBSi coating. *Wear,* 268**,** 325-328.

HERNANDEZ, Y., NICOLOSI, V., LOTYA, M., BLIGHE, F. M., SUN, Z., DE, S., MCGOVERN, I. T., HOLLAND, B., BYRNE, M., GUN'KO, Y. K., BOLAND, J. J., NIRAJ, P., DUESBERG, G., KRISHNAMURTHY,

S., GOODHUE, R., HUTCHISON, J., SCARDACI, V., FERRARI, A. C. & COLEMAN, J. N. 2008. High-yield production of graphene by liquid-phase exfoliation of graphite. *Nat Nano,* 3**,** 563-568.

HOSSEINI, S. M., MOGHADASSI, A. & HENNEKE, D. 2011. Modelling of the effective thermal conductivity of carbon nanotube nanofluids based on dimensionless groups. *The Canadian Journal of Chemical Engineering,* 89**,** 183-186.

HU, Z. S., LAI, R., LOU, F., WANG, L. G., CHEN, Z. L., CHEN, G. X. & DONG, J. X. 2002. Preparation and tribological properties of nanometer magnesium borate as lubricating oil additive. *Wear,* 252**,** 370-374.

HUMINIC, G. & HUMINIC, A. 2012. Application of nanofluids in heat exchangers: A review. *Renewable and Sustainable Energy Reviews,* 16**,** 5625-5638.

HYUNSOO, L., NAESUNG, L., YONGHO, S., JONGHWA, E. & SANGWOOK, L. 2009. Comparison of frictional forces on graphene and graphite. *Nanotechnology,* 20**,** 325701.

IJAM, A., MORADI GOLSHEIKH, A., SAIDUR, R. & GANESAN, P. 2014. A glycerol–water-based nanofluid containing graphene oxide nanosheets. *Journal of Materials Science,* 49**,** 5934-5944.

IZADI, M., SHAHMARDAN, M. M., BEHZADMEHR, A., RASHIDI, A. M. & AMROLLAHI, A. 2015. Modeling of Effective Thermal Conductivity and Viscosity of Carbon Structured Nanofluid. *Transport Phenomena in Nano and Micro Scales,* 3**,** 1-13.

JANG, S. P. & CHOI, S. U. S. 2004. Role of Brownian motion in the enhanced thermal conductivity of nanofluids. *Applied Physics Letters,* 84**,** 4316-4318.

JANG, W., CHEN, Z., BAO, W., LAU, C. N. & DAMES, C. 2010. Thickness-Dependent Thermal Conductivity of Encased Graphene and Ultrathin Graphite. *Nano Letters,* 10**,** 3909-3913.

JEFFREY, D. J. 1973. Conduction Through a Random Suspension of Spheres. *Proceedings of the Royal Society of London. A. Mathematical and Physical Sciences,* 335**,** 355-367.

JEONG, J., LI, C., KWON, Y., LEE, J., KIM, S. H. & YUN, R. 2013. Particle Shape Effect on the Viscosity and Thermal Conductivity of ZnO Nanofluids. *International Journal of Refrigeration.*

JIANG, W., DING, G. & PENG, H. 2009. Measurement and model on thermal conductivities of carbon nanotube nanorefrigerants. *International Journal of Thermal Sciences,* 48**,** 1108-1115.

JWO, C.-S., TENG, T.-P. & CHANG, H. 2007. A simple model to estimate thermal conductivity of fluid with acicular nanoparticles. *Journal of Alloys and Compounds,* 434–435**,** 569-571.

JYOTHIRMAYEE ARAVIND, S. S. & RAMAPRABHU, S. 2011. Surfactant free graphene nanosheets based nanofluids by in-situ reduction of alkaline graphite oxide suspensions. *Journal of Applied Physics,* 110**,** 124326.

KAKAÇ, S. & PRAMUANJAROENKIJ, A. 2009. Review of convective heat transfer enhancement with nanofluids. *International Journal of Heat and Mass Transfer,* 52**,** 3187-3196.

KEBLINSKI, P., PHILLPOT, S. R., CHOI, S. U. S. & EASTMAN, J. A. 2002. Mechanisms of heat flow in suspensions of nano-sized particles (nanofluids). *International Journal of Heat and Mass Transfer,* 45**,** 855-863.

KIM, J., KWON, S., CHO, D.-H., KANG, B., KWON, H., KIM, Y., PARK, S. O., JUNG, G. Y., SHIN, E., KIM, W.-G., LEE, H., RYU, G. H., CHOI, M., KIM, T. H., OH, J., PARK, S., KWAK, S. K., YOON, S. W., BYUN, D., LEE, Z. & LEE, C. 2015. Direct exfoliation and dispersion of two-dimensional materials in pure water via temperature control. *Nat Commun,* 6.

KIM, J. M., KIM, T. & AHN, H. S. 2014a. Experimental study of transient boiling characteristics on three-dimensional reduced graphene oxide networks. *Experimental Thermal and Fluid Science,* 59**,** 51-55.

KIM, J. M., KIM, T., KIM, J., KIM, M. H. & AHN, H. S. 2014b. Effect of a graphene oxide coating layer on critical heat flux enhancement under pool boiling. *International Journal of Heat and Mass Transfer,* 77**,** 919-927.

KIM, P., SHI, L., MAJUMDAR, A. & MCEUEN, P. L. 2001. Thermal Transport Measurements of Individual Multiwalled Nanotubes. *Physical Review Letters,* 87**,** 215502.

KINOSHITA, H., NISHINA, Y., ALIAS, A. A. & FUJII, M. 2014. Tribological properties of monolayer graphene oxide sheets as water-based lubricant additives. *Carbon,* 66**,** 720-723.

KIT, O. O., TALLINEN, T., MAHADEVAN, L., TIMONEN, J. & KOSKINEN, P. 2012. Twisting graphene nanoribbons into carbon nanotubes. *Physical Review B,* 85**,** 085428.

KITANO, T., KATAOKA, T. & SHIROTA, T. 1981. An empirical equation of the relative viscosity of polymer melts filled with various inorganic fillers. *Rheologica Acta,* 20**,** 207-209.

KLEINSTREUER, C. & FENG, Y. 2011. Experimental and theoretical studies of nanofluid thermal conductivity enhancement: a review. *Nanoscale Research Letters,* 6**,** 229.

KLEMENS, P. G. 2000. Theory of the A-Plane Thermal Conductivity of Graphite. *Journal of Wide Bandgap Materials,* 7**,** 332-339.

KOLE, M. & DEY, T. K. 2013. Investigation of thermal conductivity, viscosity, and electrical conductivity of graphene based nanofluids. *Journal of Applied Physics,* 113**,** -.

KOO, J., KANG, Y. & KLEINSTREUER, C. 2008. A nonlinear effective thermal conductivity model for carbon nanotube and nanofiber suspensions. *Nanotechnology,* 19**,** 375705.

KOO, J. & KLEINSTREUER, C. 2004. A new thermal conductivity model for nanofluids. *Journal of Nanoparticle Research,* 6**,** 577-588.

KOSARIEH, S., MORINA, A., LAINÉ, E., FLEMMING, J. & NEVILLE, A. 2013. The effect of MoDTC-type friction modifier on the wear performance of a hydrogenated DLC coating. *Wear,* 302**,** 890-898.

KOSYNKIN, D. V., HIGGINBOTHAM, A. L., SINITSKII, A., LOMEDA, J. R., DIMIEV, A., PRICE, B. K. & TOUR, J. M. 2009. Longitudinal unzipping of carbon nanotubes to form graphene nanoribbons. *Nature,* 458**,** 872-876.

KOTOV, N. A., DÉKÁNY, I. & FENDLER, J. H. 1996. Ultrathin graphite oxide–polyelectrolyte composites prepared by self-assembly: Transition between conductive and non-conductive states. *Advanced Materials,* 8**,** 637-641.

KOZLOV, S. M., VIÑES, F. & GÖRLING, A. 2012. Bonding Mechanisms of Graphene on Metal Surfaces. *The Journal of Physical Chemistry C,* 116**,** 7360-7366.

KRIEGER, I. M. & DOUGHERTY, T. J. 1959. A Mechanism for Non-Newtonian Flow in Suspensions of Rigid Spheres. *Transactions of The Society of Rheology (1957-1977),* 3**,** 137-152.

KUILA, T., BOSE, S., MISHRA, A. K., KHANRA, P., KIM, N. H. & LEE, J. H. 2012. Chemical functionalization of graphene and its applications. *Progress in Materials Science,* 57**,** 1061-1105.

KUMAR, D. H., PATEL, H. E., KUMAR, V. R. R., SUNDARARAJAN, T., PRADEEP, T. & DAS, S. K. 2004. Model for Heat Conduction in Nanofluids. *Physical Review Letters,* 93**,** 144301.

KWON, T. M., JHON, M. S. & CHOI, H. J. 1998. Viscosity of magnetic particle suspension. *Journal of Molecular Liquids,* 75**,** 115-126.

LAAD, M. & JATTI, V. K. S. 2016. Titanium oxide nanoparticles as additives in engine oil. *Journal of King Saud University - Engineering Sciences*.

LAHIRI, J., LIN, Y., BOZKURT, P., OLEYNIK, I. I. & BATZILL, M. 2010. An extended defect in graphene as a metallic wire. *Nat Nano,* 5**,** 326-329.

LAHOUIJ, I., VACHER, B., MARTIN, J.-M. & DASSENOY, F. 2012. IF-MoS2 based lubricants: Influence of size, shape and crystal structure. *Wear,* 296**,** 558-567.

LEE, C., LI, Q., KALB, W., LIU, X.-Z., BERGER, H., CARPICK, R. W. & HONE, J. 2010. Frictional Characteristics of Atomically Thin Sheets. *Science,* 328**,** 76-80.

LEE, C., WEI, X., KYSAR, J. W. & HONE, J. 2008. Measurement of the Elastic Properties and Intrinsic Strength of Monolayer Graphene. *Science,* 321**,** 385-388.

LEE, S., CHOI, S. U. S., LI, S. & EASTMAN, J. A. 1999. Measuring Thermal Conductivity of Fluids Containing Oxide Nanoparticles. *Journal of Heat Transfer,* 121**,** 280-289.

LEHRLE, R. S., DUNCAN, R., LIU, Y., PARSONS, I. W., ROLLINSON, M., LAMB, G. & BARR, D. 2002. Mass spectrometric methods for assessing the thermal stability of liquid polymers and oils: study of some liquid polyisobutylenes used in the production of crankcase oil additives. *Journal of Analytical and Applied Pyrolysis,* 64**,** 207-227.

LEONG, K. C., YANG, C. & MURSHED, S. M. S. 2006. A model for the thermal conductivity of nanofluids – the effect of interfacial layer. *Journal of Nanoparticle Research,* 8**,** 245-254.

LI, C. H. & PETERSON, G. P. 2007. The effect of particle size on the effective thermal conductivity of Al2O3-water nanofluids. *Journal of Applied Physics,* 101**,** 044312-044312-5.

LI, D., XIE, W. & FANG, W. 2011. Preparation and properties of copper-oil-based nanofluids. *Nanoscale Research Letters,* 6**,** 373-373.

LI, F.-C., YANG, J.-C., ZHOU, W.-W., HE, Y.-R., HUANG, Y.-M. & JIANG, B.-C. 2013. Experimental study on the characteristics of thermal conductivity and shear viscosity of viscoelastic-fluid-based nanofluids containing multiwalled carbon nanotubes. *Thermochimica Acta,* 556**,** 47-53.

LI, Q., LEE, C., CARPICK, R. W. & HONE, J. 2010. Substrate effect on thickness-dependent friction on graphene. *physica status solidi (b),* 247**,** 2909-2914.

LI, X., CHEN, Y., MO, S., JIA, L. & SHAO, X. 2014. Effect of surface modification on the stability and thermal conductivity of water-based SiO2-coated graphene nanofluid. *Thermochimica Acta,* 595**,** 6-10.

LI, Y. & CHOPRA, N. 2015a. Progress in Large-Scale Production of Graphene. Part 1: Chemical Methods. *JOM,* 67**,** 34-43.

LI, Y. & CHOPRA, N. 2015b. Progress in Large-Scale Production of Graphene. Part 2: Vapor Methods. *JOM,* 67**,** 44-52.

LIM, S., HORIUCHI, H., NIKOLOV, A. D. & WASAN, D. 2015. Nanofluids Alter the Surface Wettability of Solids. *Langmuir,* 31**,** 5827-5835.

LIN, J., WANG, L. & CHEN, G. 2011. Modification of Graphene Platelets and their Tribological Properties as a Lubricant Additive. *Tribology Letters,* 41**,** 209-215.

LIU, H., BAI, M., LV, J., ZHANG, L., WANG, P. & HU, C. 2014. Experimental Study and Analysis of Lubricants Dispersed With Nanodiamond Particles on Diesel Engine. *Journal of Nanotechnology in Engineering and Medicine,* 5**,** 041001-041001.

LIU, Z., MA, L., SHI, G., ZHOU, W., GONG, Y., LEI, S., YANG, X., ZHANG, J., YU, J., HACKENBERG, K. P., BABAKHANI, A., IDROBO, J.-C., VAJTAI, R., LOU, J. & AJAYAN, P. M. 2013. In-plane heterostructures of graphene and hexagonal boron nitride with controlled domain sizes. *Nat Nano,* 8**,** 119-124.

LOTFI, H. & SHAFII, M. B. 2009. Boiling heat transfer on a high temperature silver sphere in nanofluid. *International Journal of Thermal Sciences,* 48**,** 2215-2220.

LUNDGREN, T. S. 1972. Slow flow through stationary random beds and suspensions of spheres. *Journal of Fluid Mechanics,* 51**,** 273-299.

MA, L., ZENG, X. C. & WANG, J. 2015. Oxygen Intercalation of Graphene on Transition Metal Substrate: An Edge-Limited Mechanism. *The Journal of Physical Chemistry Letters,* 6**,** 4099-4105.

MA, S., ZHENG, S., CAO, D. & GUO, H. 2010. Anti-wear and friction performance of ZrO2 nanoparticles as lubricant additive. *Particuology,* 8**,** 468-472.

MA, W., YANG, F., SHI, J., WANG, F., ZHANG, Z. & WANG, S. 2013. Silicone based nanofluids containing functionalized graphene nanosheets. *Colloids and Surfaces A: Physicochemical and Engineering Aspects,* 431**,** 120-126.

MAHBUBUL, I. M., SAIDUR, R. & AMALINA, M. A. 2012. Latest developments on the viscosity of nanofluids. *International Journal of Heat and Mass Transfer,* 55**,** 874-885.

MAHIAN, O., KIANIFAR, A., KALOGIROU, S. A., POP, I. & WONGWISES, S. 2013. A review of the applications of nanofluids in solar energy. *International Journal of Heat and Mass Transfer,* 57**,** 582-594.

MARTIN-GALLEGO, M., VERDEJO, R., KHAYET, M., DE ZARATE, J., ESSALHI, M. & LOPEZ-MANCHADO, M. 2011. Thermal conductivity of carbon nanotubes and graphene in epoxy nanofluids and nanocomposites. *Nanoscale Research Letters,* 6**,** 610.

MARTIN, J. M. & OHMAE, N. (eds.) 2008. *Nanolubricants*: John Wiley & Sons, Ltd.

MASUDA, H., EBATA, A., TERAMAE, K. & HISHINUMA, N. 1993. Alteration of thermal conductivity and viscosity of liquid by dispersing ultra-fine particles. *Netsu Bussei,* 7**,** 227–233.

MATTEVI, C., KIM, H. & CHHOWALLA, M. 2011. A review of chemical vapour deposition of graphene on copper. *Journal of Materials Chemistry,* 21**,** 3324-3334.

MAXWELL, J. C. 1873 *A Treatise on Electricity and Magnetism,* London, Oxford: Macmillan and Co.,.

MAXWELL, J. C. 1892. A Treatise on Electricity and Magnetism. *Oxford: Clarendon,* 2**,** 68-73.

MEHRALI, M., SADEGHINEZHAD, E., LATIBARI, S., KAZI, S., MEHRALI, M., ZUBIR, M. N. B. M. & METSELAAR, H. S. 2014. Investigation of thermal conductivity and rheological properties of nanofluids containing graphene nanoplatelets. *Nanoscale Research Letters,* 9**,** 15.

MEHRALI, M., SADEGHINEZHAD, E., RASHIDI, M. M., AKHIANI, A. R., TAHAN LATIBARI, S., MEHRALI, M. & METSELAAR, H. S. C. 2015. Experimental and numerical investigation of the effective electrical conductivity of nitrogen-doped graphene nanofluids. *Journal of Nanoparticle Research,* 17**,** 1-17.

MIAO, F., WIJERATNE, S., ZHANG, Y., COSKUN, U. C., BAO, W. & LAU, C. N. 2007. Phase-Coherent Transport in Graphene Quantum Billiards. *Science,* 317**,** 1530-1533.

MINGZHENG, Z., GUODONG, X., JIAN, L., LEI, C. & LIJUN, Z. 2012. Analysis of factors influencing thermal conductivity and viscosity in different kinds of surfactant solutions. *Experimental Thermal and Fluid Science,* 36**,** 22-29.

MINTSA, H. A., ROY, G., NGUYEN, C. T. & DOUCET, D. 2009. New temperature dependent thermal conductivity data for water-based nanofluids. *International Journal of Thermal Sciences,* 48**,** 363-371.

MIURA, K. & ISHIKAWA, M. 2010. C60 Intercalated graphite as nanolubricants. *Materials,* 3**,** 4510-4517.

MOGHADASSI, A. R., MASOUD HOSSEINI, S., HENNEKE, D. & ELKAMEL, A. 2009. A model of nanofluids effective thermal conductivity based on dimensionless groups. *Journal of Thermal Analysis and Calorimetry,* 96**,** 81-84.

MOGHADDAM, M. B., GOHARSHADI, E. K., ENTEZARI, M. H. & NANCARROW, P. 2013. Preparation, characterization, and rheological

properties of graphene–glycerol nanofluids. *Chemical Engineering Journal,* 231**,** 365-372.

MOHAMAD, S. A., AHMED, N. S., HASSANEIN, S. M. & RASHAD, A. M. 2012. Investigation of polyacrylates copolymers as lube oil viscosity index improvers. *Journal of Petroleum Science and Engineering,* 100**,** 173-177.

MOHAMMED, H. A., AL-ASWADI, A. A., SHUAIB, N. H. & SAIDUR, R. 2011. Convective heat transfer and fluid flow study over a step using nanofluids: A review. *Renewable and Sustainable Energy Reviews,* 15**,** 2921-2939.

MOHD ZUBIR, M. N., BADARUDIN, A., KAZI, S. N., HUANG, N. M., MISRAN, M., SADEGHINEZHAD, E., MEHRALI, M. & YUSOFF, N. 2015. Highly dispersed reduced graphene oxide and its hybrid complexes as effective additives for improving thermophysical property of heat transfer fluid. *International Journal of Heat and Mass Transfer,* 87**,** 284-294.

MOONEY, M. 1951. The viscosity of a concentrated suspension of spherical particles. *Journal of Colloid Science,* 6**,** 162-170.

MUFTI, R. A. & PRIEST, M. 2009. Effect of Engine Operating Conditions and Lubricant Rheology on the Distribution of Losses in an Internal Combustion Engine. *Journal of Tribology,* 131**,** 041101-041101.

MURSHED, S. M. S., DE CASTRO, C. A. N. & LOURENÇO, M. J. V. 2012. Effect of Surfactant and Nanoparticle Clustering on Thermal Conductivity of Aqueous Nanofluids. *Journal of Nanofluids,* 1**,** 175-179.

MURSHED, S. M. S., LEONG, K. C. & YANG, C. 2005. Enhanced thermal conductivity of TiO2--water based nanofluids. *International Journal of Thermal Sciences,* 44**,** 367-373.

MURSHED, S. M. S., LEONG, K. C. & YANG, C. 2008a. Investigations of thermal conductivity and viscosity of nanofluids. *International Journal of Thermal Sciences,* 47**,** 560-568.

MURSHED, S. M. S., LEONG, K. C. & YANG, C. 2008b. Thermophysical and electrokinetic properties of nanofluids - A critical review. *Applied Thermal Engineering,* 28**,** 2109-2125.

MURSHED, S. M. S., NIETO DE CASTRO, C. A., LOURENÇO, M. J. V., LOPES, M. L. M. & SANTOS, F. J. V. 2011. A review of boiling and convective heat transfer with nanofluids. *Renewable and Sustainable Energy Reviews,* 15**,** 2342-2354.

NAIR, R. R., BLAKE, P., GRIGORENKO, A. N., NOVOSELOV, K. S., BOOTH, T. J., STAUBER, T., PERES, N. M. R. & GEIM, A. K. 2008. Fine Structure Constant Defines Visual Transparency of Graphene. *Science,* 320**,** 1308.

NAN, C.-W., BIRRINGER, R., CLARKE, D. R. & GLEITER, H. 1997. Effective thermal conductivity of particulate composites with interfacial thermal resistance. *Journal of Applied Physics,* 81**,** 6692-6699.

NAN, C. W., SHI, Z. & LIN, Y. 2003. A simple model for thermal conductivity of carbon nanotube-based composites. *Chemical Physics Letters,* 375**,** 666-669.

NASIRI, A., SHARIATY-NIASAR, M., RASHIDI, A. M. & KHODAFARIN, R. 2012. Effect of CNT structures on thermal conductivity and stability of nanofluid. *International Journal of Heat and Mass Transfer,* 55**,** 1529-1535.

NASSAR, A. M., AHMED, N. S., ABDEL-HAMEED, H. S. & EL-KAFRAWY, A. F. 2016. Synthesis and utilization of non-metallic detergent/dispersant and antioxidant additives for lubricating engine oil. *Tribology International,* 93, Part A**,** 297-305.

NGUYEN, C. T., DESGRANGES, F., GALANIS, N., ROY, G., MARE, T., BOUCHER, S. & ANGUE MINTSA, H. 2008. Viscosity data for Al_2O_3-water nanofluid-hysteresis: is heat transfer enhancement using nanofluids reliable? *International Journal of Thermal Sciences,* 47**,** 103-111.

NIELSEN, L. E. 1970. Generalized Equation for the Elastic Moduli of Composite Materials. *Journal of Applied Physics,* 41**,** 4626-4627.

NIKA, D. L., ASKEROV, A. S. & BALANDIN, A. A. 2012. Anomalous Size Dependence of the Thermal Conductivity of Graphene Ribbons. *Nano Letters,* 12**,** 3238-3244.

NKURIKIYIMFURA, I., WANG, Y. & PAN, Z. 2013. Heat transfer enhancement by magnetic nanofluids—A review. *Renewable and Sustainable Energy Reviews,* 21**,** 548-561.

NOMÈDE-MARTYR, N., DISA, E., THOMAS, P., ROMANA, L., MANSOT, J.-L., DUBOIS, M., GUÉRIN, K., ZHANG, W. & HAMWI, A. 2012. Tribological properties of fluorinated nanocarbons with different shape factors. *Journal of Fluorine Chemistry,* 144**,** 10-16.

NOVOSELOV, K. S., GEIM, A. K., MOROZOV, S. V., JIANG, D., ZHANG, Y., DUBONOS, S. V., GRIGORIEVA, I. V. & FIRSOV, A. A. 2004. Electric Field Effect in Atomically Thin Carbon Films. *Science,* 306**,** 666-669.

OU, J., WANG, J., LIU, S., MU, B., REN, J., WANG, H. & YANG, S. 2010. Tribology Study of Reduced Graphene Oxide Sheets on Silicon Substrate Synthesized via Covalent Assembly. *Langmuir,* 26**,** 15830-15836.

ÖZERINÇ, S., KAKAÇ, S. & YAZıCıOĞLU, A. 2010. Enhanced thermal conductivity of nanofluids: a state-of-the-art review. *Microfluidics and Nanofluidics,* 8**,** 145-170.

PARK, S. D. & BANG, I. C. 2014. Experimental study of a universal CHF enhancement mechanism in nanofluids using hydrodynamic instability. *International Journal of Heat and Mass Transfer,* 70**,** 844-850.

PARK, S. D., LEE, S. W., KANG, S., BANG, I. C., KIM, J. H., SHIN, H. S., LEE, D. W. & LEE, D. W. 2010. Effects of nanofluids containing graphene/graphene-oxide nanosheets on critical heat flux. *Applied Physics Letters,* 97**,** 023103-3.

PARK, S. D., LEE, S. W., KANG, S., KIM, S. M. & BANG, I. C. 2012. Pool boiling CHF enhancement by graphene-oxide nanofluid under nuclear coolant chemical environments. *Nuclear Engineering and Design,* 252**,** 184-191.

PARK, S. S. & KIM, N. J. 2014. Influence of the oxidation treatment and the average particle diameter of graphene for thermal conductivity enhancement. *Journal of Industrial and Engineering Chemistry,* 20**,** 1911-1915.

PARK, S. S., KIM, Y. H., JEON, Y. H., HYUN, M. T. & KIM, N. J. 2015. Effects of spray-deposited oxidized multi-wall carbon nanotubes and graphene on pool-boiling critical heat flux enhancement. *Journal of Industrial and Engineering Chemistry,* 24**,** 276-283.

PASRICHA, R., GUPTA, S. & SRIVASTAVA, A. K. 2009. A Facile and Novel Synthesis of Ag–Graphene-Based Nanocomposites. *Small,* 5**,** 2253-2259.

PATEL, H., SUNDARARAJAN, T., PRADEEP, T., DASGUPTA, A., DASGUPTA, N. & DAS, S. 2005. A micro-convection model for thermal conductivity of nanofluids. *Pramana,* 65**,** 863-869.

PATEL, H. E., DAS, S. K., SUNDARARAJAN, T., SREEKUMARAN NAIR, A., GEORGE, B. & PRADEEP, T. 2003. Thermal conductivities of naked and monolayer protected metal nanoparticle based nanofluids: Manifestation of anomalous enhancement and chemical effects. *Applied Physics Letters,* 83**,** 2931-2933.

PATON, K. R., VARRLA, E., BACKES, C., SMITH, R. J., KHAN, U., O'NEILL, A., BOLAND, C., LOTYA, M., ISTRATE, O. M., KING, P., HIGGINS, T., BARWICH, S., MAY, P., PUCZKARSKI, P., AHMED, I., MOEBIUS, M., PETTERSSON, H., LONG, E., COELHO, J., O'BRIEN, S. E., MCGUIRE, E. K., SANCHEZ, B. M., DUESBERG, G. S., MCEVOY, N., PENNYCOOK, T. J., DOWNING, C., CROSSLEY, A., NICOLOSI, V. & COLEMAN, J. N. 2014. Scalable production of large quantities of defect-free few-layer graphene by shear exfoliation in liquids. *Nat Mater,* 13**,** 624-630.

PAUL, G., CHOPKAR, M., MANNA, I. & DAS, P. K. 2010. Techniques for measuring the thermal conductivity of nanofluids: A review. *Renewable and Sustainable Energy Reviews,* 14**,** 1913-1924.

PENG, W., JIZU, L., MINLI, B., YUYAN, W., CHENGZHI, H. & LIANG, Z. 2014. Numerical Simulation on the Flow and Heat Transfer Process of Nanofluids Inside a Piston Cooling Gallery. *Numerical Heat Transfer, Part A: Applications,* 65**,** 378-400.

PRASHER, R., BHATTACHARYA, P. & PHELAN, P. E. 2005. Thermal Conductivity of Nanoscale Colloidal Solutions (Nanofluids). *Physical Review Letters,* 94**,** 025901.

PRASHER, R., EVANS, W., MEAKIN, P., FISH, J., PHELAN, P. & KEBLINSKI, P. 2006. Effect of aggregation on thermal conduction in colloidal nanofluids. *Applied Physics Letters,* 89**,** 143119.

RAJASEKARAN, G., NARAYANAN, P. & PARASHAR, A. 2016. Effect of Point and Line Defects on Mechanical and Thermal Properties of Graphene: A Review. *Critical Reviews in Solid State and Materials Sciences,* 41**,** 47-71.

RAO, C. N. R., SUBRAHMANYAM, K. S., MATTE, H. S. S. R., ABDULHAKEEM, B., GOVINDARAJ, A., DAS, B., KUMAR, P., GHOSH, A. & LATE, D. J. 2010. A study of the synthetic methods and properties of graphenes. *Science and Technology of Advanced Materials,* 11**,** 054502.

RAO, Y. 2010. Nanofluids: Stability, phase diagram, rheology and applications. *Particuology,* 8**,** 549-555.

RASHEED, A. K., KHALID, M., WALVEKAR, R., GUPTA, T. C. S. M. & CHAN, A. 2015. Study of graphene nanolubricant using thermogravimetric analysis. *Journal of Materials Research***,** 1-8.

RASHEED, A. K., KHALID, M., RASHMI, W., GUPTA, T. C. S. M. & CHAN, A. 2016. Graphene based nanofluids and nanolubricants – Review of recent developments. *Renewable and Sustainable Energy Reviews,* 63**,** 346-362.

RASHMI, W., ISMAIL, A. F., SOPYANC, I., JAMEEL, A. T., YUSOF, F., KHALID, M. & MUBARAK, N. M. 2010. Stability and thermal conductivity enhancement of carbon nanotube nanofluid using gum arabic. *Journal of Experimental Nanoscience***,** 1-13.

RASHMI, W., KHALID, M., ONG, S. S. & SAIDUR, R. 2014. Preparation, thermo-physical properties and heat transfer enhancement of nanofluids. *Materials Research Express,* 1**,** 032001.

REGUZZONI, M., FASOLINO, A., MOLINARI, E. & RIGHI, M. C. 2012. Friction by Shear Deformations in Multilayer Graphene. *The Journal of Physical Chemistry C,* 116**,** 21104-21108.

ROBERTS, A., BROOKS, R. & SHIPWAY, P. 2014. Internal combustion engine cold-start efficiency: A review of the problem, causes and potential solutions. *Energy Conversion and Management,* 82**,** 327-350.

RUAN, B. & JACOBI, A. 2012. Ultrasonication effects on thermal and rheological properties of carbon nanotube suspensions. *Nanoscale Research Letters,* 7**,** 127.

RUDENKO, P. & BANDYOPADHYAY, A. 2013. Talc as friction reducing additive to lubricating oil. *Applied Surface Science,* 276**,** 383-389.

SADEGHINEZHAD, E., TOGUN, H., MEHRALI, M., SADEGHI NEJAD, P., TAHAN LATIBARI, S., ABDULRAZZAQ, T., KAZI, S. N. & METSELAAR, H. S. C. 2015. An experimental and numerical investigation of heat transfer enhancement for graphene nanoplatelets nanofluids in turbulent flow conditions. *International Journal of Heat and Mass Transfer,* 81**,** 41-51.

SADEGHINEZHAD, E., MEHRALI, M., SAIDUR, R., MEHRALI, M., TAHAN LATIBARI, S., AKHIANI, A. R. & METSELAAR, H. S. C. 2016. A comprehensive review on graphene nanofluids: Recent research, development and applications. *Energy Conversion and Management,* 111**,** 466-487.

SADRI, R., AHMADI, G., TOGUN, H., DAHARI, M., KAZI, S., SADEGHINEZHAD, E. & ZUBIR, N. 2014. An experimental study on thermal conductivity and viscosity of nanofluids containing carbon nanotubes. *Nanoscale Research Letters,* 9**,** 151.

SAIDUR, R., KAZI, S. N., HOSSAIN, M. S., RAHMAN, M. M. & MOHAMMED, H. A. 2011. A review on the performance of nanoparticles suspended with refrigerants and lubricating oils in refrigeration systems. *Renewable and Sustainable Energy Reviews,* 15**,** 310-323.

SALEHI, M., CLEMENS, F., GRAULE, T. & GROBÉTY, B. 2012. Kinetic analysis of the polymer burnout in ceramic thermoplastic processing of the YSZ thin electrolyte structures using model free method. *Applied Energy,* 95**,** 147-155.

SALMAN, B. H., MOHAMMED, H. A., MUNISAMY, K. M. & KHERBEET, A. S. 2013. Characteristics of heat transfer and fluid flow in microtube and microchannel using conventional fluids and nanofluids: A review. *Renewable and Sustainable Energy Reviews,* 28**,** 848-880.

SASTRY, N. N. V., BHUNIA, A., SUNDARARAJAN & DAS, S. K. 2008. Predicting the effective thermal conductivity of carbon nanotube based nanofluids. *Nanotechnology,* 19.

SEN GUPTA, S., MANOJ SIVA, V., KRISHNAN, S., SREEPRASAD, T. S., SINGH, P. K., PRADEEP, T. & DAS, S. K. 2011. Thermal conductivity enhancement of nanofluids containing graphene nanosheets. *Journal of Applied Physics,* 110**,** -.

SENATORE, A., D'AGOSTINO, V., PETRONE, V., CIAMBELLI, P. & SARNO, M. 2013. Graphene Oxide Nanosheets as Effective Friction

Modifier for Oil Lubricant: Materials, Methods, and Tribological Results. *ISRN Tribology,* 2013**,** 9.

SHAHRIARI, E., MAT YUNUS, W. M. & ZAMIRI, R. 2013. The effect of nanoparticle size on thermal diffusivity of gold nano-fluid measured using thermal lens technique. *JOURNAL OF THE EUROPEAN OPTICAL SOCIETY,* 8.

SHARMA, A. K., TIWARI, A. K. & DIXIT, A. R. 2016. Rheological behaviour of nanofluids: A review. *Renewable and Sustainable Energy Reviews,* 53**,** 779-791.

SHENOY, V. B., REDDY, C. D., RAMASUBRAMANIAM, A. & ZHANG, Y. W. 2008. Edge-Stress-Induced Warping of Graphene Sheets and Nanoribbons. *Physical Review Letters,* 101**,** 245501.

SHERIF, I. I. & MAHMOUD, N. S. 1966. Measurements of Thermal Conduction and Surface Finish by the Thermal Comparator. *Journal of Applied Physics,* 37**,** 2193-2194.

SHUKLA, R. K. & DHIR, V. K. Study of the effective thermal conductivity of nanofluids International Mechanical Engineering Congress and Exposition, 2005 Orlando, Florida, USA. ASME Int.

SMOLYANITSKY, A., KILLGORE, J. P. & TEWARY, V. K. 2012. Effect of elastic deformation on frictional properties of few-layer graphene. *Physical Review B,* 85**,** 035412.

SOME, S., KIM, Y., YOON, Y., YOO, H., LEE, S., PARK, Y. & LEE, H. 2013. High-Quality Reduced Graphene Oxide by a Dual-Function Chemical Reduction and Healing Process. *Sci. Rep.,* 3.

SRIDHARA, V. & SATAPATHY, L. N. 2011. Al2O3-based nanofluids: a review. *Nanoscale Research Letters,* 6**,** 456.

STANKOVICH, S., DIKIN, D. A., DOMMETT, G. H. B., KOHLHAAS, K. M., ZIMNEY, E. J., STACH, E. A., PINER, R. D., NGUYEN, S. T. & RUOFF, R. S. 2006a. Graphene-based composite materials. *Nature,* 442**,** 282-286.

STANKOVICH, S., PINER, R. D., CHEN, X., WU, N., NGUYEN, S. T. & RUOFF, R. S. 2006b. Stable aqueous dispersions of graphitic nanoplatelets via the reduction of exfoliated graphite oxide in the presence of poly(sodium 4-styrenesulfonate). *Journal of Materials Chemistry,* 16**,** 155-158.

STEVEN, C. & MARKUS, J. B. 2011. Twisted and coiled ultralong multilayer graphene ribbons. *Modelling and Simulation in Materials Science and Engineering,* 19**,** 054003.

SUN, Z., PÖLLER, S., HUANG, X., GUSCHIN, D., TAETZ, C., EBBINGHAUS, P., MASA, J., ERBE, A., KILZER, A., SCHUHMANN,

W. & MUHLER, M. 2013. High-yield exfoliation of graphite in acrylate polymers: A stable few-layer graphene nanofluid with enhanced thermal conductivity. *Carbon,* 64**,** 288-294.

SUN, Z., YAN, Z., YAO, J., BEITLER, E., ZHU, Y. & TOUR, J. M. 2010. Growth of graphene from solid carbon sources. *Nature,* 468**,** 549-552.

TAHA-TIJERINA, J., NARAYANAN, T. N., GAO, G., ROHDE, M., TSENTALOVICH, D. A., PASQUALI, M. & AJAYAN, P. M. 2012. Electrically Insulating Thermal Nano-Oils Using 2D Fillers. *ACS Nano,* 6**,** 1214-1220.

TAHA-TIJERINA, J., PEÑA-PARAS, L., NARAYANAN, T. N., GARZA, L., LAPRAY, C., GONZALEZ, J., PALACIOS, E., MOLINA, D., GARCÍA, A., MALDONADO, D. & AJAYAN, P. M. 2013. Multifunctional nanofluids with 2D nanosheets for thermal and tribological management. *Wear,* 302**,** 1241-1248.

TARANEH, J. B., RAHMATOLLAH, G., HASSAN, A. & ALIREZA, D. 2008. Effect of wax inhibitors on pour point and rheological properties of Iranian waxy crude oil. *Fuel Processing Technology,* 89**,** 973-977.

TAYLOR, R. A. & PHELAN, P. E. 2009. Pool boiling of nanofluids: Comprehensive review of existing data and limited new data. *International Journal of Heat and Mass Transfer,* 52**,** 5339-5347.

TEXTER, J. 2014. Graphene dispersions. *Current Opinion in Colloid & Interface Science,* 19**,** 163-174.

THOMAS, S. & CHOONDAL, B. P. S. 2011. A review of experimental investigations on thermal phenomena in nanofluids. *Nanoscale Research Letters,* 6.

TIAN, L. & AHMADI, G. 2013. Fiber transport and deposition in human upper tracheobronchial airways. *Journal of Aerosol Science,* 60**,** 1-20.

TIAN, L., AHMADI, G., WANG, Z. & HOPKE, P. K. 2012. Transport and deposition of ellipsoidal fibers in low Reynolds number flows. *Journal of Aerosol Science,* 45**,** 1-18.

TIMOFEEVA, E. V., GAVRILOV, A. N., MCCLOSKEY, J. M., TOLMACHEV, Y. V., SPRUNT, S., LOPATINA, L. M. & SELINGER, J. V. 2007. Thermal conductivity and particle agglomeration in alumina nanofluids: Experiment and theory. *Physical Review E,* 76**,** 061203.

TIMOFEEVA, E. V., ROUTBORT, J. L. & SINGH, D. 2009. Particle shape effects on thermophysical properties of alumina nanofluids. *Journal of Applied Physics,* 106**,** -.

TOMBROS, N., JOZSA, C., POPINCIUC, M., JONKMAN, H. T. & VAN WEES, B. J. 2007. Electronic spin transport and spin precession in single graphene layers at room temperature. *Nature,* 448**,** 571-574.

TSAI, T.-H., KUO, L.-S., CHEN, P.-H. & YANG, C.-T. 2008. Effect of viscosity of base fluid on thermal conductivity of nanofluids. *Applied Physics Letters,* 93**,** 233121-3.

UDDIN, M. E., KUILA, T., NAYAK, G. C., KIM, N. H., KU, B.-C. & LEE, J. H. 2013. Effects of various surfactants on the dispersion stability and electrical conductivity of surface modified graphene. *Journal of Alloys and Compounds,* 562**,** 134-142.

UNDATA. 2013. *Industrial Commodity Statistics Database* [Online]. United Nations Statistics Division: UN data. Available: http://data.un.org/Data.aspx?q=Other+Asia&d=EDATA&f=cmID%3aLU %3byr%3a2010&c=2,5,6,7,8&s=_crEngNameOrderBy:asc,_enID:asc,yr:d esc&v=1.

VAKILI-NEZHAAD, G. & DORANY, A. 2012. Effect of Single-Walled Carbon Nanotube on the Viscosity of Lubricants. *Energy Procedia,* 14**,** 512-517.

VARRLA, E., PATON, K. R., BACKES, C., HARVEY, A., SMITH, R. J., MCCAULEY, J. & COLEMAN, J. N. 2014. Turbulence-assisted shear exfoliation of graphene using household detergent and a kitchen blender. *Nanoscale,* 6**,** 11810-11819.

WALVEKAR, R., FARIS, I. A. & KHALID, M. 2012. Thermal conductivity of carbon nanotube nanofluid—Experimental and theoretical study. *Heat Transfer—Asian Research,* 41**,** 145-163.

WAN, Q., JIN, Y., SUN, P. & DING, Y. 2015. Tribological Behaviour of a Lubricant Oil Containing Boron Nitride Nanoparticles. *Procedia Engineering,* 102**,** 1038-1045.

WANG, B.-X., ZHOU, L.-P. & PENG, X.-F. 2003. A fractal model for predicting the effective thermal conductivity of liquid with suspension of nanoparticles. *International Journal of Heat and Mass Transfer,* 46**,** 2665-2672.

WANG, F., HAN, L., ZHANG, Z., FANG, X., SHI, J. & MA, W. 2012. Surfactant-free ionic liquid-based nanofluids with remarkable thermal conductivity enhancement at very low loading of graphene. *Nanoscale Research Letters,* 7**,** 314.

WANG, X., XU, X. & S. CHOI, S. U. 1999. Thermal Conductivity of Nanoparticle - Fluid Mixture. *Journal of Thermophysics and Heat Transfer,* 13**,** 474-480.

WASP, E. J., KENNY, J. P. & GHANDI, R. L. 1998. *Solid Liquid Slurry Pipeline Transportation, Series on Bulk Materials Handling*, Trans Tech Publications Inc.

WEI, N., XU, L., WANG, H.-Q. & ZHENG, J.-C. 2011a. Strain engineering of thermal conductivity in graphene sheets and nanoribbons: a demonstration of magic flexibility. *Nanotechnology,* 22**,** 105705.

WEI, X., MENG, Z., RUIZ, L., XIA, W., LEE, C., KYSAR, J. W., HONE, J. C., KETEN, S. & ESPINOSA, H. D. 2016. Recoverable Slippage Mechanism in Multilayer Graphene Leads to Repeatable Energy Dissipation. *ACS Nano,* 10**,** 1820-1828.

WEI, Z., MING, Z., HONGWEI, Z., YU, T., KUNLIN, W., JINQUAN, W., FEI, J., XIAO, L., ZHEN, L., PENG, Z. & DEHAI, W. 2011b. Tribological properties of oleic acid-modified graphene as lubricant oil additives. *Journal of Physics D: Applied Physics,* 44**,** 205303.

WEN, D., LIN, G., VAFAEI, S. & ZHANG, K. 2009. Review of nanofluids for heat transfer applications. *Particuology,* 7**,** 141-150.

WILSON, R. W. & LYON, S. B. 2010. 2.26 - Corrosion in Lubricants/Fuels. *In:* EDITOR-IN-CHIEF: TONY, J. A. R. (ed.) *Shreir's Corrosion.* Oxford: Elsevier.

XIE, G., SHEN, Y., WEI, X., YANG, L., XIAO, H., ZHONG, J. & ZHANG, G. 2014. A Bond-order Theory on the Phonon Scattering by Vacancies in Two-dimensional Materials. *Sci. Rep.,* 4.

XIE, H., FUJII, M. & ZHANG, X. 2005. Effect of interfacial nanolayer on the effective thermal conductivity of nanoparticle-fluid mixture. *International Journal of Heat and Mass Transfer,* 48**,** 2926-2932.

XU, J., YU, B., ZOU, M. & XU, P. 2006. A new model for heat conduction of nanofluids based on fractal distributions of nanoparticles. *Journal of Physics D: Applied Physics,* 39**,** 4486.

XU, X., PEREIRA, L. F. C., WANG, Y., WU, J., ZHANG, K., ZHAO, X., BAE, S., TINH BUI, C., XIE, R., THONG, J. T. L., HONG, B. H., LOH, K. P., DONADIO, D., LI, B. & ÖZYILMAZ, B. 2014. Length-dependent thermal conductivity in suspended single-layer graphene. *Nat Commun,* 5.

XUAN, Y., LI, Q. & HU, W. 2003. Aggregation structure and thermal conductivity of nanofluids. *AIChE Journal,* 49**,** 1038-1043.

XUE, L., KEBLINSKI, P., PHILLPOT, S. R., CHOI, S. U. S. & EASTMAN, J. A. 2004. Effect of liquid layering at the liquid-solid interface on thermal transport. *International Journal of Heat and Mass Transfer,* 47**,** 4277-4284.

XUE, Q.-Z. 2003. Model for effective thermal conductivity of nanofluids. *Physics Letters A,* 307**,** 313-317.

XUE, Q. & XU, W.-M. 2005. A model of thermal conductivity of nanofluids with interfacial shells. *Materials Chemistry and Physics,* 90**,** 298-301.

YANG, B. & HAN, Z. H. 2006. Temperature-dependent thermal conductivity of nanorod-based nanofluids. *Applied Physics Letters,* 89**,** 083111.

YANG, P., TANG, Y., YANG, H., GONG, J., LIU, Y., ZHAO, Y. & YU, X. 2013. Thermal management performance of bent graphene nanoribbons. *RSC Advances,* 3**,** 17349-17354.

YONGPING, Z., NING, W., ZHEYONG, F., LANQING, X. & ZHIGAO, H. 2011. Mechanical properties of grafold: a demonstration of strengthened graphene. *Nanotechnology,* 22**,** 405701.

YU-HUA, L., WEI, Q. & JIAN-CHAO, F. 2008. Temperature Dependence of Thermal Conductivity of Nanofluids. *Chinese Physics Letters,* 25**,** 3319.

YU, F., STOOT, A. C., BOGGILD, P. & CAMILLI, L. 2016. Failure of multi-layer graphene coatings in acidic media. *RSC Advances,* 6**,** 21497-21502.

YU, W. & CHOI, S. U. S. 2003. The Role of Interfacial Layers in the Enhanced Thermal Conductivity of Nanofluids: A Renovated Maxwell Model. *Journal of Nanoparticle Research,* 5**,** 167-171.

YU, W. & CHOI, S. U. S. 2004. The role of interfacial layers in the enhanced thermal conductivity of nanofluids: A renovated Hamilton–Crosser model. *Journal of Nanoparticle Research,* 6**,** 355-361.

YU, W., FRANCE, D. M., CHOI, S. U. S., ROUTBORT, J. L. & SYSTEMS, E. 2007. Review and assessment of nanofluid technology for transportation and other applications.

YU, W., FRANCE, D. M., ROUTBORT, J. L. & CHOI, S. U. S. 2008. Review and Comparison of Nanofluid Thermal Conductivity and Heat Transfer Enhancements. *Heat Transfer Engineering,* 29**,** 432 - 460.

YU, W. & XIE, H. 2012. A Review on Nanofluids: Preparation, Stability Mechanisms, and Applications. *Journal of Nanomaterials,* 2012.

YU, W., XIE, H. & BAO, D. 2010a. Enhanced thermal conductivities of nanofluids containing graphene oxide nanosheets *Nanotechnology,* 21**,** 055705.

YU, W., XIE, H. & CHEN, W. 2010b. Experimental investigation on thermal conductivity of nanofluids containing graphene oxide nanosheets. *Journal of Applied Physics,* 107**,** 094317-6.

YU, W., XIE, H., WANG, X. & WANG, X. 2011. Significant thermal conductivity enhancement for nanofluids containing graphene nanosheets. *Physics Letters A,* 375**,** 1323-1328.

ZAWRAH, M. F., KHATTAB, R. M., GIRGIS, L. G., EL DAIDAMONY, H. & ABDEL AZIZ, R. E. 2015. Stability and electrical conductivity of water-base Al2O3 nanofluids for different applications. *HBRC Journal*.

ZHANG, L., PU, J., WANG, L. & XUE, Q. 2014. Frictional dependence of graphene and carbon nanotube in diamond-like carbon/ionic liquids hybrid films in vacuum. *Carbon,* 80**,** 734-745.

ZHANG, T., LI, X. & GAO, H. 2015. Fracture of graphene: a review. *International Journal of Fracture***,** 1-31.

ZHANG, W., DEMYDOV, D., JAHAN, M. P., MISTRY, K., ERDEMIR, A. & MALSHE, A. P. 2012. Fundamental understanding of the tribological and thermal behavior of Ag–MoS2 nanoparticle-based multi-component lubricating system. *Wear,* 288**,** 9-16.

ZHANG, X., GU, H. & FUJII, M. 2007. Effective thermal conductivity and thermal diffusivity of nanofluids containing spherical and cylindrical nanoparticles. *Experimental Thermal and Fluid Science,* 31**,** 593-599.

ZHENG, J., WANG, Y., WANG, L., QUHE, R., NI, Z., MEI, W.-N., GAO, Z., YU, D., SHI, J. & LU, J. 2013. Interfacial Properties of Bilayer and Trilayer Graphene on Metal Substrates. *Scientific Reports,* 3**,** 2081.

ZHMUD, B. & PASALSKIY, B. 2013. Nanomaterials in Lubricants: An Industrial Perspective on Current Research. *Lubricants,* 1**,** 95.

ZHOU, S., TAO, X. & GU, Y. 2016. Thickness-Dependent Thermal Conductivity of Suspended Two-Dimensional Single-Crystal In2Se3 Layers Grown by Chemical Vapor Deposition. *The Journal of Physical Chemistry C,* 120**,** 4753-4758.

ZHU, D., LI, X., WANG, N., WANG, X., GAO, J. & LI, H. 2009. Dispersion behavior and thermal conductivity characteristics of Al2O3-H2O nanofluids. *Current Applied Physics,* 9**,** 131-139.

APPENDIX 1

Source code for TMDLS

```
#include <SPI.h>

#include <SD.h>

            const int numReadings = 10;

            const int chipSelect = 4;

        float temp = 0;

        float temp1 = 0;

        float temp2 = 0;

        float temp3 = 0;

const int tempPin = A0;

const int tempPin1 = A1;

const int tempPin2 = A2;

const int tempPin3 = A3;

        int readings[numReadings];          // the readings from the analogue
        input

        int readings1[numReadings];

        int readings2[numReadings];

        int readings3[numReadings];

        int index = 0;                      // the index of the current reading

        int total = 0;                      // the running total

        int total1 = 0;

        int total2 = 0;

        int total3 = 0;

        int average = 0;                     // the average

        int average1 = 0;
```

```
int average2 = 0;

int average3 = 0;

int inputPin = A0;

int inputPin1 = A1;

int inputPin2 = A2;

int inputPin3 = A3;

void setup()
{
                                // initialize serial communication with computer:
  Serial.begin(9600);
  while (!Serial) {
  ;                             // wait for serial port to connect.
                                //Needed for Leonardo only
  }
//////////////////////////////////////////////////////////////////////////////////////////////////////
Serial.print ("Initializing SD card...");
delay (1000);
        pinMode (53, OUTPUT);
if (!SD.begin(chipSelect)) {
        Serial.println("Card failed, or not present");
delay (1000);
        return;
}
        Serial.println("card initialized.");
        delay (1000);
//////////////////////////////////////////////////////////////////////////////////////////Appendix///
```

```
                                        // initialize all the readings to 0:
for (int thisReading = 0; thisReading < numReadings; thisReading++)
        readings[thisReading] = 0;
for (int thisReading1 = 0; thisReading1 < numReadings; thisReading1++)
        readings1[thisReading1] = 0;
for (int thisReading2 = 0; thisReading2 < numReadings; thisReading2++)
        readings2[thisReading2] = 0;
for (int thisReading3 = 0; thisReading3 < numReadings; thisReading3++)
        readings3[thisReading3] = 0;
}
void loop () {
                                        // subtract the last reading:
 total= total - readings[index];
  total1= total1 - readings1[index];
   total2= total2 - readings2[index];
    total3= total3 - readings3[index];
                                        // read from the sensor:
 readings[index] = analogRead(inputPin);
  readings1[index] = analogRead(inputPin1);
   readings2[index] = analogRead(inputPin2);
    readings3[index] = analogRead(inputPin3);
                                        // add the reading to the total:
 total= total + readings[index];
  total1= total1 + readings1[index];
   total2= total2 + readings2[index];
    total3= total3 + readings3[index];
```

```
                              // advance to the next position in the
array:

index = index + 1;           // if we're at the end of the array...

if (index >= numReadings)     // ...wrap around to the beginning:

index = 0;                    // calculate the average:

  average = total / numReadings;

   average1 = total1 / numReadings;

    average2 = total2 / numReadings;

     average3 = total3 / numReadings;

  temp = 0.48828125*average;

   temp1 = 0.48828125*average1;

    temp2 = 0.48828125*average2;

     temp3 = 0.48828125*average3;

                              // send it to the computer as ASCII digits

                              // Serial.print(average);

                              //Serial.print(",");

Serial.print(temp);
Serial.print(",");

                              //Serial.print(average1);

                              // Serial.print(",");

Serial.print(temp1);
Serial.print(",");

                              // Serial.print(average2);

                              // Serial.print(",");

Serial.print(temp2);
Serial.print(",");

                              //Serial.print(average3);
```

```
                                                  // Serial.print(",");

Serial.print(temp3);

Serial.print(",");

Serial.print("\n ");

/////////////////////////////////////////////////////////////////////////////////////////////////////

File dataFile = SD.open("d1bb.txt", FILE_WRITE);

                                                  // if the file is available, write to it:

if (dataFile) {

   dataFile.print(temp);

      dataFile.print(",");

   dataFile.print(temp1);

      dataFile.print(",");

   dataFile.print(temp2);

      dataFile.print(",");

   dataFile.print(temp3);

      dataFile.print(",");

                                                  //dataFile.print(volt);

   dataFile.println(",");

                                                  // lcd.clear();

                                                  //lcd.print("CAHCET_EEE_DAS");

                                                  //dataFile.println(",");

                                                  //dataFile.close();

                                                  //dataFile.close();

                                                  //dataFile.close();

   dataFile.close();

}                                                 // if the file isn't open, pop up an error:

else {
```

```
    Serial.println("error opening datalog.txt");

}

//////////////////////////////////////////////////////////////////////////////////////////////////////

  delay(1000);        // delay in between reads for stability

}
```

APPENDIX 2

Table. American Petroleum Institute (API) Gasoline Engine Oil Service Classifications

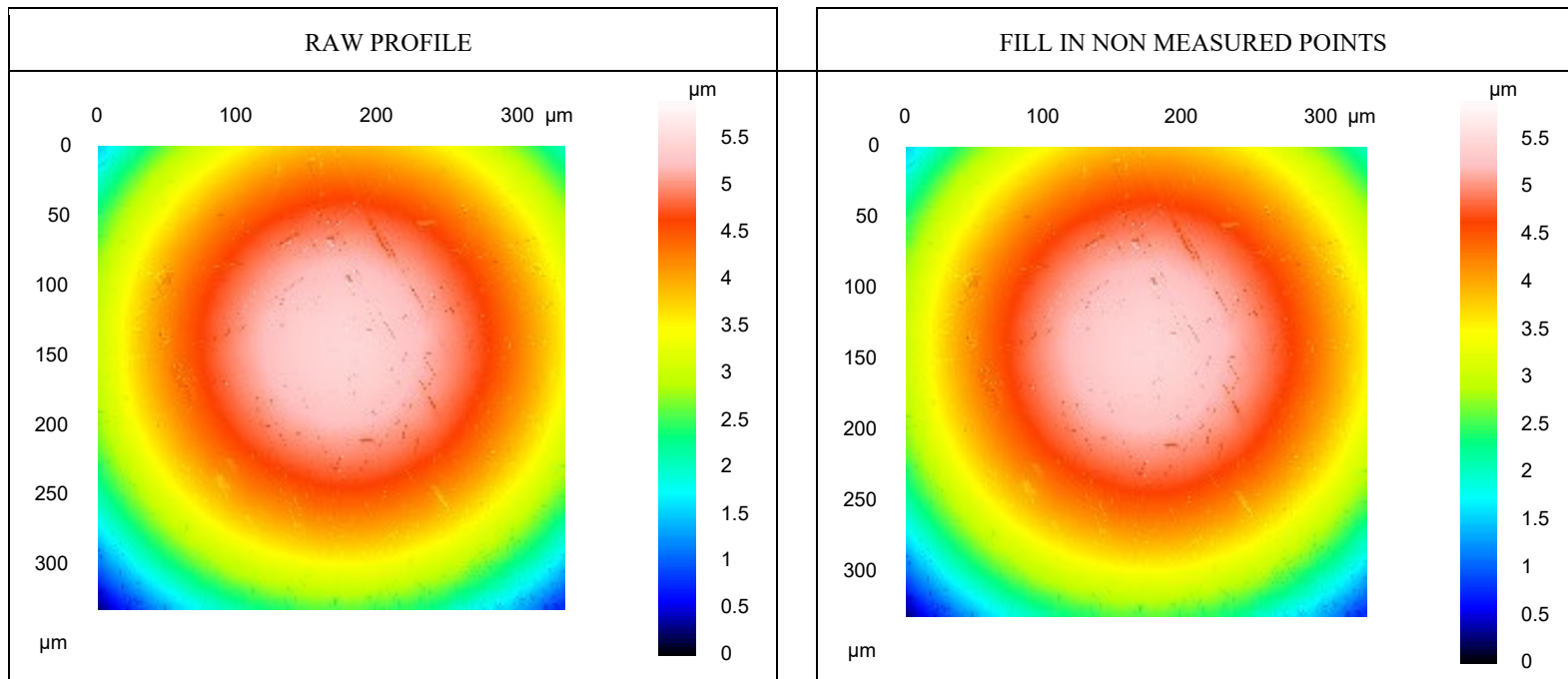| Category	Status	Service
SN	Current	Introduced in October 2010 for 2011 and older vehicles, designed to provide improved high temperature deposit protection for pistons, more stringent sludge control, and seal compatibility. API SN with Resource Conserving matches ILSAC GF-5 by combining API SN performance with improved fuel economy, turbocharger protection, emission control system compatibility, and protection of engines operating on ethanol-containing fuels up to E85.
SM	Current	For 2010 and older automotive engines.
SL	Current	For 2004 and older automotive engines.
SJ	Current	For 2001 and older automotive engines.
SH	Obsolete	Not suitable for use
SG	Obsolete	Not suitable for use
SF	Obsolete	Not suitable for use
SE	Obsolete	Not suitable for use in gasoline-powered automobile engines built after 1979.
SD	Obsolete	Not suitable for use in gasoline-powered automobile engines built after 1971. Use in more modern engines may cause unsatisfactory performance or equipment harm.
SC	Obsolete	Not suitable for use in gasoline-powered automobile engines built after 1967. Use in more modern engines may cause unsatisfactory performance or equipment harm.
SB	Obsolete	Not suitable for use in gasoline-powered automobile engines built after 1951. Use in more modern engines may cause unsatisfactory performance or equipment harm.
SA	Obsolete	Not suitable for use in gasoline-powered automobile engines built after 1930. Use in more modern engines may cause unsatisfactory performance or equipment harm.

APPENDIX 3

Test criteria for oil meeting API SN or API SN/Resource Conserving, American Petroleum Institute 2010
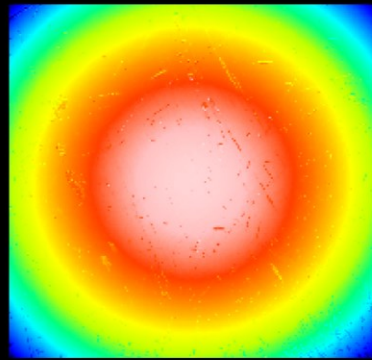
	API SN		API SN + RC
Viscosity Grades	**0W20, 0W30, 5W20, 5W30, 10W30**	**Others**	**Multi-grade variations of 0W, 5W and 10W**
Laboratory Tests			
Sulphur, max %			
0Wxx and 5Wxx	0.5	NR	0.5
10W30	0.6	NR	0.6
Others	NA	NR	0.6
High temperature deposits, max mg			
TEOST MHT	35	45	35
TEOST 33C	NR	NR	0.6
Foam	1 min. settling	10 min. settling	1 min. settling
Gelation Index	12	NR	12

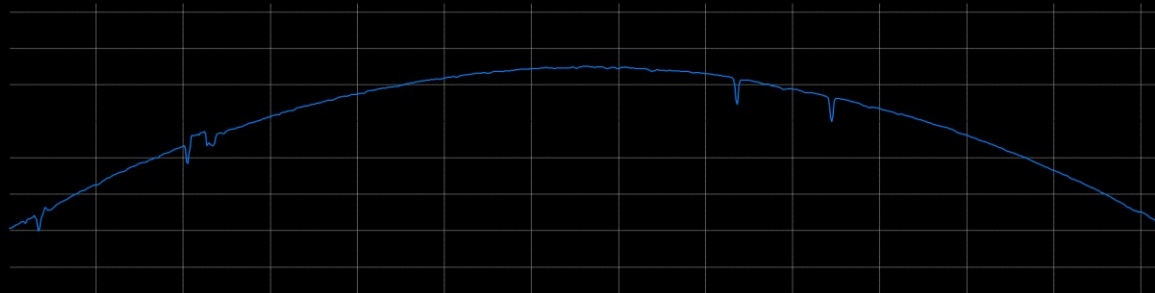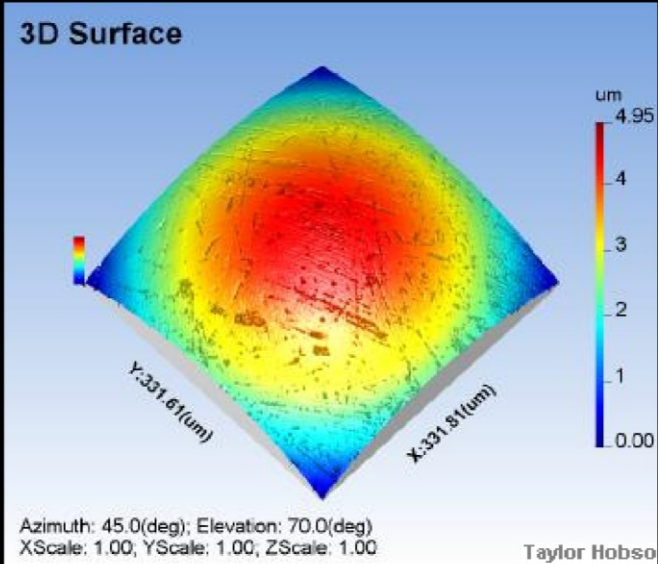|			
Emulsion Retention	NR	NR	No Water Separation
Seal Compatibility		ILSAC GF-5 limits apply	
Phosphorous, max% / min%	0.08 / 0.06	NR / 0.06	0.08 / 0.06
Engine Tests			
Sequence VID	NR	NR	Pass
ROBO or Sequence IIIGA	Pass	NR	Pass

APPENDIX 4

Typical Surface profile analysis of steel ball sample obtained after 4-ball tribometer test. Graphs were plotted using TalyMap Platinum 5.1.1.5374 software. The following data corresponds to steel ball number 94.
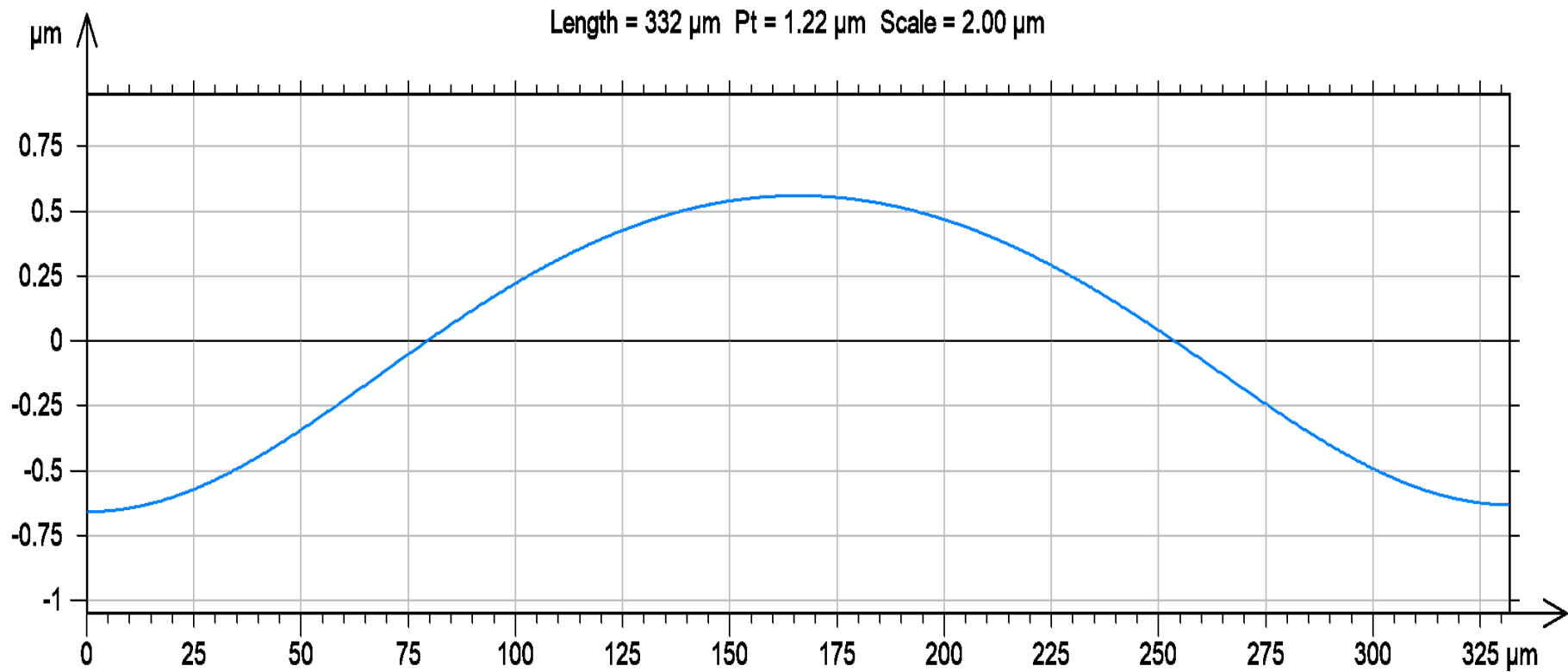
2D ROUGHNESS GRAPH

3D Surface
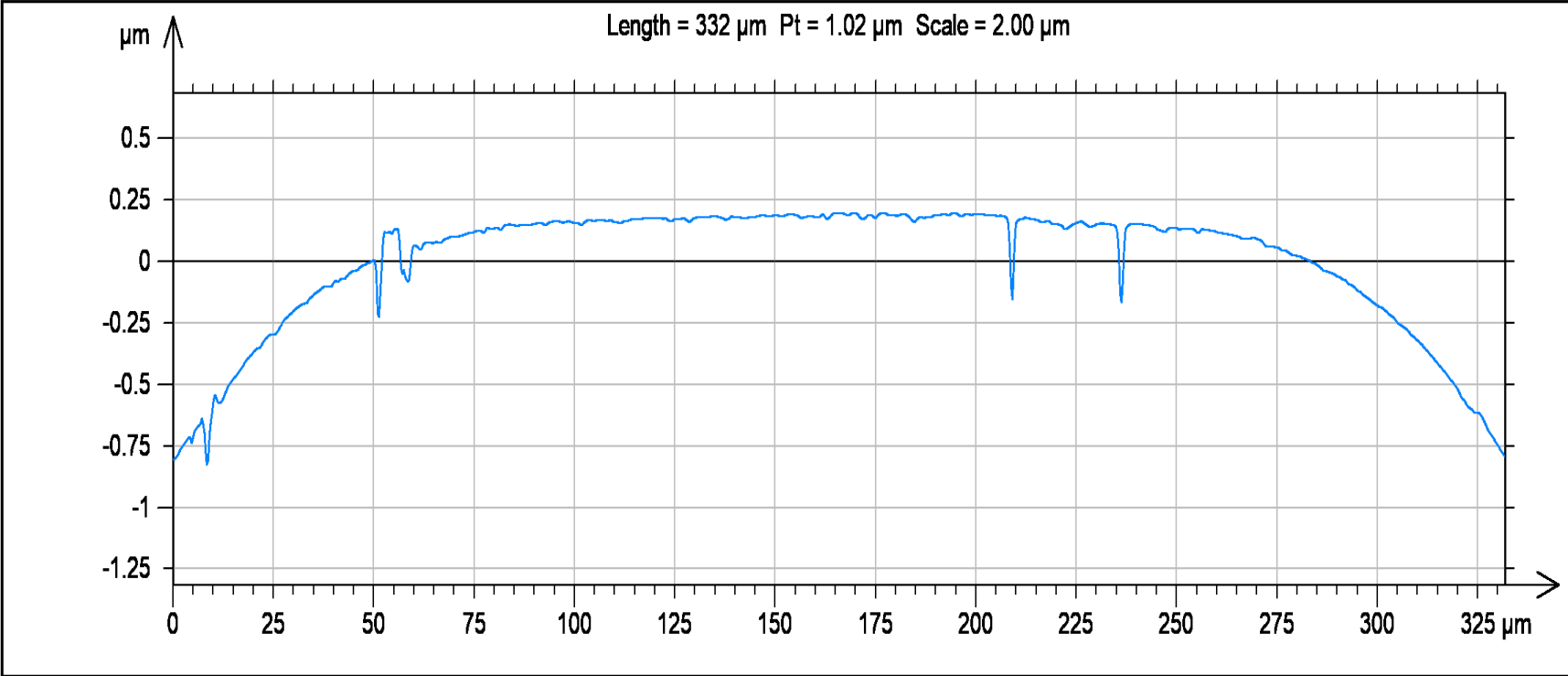
um
4.95

4

3

2

1

0.00

Y:331.61(um)

X:331.81(um)

Azimuth: 45.0(deg); Elevation: 70.0(deg)
XScale: 1.00, YScale: 1.00, ZScale: 1.00

Taylor Hobso

Filtering Waviness + Roughness Graph

Length = 332 µm Pt = 1.22 µm Scale = 2.00 µm

Length = 332 µm Pt = 1.02 µm Scale = 2.00 µm

Amplitude parameters - Roughness profile   **ISO 4287**

Rp	0.055	μm	*Rp: Maximum Peak Height of the roughness profile.*
Rv	0.189	μm	*Rv: Maximum Valley Depth of the roughness profile.*
Rz	0.244	μm	*Rz: Maximum Height of roughness profile.*
Rc	0.171	μm	*Rc: Mean height of the roughness profile elements.*
Rt	0.449	μm	*Rt: Total Height of roughness profile.*
Ra	0.0154	μm	*Ra: Arithmetic Mean Deviation of the roughness profile.*
Rq	0.0316	μm	*Rq: Root-Mean-Square (RMS) Deviation of the roughness profile.*
Rsk	-5.99		*Rsk: Skewness of the roughness profile.*
Rku	59.8		*Rku: Kurtosis of the roughness profile.*
Rmr	100	%	*Rmr: Relative Material Ratio of the roughness profile.*
Rdc	0.022	μm	*Rdc: roughness profile Section Height difference*